DISSERTATION

Transcriptional timing and noise of yeast cell cycle regulators —

a single-cell and single-molecule approach

zur Erlangung des akademischen Grades

d o c t o r r e r u m n a t u r a l i u m (Dr. rer. nat.)

im Fach Biophysik

eingereicht an der Lebenswissenschaftlichen Fakultät

der Humboldt Universität zu Berlin von

MSc. Aouefa Amoussouvi

Präsidentin der Humboldt Universität zu Berlin: Prof. Dr.-Ing. Dr. Sabine Kunst

Dekan der Lebenswissenschaftlichen Fakultät: Prof. Dr. Bernhard Grimm

Gutachter/in: 1. Prof. Dr. Andreas Herrmann

2. Prof. Dr. Dr. Edda Klipp

3. Prof. Dr. Alexander Löwer

Datum der Einreichung: 01.11.2018

Datum der Promotion: 20.06.2019

Zusammenfassung

Die Genexpression ist ein stochastischer Prozess und ihre angemessene Regulierung ist entscheidend für den Verlauf des Zellzyklus. Die Reaktion auf zellulären Stress erfordert eine Umprogrammierung, dessen strenge Regulation einen ungestörten Zellzyklusverlauf ermöglicht. Jeglicher Stress löst eine Neuprogrammierung der Expression somit einen temporären Stillstand des Zellzyklus aus. Da Messungen an Zellpopulationen oft nicht alle notwendigen Informationen liefern, um z.B. den eukaryotischen Zellzyklus im Kontext einer verrauschten Genexpression und externer Störungen zu verstehen, sind zeitaufgelöste quantitative Methoden an einzelnen Zellen notwendig.

Die wichtigsten Regulatoren der G1/S-Zellzyklusphasen in *S. cerevisiae* sind die Gene *SIC1*, *CLN2* und *CLB5*. Wir haben Einzelzellen-Fluoreszenzmikroskopie und auf experimentellen Daten basierende stochastische Modellierung auf die quantitative Charakterisierung der Expression dieser Gene angewendet. Mit dem fluoreszierendem MS2-CP-System haben wir den *SIC1*-mRNA-Gehalt quantifiziert und die verschiedenen Arten des Transports von *SIC1* mRNA-Partikeln in lebenden Zellen visualisiert. Mittels RNA-FISH und der Verwendung genetischer und morphologischer Marker konnten wir die absolute Anzahl von mRNA-Molekülen und das transkriptionelle Rauschen über alle Zellzyklusphasen unter normalen Bedingungen und unter osmotischem Stress verfolgen und vergleichen.

Die stochastische Modellierung ermöglichte eine *in silico* Synchronisation der Expressionsdaten und damit die Transformation der stationären mRNA-Daten in Zeitreihen der Expression der mRNA-Moleküle, der kodierten Proteine und deren Rauschen. Das Modell gestattete dafür die Extraktion kinetischer Parameter von Transkription und Abbau einzelner mRNA-Species. Alle drei Gene zeigten während des gesamten Zellzyklus eine basale Expression. Dieses lässt schlussfolgern, dass die Transkription nicht in ‚on' und ‚off', sondern in ‚high' und ‚low' Phasen der Genexpression unterteilt ist.

Basierend auf unseren experimentellen Daten entwickelten wir zuerst ein stochastisches Modell des G1/S-Überganges, bei dem *SIC1* im Mittelpunkt steht. Ein zweites stochastisches Modell berücksichtigt sowohl den gesamten Zellzyklus als auch *SIC1*, *CLN2* und *CLB5* sowie den Einfluss eines osmotischen Stresses. Ein niedriger *SIC1*-Transkriptionspegel sorgte für ein geringes Proteinrauschen und einen robusten Zeitablauf des G1/S-Übergangs. *CLN2* und *CLB5* zeigten eine hohe Expression in der G1-Phase sowie ein Absinken der Expression in der späten Mitose. Osmostress induzierte verschiedene Perioden der Transkriptionshemmung für *CLN2* und *CLB5* und länger anhaltende Auswirkungen auf die Dauer der Zellzyklusphasen.

Unser Ansatz ermöglicht den Zugang zu detaillierten quantitativen Erkenntnissen über die Genexpression und die Taktung des Zellzyklus, die aus populationsbasierten Untersuchungen nicht erhältlich sind. Einige für *SIC1*, *CLN2* und *CLB5* spezifische Regulationsmechanismen können für andere Gene sowie für andere Organismen verallgemeinert werden.

Abstract

Gene expression is a stochastic process and its appropriate regulation is critical for cell cycle progression. Cell survival in response to external stresses requires expression reprogramming and cell cycle arrest. Qualitative and bulk-scale population measurements do not provide sufficient information to understand eukaryotic cell cycle in context of noisy gene expression and external perturbations, and time-resolved quantitative methods on single cells are, therefore, required.

We applied single-cell fluorescence microscopy and stochastic modeling to *SIC1*, *CLN2* and *CLB5*, the main G1/S regulators in *S. cerevisiae*. Using MS2-CP system we estimated *SIC1* mRNA levels and visualized different types of transport for *SIC1* mRNA particles in living cells. With RNA-FISH combined to genetic and morphological markers we monitored absolute numbers of mRNA and transcriptional noise over cell cycle phases with and without osmostress.

Stochastic modeling enabled *in silico* synchronization from the mRNA expression experiments and expanded the static mRNA data into time courses for mRNAs, proteins and their respective noise levels. This required extracting kinetic parameters for mRNA production and decay of the single mRNA species. All three genes exhibited basal expression throughout cell cycle enlightening that transcription is not divided in “on” and “off” but rather in “high” and “low” phases.

Based on our experimental data we developed a stochastic model of G1/S timing centered on *SIC1* and a second one for the entire cell cycle involving *SIC1*, *CLN2* and *CLB5* and the response to osmostress. A low *SIC1* transcript level ensured a low protein noise and a robust timing of the G1/S transition. *CLN2* and *CLB5* showed main expression peaks in G1 as well as an expression upshift in late mitosis. Osmostress induced different periods of transcriptional inhibition for *CLN2* and *CLB5* and long-term impact on cell cycle phase duration.

Our approach disclosed detailed quantitative insights into gene expression and cell cycle timing, not available from bulk experiments. Importantly some regulation mechanisms specific to *SIC1*, *CLN2* and *CLB5* might be generalized to other genes as well as to other organisms.

Schlagwörter / Keywords

Schlagwörter:

Eukaryotische Zellzyklus, MS2-CP Methode, Einzelmolekül RNA-FISH, Einzelzell-Mikroskopie, G1/S-Übergangs, Stochastische Modellierung, Antworten auf osmotischen Stress.

Keywords:

Eukaryotic cell cycle, MS2-CP, single-molecule RNA-FISH, single-cell microscopy, G1/S transition, stochastic modeling, osmotic stress response

Table of Content

List of Abbreviations

(m)RNA	(messenger)RiboNucleic Acid
3'UTR	3' Untranslated Region
Ana	Anaphase
CCD camera	Charge Coupled Device camera
CDK	Cyclin Dependent Kinase
CDKI	Cyclin Dependent Kinase-Inhibitor
cDTA	Comparative Dynamic Transcriptome Analysis
CFP	Cyan Fluorescent Protein
Clb	B-type cyclin
Cln	G1 phase cyclin
CPU	Central Processing Unit
CV	Coefficient of Variation
Cys	Cysteine
DAPI	4',6-diamidino-2-phenylindole
DIC	Differential Interference Contrast
DNA	DeoxydriboNucleic Acid
dNTP	Deoxynucleotide
FACS	Fluorescence Activated Cell Sorting
FISH	Fluorescence *In Situ* Hybridization
G0	Gap-phase 0
G1	Gap-phase 1
G2	Gap-phase 2
GFP	Green Fluorescent Protein
GO	significantly enriched Gene Ontology method (Geijer et al., 2013)
GPU	Graphics Processing Unit
His	Histidine
Hog1	High Osmolarity Glycerol protein 1
LB medium	Luria Bertani medium
M	Mitosis
MAPK	Mitogen Activated Protein Kinase
MBF	SCB-Binding Factor, made of Swi4 and Mbp1
Met	Methionine
MS2-CP	MS2-Coat Protein
N&B	Number & Brightness method

NaCl	Sodium chloride
NLS	Nuclear Localization Signal
OD	Optical Density
ODE	Ordinary Differential Equation
ORF	Open Reading Frame
P/M	Prometa-/Metaphase
PCR	Polymerase chain Reaction
RNP	RiboNucleoprotein Particle. Is a complex of RNA(s) and protein(s).
ROI	Region Of Interest
RT	Room Temperature
S	DNA synthesis phase
S. cerevisiae	Saccharomyces cerevisiae
SAPK	Stress-Activated Protein Kinase
SBF	SCB-Binding Factor, made of Swi6 and Swi4
SD	Synthetic Dextrose
SEM	Standard Error of Mean
SSC buffer	Sodium Saline Citrate buffer
T/C	Telophase/Cytokinesis
TF	Transcription Factor
TS	Transcription Start site
URA	Uracile
WT	Wild Type
YFP	Yellow Fluorescent Protein
YPD medium	Yeast Extract Peptone Dextrose medium

“The future never just happened. It was created.”

- Mae Jemison

To my family and friends

1. INTRODUCTION

1.1 Dissecting the cell division cycle to stop a 'silent epidemic'.

Together diabetes, cancers, cardiovascular and neurodegenerative diseases are the primary causes of morbidity and mortality and engender considerable economic and social issues in industrialized countries (Vos et al., 2015). Their slow development leads to late diagnosis, when progression of irreversible symptoms can only be partially slowed down, resulting in a 'silent epidemic' through the population (Meetoo, 2008). Cancers are closely related to dysfunctions in cell division cycle and several cell cycle regulating genes have been identified as oncogenes and tumor repressors, which promotes or represses tumor development, respectively (Barberis et al., 2005; Foury, 1997; Harashima et al., 2013; Hwang and Clurman, 2005; Zhivotovsky and Orrenius, 2010). Interestingly, diabetes as well as cardiovascular or neurodegenerative diseases have also been linked to dysfunctions in cell division cycle regulation (Boehm and Nabel, 2003; Currais et al., 2009; Zhivotovsky and Orrenius, 2010). A major goal to fight this 'silent epidemic' consists of finding novel treatments especially in identifying possible drug-targets. Moreover a new challenge has been to improve the still underdeveloped early-diagnosis strategies in isolating efficient "early-phase biomarkers" to diagnose the disease at a stage where it can still be potential cured (Boehm and Nabel, 2003; Nagy, 2007; Zhivotovsky and Orrenius, 2010). Fundamental research to dissect the regulatory mechanisms of the cell cycle and its regulators offers a direction to better understand the dysfunctions of cell cycle progression and related diseases as well as to open the path toward novel diagnosis and treatments.

1.2 System biology or how computational modeling helps rationalizing large experimental, heterogeneous data set.

Although cell cycle and activation of signaling pathways in response to stress have been extensively investigated on a protein level (Adrover et al., 2011; Hohmann, 2002; Muzzey et al., 2009; Saito and Posas, 2012), their long-term regulation with regard to gene expression at single-cell level, especially transcription and noise, and cell cycle timing are not well characterized. The available research data has drastically increased and computational approaches are powerful tools to rationalize already published information and novel experimental findings and to create coherence between those interconnected processes, which are often independently addressed. Additionally mathematical models enable to extract parameters from data sets, which are experimentally not accessible, and to make predictions on the dynamics of complex regulatory networks. Further development of stochastic models require therefore better cell cycle resolved and more quantitative experimental measurements of single-cell mRNA numbers.

1.3 The eukaryotic cell cycle

1.3.1 Four phases to replicate life

The cell cycle is an essential process of life that controls growth, DNA duplication and cell division. Eukaryotic cell cycle leads from an initial unique mother cell to the production of two daughter cells with identical DNA information and consists of four distinct main phases: gap-phase 1 (G1), DNA synthesis phase (S), gap-phase 2 (G2) and mitosis (M) usually followed by cytokinesis (Alberts et al., 2002). G1, S and G2 constitute the interphase, which can be simplified as a period of growth, protein synthesis (G1 and G2) and DNA replication (S) to prepare the mitosis, i.e. the period of nuclear division. Mitosis is the most critical phase and also considerably shorter than the interphase. Indeed mitosis takes approximately only 5-20% of the full cell cycle length (Alberts et al., 2002; Cooper, 2000). Mitotic events occur rapidly and decompose into sub-phases (prometaphase, metaphase, anaphase, telophase and cytokinesis). Nucleus and DNA structure morphologically differentiate between interphase and mitosis. While in interphase DNA is uniformly distributed in chromatin form, it is packed and condensed into chromosomes during mitosis.

Cell cycle generally follows the strict progression previously described, however, a few exceptions exist. For example in early embryonic cells the two gap phases are dramatically shortened and cytokinesis, i.e. cellular division does not occurs. In those cells cell cycle only alternates between S and M phases in order to divide a fertilized egg into multiple smaller cells (Ciemerych and Sicinski, 2005; Fujii-Yamamoto et al., 2005). Additionally under unfavorable conditions cells can enter after ending a cell division in a quiescent gap-phase 0 (G0) during which they stop proliferate while still being metabolically active (Alberts et al., 2002).

1.3.2 Checkpoints and oscillating activity ensure unidirectionality through cell cycle

Strict regulation of the event order ensures a unique replication and a symmetrical division of the DNA content and consequently healthy daughter cells. This unidirectionality is mainly achieved by checkpoints (Hartwell and Weinert, 1989; López-Avilés et al., 2009) and oscillating activity of cell cycle regulators (Ball et al., 2011; Orlando et al., 2008; Simon et al., 2001; Zhang et al., 2011).

Three checkpoints serve as control and arrest cell cycle progression at a specific stage until the cell fulfills specific criteria, thus preventing any praecox entry into the next phase. These checkpoints are in the late G1, at G2/M and in metaphase. For example passing the late G1 checkpoint requires appropriate cell size, biomass and favorable external conditions to enter S phase and replicate DNA. Passing through the late G1 checkpoint is also a commitment to undergo full cell cycle (Hartwell and Weinert, 1989). The late G1 checkpoint was first characterized in *Saccharomyces cerevisiae* (*S. cerevisiae*) and was called “START” in this organism whereas in metazoans the same checkpoint was named “restriction point”. The G2/M checkpoint controls entry into M and enables the cell to detect un-replicated DNA and repair any DNA damage. Genomic integrity is also ensured by the spindle checkpoint in metaphase, which controls well alignment of chromosomes and bipolar tension (Alberts et al., 2002; Cooper, 2000).

Gene expression regulation is crucial for cell cycle progression (Andrews and Mason, 1993; Chymkowitch and Enserink, 2013; Orlando et al., 2008; Simon et al., 2001). A highly controlled

transcriptional and translational regulation of each key regulator gene provides coordinated oscillations of the respective messenger RNA (mRNA) and protein levels and ensures a robust timing of the cell cycle progression. Oscillating production and degradation rates (Eser et al., 2013) and other post-transcription and post-translation processes such as feedback loops, mRNA and protein transport and protein modifications (multi-phosphorylation, proteins complexation, multi-ubiquitination…) further fine-tune the waves of activities (Barberis et al., 2012; Barik et al., 2010; Finley et al., 2012; Jensen et al., 2006; Kõivomägi et al., 2011; Zhang et al., 2011). Appropriate gene expression becomes particularly critical in response to external stimuli and stresses since dysfunctions in adaptation mechanisms can lead to genomic instability causing diseases such as cancers (Adrover et al., 2011; Clotet et al., 2006; Duch et al., 2013a; Eser et al., 2013; Miller et al., 2011; Proft et al., 2006; Saito and Posas, 2012).

1.3.3 Cell cycle regulators and conservation among eukaryote kingdom

The main cell cycle regulators are cyclins, cyclin dependent kinases (CDK) and CDK-inhibitors (CKI). Notably cyclins and CKIs in higher eukaryotes represent potential oncogenes and tumor repressors, respectively (Zhivotovsky and Orrenius, 2010). Human cells possess at least 20 CDKs and a still growing number of cyclins and CKIs. In contrast *S. cerevisiae* has a main and essential CDK, called Cdk1 or Cdc28, which controls its entire cell cycle, nine Cdk1-related cyclins, and a main CKI, namely Sic1 (Morgan, 1997; Satyanarayana and Kaldis, 2009). Besides Cdk1, Pho85 is another CDK expressed in *S. cerevisiae*. Nevertheless deletion of Pho85 is viable under optimal growth conditions and its role in cell-cycle regulation is less investigated than the one of Cdk1 (Espinoza et al., 1994; Huang et al., 2007; Lenburg and O'Shea, 2001; Morgan, 1997).

Interestingly, genetic sequences of cell cycle regulators are not conserved throughout the eukaryotic kingdom, however, functions and regulatory network motifs are highly similar among eukaryotes (Foury, 1997; Harashima et al., 2013). Indeed dissection of the G1/S transition network revealed a high similarity in the regulatory architecture (Harashima et al., 2013) (Figure 1). For example, Sic1 from budding yeast is functionally related to mammalian $p27^{Kip1}$. Accordingly, their CDK/S-cyclin inhibitory domain is structurally conserved enough that overexpression of the mammalian *KIP1* gene encoding $p27^{Kip1}$ rescues cell cycle phenotype in *SIC1* deletion yeast mutant (sic1Δ) (Barberis et al., 2005) (Figure 2).

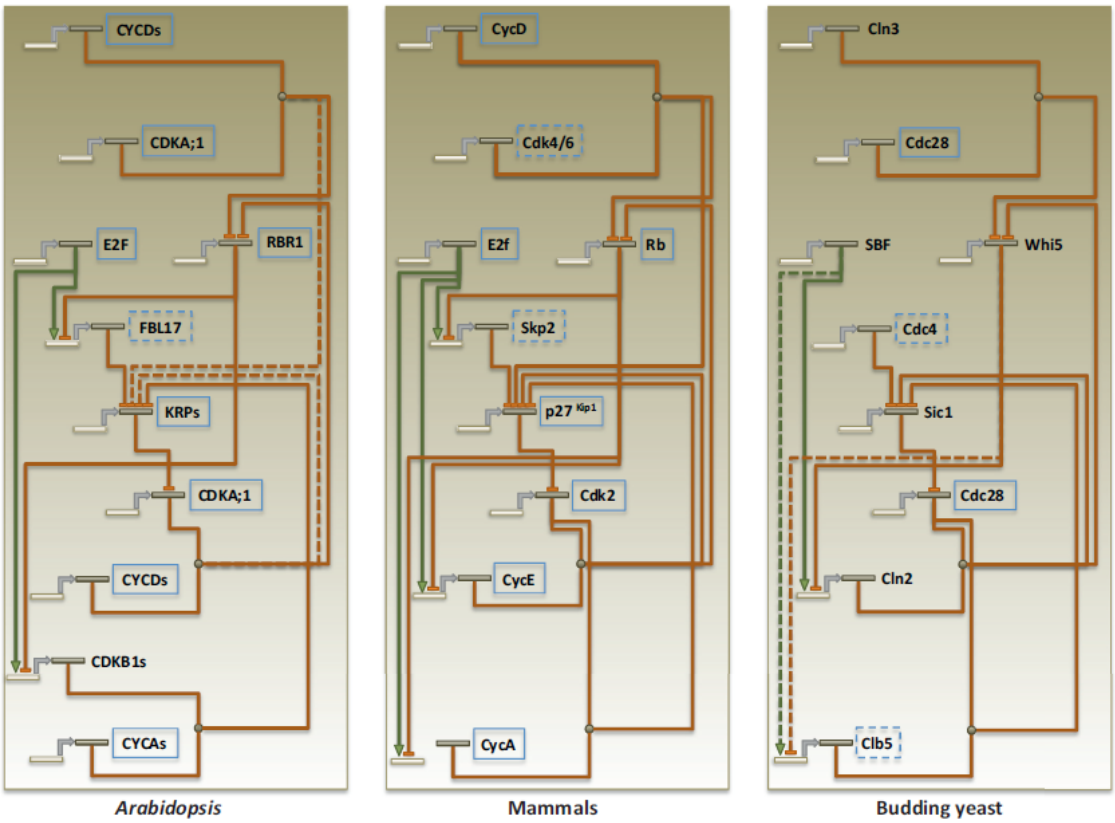

Figure 1. Architecture of the molecular network controlling the G1/S transition is highly conserved among eukaryotic organisms.

In budding yeast Cdc28, also called Cdk1, is the only essential CDK of G1/S transition while mammals have three CDKs (Cdk2, Cdk4 and Cdk6) and the plant, Arabidopsis, needs two CDKs (CDKA;1 and CDKB1). Horizontal yellow bars indicate promoters and/or mRNA, grey bars proteins, red lines with blunt ends inhibitory effects, and green lines with arrowheads positive effects on protein or promoter/mRNA. Dashed lines indicate not entirely resolved regulatory actions. The same height/position in the wiring diagram indicates analogous function. Boxes around regulators indicate homologous sequence; dashed boxes indicate that the respective regulators share similarities but that there are other, more closely related regulators in different species. Image and legend adapted from (Harashima et al., 2013).

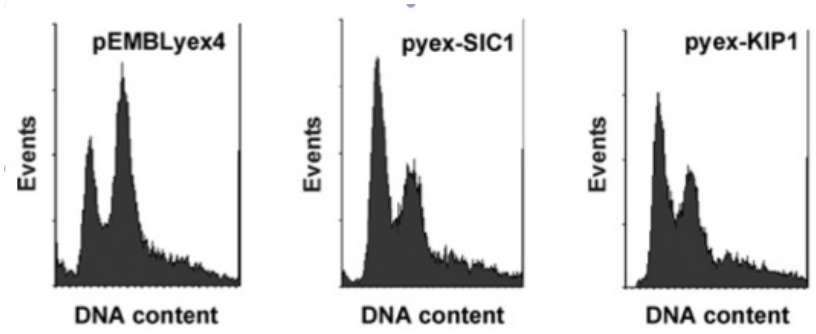

Figure 2. Budding yeast Sic1 is functionally related to mammalian p27Kip1.

Budding yeast Sic1 is functionally related to mammalian $p27^{Kip1}$. DNA content measurement of sic1Δ yeasts transformed with empty plasmid (pEMBLyex4) (left plot), *SIC1* expressing plasmid (pyex-SIC1) (middle plot) and *KIP1* expressing plasmid (pyex-KIP) (right plot). pEMBLyex4 population with no *SIC1* show an abnormal lower cell fraction in G1 (left peak, left plot) than in G2/M phases (right peak, left plot). Overexpression of *SIC1* (middle plot) as well *KIP1* gene (tight plot) rescues cell cycle phenotype in sic1Δ mutant. Image from (Barberis et al., 2005)..

1.4 Case study: G1/S transition in yeast and its main players Sic1, Cln2 and Clb5

1.4.1 *S. cerevisiae* as a model organism for eukaryotic cell cycle

The baker's or brewer's yeast, *S. cerevisiae,* is a widely used model organism to study eukaryotic cell cycle (Schneiter, 2004). It is also called budding yeast due to its asymmetric growth and division, which leads to a mother cell and a smaller newly produced daughter cell. Its metabolism and physiology are well-characterized and full sequencing of its 16 chromosomes has been a break-through in science as it was the first eukaryotic genome to be completely sequenced (Goffeau et al., 1996). Established tools for genetic manipulations (Hinnen et al., 1978; Lundblad and Struhl, 2008) and existing strain-libraries of mutants such as with green fluorescent protein (GFP) -tagged proteins (Ghaemmaghami et al., 2003) or knock-out (Baker Brachmann et al., 1998) enable to easily mutate and study the resulting phenotype. Doubling time of the budding yeast is only about 90 min und much shorter than the 24 hours cell cycle of mammalian cells in culture. Budding yeast are about 5 µm and well observable by optical microscopy. Yeast cells are also inexpensive and have simple requirements to grow in the laboratory. Main cell cycle players and events are well known in *S. cerevisiae* (Figure 3). Notably the nine Cdk1-related cyclins have partially redundant functions and are usually named with short notations as Cln1,2,3; Clb1,2; Clb3,4 and Clb5,6 (Morgan, 1995).

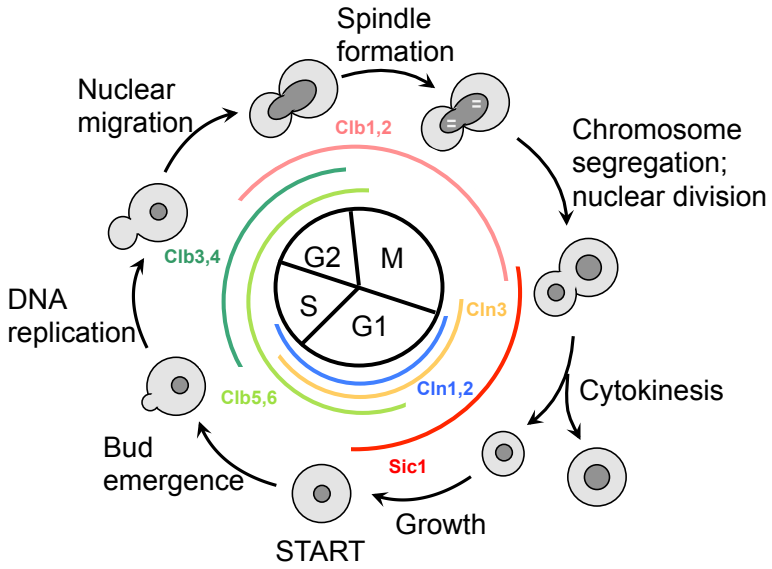

Figure 3. Cell cycle events and gene regulators in *S. cerevisiae*.
Budding yeast has an asymmetrical growth and cell division. Cdk1, the main CDK (not shown on sketch), in budding yeast has a constant concentration throughout cell cycle and becomes activated by binding with cyclins (Morgan, 1995). In contrast cyclins have oscillating expression (high expression periods are depicted by the portions of circle), activate Cdk1 by binding and give the complex specificity, hence driving the cell cycle forward (Morgan, 1995). G1 cyclins, Cln1-3 (Cln1,2 in blue and Cln3 in yellow), control growth and budding initiation (Dirick et al., 1995), S-phase cyclins Clb5,6 (in light green) trigger replication origin firing (Schwob and Nasmyth, 1993), Clb3-4 (in dark green) play a role in DNA replication and spindle assembly in S-phase and finally, Clb3-4 together with Clb1,2 (in pink) initiate entry in M-phase (Grandin and Reed, 1993). CKI Sic1, binds to and inhibits Clb5,6 in its high expression period in early G1 therefore inhibiting DNA duplication (Rossi et al., 2005; Schwob, 1994). Oscillating gene expression highly influences the cell cycle progression by regulating the amount and activity of phase specific functional partners.

1.4.2 Zoom in on G1/S transition

Three main players of the G1/S transition at the early stage of the cell cycle in *S. cerevisiae* are Sic1, Clb5 and Cln2. The cyclins Clb5 (functionally homologue to mammalian cyclin A) and Cln2 (functionally homologue to mammalian cyclin E) in complex with Cdk1 control DNA replication origin firing and bud formation, respectively, characterizing the exit from G1 and entrance into S phase (Dirick et al., 1995; Schwob and Nasmyth, 1993; Stuart and Wittenberg, 1994) (Figure 4A). The CKI Sic1 (functionally homologue to mammalian $p27^{Kip1}$) prevents premature G1/S transition by inhibiting Clb5-Cdk1 and triggers its nuclear export during G1 phase (Rossi et al., 2005; Schwob, 1994). At START in late G1, Cln2-Cdk1 initiates Sic1 hyperphosphorylation, ubiquitination and degradation and therefore activation of Clb5-Cdk1 and entrance into S phase (Berset et al., 2002; Verma, 1997). Activated Clb5-Cdk1 also induces Sic1 phosphorylation ensuring a sharp degradation of Sic1 (Cross et al., 2007).

CLN2 and *CLB5* genes belong to the G1 gene cluster for which mRNA levels peak in late G1 and dependent on the transcription factors complexes SBF (made of Swi6 and Swi4) and MBF (made of Swi4 and Mbp1) (Iyer et al., 2001; Koch et al., 1993) (Figure 3 and Figure 4B). Notably, Cln2 enhances its own transcription via a positive feedback loop (Cross and Tinkelenberg, 1991; Skotheim et al., 2008). *SIC1* expression is mainly induced by Swi5 in late mitosis in both mother and daughter cells and by Ace2 in early G1 in daughter cells only (Aerne et al., 1998; Knapp et al., 1996; Toyn et al., 1997) (Figure 3 and Figure 4B).

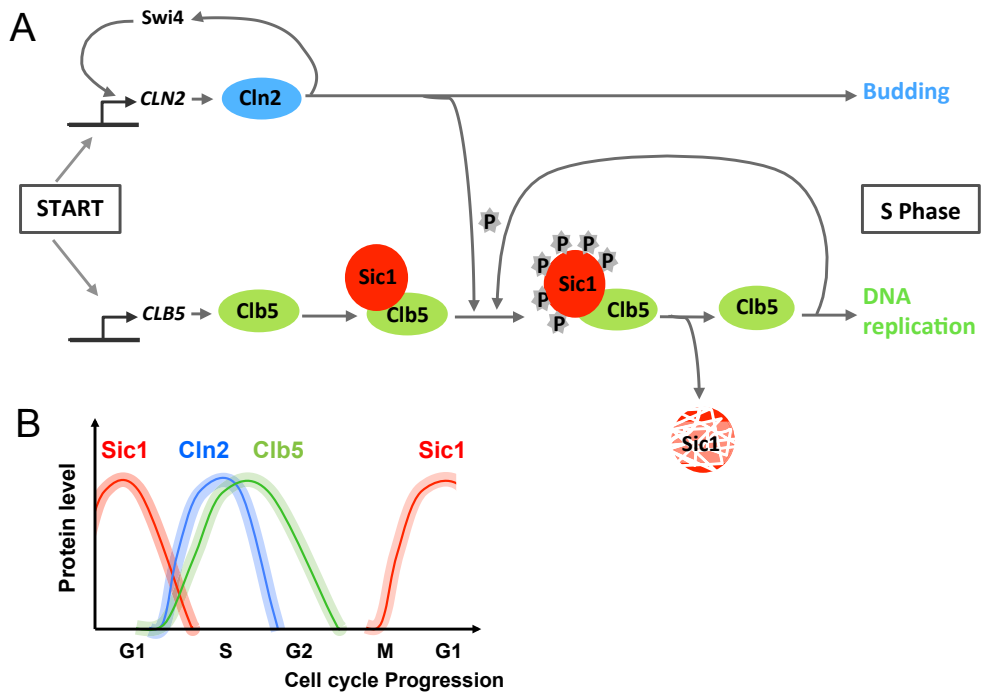

Figure 4. Cln2, Clb5 and Sic1 are the main regulators of the G1/S transition.
(A) During G1, CKI Sic1 through binding inhibits and triggers nuclear export of Cdk1-Clb5 (Rossi et al., 2005; Schwob, 1994). At START in the middle-late G1, cyclin Cln2 binds to Cdk1 inducing budding and phosphorylation of Sic1 (Berset et al., 2002; Verma, 1997). Sic1 becomes target for ubiquitination and subsequent proteasomal degradation by Cdc4 and SFC (Skp, Cullin, F-box containing complex), two parts of the proteasome. Once released of Sic1, Cdk1-Clb5 triggers replication origin firing (Schwob and Nasmyth, 1993). DNA replication initiation and budding are hallmarks of entry into S-phase. Cln2 triggers its own transcription via a positive feedback loop involving its transcription factor (TF) Swi4 (Cross and Tinkelenberg, 1991; Skotheim et al., 2008). This feedback loop ensures a sharp peak of *CLN2* expression and activity. For simplicity Cdk1-Cln2 and Cdk1-Clb5 are depicted in the sketch as Cln2 and Clb5, respectively. (B) Sketch of the oscillations of Cln2, Clb5 and Sic1 levels throughout cell cycle.

1.5 Monitoring cell cycle progression using synchronization methods

1.5.1 Traditional synchronization methods

Resolving the timing of the expression of the cell cycle regulators is critical to assess the regulation of cell cycle progression. Previous studies on chemically or physically synchronized cell populations combined with bulk scale gene expression measurements, primarily qualitative Northern and Western blots, resolved transcript and protein oscillations throughout the cell cycle (Adrover et al., 2011; Barberis et al., 2012; Eser et al., 2013; Gallego et al., 1997; Spellman et al., 1998).

Chemical synchronization is the most used synchronization method (Breeden, 1997; Day et al., 2004; Futcher, 1999; Walker, 2011). Addition of a chemical or nutrient deprivation arrest cell cycle progression at a specific cell cycle phase. Common substances are α-factor pheromone (early G1), nitrogen depravation (G1) (Figure 5AB), nocodazole (G2/M) and hydroxyurea (Adrover et al., 2011; Barberis et al., 2012; Breeden, 1997; Eser et al., 2013; Gallego et al., 1997; Spellman et al., 1998). Temperature changes applied on temperature-sensitive cdc15-2 mutant also influences the molecular network and enable synchronization at G2/M (Spellman et al., 1998). Unfortunately, chemical synchronization is known to perturb molecular networks and cell cycle regulation (Cooper, 2004; Futcher, 1999). Furthermore, synchrony is only partial making it difficult to follow one full cycle and especially to resolve late and short mitosis events (Breeden, 1997; Futcher, 1999; Hur et al., 2011; Spellman et al., 1998). Over time observed oscillations are attenuated and distributions of the measured values are broader due to the loss of synchrony between the cells (Eser et al., 2013) (Figure 5CD).

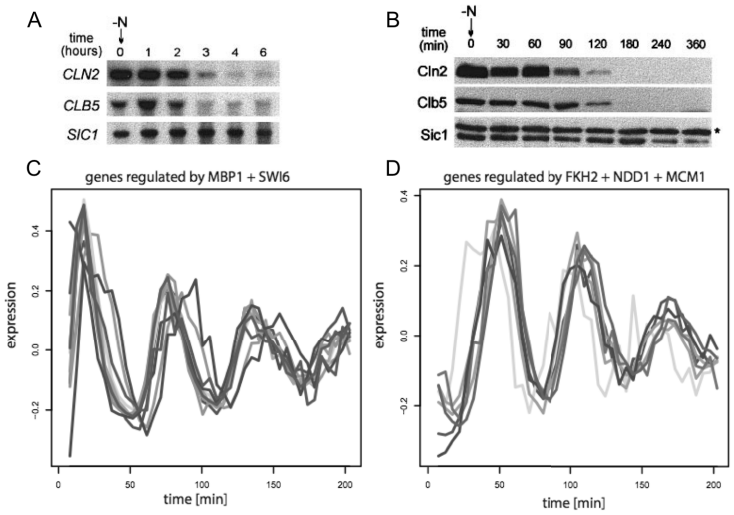

Figure 5. Expression timing of the cell cycle regulators investigated in chemically synchronized cell populations.
(A) mRNA and (B) protein level changes of Cln1, Cln2, Clb5 and Sic1 measured by Northern blot (mRNA) and Western blot (protein) in populations synchronized in G1 by nitrogen deprivation. The arrow in position 0 min (or 0 hour) indicates the deprivation of nitrogen from the culture to trigger arrest of the cell population in G1. mRNA and protein levels of the cyclins are high at the beginning in asynchronous population and later decrease and vanish while cells arrest in G1. *SIC1* and Sic1 stay present while cells accumulate in G1. In (B) An asterisk indicates a non-specific band that cross-reacts with a 12CA5 antibody. (A) and (B) are adapted from (Gallego et al., 1997). (C) and (D) Oscillations of cell cycle regulators are reduced over time after ⍰-factor synchronization. mRNA expression was measured by cDTA (comparative Dynamic Transcriptome Analysis). Four and three oscillations are observed for selected genes regulated by *MBP1* and *SWI6*, the G1/S TFs (C), and by *FKH2*, *NDD1* and *MCM1*, the mitosis TFs (D). Although oscillations are well observable over time, the peaks become broader and the amplitudes of the oscillations smaller. (C) and (D) images from (Eser et al., 2013).

1.5.2 Counterflow centrifugation elutriation as a physical synchronization method

Counterflow centrifugation elutriation, or shortly elutriation, is a non-intrusive mechanical method that collects newborn early G1 cells from an asynchronous population using centrifugation force (Bachere et al., 1988; Banfalvi, 2008; Woldringh et al., 1995). The asynchronous cell culture is subject to two opposite forces, namely the centrifugal force and the counterflow drag force. While the older and heavier cells are more sensitive to the centrifugal force and stay retained in the centrifuge, the lighter and smaller newborn cells are dragged by the counterflow medium outside the centrifuge and collected in a container (Figure 6). Early G1 cells released in fresh media will progress with synchrony through cell cycle. Apart from the purchase of the equipment, elutriation is an inexpensive and fast but laborious method. It yields to about 5% of the initial cell population with high recovery, viability, and minimal effect on the cell molecular regulation. The synchrony of the population is high due to the homogenous size of the cells (Banfalvi, 2008; Walker, 2011).

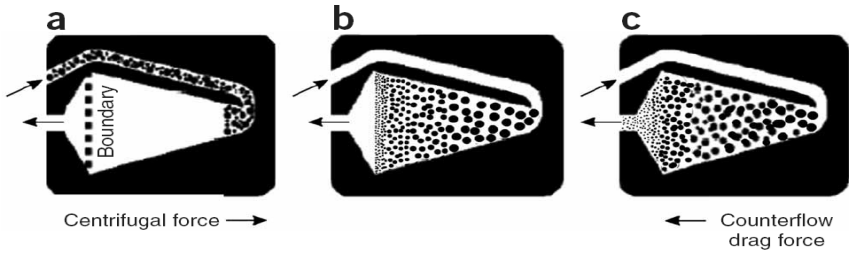

Figure 6. Counterflow centrifugation elutriation selects smallest and newly born early G1 cells.
The elutriation set up requires a centrifuge, a loading chamber installed in the centrifuge, which is linked to a pump controlling the media flow. Asynchronous cell culture is subject to two opposite forces, namely centrifugal force and counterflow drag force. (a) Asynchronous cell culture is loaded in the elutriation chamber. (b) Cells accumulate until a boundary, where there are at equilibrium between the two oppose centrifugal force and counterflow drag force. The youngest and lightest cells, which are less sensitive to centrifugal force, go further in the chamber than bigger and elder cells. (c) After the chamber is fully loaded counterflow drag force is slightly increased and centrifugal speed slightly decreased to drag and collect the youngest and lightest cells in a container outside the centrifuge. Image from (Banfalvi, 2008).

1.5.3 Cell cycle genetic and morphological markers.

Genetic and morphological markers in combination with optical microscopy can serve as hallmarks for cell cycle events (Charvin et al., 2008; Di Talia et al., 2007; Trcek et al., 2011). This strategy has the remarkable advantages to lead to no or minimal perturbation in growth and cell cycle progression and to provide single-cell information in specific cell cycle phases. Typically images of an asynchronous cell population are acquired by microscopy and each cell is assigned to a cell cycle phase using information given by genetic and/or morphological markers. Cell cycle markers can be among others the shape of the cells, the presence and size of a bud, the presence of a bud-neck visualized fluorescently tagged Cdc10, the morphology of the DAPI-stained nucleus, the localization of labeled Whi5 or the spindle or spindle pole body visualized by fluorescently beta-tubulin (Tub1) or Spc42, respectively (Figure 7A, B and E) (Charvin et al., 2008; Di Talia et al., 2007; Trcek et al., 2011). Such markers can be employed individually (Figure 7A, B) or in combination, which in the latter case provides more accuracy in the cell cycle phase resolution (Figure 7C-E).

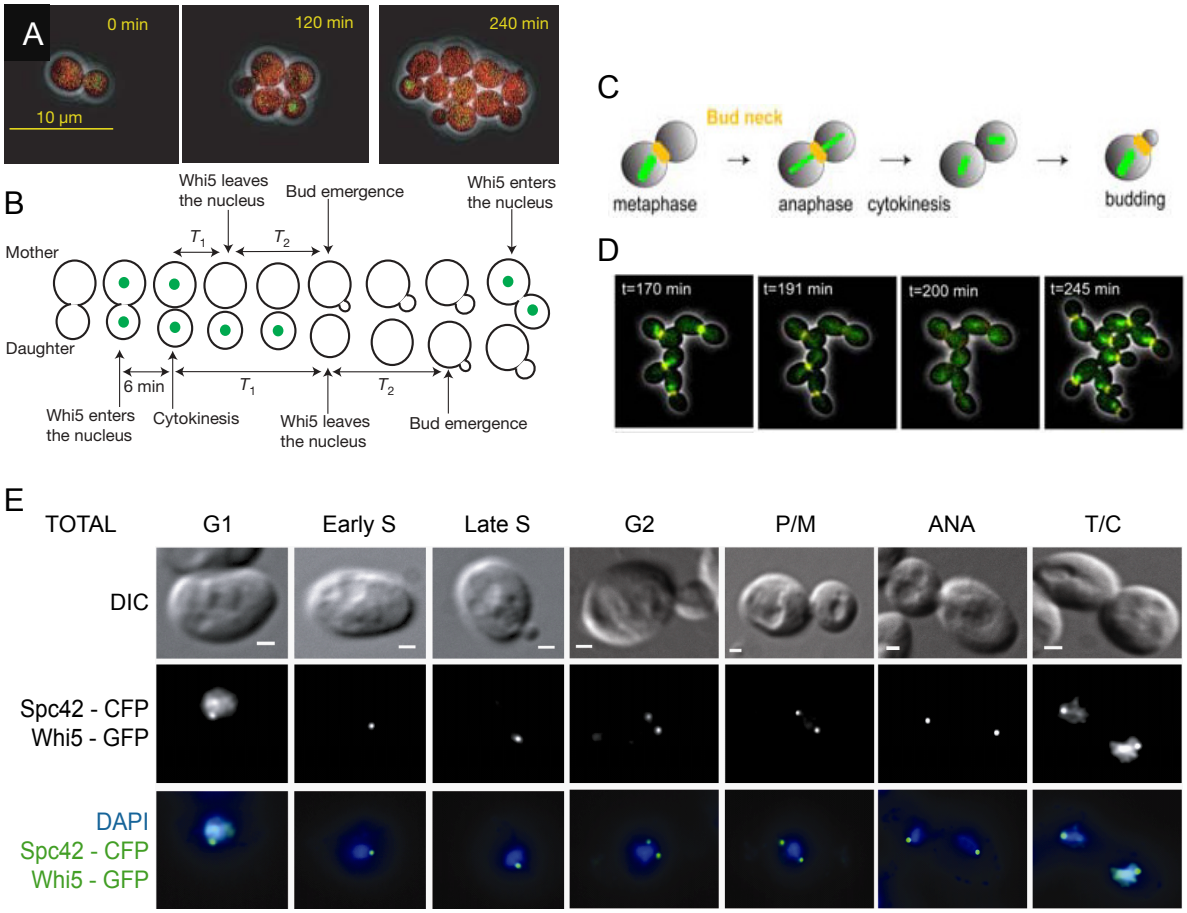

Figure 7. Genetic and morphological markers enable cell cycle segmentation of asynchronous cell population.
(A) and (B) GFP-tagged Whi5 (Whi5-GFP, in green) nuclear localization is a hallmark for early G1 and late mitosis. Images (A) and sketch (B) of Whi5-GFP nuclear import and export. Adapted from (Di Talia et al., 2007). (C) to (E) Possible combinations of genetic and morphological markers. (C) and (D) Combination of YFP-tagged Cdc10 (Cdc10-YFP) and GFP-tagged beta-tubulin (Tub1-GFP) as markers for bud neck and spindle, respectively. Adapted from (Charvin et al., 2008). (E) Combination of Whi5-GFP, Spc42-CFP (CFP-tagged Spc42, part of spindle pole body), DAPI stained nucleus (in blue), morphology of the cell and presence of a bud or daughter cell enables to discriminate between seven cell cycle periods. Adapted from (Trcek et al., 2011).

1.6 Gene expression: from qualitative to quantitative and from population to single-cell

The development of techniques to assess gene expression in the last decade was crucial to unravel regulatory mechanisms in the context of cell cycle. Two radical changes in the gene expression research were the shift from qualitative to quantitative methods and from population to single-cell resolution.

1.6.1 Bulk scale methods for gene expression provide time-courses and average numbers of cell cycle regulators

As previously described in section (1.5 Monitoring cell cycle progression using synchronization) bulk-scale gene expression measurements combined with synchronized cell populations resolved transcript and protein oscillations of cell cycle regulators (Adrover et al., 2011; Barberis et al., 2012; Eser et al., 2013; Spellman et al., 1998). Interestingly the results showed that some cell cycle players such as cyclins and CKI have oscillating molecular levels whereas others, as Cdk1, have constant expression and their oscillating activities controlled are by post-translation modifications (Morgan, 1997).

Technical advances enabled the shift from qualitative to quantitative measurement of gene expression. At first this shift provided numbers of relative changes and later absolute values for protein and mRNA. Relative changes could be obtained by quantitative Northern and Western blots, microarrays, cDTA (comparative Dynamic Transcriptome Analysis), real-time PCR (polymerase chain reaction) (Donovan et al., 1994; Miller et al., 2011; Schwob, 1994; Spellman et al., 1998). These methods, when used on a genome-wide scale in yeasts and bacteria, showed that the majority of genes, including those controlling essential biological functions, are present at very low number of transcripts with less than two copies/cell in average per cell cycle (Bon et al., 2006; Holstege et al., 1998). Although the same methods employed on larger samples revealed higher average mRNA values, the generally low transcript level, especially for regulated genes like the ones involved in cell cycle control, raises the question of how robustness of cell cycle progression is secured in context of such low mRNA numbers of key regulators. Averaging and normalization introduce biases in the resulting transcript numbers leading to up to 5 folds discrepancy between the values obtained with the different methods (Ball et al., 2013; Gandhi et al., 2011; Holstege et al., 1998; Miller et al., 2011). Thus further investigations of this key question of life strongly benefit from new quantitative methods that provide absolute values of transcripts per single cell.

1.6.2 MS2-CP and RNA-FISH methods enable mRNA visualization at single-cell level

Development of single cell resolution methods such as single cell real-time PCR and a range of fluorescence spectroscopy and microscopy strategies such as FACS (Fluorescence Activated Cell Sorting), RNA-FISH (RNA-Fluorescence *in situ* Hybridization), MS2-Coat Protein (MS2-CP) tagging strategy revealed the existence of large variability in biological properties such as RNA and protein abundances between genetically identical single cells grown in a homogenous environment, called gene expression noise (Elowitz et al., 2002; Ladbury and Arold, 2012; Munsky et al., 2012; Taniguchi et al., 2010). MS2-CP and RNA-FISH systems are nowadays widely employed microscopy technics to study RNA level in single cells.

MS2-CP tagging strategy and RNA-FISH were primarily established in the Robert Singer's Lab (Bertrand et al., 1998; Singer and Ward, 1982) and are two fluorescent microscopy based methods for single cells RNA detection. The labeled RNA molecules with fluorescent proteins (FP) or fluorophores can be visualized by fluorescence microscopy as diffraction-limited points allowing localization and quantification of transcript abundance in single cells and related transcriptional variability within a population (Figure 8).

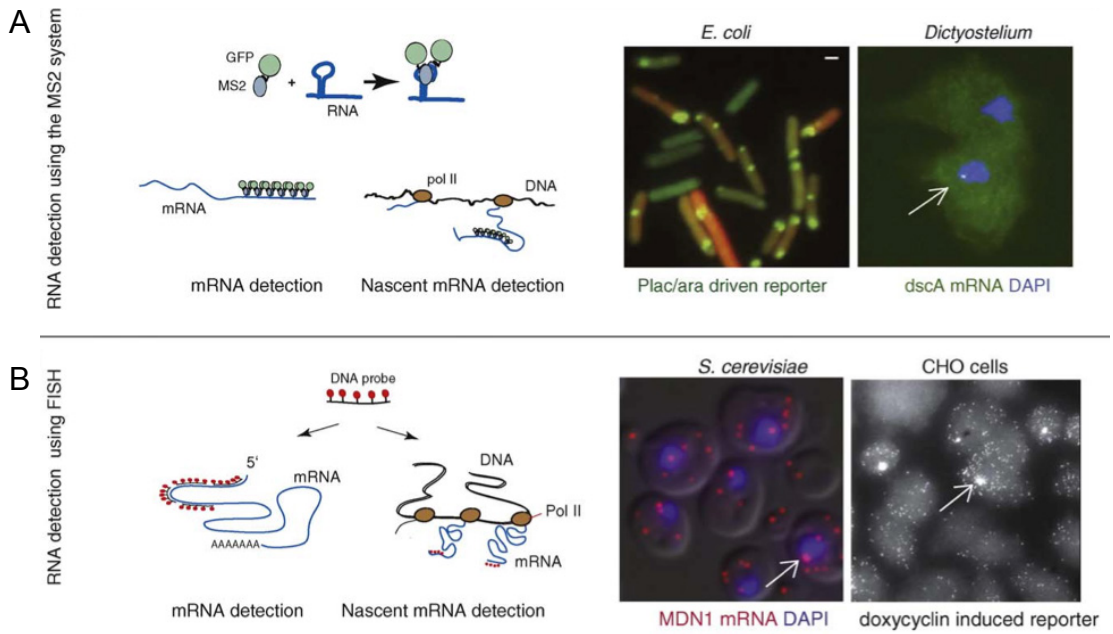

Figure 8. MS2-CP and RNA-FISH enable single cell transcription microscopy.

(A) The MS2 system uses the specific interaction between the MS2 RNA stem-loop and a fusion of a fluorescent protein and the MS2 phage coat protein to create a fluorescent labeled mRNA. Inserting multiple binding sites into an mRNA allows the detection of single mRNAs in living cells. The MS2 system has been used to count single mRNAs in different organisms, for example in *E. coli* as shown here (Golding and Cox, 2004), or to determine transcription kinetics in Dictyostelium in real time (Chubb et al., 2006). Sites of active transcription are marked by arrows. (B) Single-molecule-resolution fluorescence *in situ* hybridization (FISH) uses synthetic oligonucleotides labeled at multiple positions with fluorescent dyes to detect single mRNAs. Multiple fluorescent probes are hybridized to paraformaldehyde-fixed cells. FISH allows the detection of single mRNAs in the cytoplasm as well as nascent mRNAs at the site of transcription. On the right, yeast cells expressing *MDN1* mRNA (Zenklusen et al., 2008) and mammalian CHO cells (hamster cell line) expressing a doxycycline-induced reporter (Raj et al., 2006) are shown. Adapted from (Larson et al., 2009).

1.6.2.1 MS2-CP method for *in vivo* mRNA tracking in living cells

In the MS2-CP method the transcript of interest is genomically tagged in the 3′ UTR (Untranslated Transcribed Region) with a sequence coding for stem-loop structures from MS2 bacteriophage (Figure 8A and Figure 9A). The stem-loop is the binding site for a MS2-coat protein (CP) dimer fused to one or a series of fluorescent proteins that are co-expressed in the MS2 tagged cells. In more rare case the CPs are labeled with a synthetic fluorescent dye (Figure 9B). The binding of MS2-CP complexes to the mRNA results in the accumulation of detectable fluorescence in living cells and therefore enables *in vivo* studies of mRNA numbers, transport and localization and transcription processes. In 1998 for the first time Bertrand and colleagues described and employed MS2-CP on *ASH1* in *S. cerevisiae* (Bertrand et al., 1998). The method has then been improved and extended to several organisms (Ben-Ari et al., 2010; Golding and Cox, 2004; Halstead et al., 2015).

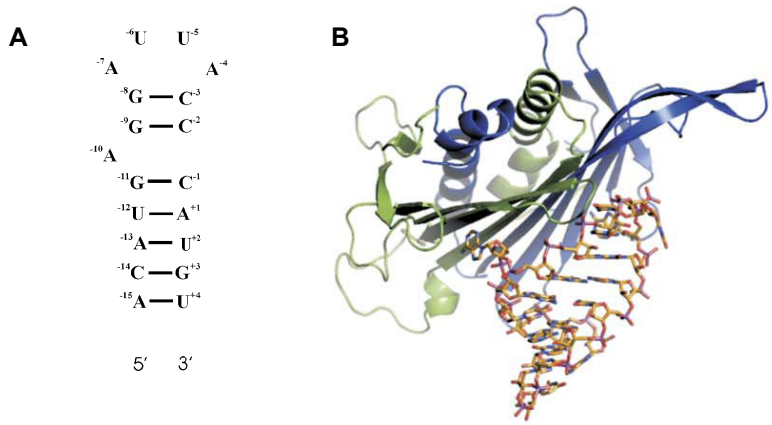

Figure 9. Structures of the MS2 RNA stem-loop.
(A) Secondary structure in stem-loop shape of the MS2 RNA sequence. Numbering is relative to the first nucleotide (+1) of the replicase start codon. (B) Stereoimage of the complex between the MS2 RNA stem-loop and an MS2 AB protein dimer (Valegård et al., 1997). Subunit A of the dimer is shown in blue, subunit B is shown in green, and the RNA is shown in stick format. Adapted from (Horn et al., 2006)

1.6.2.2 RNA-FISH for single-molecule RNA detection in fixed cells

The RNA-FISH method is based on the hybridization of a transcript of interest with several synthetic, single-stranded, antisense DNA oligonucleotides that are labeled with a fluorescent dye (Figure 8B) (Ball et al., 2013; Femino, 1998; Raj et al., 2008; Trcek et al., 2012; Zenklusen et al., 2008). The imaging and quantitative analysis of these diffraction-limited points provides information of the position and abundance of transcripts in fixed cells in the place of their natural occurrence (*in situ*) and without the requirement of any genetic manipulation or growth perturbation.

The first version of the RNA-FISH technology to visualize mRNA molecules in chicken muscle tissue was published in 1982(Singer and Ward, 1982). Improvements of new fluorochromes, labeling and hybridization protocols, microscope setting and image analysis tools over the last decades made RNA-FISH a well-established method for quantification of mRNA molecules in single yeast cells (Trcek et al., 2012) as well as bacteria (Taniguchi et al., 2010), mammalian cells (Vargas et al., 2011), drosophila (Ghosh et al., 2012) or *C. elegans* (Raj et al., 2010).

The main advantages of the RNA-FISH method are the high specificity of the probes for the gene of interest, the possibility to detect simultaneously several gene transcripts in the same cell, the high signal to noise ratio that results in a very sensible spatial resolution, the non-intrusiveness of the technique that preserves the cellular spatial information and the existence of well-established protocols and software for the analysis of microscopic images and quantification of the fluorescent RNA signal. Therefore RNA-FISH has been a method of choice for single molecule detection and absolute enumeration of transcripts in single cells and their transcriptional variability in populations (Ball et al., 2013; Raj et al., 2010; Taniguchi et al., 2010; Trcek et al., 2011; Vargas et al., 2011; Zenklusen et al., 2008).

1.7 Molecular noise – causes and effects

1.7.1 Definition of molecular noise and its sources

Noise in gene expression is a well-recognized phenomenon and has been studied experimentally as well as by mathematical modeling (Ball et al., 2013; Colman-Lerner et al., 2005; Elowitz et al., 2002; Kar et al., 2009; Munsky et al., 2012; Raj and van Oudenaarden, 2009; Schmiedel et al., 2015; Shahrezaei and Swain, 2008). This noise is the result of two distinct sources of stochasticity (Elowitz et al., 2002). The first contribution, called intrinsic noise, is due to stochasticity in the biochemical process of gene expression itself. The second contribution, called extrinsic noise, describes the fluctuations in the amount and activity of cellular components, e.g. ribosomes or transcription factors, between each cell. The consequence is the observation of a broadly varying distribution of both mRNA and protein level within the cell population (Taniguchi et al., 2010). Noise is represented as the coefficient of variation (CV), i.e. ratio of standard deviation to mean (sometimes it is also represented as the ratio of square of standard deviation to mean) and is the quantity of dispersion of a data group from the mean value of this data group. The use of CV enables to quantitatively compare the changes of noise over time, under different conditions or between different systems.

1.7.2 The two-state model, a stochastic model for gene expression.

Deterministic models based on ODEs (Ordinary Differential Equations) are commonly employed to assess signaling processes (Adrover et al., 2011; Barberis et al., 2007). Deterministic models suppose that the changes over time are continuous. It is a reasonable assumption for protein regulations and protein modifications since protein and protein complex levels are relatively high and the variation of protein numbers is low compared to its average value (Rangamani and Iyengar, 2008). Such models lack, however, precision when dealing with the dynamics of low and discrete mRNA numbers whose fluctuations are high compared to the average value and whose changes over time are not continuous. Therefore, stochastic models are a preferred approach to assess gene expression and, especially, transcriptional regulation (Neuert et al., 2013).

Gene expression can be seen as a probabilistic multi-step process, which is formalized in the two-state model (Ko, 1991; Peccoud and Ycart, 1995). This model integrates the stochastic component of gene expression and enables to assess and predict noise in mRNA and protein levels (Ko, 1991; Peccoud and Ycart, 1995). The two-state model of gene expression is a mathematical model for gene expression also known as 'Random Telegraph' model. In 1991 Ko first proposed that genes switch between an active 'On' and an inactive 'Off' state of transcription (Ko, 1991) (Figure 10AB). The two 'On' and 'Off' states represent an open, accessible structure of chromatin to transcription machinery and a closed, inaccessible form, respectively. Consequently the promoter also oscillates between high and low periods of activity. This stochastic model was later expanded by Peccoud & Ycard (Peccoud and Ycart, 1995). The transition rate constants between the 'On' and 'Off' states are defined as k_{On} and k_{Off}, respectively. In the 'On' state the transcription occurs with a transcription rate, k_R and the produced mRNA is translated with a rate k_P and degraded with a rate γ_R. The produced protein is also degraded with a specific rate γ_P.

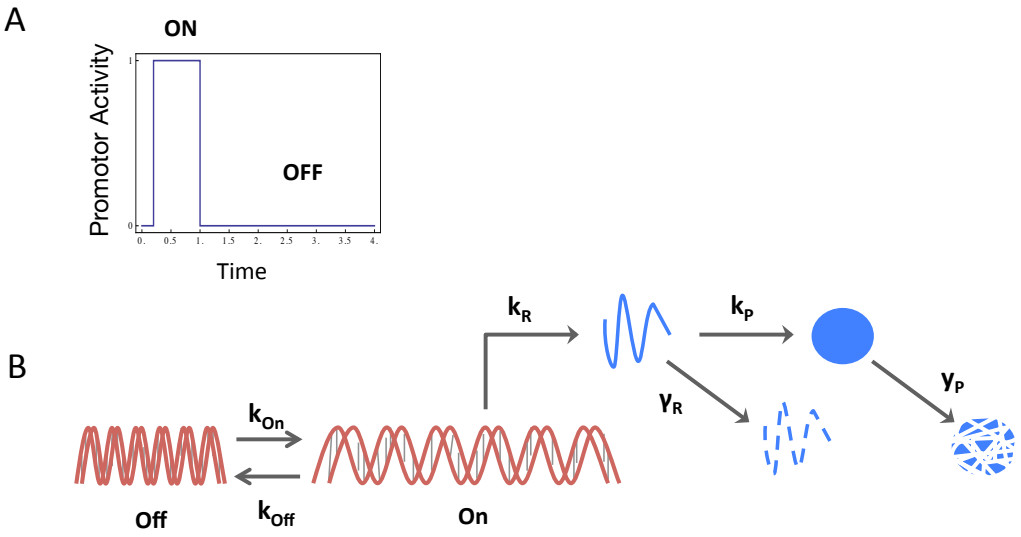

Figure 10. Two-states model of gene expression regulation.

Central dogma of gene expression. (A) In the two-states model of gene expression, the promoter activity is predicted to oscillate between a high and a low period, corresponding to 'On' and 'Off' states of transcription, respectively. (B) The 'On' active and 'Off' inactive states of transcription correspond to a closed and open structure of the chromatin, respectively. The gene (red) switches between those two states with the rates k_{On} and k_{Off}. In the 'On' state the transcription occurs with k_R, transcription rate. Molecules of mRNA (blue line) are translated into proteins (blue circle) with a rate k_P and degraded with a rate γ_R. The produced protein is degraded with a rate γ_P.

Static mRNA and protein distributions obtained from single-molecule experiments can be fitted to extract kinetic properties of the transcription and translation processes (Choi et al., 2010; Coulon et al., 2013; Larson et al., 2009; Munsky et al., 2012; Neuert et al., 2013; Raj and van Oudenaarden, 2009). Thus, cell variability hides precious information on the regulatory mechanisms of gene expression. The majority of the housekeeping genes, which are continuously expressed, have transcript and protein distributions following a Poisson distribution (constitutive model), however, expression of regulated genes, such as the ones coding for cell cycle regulators, results in distributions deviating from a Poisson distribution (regulated model) (Gandhi et al., 2011; Silverman et al., 2010).

Interestingly, comparison of the molecule distribution of a set of genes can also reveals regulatory mechanism between them. Similarities in the shape of the distribution may indicate a common gene expression regulation such as a common TF activator or TF inhibitor. Moreover, changes of the molecule distribution in context of cell cycle or stress indicate changes of the kinetics of gene expression (Munsky et al., 2012; Neuert et al., 2013).

1.7.3 Effects of molecular noise on biological processes

Nature sets mechanisms such as thresholds, positive and negative feedback loops, post-transcriptional and post-translational modifications (complex formations, multi-phosphorylation, multi-ubiquitination…), molecular transport to counter act stochasticity and ensure robustness of vital processes (Ladbury and Arold, 2012; Stewart-Ornstein et al., 2012).

Interestingly, noise can be an advantage in some situations. For example cellular variability establishes initial asymmetries in molecule abundances, which can be amplified by feedback loops, and therefore helps to create different phenotypes leading to different responses to stress. As a result, while some individuals will be deadly affected, the diversity of responses increases the survival and fitness of the overall population (Cağatay et al., 2009).

Gene expression noise in the context of cell cycle at the level of transcript (Ball et al., 2013) or of protein (Bean et al., 2006; Di Talia et al., 2007), throughout cell cycle progression or under external stress (Mettetal et al., 2008; Neuert et al., 2013; Pelet et al., 2011) were usually separately investigated. Effects and regulation of gene expression noise are, especially, challenging in context of cell cycle progression and external stress as the genes involved are expressed at low mRNA copies and their gene expression necessities precise timing for production and degradation. Moreover, studying the recovery to normal condition after a perturbation is a common practice to assess the mechanisms of cell regulation and the function of the different players involved in the system.

1.8 Yeast response to hyperosmolarity – The Hog pathway

Osmotic stress response is commonly observed in the nature. For example it is critical for plants during drought periods (Golldack et al., 2014), for yeasts living on ripening fruits, in which sugar content increases, (Hohmann, 2002) or for animals to maintain proper processing of urine by kidney (Yoshida et al., 1997). Therefore osmotic stress response has been intensively studied. Hyperosmolarity induces shrinking and increase of the turgor pressure. In *S. cerevisiae* sensing of this pressure triggers phosphorylation and subsequent activation of the high osmolarity glycerol (Hog1) protein (Figure 11A). Hog1 is an mitogen-activated protein kinase (MAPK) and stress-activated protein kinase (SAPK) protein, which is evolutionary conserved and homologous to the mammalian p38 MAPK/SAPK (Duch et al., 2012; Han et al., 1994). Upon external stimuli activated Hog1 triggers a cellular survival response program including several biological processes as gene expression adaptation and cell cycle arrest (Geijer et al., 2013; Hohmann, 2002; Miller et al., 2011; de Nadal et al., 2011; Saito and Posas, 2012) (Figure 11AB). The signaling pathway containing Hog1, the receptors sensing the turgor pressure and the proteins responsible for Hog1 activation and the subsequent cellular responses is named Hog pathway.

To adapt to environmental stresses cell cycle progression is delayed of about 20 to 30 min and each phase is regulated. Studies using synchronized cell populations showed that cell cycle arrest in early G1 (Adrover et al., 2011; Bellí et al., 2001) and in G2 (Alexander et al., 2001; Clotet et al., 2006), the delay and elongation of the S phase (Duch et al., 2013b; Yaakov et al., 2009) and the exit from mitosis driven by Hog1 (Reiser et al., 2006).

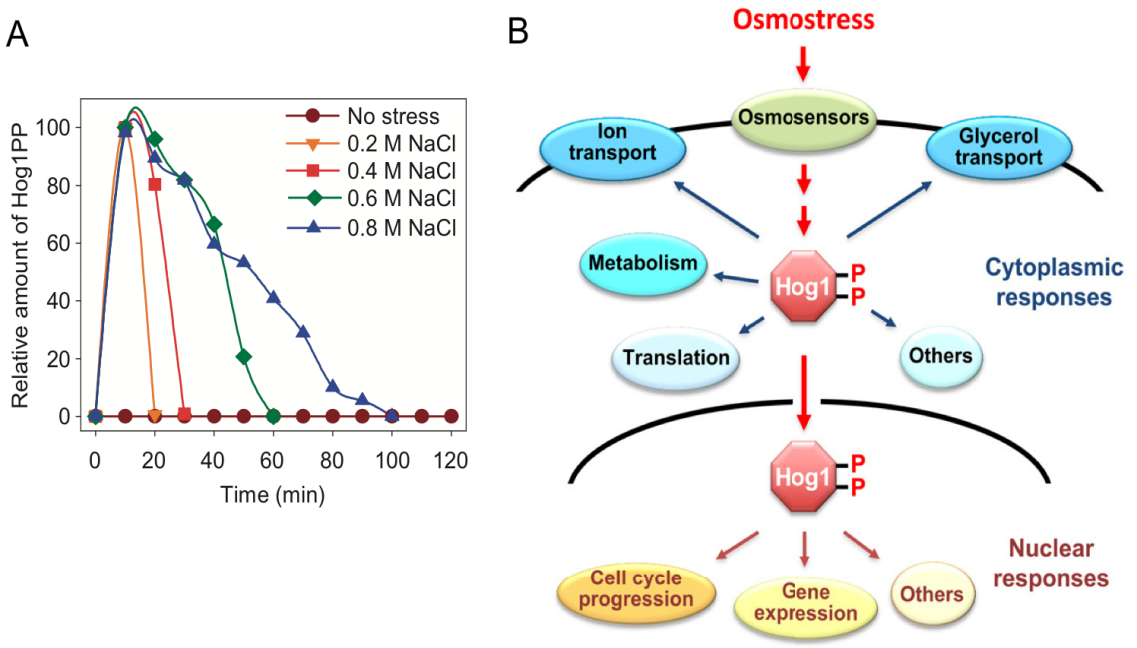

Figure 11. Activated Hog pathway by hyperosmolarity regulates large range of biological processes.
(A) Relative amount of phosphorylated Hog1 (Hog1PP) was plotted as the percentage of its maximum level. Cell population was synchronized in early G1 with α-factor and subjected to osmotic stress (0.2 to 0.8 M NaCl). Adapted from (Adrover et al., 2011). (B) Osmo-adaptive response via Hog pathway in yeast. In response to an increase in extracellular osmolarity, the Hog1 MAPK is activated, which leads to the induction of cytoplasmic and nuclear adaptive responses. Cytoplasmic responses include the control of ionic fluxes, glycerol transport, metabolic enzymes, and protein translation. Nuclear responses include the modulation of cell-cycle progression and the control of gene expression. Adapted from (Saito and Posas, 2012).

Furthermore stress response includes a gene expression reprogramming that results in dramatic changes in the transcriptome landscape (Geijer et al., 2013; Miller et al., 2011; Molin et al., 2009; Nadal-Ribelles et al., 2012; Romero-Santacreu et al., 2009). Indeed cells rapidly regulate the expression of a set of specific osmo-sensitive genes to slow down growth and metabolic activities and induce response mechanisms to environmental stress conditions. Miller and colleagues distinguished in their genome scale study three stages in the osmotic stress transcriptional response of the cell (Miller et al., 2011) (Figure 12A). In the initial shock stage, the cell triggers global mRNAs storage by decreasing mRNA synthesis and degradation. In the following induction stage, mRNA synthesis and degradation of specific osmo-sensitive genes strongly increase to allow a fast production and degradation of those osmo-sensitive genes. Finally, in the recovery stage mRNA decay and synthesis rates are restored.

Specifically at G1/S transition, the activated Hog1 down-regulates *CLN2* and *CLB5* transcription and stabilizes Sic1 through direct phosphorylation at Threonin^{173}, preventing its ubiquitination and consequently delays exit from G1 (Adrover et al., 2011; Escoté et al., 2004; Yaakov et al., 2009) (Figure 12B). Interestingly, studies using synchronized populations demonstrated that cells differently adapt their gene expression depending on which cell cycle phase they were in when hit by the stress (Adrover et al., 2011; Escoté et al., 2004; Yaakov et al., 2009) Figure 12C-F). As a result Sic1, Cln2 and Clb5 levels as well as the related bud initiation and DNA origin firing have different timings if the stress hit the cell before, at or after START (Adrover et al., 2011).

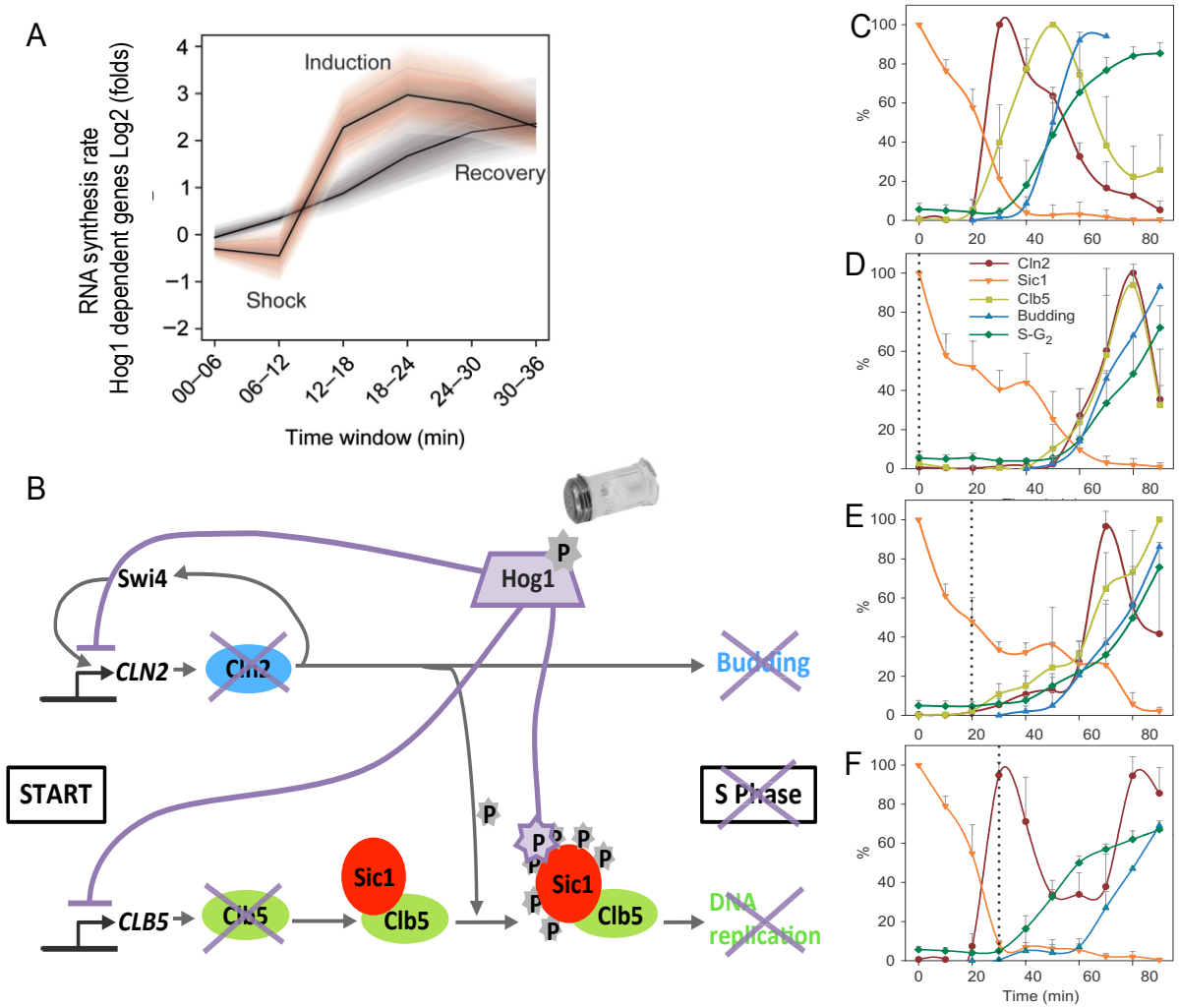

Figure 12. Osmotic stress affects gene expression in S. cerevisiae.

(A) Increased sensitivity and temporal resolution of cDTA transcriptomic (in red, Miller et al., 2011) revealed three clear response phases for the synthesis rates compared to the monotonically increase of total mRNA previously measured (in grey, Capaldi et al, 2008). The solid lines represent the time course of the median, the shaded bands are the central 95% regions. Image adapted from (Miller et al., 2011). (B) Scheme of the effects of Hog1 activation on *SIC1*, *CLN2* and *CLB5*. Activated Hog1 down-regulates *CLN2* and *CLB5* transcription and stabilizes Sic1 through direct phosphorylation at Threonin[173], preventing Sic1 degradation and consequently delays exit from G1. (C) to (F) Measurements of cell cycle arrest and alternation of protein expression profiles for Sic1, Cln2 and Clb5 upon hyperosmolarity in population synchronized in early G1 with α-factor. Cell cycle arrest is represented by the DNA content (green, representing cells in S or G2), and budding index (blue). Sic1 (orange), Cln2 (brown), and Clb5 (yellow) proteins (expressed as percentage of their maximal abundance) measured with Western-Blot are depicted. Error bars represent means and Standard deviation (SD) of three independent experiments. (C) Progression throughout the cell cycle in the absence of stress. (D-F) Cells regulation is differentially affected whether cells were stressed with 0.4 M NaCl at 0 min (D), 20 min (E) or 30 min (F) after release from pheromone. The cells were released from pheromone arrest and sampled every 10 min. Dotted lines in D, E, and F represent the time after release from pheromone arrest that osmotic stress was initiated. Adapted from (Adrover et al., 2011).

Although activation of signaling pathways in response to stress has been extensively investigated, the long-term changes with regard to gene expression at single-cell level, especially transcription and noise, and cell cycle timing are not well characterized. Interesting open questions are: What is the mRNA/protein noise level of cell cycle genes? How does mRNA/protein noise change throughout the cell cycle? How does noise propagates from mRNA to protein level? Are some cell cycle genes “noisier” are others? How does mRNA/protein noise change in response to perturbations? How does mRNA/protein noise level influence the response of single cell to external perturbations?

To investigate these questions there is a strong need for coherent studies providing consequent quantification of absolute transcript levels at single cell and their fluctuations and timing over the full cell cycle. Finally, such quantitative data need to be rationalized with already existing data to assess the relation between transcript and protein levels and the effect of specific stresses on gene expression and cell cycle timing.

2. AIM & STRATEGY OF THIS STUDY

Gene expression is a driving force of the cell division cycle (Andrews and Mason, 1993; Chymkowitch and Enserink, 2013; Orlando et al., 2008; Simon et al., 2001) and is subject to stochasticity (Ball et al., 2013; Raj et al., 2010; Taniguchi et al., 2010; Trcek et al., 2011; Vargas et al., 2011; Zenklusen et al., 2008). Importantly, cellular survival under external perturbations requires gene expression reprogramming and cell cycle arrest (Geijer et al., 2013; Hohmann, 2002; Miller et al., 2011; de Nadal et al., 2011; Saito and Posas, 2012). So the question rose on how are proper cell cycle progression and efficient cell cycle response to stress ensure in the presence of stochastic fluctuations of low transcript numbers as observed for cell cycle regulators? Indeed dysfunctional regulation of cell cycle progression can lead to genetic disorders, abnormal growth or cell death (Barberis et al., 2005; Foury, 1997; Harashima et al., 2013; Hwang and Clurman, 2005; Zhivotovsky and Orrenius, 2010).

This project aimed for a **quantitative understanding at a single cell level of the interplay between gene expression and eukaryotic cell cycle in the context of external stress.** Especially we ambitioned to fulfill the strong need for consequent absolute numbers and timing of transcript levels and their related noise levels over the full cell cycle as well as the effect of specific stresses on this timing and the relation between transcript and protein levels.

We worked with the budding yeast *Saccharomyces cerevisiae* as a model organism for eukaryotic cell cycle. We focused on the **CKI, Sic1, and the two cyclins, Cln2 and Clb5, which regulate the G1/S transition** at the early stage of the yeast cell cycle (Dirick et al., 1995; Morgan, 1995; Schwob, 1994). The G1/S transition is critical as it is a commitment for undergoing a full cell cycle (Hartwell and Weinert, 1989).

We employed the **single-cell mRNA fluorescence microscopy technologies, MS2-CP and RNA-FISH** to provide absolute numbers of mRNA in single-cells and related noise within a population (Bertrand et al., 1998; Femino, 1998). Those methods were usually employed on small samples also one challenge in this project was to adapt the currently published protocols for larger samples and to develop a semi-automatic pipeline for quantitative analysis of microscopy images.

Previous studies had extensively assessed the oscillations of the cell cycle players with chemical synchronization methods, which unfortunately perturb molecular networks and cell cycle regulation (Cooper, 2004; Futcher, 1999). **We combined single-cell mRNA microscopy with less intrusive synchronization methods such as the mechanical elutriation** (Bachere et al., 1988). Additionally, using **morphological and genetic markers** we sought to monitor transcript and transcriptional noise levels in each cell cycle phase and especially to resolve the late and short mitosis events(Charvin et al., 2008; Di Talia et al., 2007; Trcek et al., 2011).

We applied our approach to study cellular response to **osmotic stress**. Activation of signaling pathways in response to osmotic stress is well-known (Geijer et al., 2013; Hohmann, 2002; Miller et al., 2011; de Nadal et al., 2011; Saito and Posas, 2012), however, our objective was to monitor the

short, middle and especially long-term effects with regard to gene expression and cell cycle timing. Indeed signaling pathway, gene expression noise and cell cycle are usually separately investigated. Moreover, it is a common practice to disturb a system and study its recovery to equilibrium in order to learn about its regulation.

We employed **stochastic modeling** to rationalize our experimental data on mRNA, noise and cell cycle timing with previously measured and published dynamics of the respective proteins and their complexes. Furthermore our mathematical models enabled to extract gene specific rates of mRNA production and decay and we also expanded our static mRNA experimental data into time courses of mRNA, protein and related noise. Hence, our model provided the missing link between different types of data, which was needed to understand the interplay between transcription and translation and the propagation of noise between these levels of regulation in the critical context of environmental stimulus.

I divided the results of this thesis into two parts: RESULTS I and RESULTS II. The first part, RESULTS I, focuses on the MS2- CP tagging system and our minimalistic stochastic model centered on *SIC1* and the G1/S transition. In the second part, RESULTS II, I describe how we assessed the gene expression of *SIC1*, *CLN2* and *CLB5*, their changes over the entire cell cycle and their regulation upon osmotic stress with RNA-FISH and our extended stochastic model. I discuss the results of each part in DISCUSSION I and DISCUSSION II, respectively. Finally, in GENERAL DISCUSSION I compare the methods employed in this study and further discuss the results and their implications.

3. MATERIAL AND METHODS

3.1 Material

3.1.1 Equipment

Table 1. Equipment and companies, which equipment pieces were purchased from.

General equipment	Company
Centrifuge Avanti j-20xp (rotor jla10.500)	Beckmann Coulter, Krefeld, Germany
Table top centrifuge biofuge	Heraeus, Berlin, Germany
pH-meter 761 climatic	Knick, Berlin, Germany
Biophotometer plus spectrophotometer	Eppendorf, Hamburg, Germany
Phosphoimager image analyser fla3000 bas reader software	Fujifilm, Tokyo, Japon
Thermal cycler MyCycler	Biorad, Munich, Germany
CASY ® cell counter Model TTC 45/60/150	OLS Omni Life Sciences, Bremen, Germany
Vortex (Genie2, 12-812)	Thermo Fisher Scientific, Waltham, USA
Plasma-cleaner ZEPTO version B	Diener Electronic, Ebhausen, Germany
Plate reader spectrophotometer FLUOstar Optima	BMG-LabTech, Ortenberg, Germany
JE-6 counterflow centrifugal elutriator system	Beckmann Coulter, Brea, USA
Incubator IG-150	Thermo electron corporation, USA
Microscopy equipment	**Company**
Epi-fluorescence microscope IX81	Olympus, Hamburg, Germany
Clara E Interline CCD camera (mounted on IX81 microscope)	Andor Technology, Belfast, Ireland
Objective 100x/1.35 Oil UPlanFL, DIC (mounted on IX81 microscope)	Olympus, Hamburg, Germany
Filters for microscope settings	See Table 2

Table 2. Filters used in the microscopy settings for fluorescence microscopy acquisition.
All filters were purchased at Olympus, Germany, except the Sp. Red HC mFISH filter set, which was purchased at Semrock, USA.

Filter set	$\lambda_{Excitation}$ (mn)	$\lambda_{Emission}$ (mn)	Fluorophores	Company
U-MWU2	330-385	420	DAPI	Olympus
U-MCFPHQ	425-445	460-510	mTurquoise	Olympus
U-MWNiba	470-495	520IF	GFP/ TagGFP/ YFP/ FlAsH	Olympus
Sp. Red HC mFISH	576-596	612-644	Cal Fluor Red® 610	Semrock
U-MNG2 modified	530-550	572-612	Quasar® 570	Olympus
DIC	-	-	-	Olympus

3.1.2 Chemical material

All chemicals and reagents were obtained from Sigma-Aldrich (Munich, Germany) unless indicated as below.

- Blue fluorescent beads 0,2 μm (Fisher Technology)
- Recombinant purified GFP solution (Roche Cat. No 11814 524 001)
- 4,6-diamidino-2-phenylindole (DAPI) (Invitrogen, Darmstadt, Germany)
- 32% Paraformaldehyde (Electron Microscopy Sciences; Hatfield, PA, cat. n. 15714)
- Sheared salmon sperm DNA (Sigma-Aldrich, Munich, Germany, D7656)
- SYBR Safe DNA gel stain (Invitrogen, Darmstadt, Germany)
- TC-FlAsH™ II In-Cell Tetracysteine Tag Detection Kit (Green Fluorescence), (Invitrogen, Darmstadt, Germany, T34561)
- Bacto Agar, Bacto Tryptone and Yeast Extract (Becton and Dickinson (DB) company, Lepont de Claix, France)
- PBS buffer (PAA, Pasching, Austria, H15-002)
- Distilled, deionized water (ddH_20) (MilliQ, Merck Millipore, Darmstadt, Germany)

Kits for molecular cloning:

- QIAprep Spin Miniprep kit (Quiagen, Hilden, Germany)
- QIAquick gel extraction kit (Quiagen, Hilden, Germany)
- High Pure mRNA Isolation Kit (Roche, Mannheim, Germany)
- Transcriptor High Fidelity cDNA Synthesis Kit (Roche, Mannheim, Germany)

Chemicals for RNA-FISH protocol:

- Sorbitol (Sigma-Aldrich, Munich, Germany, S1876)
- Mowiol® 4-88 (Sigma-Aldrich, Munich, Germany)
- ProLong® Gold (Thermo Fisher Scientific, Waltham, USA)
- Vectashield Hardset (Vector Laboratories, Burlingame, CA, USA)
- 32% Paraformaldehyde (Electron Microscopy Sciences; Hatfield, PA, cat. n. 15714)
- Ribonucleoside Vanadyl Complex (VRC) (New England Biolabs (NEB), Frankfurt, Germany S1402S)
- Lyticase from arthrobacter luteus (1200 units/mg of solid) (Sigma-Aldrich, Munich, Germany, L5263)
- 70 % Ethanol (Sigma-Aldrich, Munich, Germany)
- 20x SSC (Roche, Mannheim, Germany, 11 666 681 001)
- 99% Deionized formamide (Arcos Organics; 327235000)
- *E .coli* tRNA (Roche, Mannheim, Germany, 1010951001)
- Long RNA-FISH probes against MS2 sequences (Tib MolBiol, Berlin, Germany)
- Short RNA-FISH probes (Biosearch Technologies, Novato, USA)
- KH_2PO_4 (Sigma-Aldrich, Munich, Germany, P8416)
- K_2HPO_4 (Sigma-Aldrich, Munich, Germany, P8281)
- 100x TE (Tris-EDTA) solution, pH 8.0, (Sigma-Aldrich, Munich, Germany, T9285)
- Bovine Serum Albumin (BSA) 20 mg/mL in H2O (Sigma-Aldrich, Munich, Germany, B8667)
- dNTPs (NEB, Frankfurt, Germany)

3.1.3 Biological material

3.1.3.1 Enzymes

Restriction enzymes: NEB, Frankfurt, Germany & Fermentas, Waltham, USA

Ligase: T4-DNA ligase (NEB, Frankfurt, Germany)

Polymerase:

Phusion High-Fidelity DNA Polymerase (Finnzymes, Waltham, USA)

Taq DNA polymerase (PEQLAB Biotechnologie GmbH, Erlangen, Germany)

Superscript II reverse transcriptase (Life technologies, Waltham, USA)

3.1.3.2 Yeast strains

All yeast strains used in this project are listed in Table 3. We used the BY4741 (*MATa his3 leu2 met15 ura3*) haploid yeast strain and its derivatives: deletion mutants (sic1Δ, cln2Δ, clb5Δ), MS2 mutants (*SIC1* mRNA-MS2, *CLN2* mRNA-MS2) and mutant with cell cycle morphological markers (Whi5-TagGFP/Spc42-mTurquoise). The deletion strains are part of the *Saccharomyces* Genome Deletion Collection Project at Stanford University, San Francisco, USA: http://www-sequence.stanford.edu/group/yeast_deletion_project/deletions3.html

The strains MS2-CP strains were established within this work and the cloning procedure is separately presented in detail in section 3.2.2.1 Cloning of the SIC1 and CLN2 MS2-GFP strains.

We cloned the strain Whi5-TagGFP/Spc42-mTurquoise with mTurquoise labeled spindle-pole bodies and TagGFP labeled Whi5 for allocation of the cell cycle state of individual cells (Trcek et al., 2012). We used BY4741 (*MATa his3Δ1 leu2Δ0 met15Δ0 ura3Δ0*) haploid yeast strain as parental strain. pUG72 (Euroscarf accession number P30117) was used to clone plasmids with removable selection a marker and fluorescent proteins as polymerase chain reaction (PCR) template. TagGFP and mTurquoise have been respectively amplified by PCR and cloned in PstI site of pUG72. The generated plasmids contain Open Reading Frames (ORF) for fluorescent proteins and Ura3 selection marker flanked by two loxP sites.

Transformation cassettes for homologous integration were PCR amplified with primer pairs indexed number 20-23 in Table 5. Integration cassettes were transformed in BY4741 and transformed clones were selected on minimal medium agar-plates lacking uracil. Successful integration was controlled microscopically. The Ura3 selection marker was removed by expression of Cre recombinase from plasmid pSH68 (Euroscarf accession number P30674). We observed similar growth rates for the wild type and the Whi5-TagGFP/Spc42-mTurquoise double-tagged strain, indicating that the tagging did not affect cell growth and viability (Figure 13B).

Table 3. List of yeast strains used in this study.

All strains are derivatives from the BY4741 haploid wild type strain. NLS stands for Nuclear Localization Signal.

Name	Comments	Comments
BY4741	MATa his3Δ1 leu2Δ0 met15Δ0 ura3Δ0	Wild Type
Whi5-TagGFP/Spc42-mTurquoise	MATa, his3Δ1, leu2Δ0 met15Δ0 ura3Δ0 (Whi5::Whi5-TagGFP, Spc42::Spc42-mTurquoise)	Spc42 and Whi5 genomically tagged with mTurquoise and TagGFP, respectively (this work)
sic1Δ	MATa his3Δ1 leu2Δ0 met15Δ0 ura3Δ0 (sic1Δ::KanMX4)	Deletion *SIC1* gene (Genome Deletion Collection Project, Stanford University)
cln2Δ	MATa his3Δ1 leu2Δ0 met15Δ0 ura3Δ0 (cln2Δ::KanMX4)	Deletion *CLN2* gene (Genome Deletion Collection Project, Stanford University)
clb5Δ	MATa his3Δ1 leu2Δ0 met15Δ0 ura3Δ0 (clb5Δ::KanMX4)	Deletion *CLB5* gene (Genome Deletion Collection Project, Stanford University)
pCP-MS2-GFP(x3)	MATa his3Δ1 leu2Δ0 met15Δ0 ura3Δ0 (MS2::MS2-GFP(x3))	Expression MS2-GFP(x3) for control (Singer lab, USA)
pG14-MS2-GFP	MATa his3Δ1 leu2Δ0 met15Δ0 ura3Δ0 (MS2::MS2-GFP) + (NLS)	Expression MS2-GFP with NLS (Singer lab, USA)
***CLN2* mRNA MS2 hairpins (HP)**	MATa his3Δ1 leu2Δ0 met15Δ0 ura3Δ0 (Cln2 3'UTR:: 12xMS2HP, ATP2::loxP::MS2L::ATP2$^{3'\text{-}UTR}$)	12 hairpins on *CLN2* mRNA, genomically inserted from pLOXHis5MS2L (this work)
***SIC1* mRNA MS2 hairpins**	MATa his3Δ1 leu2Δ0 met15Δ0 ura3Δ0 (Sic1 3'UTR::12xMS2HP)	12 hairpins on *SIC1* mRNA, genomically inserted from pLOXHis5MS2L (this work)
***CLN2* mRNA MS2-GFP(x3)**	MATa leu2Δ0 ura3Δ0 (Cln2 3'UTR:: 12xMS2HP, HIS3, MET, MS2::MS2-GFP(x3))	Expression MS2-GFP(x3) + 12 hairpins on *CLN2* mRNA, Histidine selection marker, Methionine promoter
***SIC1* mRNA MS2-GFP(x3)**	MATa leu2Δ0 ura3Δ0 (Sic1 3'UTR::12xMS2HP, HIS3, MET, MS2::MS2-GFP(x3))	Expression MS2-GFP(x3) + 12 hairpins on *SIC1* mRNA, Histidine selection marker, Methionine promoter
***SIC1* mRNA MS2-GFP**	MATa leu2Δ0 met15Δ0 ura3Δ0 (Sic1 3'UTR::12xMS2HP, HIS3, MET) + pG14-MS2-GFP – NLS -Leu	Expression MS2-GFP+ 12 hairpins on *SIC1* mRNA, Histidine selection marker, Leucine promoter
***SIC1* mRNA MS2-YFP**	MATa leu2Δ0 ura3Δ0 (Sic1 3'UTR::12xMS2HP, HIS3, MET) + MS2-YFP	Expression MS2-YFP + 12 hairpins on *SIC1* mRNA, Histidine selection marker, Methionine promoter
***SIC1* mRNA MS2-TetraCystein**	MATa leu2Δ0 ura3Δ0 (Sic1 3'UTR::12xMS2HP, HIS3, MET) + MS2-4xCYS	Expression MS2-TetraCystein + 12 hairpins on *SIC1* mRNA, Histidine selection marker, Methionine promoter

3.1.3.3 Bacteria strain

We used the chemically competent bacteria strain *E.coli* DH5α (Thermo Fisher Scientific, USA) for cloning procedure. Genotype:

F$^-$ *endA1 recA1 hsdR17*(rk$^-$ mk$^+$) *supE44* λ$^-$ *thi-1* gyr*A*(Na1) *relA1* ϕ80 *lacZ*ΔM15Δ *(lacZY* A-*argF)*

3.1.3.4 Oligonucleotides and plasmids

Table 4. List of plasmids used in this study.

Name Vector	Phenotype	Source
pUG72	loxP-flanked marker gene deletion cassette: loxP-pKlURA3-KlURA3-tKlURA3-loxP, selectable phenotype: uracil prototrophy, ampicillin resistance	Euroscarf Ref. P30117
pSH68	Cre-expressing (pGAL1-cre) CEN/ARS plasmid, marker gene: pScHIS3-ScLEU2-tScHIS3, selectable phenotype: leucine prototrophy	Euroscarf ref.P30674
pSH47	Expression of Cre recombinase	Euroscarf ref. P30119
pESC-ura	Empty vector, URA selection marker	Agilent Technologies
pMS2-CP-GFP(x3)	Expression of MS2 coat protein linked to GFP triplet	Gerst Lab, Isreal, SD-His - Met
pLOXHis5MS2L	PCR template vector of 12 hairpins MS2 binding sites	Singer Lab, US
pMS2-CP-YFP	Expression of MS2 coat protein linked to YFP	this work
pG14-MS2_GFP	Expression of MS2 coat protein linked to GFP	Singer Lab, US
pCP MS2 Tetra Cys	Expression of MS2 coat protein linked to Tetracystein binding site for Flash dye	this work

Table 5. List of primers used in this study.

Index	Name	Sequences (5'→ 3')	Comments
1	fw_*Sic1*-MS2-tag	GCCAAAGGCATTGTTTCAATCTAGGGATCAAGAGCATTGAAACGC TGCAGGTCGACAACCC	Cloning MS2 loops
2	rev_*Sic1*-MS2-tag	TAAAATATAATCGTTCCAGAAACTTTTTTTTTTCATTTCTGCATAGG CCACTAGTGGATC	Cloning MS2 loops
3	fw-CLN2-MS2-tag	CTTTAATTTCTTTTGGTATGGGCAATACCCAAGTAATATAGAACGC TGCAGGTCGACAACCC	Cloning MS2 loops
4	rev-CLN2-MS2-tag	GTTTGGCAAATTGGCATTCATTTATCATGAAAAGAACAGGAAGCA TAGGCCACTAGTGGATC	Cloning MS2 loops
5	Sic1-DetR	GTTGATGTTAATGCCCCTTTGC	Cloning MS2 loops
6	Sic1-DetF	CCTACATCTGCCAGGCAGTTAC	Cloning MS2 loops
7	His5-DetR	GACTGTCAAGGAGGGTATTCTG	Cloning MS2 loops
8	CLN2-DetR	CTCTCTTTTCCCGCAGAATATG	Cloning MS2 loops
9	CLN2-DetF	TCCTCATCTCAAAGCCACACTC	Cloning MS2 loops
10	rev_pCP_MS2	CACTATAGGGCGAATTGG	Cloning MS2-YPF
11	fw_mYFP_XmaI	CGGATCCCCCGGGATGGTGAGC	Cloning MS2-YPF
12	rev_mYFP_NotI	CATAGCGGCCGCCTTGTACAG	Cloning MS2-YPF
13	fw_mYFP_NotI	CAAGGCGGCCGCTATGGTGAGC	Cloning MS2-YPF
14	rev_mYFP_XhoI	CACCATCTCGAGCTTGTACAG	Cloning MS2-YPF
15	fw_mYFP_XhoI	GTACAAGCTCGAGATGGTGAGC	Cloning MS2-YPF
16	rev_mYFP-Stop_MluI	GCGTACACGCGTTTACTTGTAC	Cloning MS2-YPF
17	rev_Tetra_Cys linker	CGCGTTAGCAACAGCCAGGACAACAAC	Cloning MS2-Tetracystein
18	fw_Tetra_Cys linker	CCGGGTTGTTGTCCTGGCTGTTGCTAA	Cloning MS2-Tetracystein
19	rev_Tetra_Cys_intern	AGCAACAGCCAGGACAAC	Cloning MS2-Tetracystein
20	fw_Spc42_integ	CTGAAAATAATATGTCAGAAACATTCGCAACTCCCACTCCCAATAA TCGAGGAGCAGGTGCTGGTGCT	Cloning cell cycle markers
21	rev_Spc42_integ	GCTTTAAGAATGCGCCATACTCCTTAACTGCTTTTTAAATCATCAAT TAGAAAAACTCATCGAGCATC	Cloning cell cycle markers
22	fw_mTurquoise_BamHI	CTGCAGGTCGACGGATCCGGAGCAGGTGCTGGTGCTGGTGCTGG AGCAATGGTGAGCAAGGGCGAGGAGCTG	Cloning cell cycle markers
23	rev_mTurquoise_zBssHII	CGCTTATTTAGAAGTGGCGCGCAGTTACTTGTACAGCTCGTCCATG CCGAGAGTG	Cloning cell cycle markers

3.1.3.5 Media and buffers

- Cell culture (for solid media and growth on plates, 2% agar was added into liquid media.)

Synthetic Dextrose (SD) medium: 0,17% (w/v) Yeast Nitrogen Base, 0,5% (w/v) Ammonium sulfate, 5,5‰ (w/v) Adenine, 5,5‰ (w/v) L-Thyrosin, 5,5‰ (w/v) Uracil, 2% (w/v) D-glucose, 1% (w/v) amino-acids stock* in ddH_2O, pH 7.

* Amino-acids stock is composed of the following listed amino-acids in ddH_2O, pH 10 with NaOH. Selected amino-acids were omitted in case they served as selection markers or to maintain a plasmid inside the cell. Amino-acids stock is stored at 4 °C.

0,2% (w/v) L-Arginin, 0,1% (w/v) L-Histidin, 0,6% (w/v) L-Leucin, 0,6% (w/v) L-Isoleucin, 0,4% (w/v) L-Lysin, 0,1% (w/v) L-Methionin, 0,6% (w/v) L-Phenylalanin, 0,5% (w/v) L-Threonin, 0,4% (w/v) L-Tryptophan

Yeast Extract Peptone Dextrose (YPD) medium: 1% (w/v) yeast extract, 2% (w/v) peptone, 2% (w/v) dextrose (D-glucose) in ddH_2O, pH 7.

Luria-Bertani (LB) medium: 1% Bacto™ Tryptone, 0,5% Bacto™ Yeast Extract, 0,5% NaCl, in ddH_2O, pH 7. Ampicilin was optionally added to the medium in concentration of 100 μg/mL.

- Mounting media for microscopy

Mowiol mounting medium for microscopy: 2,4 g of Mowiol 4-88 were mixed with 6 g of glycerol and 6 mL of ddH_2O and leave for several hours at room temperature. 12 mL of 0.2 M Tris-Cl pH 8,5 were added and the mix was heated to 50°C for 10 min with occasional mixing. After the Mowiol dissolved, the mix was clarified by centrifugation at 5000g for 15 min, the supernatant was aliquoted in 2 mL tubes and stored at −20 °C. These aliquots are stable at room temperature for several weeks after thawing.

Mowiol and Vectashield mix as mounting medium: These mix 20% of Mowiol and 80% Vectashield was stored at 4 °C for one week after preparation.

- Buffers for RNA-FISH

1x TE (Tris-Ethylene-diamine-tetra acetic acid (EDTA)) solution: 100x TE was diluted into ddH_20 to a final concentration of 1x TE, pH 8. This buffer is used to dissolve dry RNA-FISH probes to a working concentration of 25 μM in solution. In the case of the Stellaris probes 5 nmol is dissolved in 200 μL of 1x TE. The RNA-FISH probes working solution was aliquoted into 5 and 10 μL and kept at -80 °C in dark for several years.

1x Buffer B: 1,2 M Sorbitol, 0,1 M potassium phosphate, dissolved in ddH_20, pH 7,5 and stored at 4 °C.

1,4x Buffer B: 1,7 M sorbitol, 140 mM potassium phosphate, dissolved in ddH_20, pH 7,5 and stored at 4 °C.

Potassium phosphate buffer (100 mM, pH 7,5): 83.4 mL of 1M K_2HPO_4 and 16,7 mL of 1 M KH_2PO_4 were mixed and ddH_20 was added to 1 L with. Mix was stored at RT.

DAPI solution: 0,5 µg/mL DAPI solution in 1x PBS-/- was stirred overnight at room temperature in an aluminum foil wrapped flask and then stored at 4 °C in the dark.

DNA competitor mix: A mix of 1:1 of 10 mg/mL sheared salmon sperm DNA (ssDNA) and 10 mg/mL *E.coli* tRNA. *E. coli* tRNA solution was previously prepared by dissolving 10 mg of dry *E. coli* tRNA into 1 mL of ddH_20. Both DNA competitor mix solution and *E. coli* tRNA solution were stored at −20 °C for several years.

Hybridization washing solution: 10% deionized formamide and 2x SSC in ddH_20. Should be prepared fresh.

Spheroplasting buffer: 1,2 M sorbitol, 0,1 M potassium phosphate, 100 U/mL lyticase, 20 mM ribonucleoside vanadyl complex (VRC), 2% (v/v) β-mercaptoethanol, pH 7,5. Should be prepared fresh. 1ml of spheroplasting buffer was prepared as below and is needed for 50 ml of cell culture.

Spheroplasting buffer	STOCK	Final concentrations	1 mL
1,4x buffer B	1,4x	1x	720 µL
β-mercaptoethanol	100%	2% (v/v)	2 µL
VRC	200 mM	20 mM	100 µL
Lyticase	8000 U/mL	200 U/mL	25 µL
ddH_2O	-	-	153 µL

Hybridization buffer:2x SSC, 10% formamide, 1 mg/mL BSA, 10 mM VRC, 0,5 mg/mL *E. coli* tRNA, 0,5 mg/mL salmon sperm DNA, 0,1 g/mL dextran sulfate, 5 mM sodium phosphate pH 7,5 and 0,25 µM (or 0,025 µM)** labeled FISH DNA probes. Preparation for 10ml of hybridization mix is described below.

		STOCK	Final concentrations	Quantities for 10 ml mix
Deionized formamide		100%	10%	1 mL
*Sodium phosphate buffer pH 7,5		100 mM	5 mM	500 µL
*20x SSC		2x SSC	2x SCC	1 mL
*BSA		20 mg/mL	1% = 0,2 mg/mL	100 µL
*VRC µL		200 mM	10 mM final C	500 µL
*Competitor mix DNA 1:1 *E. coli* tRNA: ssDNA		10 mg/mL	1 mg/mL	1 mL
*Dextran Sulfate Sodium M = 10 000 g/mol		100%	10% w/w	1 g
*ddH20 µL		-	-	until 10 mL
**RNA-FISH probes	Hybridization made in an Eppendorf tube with initial 50 mL cell culture	25 µM of probes in 50 µL solution	0,25 µM	0,5 µL
	Hybridization made with cells attached to a coated microscopy glass coverslide	1,25 µM of probes in 25 µL solution	0,025 µM	0,5 µL

* These components were mixed together to make a stock solution, which was aliquoted in 50, 100, 200, 500 and 1000 µL and stored at -20°C. Before use, an aliquot was thawed and the required amount of deionized formamide was added to it to a final concentration of 10% of deionized formamide.

** We used two different initial and final concentrations of RNA-FISH probes depending of whether the hybridization was done an Eppendorf tube or on a coated microscopy coverslide.

3.2 Methods

3.2.1 Cell culture and cell preparation

3.2.1.1 Cell culture

Cells were grown overnight at 30 °C in liquid SD medium or in YPD. The next morning cells were diluted into fresh medium to an optical density at 600 nm (OD_{600nm}) of ~0,05 and let grow until OD_{600nm} of ~0,3 for later procedures.

For induction of MS2–CP fused to fluorescent complexes (mostly GFP(x3)), cells were shifted to medium lacking histidine (selection of the cells with MS2 hairpin loops) and methionine (induction of MS2-CP complexes) for 1,5 h at 30 °C.

For fixation, formalin solution (Sigma-Aldrich) or 32% paraformaldehyde (Electron Microscopy Sciences) were added to the cell culture to a final concentration of 4% (w/v) and culture was incubated for 30 min at room temperature. Yeast samples were then washed from fixative, re-suspended into PBS or required buffer and stored at 4 °C before microscopic acquisition.

For application of osmotic stress to the cells, cell cultures were supplemented with 0.4M NaCl (final concentration), when culture reached early logarithmic growth phase (OD_{600nm} ~0.3). After 15, 30, 45, 60 and 90 min, culture samples were taken and fixed with paraformaldehyde.

3.2.1.2 Growth test

We tested the growth behavior of the yeast strains by long time absorption measurements at 600 nm and 30° C using a plate reader spectrophotometer and manually. Mutant strain behavior was always compared to wild type strains.

- Plate reader: Cells at a low OD_{600nm} ~0,1 were grown in a 96-well plate at 30 °C and measurements were performed every 10 min with 5 min shaking prior to every measurement. Each well was measured 20x in every cycle and obtained values were averaged.

- Manual: Cells were grown overnight due to standard conditions, diluted the next morning to approximately OD_{600nm} 0,05 and let grow. Every 30 or 60 min, 1 ml of the culture was extracted in a cuvette and OD_{600nm} was measured with a spectrophotometer. To calculate the duplication time (in min) data was fitted with an exponential growth equation:

$$N(t) = N_0 . e^{kt} ,$$

where $N(t)$ is the number of cells at time t, No is the initial number of cell at time $t = 0$ and k is the growth rate in number of cells per minute. The duplication time, T_d, in minutes is calculated as $T_d = \ln(2)/k$. Calculation was made using an internet software http://www.doubling-time.com/compute.php .

3.2.1.3 Calculation of budding index

At least 200 cells in bright field microscope images were counted and scored for the presence of a bud. Budding is a morphological hallmark for G1/S transition and the value of 5% of budding cells was taken as threshold to determine the timing of the G1/S transition (Labib et al., 1999).

3.2.1.4 Counterforce elutriation for cell population synchronization

Cell culture was grow overnight and diluted the next morning to OD_{600nm} ~0,05 in typically 3 liters. When cell culture reached OD_{600nm} ~0,5, cells were synchronized using the JE-6 counterflow centrifugal elutriator system (Beckmann Coulter Inc.). Small G1 synchronized cells were collected at a flow rate of 40 ml/min at 1500 rpm and 20 °C; they were then centrifuged and re-suspended in culture media to increase the cell concentration. Afterwards cells were let grow and then harvested at specific times for further procedures, for example microscopy acquisition.

3.2.1.5 Genetic and morphological markers for *in silico* synchronization

For assignment of cells to specific cell cycle phases, we used a reporter strain with two labeled cell cycle markers Whi5-TagGFP and Spc42-mTurquoise (cloning procedure explained in section 3.1.3.2 Yeast strains). We acquired bright field and fluorescence microscopy images of a non-synchronized population of this reporter strain. Each single cell from the non-synchronized cell population was assigned to different cell cycle phases according to the patterns of the genetic and morphological cell cycle markers (Table 6).

The markers were the presence and size of a bud, the morphology of the DAPI stained nucleus, the number and localization of spindle pole body visualized by mTurquoise-labeled Spc42, and finally, the localization of TagGFP-labeled Whi5 (Trcek et al., 2011). Whi5 is recruited to the nucleus between late M and early G1 and is cytoplasmic during the rest of the cell cycle (Costanzo et al., 2004). We distinguished early G1, late G1, S, G2, prometa-/meta-phase (P/M), anaphase (Ana) and telophase/cytokinesis (T/C) (Table 6). The duplication time of this strain was about 129 min in YPD at 30 °C and the duration of each phase was proportional to the number of cells in each specific phase (Trcek et al., 2011).

The images of Whi5-TagGFP/Spc42-mTurquoise yeast cells were acquired with an inverted Olympus IX81 epi-fluorescence microscope with UPlanApo 100X, 1,35 numerical aperture oil-immersion objective (Olympus). Vertical stacks of fifteen images with a *z*-step size of 0,25 µm were acquired using a Clara E Interline charge-coupled device (CCD) camera (Andor) with a 0,0645 µm pixel size. An HBO 100 watts light source was used for illumination. GFP fluorescence was acquired with NIBA filter for 500 ms. mTurquoise fluorescence was acquired with U-MCFPHQ filter for 300 ms. Bright field images were acquired with DIC filter for 10 ms. DAPI images were acquired with U-MWU2 filter for 25 ms. When cell cycle markers were combined with RNA-FISH, the acquisition of the cell cycle markers was prior to the acquisition of the fluorescently tagged mRNAs to avoid bleaching of the fluorescence of the proteins employed as cell cycle markers. Instrument control was accomplished using MetaMorph Software and images were acquired using the associated Multi-dimensional acquisition (MDA) module.

Table 6. Rules for *in silico* cell cycle phase segmentation using genetic and morphological markers.
Single cells from bright field and fluorescent microscopy images were assigned to cell cycle phases using morphological markers: the presence and size of the bud/daughter cell (1st line), the nuclear or cytosolic localization of the TagGFP tagged Whi5 protein (2nd line), the number and orientation of the spindle pole body (SPB) (3rd line), observable thanks to its mTurquoise tagged Spc42 component protein, the size and number of DAPI labeled nucleus (4th line) and finally, the shape of the cell (5th line). The abbreviations used in the table are described as follow. Whi5_nuc: fluorescence intensity of Whi5 signal in nucleus; Whi5_cyt: fluorescence intensity of Whi5 signal in cytoplasm, SPB_i: fluorescence intensity of SPB, d: distance separating the two SPBs, D: diameter of the nucleus, L: length of the yeast, Nuc_i: fluorescence intensity of the nucleus.

	Early G1	**Late G1**	**S**	**G2**	**P/M**	**ANA**	**T/C**	**No bud/2 SPBs**
Bud	no	no	little	bigger	bigger	bigger	bigger	no
Whi5 localization	Nuclear Whi5_nuc > Whi5_cyt	Cytoplasmic Whi5_nuc ≈ Whi5_cyt	Cytoplasmic Whi5_nuc ≈ Whi5_cyt	Cytoplasmic Whi5_nuc ≈ Whi5_cyt	Cytoplasmic Whi5_nuc ≈ Whi5_cyt	Cytoplasmic Whi5_nuc ≈ Whi5_cyt	Nuclear Whi5_nuc > Whi5_cyt	Cytoplasmic Whi5_nuc ≈ Whi5_cyt
Spindle Pole Body (SPB) number and localization seen with Spc42	1 SPB of fluorescence intensity SPB_i=i	1 SPB of fluorescence intensity SPB_i=i	1 SPB brighter of intensity SPB_i=2i	2 SPBs separated by a distance, d, shorter than diameter of nucleus, D. d < D Intensity in each SPB SPB_i=i	2SPBs separated in 1 nucleus d≈D and oriented toward bud.	2 SPBs in 2 separated nucleus D<d<L. L=length of the yeast Intensity in each SPB SPB_i=i	2 SPBs in 2 extremely separated nucleus. SPBs and nucleus on same axis d≈L. Intensity in each SPB SPB_i=i	2 SPBs Intensity in each SPB SPB_i=i
Nucleus	1 round of intensity Nuc_I= I	1 round Nuc_I= I	1 round I ≤ Nuc_I ≤ 2I	1 round Nuc_I = 2I	1 round Nuc_I = 2I	1 elongated or 2 separated	2 separated with each Nuc_I= I	1 round or elongated I ≤ Nuc_I ≤ 2I
Cell morphology	round	elongated	Round with bud	Round with daughter cell	Round with daughter cell	Round with daughter cell	Bud neck still present	round

For the analysis, the 3D image stacks were reduced to 2D image projections along the z-axis using ImageJ. Stacks of bright field images were reduced to best focus projections. Stacks of fluorescence microscopy images of DAPI stained nucleus and of mTurquoise-labeled spindle pole body were reduced to maximal intensity projections. Stacks of fluorescence microscopy images of TagGFP-labeled Whi5 were reduced to average intensity projections. Number and localization of spindle pole body were measured using a semi-automatic spot detection workflow developed during this work with open source and free software. The workflow was similar to the one used for the detection of the mRNA fluorescent spots described in the section 3.2.4 Analysis of microscopy images. The presence and size of the bud, the morphology of the DAPI stained nucleus and the localization of GFP-labeled Whi5 were analyzed per hand. All information was collected in an excel sheet, where cell cycle phase was sorted using customer defined rules shown in Table 6. The fractions of cell population in each cell cycle phase were processed using a pivot table in excel.

We tested whether the tagging of Whi5 and Spc42 proteins altered the growth of the cell culture or the expression of our genes of interest and obtained similar growth curves and similar mRNA distributions of *SIC1*, *CLN2* and *CLB5* for the wild type strain and the Whi5-TagGFP/Spc42-mTurquoise strain (Figure 13).

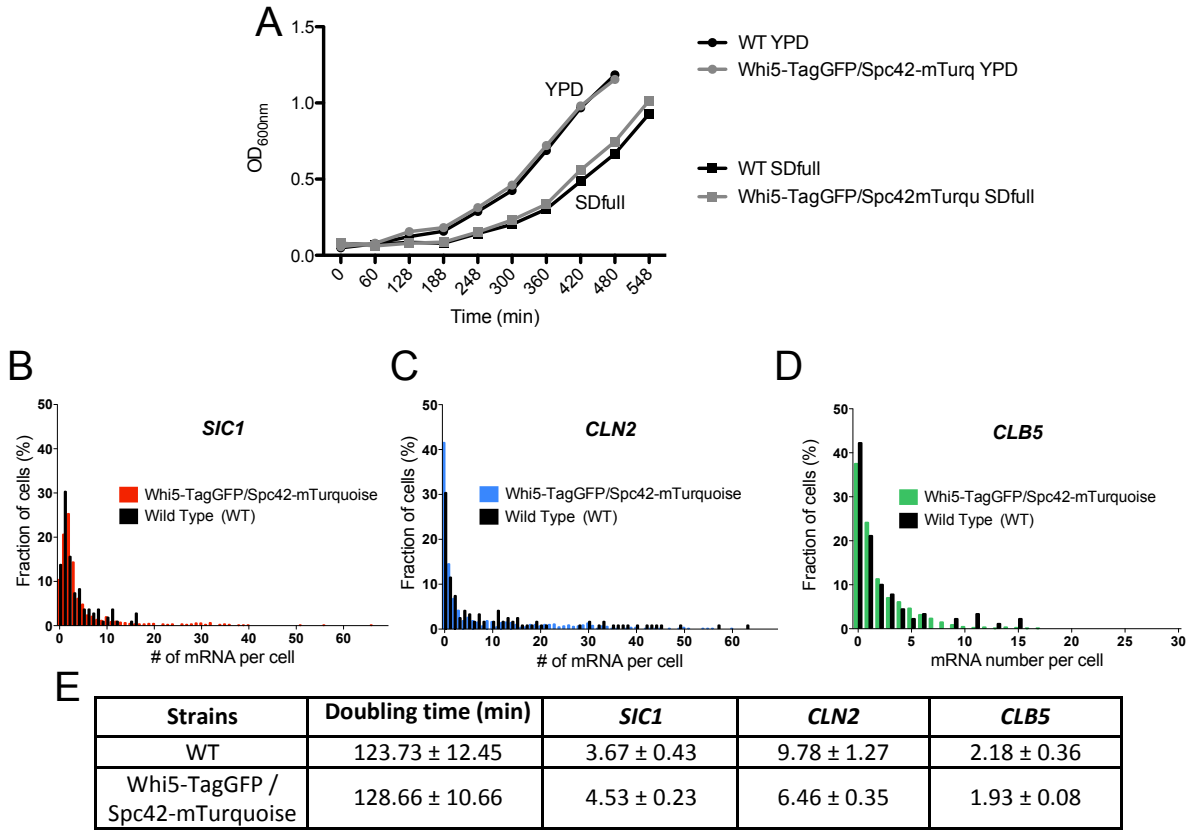

E

Strains	Doubling time (min)	*SIC1*	*CLN2*	*CLB5*
WT	123.73 ± 12.45	3.67 ± 0.43	9.78 ± 1.27	2.18 ± 0.36
Whi5-TagGFP / Spc42-mTurquoise	128.66 ± 10.66	4.53 ± 0.23	6.46 ± 0.35	1.93 ± 0.08

Figure 13. Comparison of the growth and mRNA distributions of *SIC1*, *CLN2*, and *CLB5* in wild type and Whi5-TagGFP/Spc42-mTurquoise strains.

(A) Growth of the wild type (black curves) and Whi5-TagGFP/Spc42-mTurquoise (grey curves) strains in YPD (circles) and SD full (squares) media at 30 °C. (B) to (D) mRNA distributions of *SIC1*, *CLN2*, and *CLB5* in the two strains obtained with RNA-FISH. Data in Whi5-TagGFP/Spc42-mTurquoise strain are shown in colors and represent approximately 900 cells. Data in wild type strain are shown in black and represent approximately 100 cells. Data for *SIC1*, *CLN2*, and *CLB5* are shown in (B), (C) and (D), respectively. (E) Doubling time (minutes) of the two strains grown in YPD at 30°C and mean +/- SEM of mRNA/cell for *SIC1*, *CLN2*, and *CLB5* obtained with RNA-FISH in wild type strain (approximately 100 cells) and in Whi5-TagGFP/Spc42-mTurquoise strain (approximately 900 cells) YPD at 30 °C.

3.2.2 MS2-CP system

The method was initially established at Robert Singer's Lab (Bertrand et al., 1998) and since then was continuously improved. The 3' untranslated region (3'UTR) of the gene of interest is tagged with a series of hairpin loops from MS2 bacteriophage by homologous recombination (Bertrand et al., 1998; Haim et al., 2007). The hairpins are binding sites for a dimer of MS2 coat protein (MS2–CP) fused to a fluorescent element, typically a GFP (MS2–CP–GFP), which is expressed in yeast cells (Figure 14). The target mRNAs are visualized as bright fluorescent spots due to the accumulation of fluorescently tagged MS2–CP.

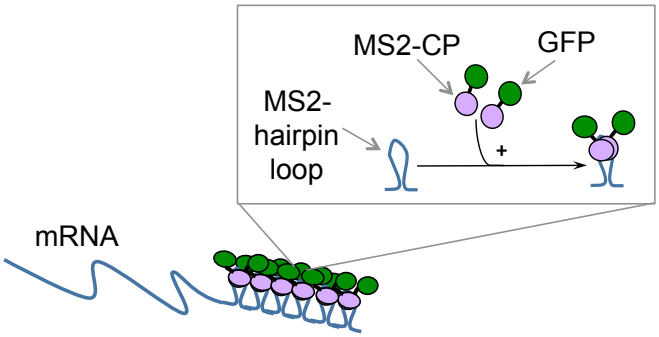

Figure 14. Principle of the MS2-CP system.
In the MS2-CP system a series of hairpin loops from MS2 bacteriophage is integrated in the 3' untranslated region (3'UTR) of a target gene by homologous recombination. The hairpins are binding sites for a dimer of MS2 coat protein (MS2–CP) fused to a fluorescent element, for example a GFP (MS2–CP–GFP), which is expressed in the cell via a plasmid. This technique enables single cell mRNA detection using fluorescent microscopy.

3.2.2.1 Cloning of the *SIC1* and *CLN2* MS2-GFP strains

The cloning of stable strains with *SIC1* and *CLN2* tagged with MS2 system was performed following the m-TAG gene-tagging procedure (Haim-Vilmovsky and Gerst, 2009; Haim et al., 2007) (Figure 15). First the hairpins sequence were designed to match the end of the coding region and the beginning of the 3'UTR of the gene of interest by PCR using the plasmid pLOXHis5MS2L and the pairs of primers Sic1-Det R/Sic1-Det F and CLN2-Det R/CLN2-Det F for *SIC1* and *CLN2*, respectively. The PCR product was transformed into yeast to enable homological recombination into chromosomal target site and therefore tagging of *SIC1* or *CLN2* mRNA with MS2 hairpins. As selective marker HIS5 gene flanked by loxP sites was employed and removed after successful recombination, leading to minimal gene perturbations, were only MS2 hairpins were inserted between the stop codon and the full length 3'UTR. In the following part "GENE" refers to *SIC1* or *CLN2*. The transformed cell colonies were selected with a histidine selection marker and the yeast cells with proper integrated sequence were detected by colony-PCR using the GENE-Det F and HIS3-Det R primers. Cells were transformed with the plasmid pSH47, selected with a uracil selection marker and grown on galactose containing medium to induce the expression of Cre recombinase. Cre recombinase cut the histidine marker sequence, which was not needed after the histidine selection and which separated the gene-coding region from the MS2 hairpins and the 3'UTR. Finally, the cells were transformed with a plasmid, MS2-CP-X, coding for the MS2-CP bound to a fluorescent molecule or molecule complex, X, and selected with a histidine marker. We used in this studied four different MS2-CP-X plasmids, i.e. pG14-MS2_GFP, pMS2-CP-GFP(x3), pMS2-CP-YFP(x3) or pCP-MS2-Tetra Cys. All these MS2-CP-X plasmids contain a methionine promoter. In the case of pCP-MS2-Tetra Cys, the MS2-CP is bound to a quadruplet of cysteine that forms a binding site for a green fluorescent FlAsH dye..

Similar growth curves were observed for the wild type and the MS2-CP modified strains (Figure 21 in RESULTS I).

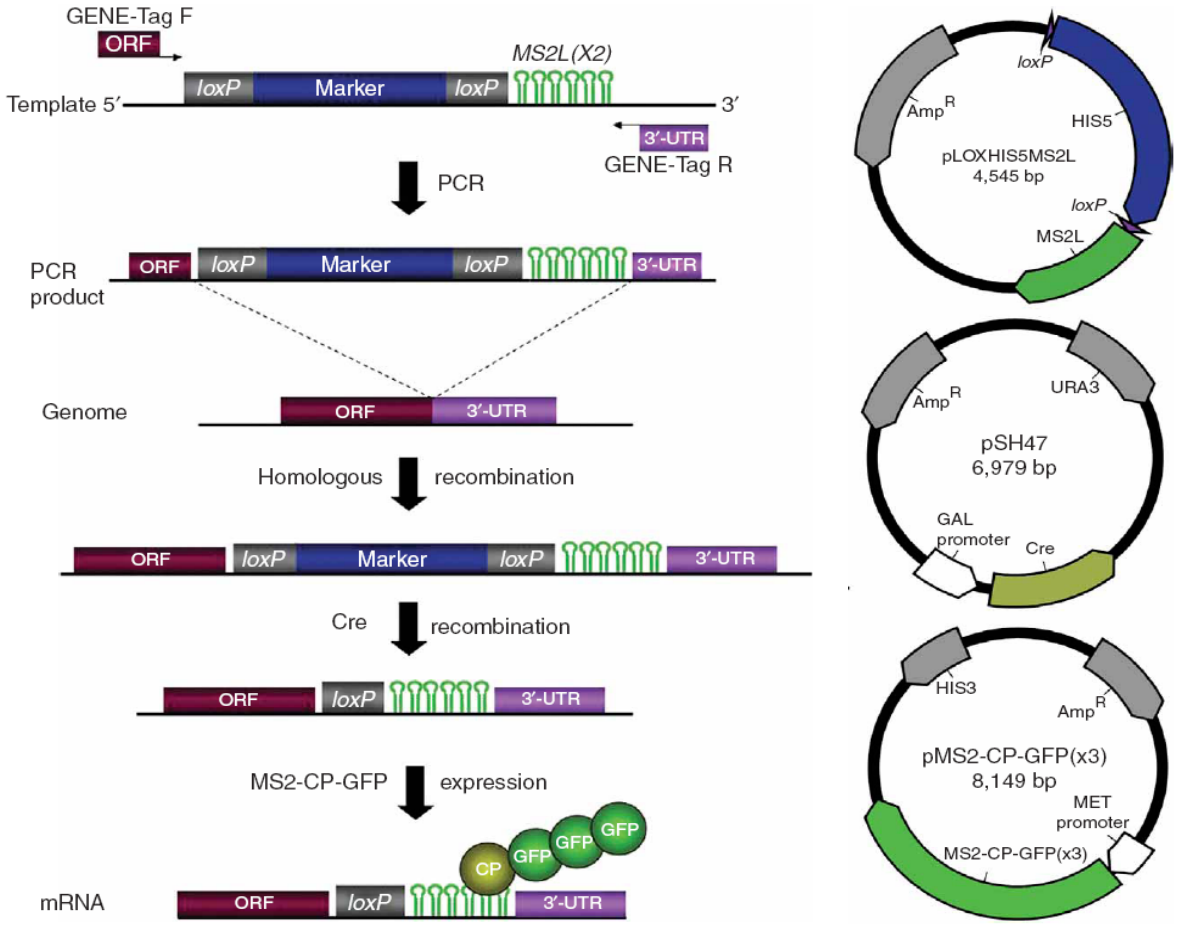

Figure 15. Cloning procedure for the tagging of a specific gene with the MS2-CP system.
Left part. Procedure of molecular cloning for tagging with the MS2-CP. "GENE" refers in this study to *SIC1* or *CLN2*. Right part. Maps of the three plasmids used in the cloning procedure. pLOXHis5MS2L codes for the MS2 loops, binding sites of the MS2 coat proteins. Note that the last plasmid pMS2-CP-GFP(x3) is shown as an example for plasmid coding for the MS2-CP bound to a fluorescent molecule. In this study we used four different plasmids coding for the MS2-CP bound to a fluorescent molecule, namely pG14-MS2_GFP, pMS2-CP-GFP(x3), pMS2-CP-YFP(x3) and pCP-MS2-Tetra Cys. In the case pCP-MS2-Tetra Cys, the MS2-CP is bound to a quadruplet of cysteine that forms a binding site for a green fluorescent FlAsH dye. Adapted from (Haim-Vilmovsky and Gerst, 2009).

3.2.2.2 Preparation of cells and microscopy measurement of MS2 mutant strains

For cell imaging of MS2 labeled mRNA, cells were grown overnight at 30 °C in SD lacking histidine (SD-His) to retain the MS2-CP-X plasmid in the cells. In the morning cells were diluted to OD_{600mn} 0,05 in SD lacking histidine and methionine (SD -His -Met) to induce expression of the MS2-CP-X and were grown several cell cycles to OD_{600mn} ~0,3. From this point cells were labeled with FlAsh dye, fixed in formalin or directly used for microscopy acquisition.

In the case of pCP-MS2-Tetra Cys, 200 µL cells in SD -His -Meth were labeled overnight (12 hours) with 2µL of 200 µM FlAsH dye solution (2µM final concentration) at 30 °C, then washed twice 30 min in BAL buffer (provided in the purchased Tetra Cysteins FlAsH labeling kit) and resuspended in SD -His -Meth. From this point cells were used for microscopy acquisition.

To study the changes of *SIC1* mRNA level over cell cycle using MS2-CP-GFP(x3) tagging we monitored *SIC1* level in a population of cells synchronized in early G1 via counterflow centrifugation elutriation (section 3.2.1.4) (Figure 16). We transferred this synchronized population into SD -His – Meth, harvested a sample every 2 min and fixed it in 4% w/v paraformaldehyde. The population was grown for 250min. We performed fluorescence microscopy of each sample to monitor the level of *SIC1* tagged with MS2-CP-GFP(x3). Beside the fluorescent images, we took bright field images to measure the fraction of budding cells, i.e. budding index, and therefore to identify the timing of the G1/S transition.

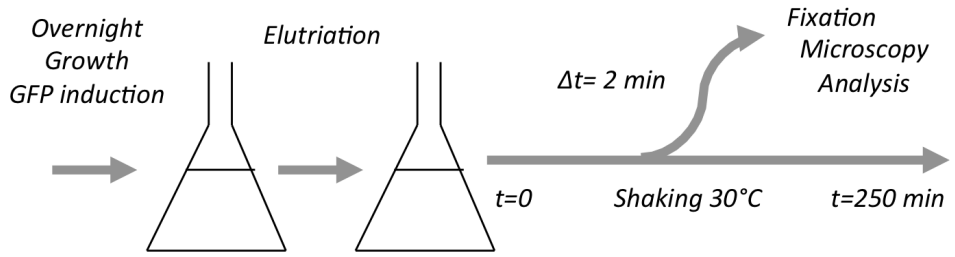

Figure 16. Experimental set up to follow the *SIC1* expression over cell cycle progression.
A cell population modified with the MS2-CP system tagging the *SIC1* gene was grown until logarithmic phase and applied to counterflow centrifugation elutriation. Early G1 synchronized cell population was then moved at 30°C with a slight shaking to ensure optimal growth conditions. Every 2 minutes a sample was taken, fixed in 4% w/v paraformaldehyde and observed using fluorescent and bright field microscopy to obtain the level of *SIC1* RNPs per cell and the budding index, respectively.

For microscopy cells were placed between a microscope slide and a coverslip. Images were acquired on an Olympus IX81 epi-fluorescence microscope with an UPlanApo 100x, 1,35 numerical aperture oil-immersion objective (Olympus). An HBO 100 watts light source was used for illumination with a U-MWNiba filter (Olympus). The excitation and emission wavelengths for Tag-GFP, YPF and FlAsH dye were 480 nm and 530 nm, respectively using a U-WNIBA filter. Exposure time for GFP, YPF and FlAsH dye was 300ms. Bright field images were taken with DIC filter with 10 ms exposure time. Vertical stacks of 21 images with a z step size of 0,2 mm were acquired using a Clara E Interline camera (Andor) with a 6,45 mm pixel size CCD. Metamorph (Molecular Devices) software platform was used for instrument control and image acquisition.

3.2.3 RNA-FISH approach

RNA-Fluorescence *in situ* Hybridization (RNA-FISH) is a well-established method for single RNA molecule detection and absolute enumeration of transcripts in single cells and their transcriptional variability in populations (Ball et al., 2013; Femino et al., 1998; Raj et al., 2010; Taniguchi et al., 2010; Trcek et al., 2012; Vargas et al., 2011; Zenklusen et al., 2008). The RNA sequence of each gene of interest is hybridized by a set of fluorescently labeled DNA probes (Figure 17). The following improved protocol is based on the experimental procedures and analysis workflows described in (Raj et al., 2008; Trcek et al., 2012).

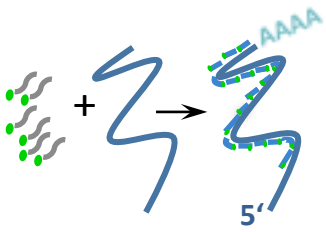

Figure 17. Principle of the RNA-FISH method.
A set of fluorescently labeled DNA probes (grey line with green dot) hybridizes the target mRNA sequence (blue line). Single mRNA molecules can be detected with fluorescence microscopy.

3.2.3.1 Design of RNA-FISH probes

Two types of RNA-FISH probes were employed. The first RNA-FISH strategy used a unique FISH probe sequence, which was complementary to the sequence coding for a MS2 binding site hairpin. A set of this unique FISH probe bound to the 12 hairpins, previously genomically integrated in the mRNA sequence of interest. We employed the MS2-FISH sequence published in (Gallardo et al., 2011) with five Cy3 fluorophore labels on three modified thymines at the two ends and in the middle of the sequence (Table 7). Maxima of absorption and emission of Cy3 occur at 548 and 562 nm, respectively (Figure 18). The MS2-FISH probes were purchased at BioTeZ Berlin Buch GmbH, Berlin, Germany. Unfortunately, we did not obtain relevant microscopy images with this set up.

Table 7. Properties of the FISH oligonucleotide tagging the MS2 hairpin sequences.
* indicates the Cy3 fluorescently labeled nucleotides. The MS2-FISH sequence is the one published in (Gallardo et al., 2011). The Cy3 labeled MS2-FISH probes were purchased at BioTeZ Berlin Buch GmbH, Berlin, Germany.

Probe name	Sequence (5' to 3')	Length (nucleotides)
MS2_loop_FISH	C*TAGGCAAT*TAGGTACCTTAGGATCTAAT*GAACCCGGGAAT*ACTGCAGAC*	50

The second RNA-FISH strategy used gene specific Stellaris® FISH probes purchased at Biosearch Technologies, Novato, USA. For each gene of interest, namely *SIC1*, *CLN2* and *CLB5*, a set of approximately 34 DNA probes, each labeled with one fluorophore was designed for selective binding to the target transcript sequence (Raj et al., 2008). The RNA-FISH probes were 20 nucleotide long oligo-nucleotides with a GC content close to 45%. The 3'-amine served as a reactive group for the succinomidyl-ester coupling of the fluorophore. A spacing of at least two nucleotides separated two adjacent RNA-FISH probes. The fluorophores used were Quasar® 570 (Cy3™ replacement) and CAL Fluor Red 610 (Alexa Fluor® 594 replacement). The excitation and emission maxima for Quasar® 570 are 548 nm and 566 nm, and for CAL Fluor Red® 610 and 590nm and 610nm, respectively (Figure 18). The RNA-FISH probe sets for *SIC1*, *CLN2* and *CLB5* used in this study are listed in (Table 8, Table 9 and Table 10). We tested the specificity of a probe set for a single gene by performing RNA-FISH in a knockout strain of this specific gene (Figure 31 in RESULTS II).

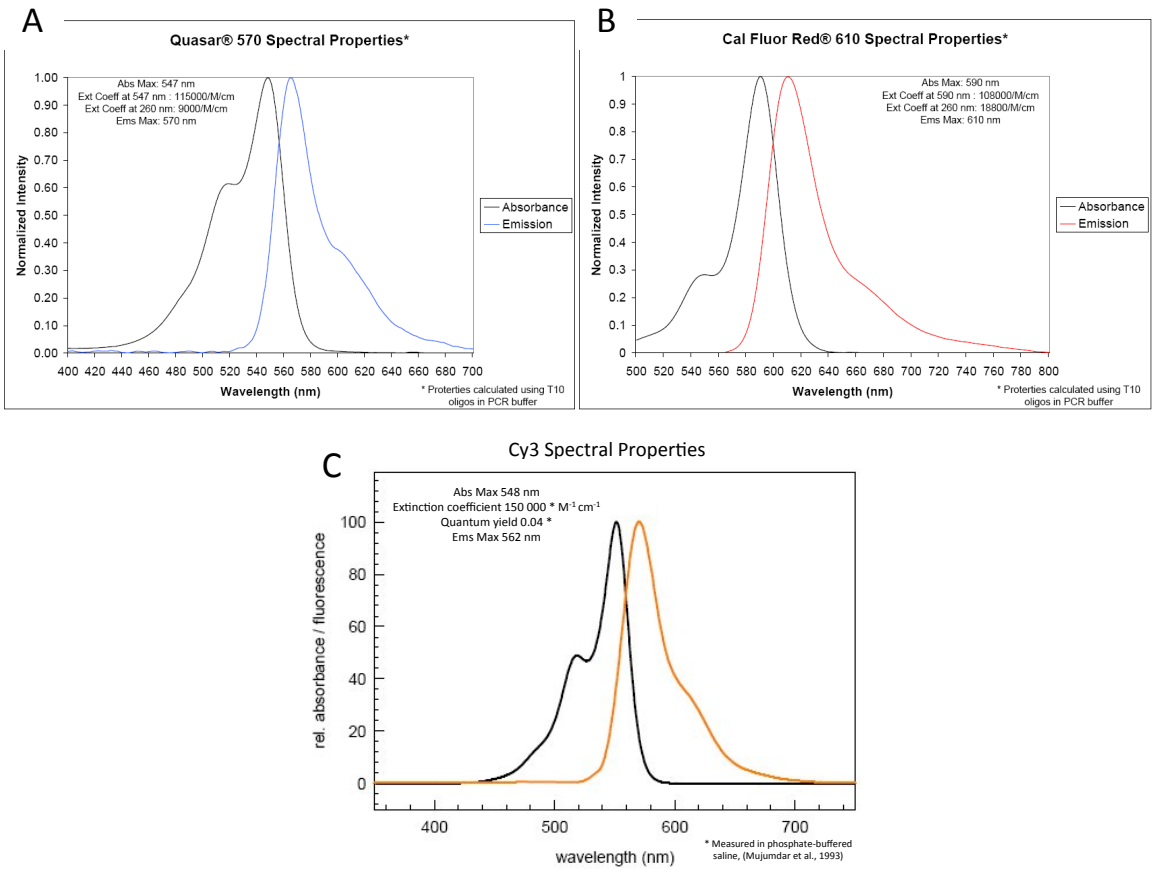

Figure 18. Spectral properties of the fluorophores labeling the RNA-FISH probes.

Absorption (black curves) and emission (color curves) spectra of Quasar® 570 (Cy3™ Replacement) (A), Quasar® 610 (Alexa Fluor® 594 Replacement) (B) and Cy3 (C) used as labels of the RNA-FISH probes. The maxima of excitation and emission for Quasar® 570 are 548 nm and 566 nm, for CAL Fluor Red® 610 are 590nm and 610nm, for Cy3 are 548 and 562, respectively.

Table 8. Properties of the FISH oligonucleotide set for *SIC1*.

Start and end positions are relative to the ORF of the gene. The 3'-amine of each RNA-FISH probe was labeled with one fluorophore Quasar® 570 (Cy3™ Replacement) or CAL Fluor Red 610 (Alexa Fluor® 594 Replacement). Stellaris® FISH probes purchased at Biosearch Technologies, Novato, USA.

Index	Name Probe	Sequence (5' to 3')	Start Position	End Position	Length (nucleotides)
1	Sic1_yeast_570_1	TTGGTGGGGTGGAAGGAGTC	3	22	20
2	Sic1_yeast_570_2	GCTGCGCAAGGTACCTAGTC	33	52	20
3	Sic1_yeast_570_3	TGCATTAGGGCACTAGAAC	68	86	19
4	Sic1_yeast_570_4	TAGGTTCTGTGAAGGCTTTT	104	123	20
5	Sic1_yeast_570_5	AGTTGTTGAGGGAGTGACAG	128	147	20
6	Sic1_yeast_570_6	TGCTAATAATGGCGCATTTT	158	177	20
7	Sic1_yeast_570_7	AGAGGTCATACCCATGTTCG	188	207	20
8	Sic1_yeast_570_8	GAGCGTTGAGGAGACGTAAG	220	239	20
9	Sic1_yeast_570_9	CACTGAAGATTTTGGAAACGG	241	261	21
10	Sic1_yeast_570_10	TCAAATTGGAATAGTGTCCTC	264	284	21
11	Sic1_yeast_570_11	ACTGTTCCATTATCATGACTT	285	305	21
12	Sic1_yeast_570_12	TGGTTCCTGCTCTTCCCT	307	324	18
13	Sic1_yeast_570_13	ATCCTATTTACACGACCCAA	325	344	20
14	Sic1_yeast_570_14	CACATTTTGCTGCGTGGGAA	350	369	20
15	Sic1_yeast_570_15	CTTCTTCTGCTGCATCTATA	372	391	20
16	Sic1_yeast_570_16	AGATGTAGGTCTGCTGGGG	417	435	19
17	Sic1_yeast_570_17	AGTGATAAATGTAACTGCCT	439	458	20
18	Sic1_yeast_570_18	TGTCTGATCAAACTCATCTCT	463	483	21
19	Sic1_yeast_570_19	GGCGTACCAGGTACATCTTT	502	521	20
20	Sic1_yeast_570_20	AATGTTATCACCTTGTCGCT	523	542	20
21	Sic1_yeast_570_21	CACTTTCTTGACTCCTGGCG	585	604	20
22	Sic1_yeast_570_22	CACCCGCACTGGATTGATGA	623	642	20
23	Sic1_yeast_570_23	TTCCTGAGTGACCAGTTCAT	665	684	20
24	Sic1_yeast_570_24	AACATTGCCCTTTTACGTTC	694	713	20
25	Sic1_yeast_570_25	ACGTCTTCTATATCTGGGTT	721	740	20
26	Sic1_yeast_570_26	CCCTTCTTATTGACATATGTTAT	742	764	23
27	Sic1_yeast_570_27	TCATCCGTTAACCTTCGTTT	778	797	20
28	Sic1_yeast_570_28	GGCTTGAATCTTCTCTTTTCT	798	818	21
29	Sic1_yeast_570_29	CAATGCTCTTGATCCCTAG	836	854	19

Table 9. Properties of the FISH oligonucleotide set for *CLN2*.

Start and end positions are relative to the ORF of the gene. The 3'-amine of each RNA-FISH probe was labeled with one fluorophore Quasar® 570 (Cy3™ Replacement) or CAL Fluor Red 610 (Alexa Fluor® 594 Replacement). Stellaris® FISH probes purchased at Biosearch Technologies, Novato, USA.

Index	Name Probe	Sequence (5' to 3')	Start Position	End Position	Length (nucleotides)
1	Cln2_yeast_570_1	CTTGGTTCAGCACTAGCCAT	1	20	20
2	Cln2_yeast_570_2	TAGCATTGATGACGAGTCCC	30	49	20
3	Cln2_yeast_570_3	CTGCATTAGATAGCTCAATCGG	64	85	22
4	Cln2_yeast_570_4	GGTGGTATTCTTGCAGCATT	105	124	20
5	Cln2_yeast_570_5	CTGCTGGTCTATTAGTTTTGGAT	173	195	23
6	Cln2_yeast_570_6	CTTGTTTCCACGGGGTTCAT	202	221	20
7	Cln2_yeast_570_7	GACCACAGACAGCTCGAACA	242	261	20
8	Cln2_yeast_570_8	CTCTTGGAACAATAGCGGTC	307	326	20
9	Cln2_yeast_570_9	ATTTGGCTTGGTCCCGTAAC	333	352	20
10	Cln2_yeast_570_10	TTAGCAGCCAACCAGAGACA	367	386	20
11	Cln2_yeast_570_11	GTGATTACAACCGCCCCAAG	389	408	20
12	Cln2_yeast_570_12	ATCTTCCGCCAGTAGGGATG	426	445	20
13	Cln2_yeast_570_13	GAGAGTCGAGGTATACGTGC	466	485	20
14	Cln2_yeast_570_14	AAGACCTGACCATCACCACA	502	521	20
15	Cln2_yeast_570_15	AGTTCGTATTGCATCAAACAATT	625	647	23
16	Cln2_yeast_570_16	GGGATAATTGAGACTGACGTT	689	709	21
17	Cln2_yeast_570_17	CCTCTCGTCTACAGTGGCAT	719	738	20
18	Cln2_yeast_570_18	TGCCACGCGGATACATCAAT	814	833	20
19	Cln2_yeast_570_19	GAATATGCCGTGCGATACTT	863	882	20
20	Cln2_yeast_570_20	CCGTGGTCTTGATTGGTGAA	898	917	20
21	Cln2_yeast_570_21	GCTTTCTGATGTCATTGGAGT	931	951	21
22	Cln2_yeast_570_22	ATGCCGTTCATTAAGGTACT	970	989	20
23	Cln2_yeast_570_23	ACACTTCCATCAAGGAGTTAGG	1000	1021	22
24	Cln2_yeast_570_24	GTAGAACACCATTGACCGTTT	1025	1045	21
25	Cln2_yeast_570_25	ATGTTCAAGTTGGATGCAATT	1098	1118	21
26	Cln2_yeast_570_26	AAAGAGCATGATGGGGTTGA	1138	1157	20
27	Cln2_yeast_570_27	TGAGGAAGCGGGCGAAGGA	1182	1200	19
28	Cln2_yeast_570_28	ATTGGAGTGTGGCTTTGAGA	1201	1220	20
29	Cln2_yeast_570_29	ATATTCCGGCTGAAAACGCT	1249	1268	20
30	Cln2_yeast_570_30	ACATACTTGGAGTGATTGGTGA	1279	1300	22
31	Cln2_yeast_570_31	CATATACTGTTTGACTGCTGCT	1313	1334	22
32	Cln2_yeast_570_32	ACCAGACTATTCACACTAACGG	1343	1364	22
33	Cln2_yeast_570_33	TGTTCGTAGATCCTTTGTTTGT	1376	1397	22
34	Cln2_yeast_570_34	ATTGCTGTTAGGACCCGTGA	1400	1419	20
35	Cln2_yeast_570_35	TGGTTTTCCTTGTTAGACTCATT	1456	1478	23
36	Cln2_yeast_570_36	ATTGAGGTAATGCGCCGTT	1488	1506	19
37	Cln2_yeast_570_37	AATGAAGCTTGTCTTGGGT	1515	1533	19
38	Cln2_yeast_570_38	CAGTTGGCGAGGGGAACATT	1542	1561	20
39	Cln2_yeast_570_39	AGGCACTGCTAGATTTACCG	1575	1594	20

Table 10. Properties of the FISH oligonucleotide set for *CLB5*.

Start and end positions are relative to the ORF of the gene. The 3'-amine of each RNA-FISH probe was labeled with one fluorophore Quasar® 570 (Cy3™ Replacement) or CAL Fluor Red 610 (Alexa Fluor® 594 Replacement). Stellaris® FISH probes purchased at Biosearch Technologies, Novato, USA.

Index	Name Probe	Sequence (5' to 3')	Start Position	End Position	Length (nucleotides)
1	Clb5_yeast_570_1	CTGCTCATGGTCGTGGTTCT	8	27	20
2	Clb5_yeast_570_2	CACAACTGCCTCTCATTTTCAT	56	77	22
3	Clb5_yeast_570_3	ATCCTGAACCTGCTGCTTAC	137	156	20
4	Clb5_yeast_570_4	CTGTTAAAGCCCTTCTTGGT	162	181	20
5	Clb5_yeast_570_5	CTCTTGTTCTGGCTTAAAGGAT	200	221	22
6	Clb5_yeast_570_6	CTTCGTACTTTGGCCGCCTT	238	257	20
7	Clb5_yeast_570_7	ACGGCGCTAACAATAGGTC	272	290	19
8	Clb5_yeast_570_8	TGCTCTGCTGCCGTTCGAT	314	332	19
9	Clb5_yeast_570_9	TGTTCACTATCGAAGCAGCAT	368	388	21
10	Clb5_yeast_570_10	ACTCACTCCTTCAGCGTCTA	401	420	20
11	Clb5_yeast_570_11	TCTAGGTCCTGCCAGCCTAC	427	446	20
12	Clb5_yeast_570_12	GCTACCATTGCAGTATCATCTTT	457	479	23
13	Clb5_yeast_570_13	TTGTGCGATGGTAACGTTTCT	525	545	21
14	Clb5_yeast_570_14	ACTTGGACGTTTTGTCGAGT	552	571	20
15	Clb5_yeast_570_15	GTTCTCATGGAAGGCCTCAA	577	596	20
16	Clb5_yeast_570_16	GCACCTCTACCAGCCAATCC	606	625	20
17	Clb5_yeast_570_17	ACGTTTCCGGATAGCATTGA	636	655	20
18	Clb5_yeast_570_18	TGCCGCGATGAAAAGTGAGG	737	756	20
19	Clb5_yeast_570_19	CGCGCCGTCAGTGATATAAG	797	816	20
20	Clb5_yeast_570_20	TGAGCATGAACATTTCCGCA	840	859	20
21	Clb5_yeast_570_21	CCTTAGGAAATTGAGTGGGTT	889	909	21
22	Clb5_yeast_570_22	ATCATCTGCCTTGGAGATCCT	910	930	21
23	Clb5_yeast_570_23	GGTGGCAGCAGTAGGCAT	974	991	18
24	Clb5_yeast_570_24	GCCATTGCGCTTACGGTAGA	1012	1031	20
25	Clb5_yeast_570_25	CTGTTGGTCATTCTTCTCGC	1042	1061	20
26	Clb5_yeast_570_26	ATGCTGTAGTGTTCCATTCCA	1078	1098	21
27	Clb5_yeast_570_27	ATTGGATCGATACCACCACT	1102	1121	20
28	Clb5_yeast_570_28	ATGCAGAGAGACTGAAACGC	1132	1151	20
29	Clb5_yeast_570_29	GTTTTGGAACTAGCGATGTCTTT	1162	1184	23
30	Clb5_yeast_570_30	TGGAAATAAACAGAGCCATACCT	1222	1244	23
31	Clb5_yeast_570_31	GCATTTCGGATGTACACCACT	1253	1273	21

3.2.3.3 Preparation of cells, hybridization and washing for RNA-FISH

The preparation of yeast cells for RNA-FISH differs from established protocols for mammalian cells mainly because of yeast cells having not only a plasma membrane as mammalian cells, but also a cell wall. Exponentially growing yeast cells were fixed with PFA and The cell wall was enzymatically digested (this step is also called "spheroplasting"). Resulting spheroplasts were stored in 70% ethanol, which leads to permeabilization of the plasma membrane in order to enable the RNA-FISH probes to enter the cells and to hybridize to the RNA molecules. The hybridization was done with the cells attached to coated coverslips or with the cells in solution in Eppendorf tubes. The hybridization on coverslips was more adapted to small amount of samples (e.g. RNA-FISH experiment with MS2_loop_FISH on MS2 tagged gene or test experiment for the specificity of a RNA-FISH probe set for a single gene) since this protocol required more manipulation of the fragile coverslip with forceps and larger amount of liquids per sample than the protocol with hybridization in Eppendorf tubes. In contrast the protocol with hybridization in Eppendorf tubes was well adapted to large amount of cells and large amount of samples (e.g. RNA-FISH experiment on *SIC1*, *CLN2* and *CLB5* under normal growth conditions and hyperosmolarity). The distinction between the two protocols is explained in Table 11 and in the following detailed protocol.

Table 11. Comparison between the RNA-FISH protocols with the hybridization step made on microscope coverslips and made in Eppendorf tubes.

Protocols with hybridization on microscope COVERSLIPS	Protocols with hybridization in Eppendorf TUBES
Cell culture + Cell fixation in tubes	
Spheroplasting in tubes = Cell wall removal	
Adherence on microscope coverslips	-
Cell membrane permeabilization in 70% ethanol at -4°C or at -20°C for long term storage	
Washing + Hybridization RNA-FISH probes on RNAs for 4 hours at 37°C. Note: the amount of cells was much higher in the Eppendorf tubes than on the microscope coverslips also the concentration of the RNA-FISH probes used in the hybridization made in Eppendorf tubes (0,25 μM) was also much higher than in the protocol with the hybridization made in microscope coverslips (0,025 μM)	
Washing	
-	**Adherence on microscope coverslips**
DAPI staining of the nucleus + Mounting on slides	
Microscopy	
Storage (Middle- or long-term storage at 4°C or -20°C, respectively)	

- Pre-treatment and coating of the microscope coverslips.

In order to remove any dirt or residual fat, microscope coverslips (⌀ 2,0 cm) were boiled in ddH_2O containing 10 mM HCl for 20 min. The microscope coverslips were rinsed ten times with ddH_2O and directly further processed or stored in 70% ethanol at 4°C for long-term storage. Microscope coverslips were coated with poly-L-lysine or concanavalin A to allow the cells to attach and facilitate the microscopy. Microscope coverslips were air-dried on paper tissues and were soaked in 1x poly-L-lysine diluted in ddH_2O or 1x concanavalin A diluted in ddH_2O for 10 min. Afterward coated coverslips were air-dried and the coating procedure was repeated twice. Microscope coverslips were directly employed or stored at room temperature (RT) protected from dust for several months.

- Preparation of the cells.

Cells were grown as previously described. For fixation 32% (w/v) paraformaldehyde (PFA) stock solution was added to the cell culture at a final concentration of 4% PFA and incubated for 45 min at RT. Cells were washed three times with 10 mL of ice-cold 1x buffer B and centrifuged at 2 000 g for 5 min at 4 °C after each washing. Cells were resuspended in 1 mL of spheroplasting buffer for 15 min at 30 °C and frequently inverted. The spheroplasting procedure partially hydrolyses the glucans contained in the yeast cell wall. The removal of the cell wall was monitored with a light microscope and wide-field illumination as spheroplasted cells have clear boarders and less contrast than the intact cells. The fragile spheroplasts were centrifuged for 4 min at 800 xg at 4 °C and washed once in 2 mL of ice-cold 1x buffer B.

- Adherence on microscope coverslips (at this stage in the case of hybridization made on microscope coverslips or after the hybridization and washing in the case of hybridization made in Eppendorf tubes)

Coated microscope coverslips were placed into a well of a 6-well tissue culture plates (Becton Dickinson, Franklin Lakes, USA) with their coated sides on the top. Cells were resuspended in 2 mL of 1x buffer B and 150 µL were used to cover the surface of a coated poly-L-lysine coverslip. The six-well dish was incubated for 30 min up to 1 hour at 4 °C to allow the cells to adhere to the coverslips. 5 mL of ice-cold 1x buffer B were slowly put in each well and aspired to remove the cells that were not attached to the microscope coverslips.

- Cell membrane permeabilization

Subsequently 70% (v/v) ethanol (2 mL in the eppis or 5 mL in the well) was added to the cells and incubated at least 20 min at -20°C. Ethanol permeabilizes the cell membrane therefore during hybridization the RNA-FISH probes could enter into the cells and bind to the mRNA molecules. Cells could be kept in this state in 70% ethanol at -20 °C for long-term storage up to several months.

- Hybridization

NOTE 1: For the subsequent steps forceps were used to manipulate the microscope coverslips. Liquids were slowly dropped off into and then aspired from the well, in which the coverslips were placed. If Eppendorf tubes were used, liquids were exchanged after centrifuging the tubes 4 min at 1500g at 4°C.

After the incubation in ethanol the cells were rehydrated in 2x saline-sodium citrate buffer (2x SSC) twice for 5 min at RT. Afterward the cells were incubated in hybridization washing solution (2x SSC / 10% (v/v) deionized formamide) for 15 min at RT and this solution was later replaced by a hybridization buffer containing the RNA-FISH probes. The hybridization was carried out for 4 h at 37 °C in the dark. The deionized formamide in the hybridization buffer loosens existing mRNA-protein interactions and lowers the melting temperature of the nucleotides thus allowing the probes to bind to the mRNA molecules.

NOTE 2: In our initial protocol we mixed per coverslide 10 ng of RNA-FISH probes with 4 µL of 10 mg/mL DNA competitor mix and dried the mixture in a Vacufuge at 25 °C for at least 30 min as described in (Trcek et al., 2012). *The dried mixture was then resuspended in 25 µL of hybridization solution and dropped off on the cells. This step was thought to enhance the binding of probes with the DNA probes and therefore the entrance of the RNA-FISH probes into the cells. Removal of this additional step did not result in any significant differences in the images or extracted numerical RNA abundances.*

- *Washing*

After addition of FISH probes the samples have to be protected from the light. The cells were washed three times with hybridization washing solution with intermediate 15 min incubation steps at 37° C in the dark. Subsequently the cells were then washed with 0,1% (v/v) Triton X-100 in 2x SSC at RT, while gently shaking on an orbital shaker for 5 min and protected from the light. Finally, the cells were washed twice with 1x SSC for 15 min at RT with gently shaking on an orbital shaker.

- Adherence on microscope coverslips (at this stage in the case that hybridization was made in Eppendorf tubes. Adherence on coverslips were made earlier after the spheroplasting in the case that hybridization was made on microscope coverslips)

Coated microscope coverslips were placed into a well of a six-well tissue plate in the coated sides on the top. Cells were resuspended in 2mL of 1x SSC and 150 µL were used to cover the surface of a coated coverslip. Afterwards the six-well dish was incubated for 30 min up to 1 hour at 4 °C to allow the cells to adhere to the coverslip. 5 ml of ice-cold 1x SSC were slowly put in the well and aspired to remove the cells that were not attached to the microscope coverslips.

- DAPI staining and Mounting

Cells were incubated in DAPI solution (0,5 µg/mL DAPI solution in 1x PBS-/-) for 5 min and washed with 1x PBS-/-. Coverslips were mounted onto microscope slides with 3-5 µL per coverslip of mounting medium (20% Mowiol + 80% Vectashield). Samples were allowed to dry and harden for 24 hours at RT. Edges were sealed with nail polish if there was no fluorescent protein (TagGFP or mTurquoise) in the sample. Finally, slides were stored at -20°C and could be imaged for several months depending of the employed fluorophore.

NOTE 3: We compared different mounting media. We employed in some experiments RNA-FISH on the cell cycle markers strain and we required for those samples a mounting medium that prevents the bleaching of the chemical fluorophores as DAPI and the labels on RNA-FISH probes (Cy3, Quasar® 570 and CAL Fluor Red 610) as well as of the fluorescent proteins (TagGFP, mTurquoise). The advantages and disadvantages of each medium are summarized in Table 12. We found that a

combination of 20% Mowiol with 80% Vectashield prevented the bleaching of fluorescent proteins as well as of chemical fluorophores.

Table 12. Comparison between the different mounting media tried in this study and used in the RNA-FISH protocol.

Media	ProLong® Gold	Mowiol ® 4-88	Vectashield® Hardset	20%Mowiol +80%Vectashield® Hardset
Company	Molecular Probes, Invitrogen	Sigma-Aldrich	Vector Laboratories	Sigma-Aldrich, Vector Laboratories
Advantages	- works well for chemical fluorophores - solidifies hard therefore can be stored long-term	- water and glycerol based and therefore highly appropriate for fluorescent proteins. - solidifies hard therefore can be stored on long-term	- water based and supposed to prevents rapid photobleaching of fluorescent proteins and fluorescent dyes.	- combines the photobleaching prevention properties of Vectashield for fluorescent proteins and fluorescent dyes and with the properties from Mowiol to enhance the stability of fluorescent proteins and nuclear staining
Disadvantages	- destabilizes fluorescent proteins (for ex. GFP, YFP, mTurquoise)	- no specific anti-fading properties and therefore not appropriate for chemical fluorophores - should be prepared in advance	- may induce diffusion out of nuclei over time of nuclear counterstains as DAPI	- Mowiol should be prepared in advance - Mix of Mowiol and Vectashield® should be prepared fresh
Base	Glycerol based	Water and glycerol based	Water based	Water and glycerol based

3.2.3.4 Microscope image acquisition of RNA-FISH samples

Images of FISH-hybridized yeast cells were acquired in three dimensions with an inverted Olympus IX81 epi-fluorescence microscope with UPlanApo 100X, 1,35 numerical aperture oil-immersion objective (Olympus). Vertical stacks of fifteen images with a *z*-step size of 0,25 µm were acquired using a Clara E Interline CCD camera (Andor) with a 0,0645 µm pixel size. An HBO 100 watts light source was used for illumination. The exposure time for each plane was 1 000 ms for the RNA-FISH probe. In the case of DAPI imaging an exposure time of 25 ms was used. The filter sets were optimized to maximize the collection of emission and to minimize the spectral overlap. The instrument control was accomplished using MetaMorph Software and images were acquired using the associated Multi-dimensional acquisition (MDA) module.

3.2.4 Analysis of microscopy images

3.2.4.1 Semi-automatic quantitative tools for analysis of cell segmentation and mRNA distribution

To process a large number of microscopy images, ensure the reproducibility of analysis and avoid human subjectivity bias, we developed a semi automatic working flow for quantitative analysis of the fluorescence microscopy images. We employed open source and free of charge software and tools (ImageJ, Python, IDL virtual machine) to favor the sharing and further improvement of our analysis protocols within and outside the lab. Our workflows were designed by Aouefa Amoussouvi, Martin Seeger, Lotte Teufel, Szymon Stoma as collaboration between the Molecular Biophysics group of Prof. Andreas Herrmann and Theoretical Biophysics group of Prof. Edda Klipp (Humboldt Universität zu Berlin, Germany).

Software:

- ImageJ, National Institute of Health, Bethesda, USA
- Python (PyQt package), Python Software Foundation, Beaverton, USA
- IDL virtual machine, Exelis Visual Information Solutions, USA
- Cell-ID, Buenos Aires, Argentina (Chernomoretz et al., 2008)

Functions & Plugins:

- Localize, IDL script, Daniel Larson, NIH, Bethesda, USA (Thompson et al., 2002)
- Make Mask Beta 1, run on ImageJ, Robert Singer, Albert Einstein College of Medicine, NYC, USA (Trcek et al., 2012)
- Maximum_ZStackProj_8bitsSave, Focus_ZStackProj_8bitsSave run on ImageJ, this work, Humboldt Universität zu Berlin, Germany
- Spotalyzer, Python script, this work, Humboldt University Berlin, Germany
- IDLmerger, Python script, this work, Humboldt University Berlin, Germany
- SQLite Data Browser, http://sqlitebrowser.org/

Step 0: The 3D z-stacks of bright field and fluorescence images were projected into single 2D images for best focus or maximum intensity projection of each pixel along the z-axis, respectively. We used the ImageJ functions "Focus_ZStackProj_8bitsSave" and "Maximum_ZStackProj_8bitsSave" on the bright field and fluorescent images, respectively, to do these projections as well convert the resulting images from 16 to 8bits images. We further processed with one of our two customer-written workflows.

- Workflow I: "Spotalyzer"

Step 1a: Cell-ID was used for cell segmentation. This tool used the enhanced contrast between the inside and the outside of the cells resulting in a "ring" around the cells in the out-of-focus bright field images.

Step 2a: The fluorescent RNA spots were identified using "find_dots" a customer written function in ImageJ. The "find_dots" function removed the (1) background, (2) inverted the grey color scale, (3) smoothed the intensity and (4) identified the local maxima with the "find-maxima" ImageJ function.

Step 3a: The cell segmentation and the information of the fluorescent spots were merged together with the Spotalyzer Python customer written script.

The cell segmentation and fluorescent spot detection with "Spotalyzer" were not sensitive enough and the handling of information was limited to small samples (approximately hundreds of cells) therefore we developed a second workflow that solved these issues.

- Workflow II: "Localize" and "IDLmerger"

The second workflow is depicted in Figure 19. It involved the cell segmentation tool "Make Mask Beta 1" run on ImageJ, the "Localize" function for fluorescent mRNA detection run on IDL virtual machineFigure 20. Subsequently the customer written "IDLmerger" script run on Python merged the spot and cell information into a SQLite Data Browser database, normalized of the spot intensity and identified of the transcription sites (Figure 19).

Step 1b: Cell boundaries were manually detected and stored in "ROI Manager" (Analyze> Tools> ROI Manager). The list of the cell boundaries was then used to create a mask with the "Make Mask Beta1" plugin.

Step 2b: The "Localize" function detected the fluorescent spots as local maxima from the maximum intensity projection images and fitted each spot with 3D Gaussian mask. The integral of a Gaussian was taken as the numerical value of fluorescent intensity of the related fluorescent spot. „Localize" generated three output files, a summary text file of the detection parameters and numbers of found spots, a image of the detected spots and a text file containing the quantitative features of each spot, i.e. coordinates (x,y), intensity and frame index (Figure 19 and Figure 20). The detection parameters were as follow. The auto bandpass was set to "ON". The photon threshold was adjusted to detect all spots with values between 9 and 14. The black level was set to "local". The "Localize" function was sensitive enough to overcome two critical issues of detecting single fluorescent particles in cells, namely the non-uniform fluorescent background in each cell and the non-uniform fluorescent features, intensity and size, of the particles.

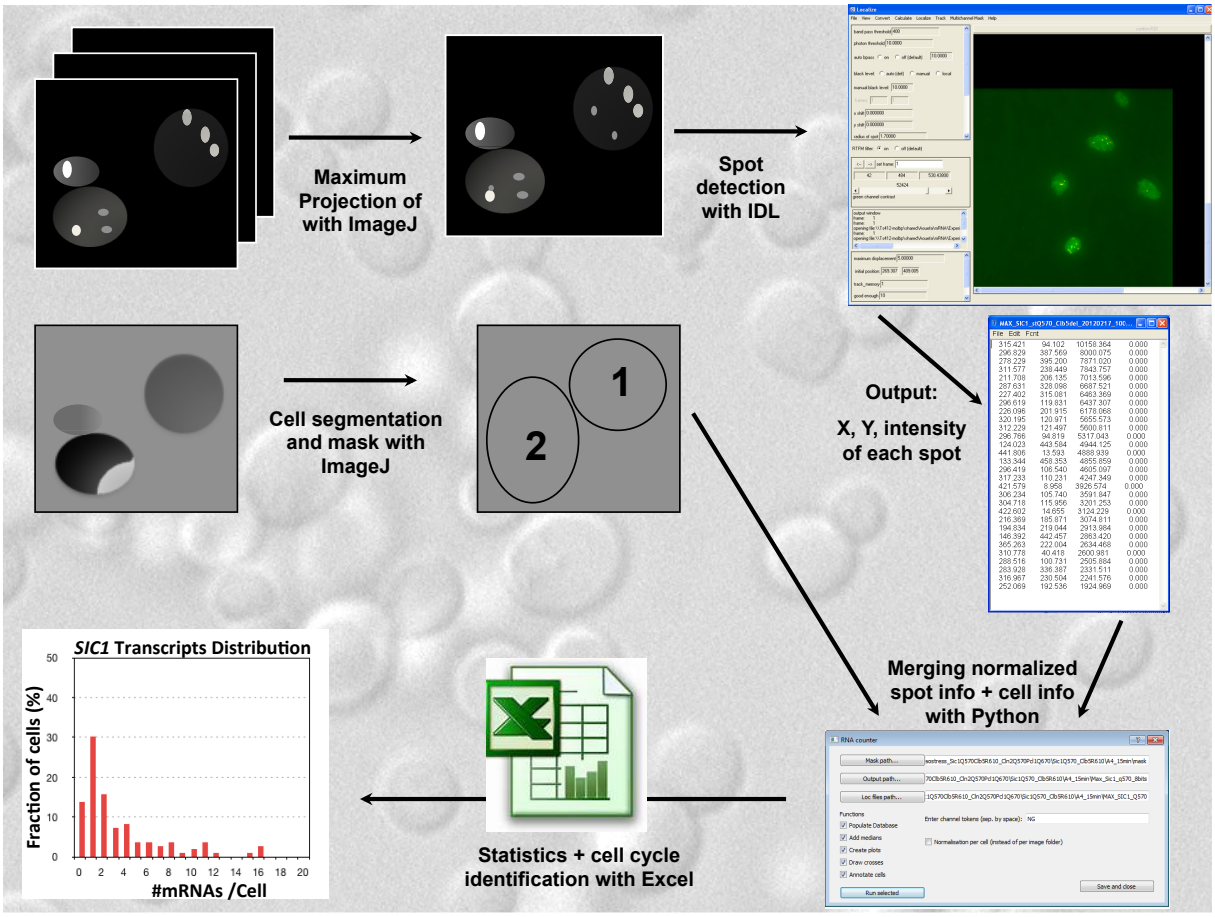

Figure 19. Workflow for microscopy image analysis with IDLmerger.
Stacks of fluorescence images were reduced to a single image by maximum pixel projection with ImageJ. Fluorescent spots of mRNA or spindle pole bodies were detected as local maxima on the projected images with Localize function on IDL. Localize function produced an output file containing a list of the coordinates and fluorescence intensities of each detected spot. In parallel cells were segmented with an ImageJ plugin, which created a mask with the cells coordinates. Cells and fluorescent spots information were merged into a database with a customer written "IDLmerger" Python script, which normalized the fluorescent spot intensity and identified transcript sites. Statistics analysis and cell cycle phase identification were made with Excel.

Step 3b: "IDLmerger" normalized the spot intensity by the median intensity of the list of detected spots to extract the number of mRNA in each fluorescent spot. The median was more robust and representative to the value of a single mRNA fluorescent spot than the average. Indeed some spots of high intensity contained several mRNA molecules and therefore strongly influenced the average and less the median. The spots with less than 50% of the median value were excluded and considered false positives. The rest of the spots were grouped related to their intensities. A spot with an intensity of 50% to 150% of the median value was considered one mRNA molecule. A spot with an intensity of 150 % to 250% was considered two mRNAs and so on (Figure 19). "IDLmerger" identified transcription sites, which were fluorescent mRNA spots containing at least three times the intensity of a single mRNA spot. The fraction of cells with transcription sites (%) was calculated as the ratio of the number of cells with transcription sites to the total number of cells in the experiment. In total between 400 and 1000 cells were analyzed per time point and gene (exact numbers in Supplementary Table S1 in Appendix) and at least 1500 cells per time point for the cell cycle length information from three independent replicated experiments pooled together.

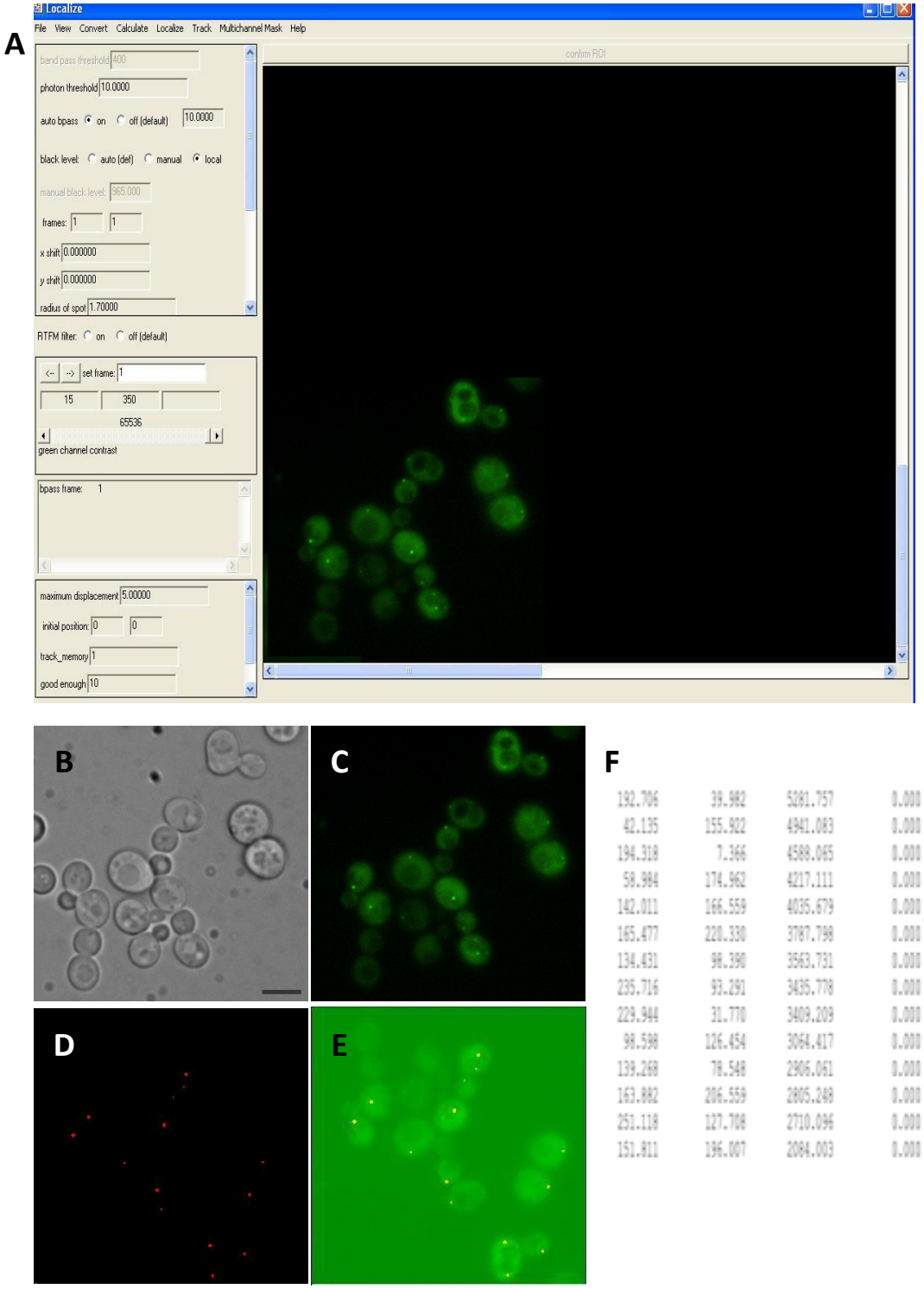

Figure 20. Quantitative localization of mRNA fluorescent spots using Localize.

(A) Snapshot of the graphic user interface of Localize run on IDL® obtained from Daniel Larson, NIH, Bethesda. Localize detected the mRNA fluorescent spots as local maxima and applied on each spot a 3D Gaussian fit. In the left column user could change sensitivity parameters for spots detection. In screen user could see the original image (in green). An example for the analysis is shown in (B-E). (B) Bright field image. Bar scale represents 5µm. (C) Maximum intensity projection image taken as input for Localize. (D) Red dots represent the detected local fluorescent intensity maxima. (E) Overlay of the input image, i.e. maximum intensity projection (C) with the detected fluorescent spots (D). (F) The output text file contained the quantitative features of spot population, i.e. coordinates (x,y), intensity and frame index. The frame index was only useful if the input file was a stack containing several images otherwise frame index was set to 0.

3.2.4.2 Tracking of MS2-CP labeled mRNA in living cells

3D z-stacks of fluorescence images of MS2-CP labeled mRNAs were reduced to a single 2D maximum intensity projection of each pixel, along the z-axis, using ImageJ "Maximum_ZStackProj_8bitsSave" function and further processed with "TrackMate" an ImageJ function (http://fiji.sc/TrackMate).

3.2.4.3 Coefficient of variation for calculation of mRNA and protein noise

The RNA-FISH assays provided distributions of mRNA number per single cell and a coefficient of variation (CV) for each data set was calculated to analyze the cell-to-cell variability, i.e. noise level. The coefficient of variation is a statistical measurement for dispersion of data points around the mean. They enable the comparison of several data series with drastically different means. For a data set with a mean, m ($m \neq 0$), and a standard deviation, s, the coefficient of variation, also called the weighted noise, is the ratio $CV = \frac{s}{m}$. In the theoretical ideal case of a constitutively expressed gene with a transcript distribution following a Poisson process CV equals 1 (Munsky et al., 2012).
Note: We also employed the coefficient of variation for calculation of the simulated mRNA and protein levels.

3.2.5 Stochastic modeling of the G1/S transition and *SIC1*, *CLN2* and *CLB5* gene expression

One of the previously published models of the G1/S transition, a deterministic model considered 52 parameters to represent a large network of biochemical reactions (Barberis et al., 2007). Deterministic modeling is based on based on a system of ordinary differential equations (ODEs) and simulates changes of molecular constants but not of discrete values. Consequently, deterministic modeling is more appropriate to study large numbers as protein levels than the small molecule numbers of mRNAs. At contrary stochastic, also called probabilistic, modeling is based on the chemical master equation (or approximations of it) and enables the study of such small quantities as well as single cell behavior and the resulting cell-to-cell variability within a population (Ko, 1991; Paulsson, 2005; Wilkinson, 2006). The rates of the biochemical reactions depend on the concentration of a species in the case of deterministic models and on the number of molecule of this species in the case of stochastic modeling.

We developed in this study a first stochastic model focusing only on the molecular abundances of the CDK inhibitor, Sic1, and the activator of DNA replication, Cdk1-Clb5, and investigated the effects of *SIC1* molecules number on the initiation timing of DNA replication under optimal growth conditions (Barberis et al., 2011). We, then, expended the system into a second model to include the initiator of budding, Cdk1-Cln2, and the activation of Hog1 upon osmotic stress (Amoussouvi et al., 2018). Our stochastic models were designed in collaboration with the Theoretical Biophysics group of Prof. Edda Klipp (Humboldt Universität zu Berlin, Germany) and based on our experimental results, which were conducted in the Molecular Biophysics group of Prof. Andreas Herrmann (Humboldt Universität zu Berlin, Germany).

3.2.5.1 Stochastic model of the G1/S transition centered on *SIC1*.

The following reduced description of our first stochastic model is based on our published manuscript (Barberis et al., 2011):

Barberis, M., Beck, C., Aoussouvi, A., Schreiber, G., Diener, C., Herrmann, A., and Klipp, E. (2011). A low number of SIC1 mRNA molecules ensures a low noise level in cell cycle progression of budding yeast. Mol. Biosyst. 7, 2804–2812. DOI: 10.1039/c1mb05073g

Contributions: Aouefa Amoussouvi (AA) and Gabriele Schreiber performed the molecular cloning, designed and conducted the experiments and analysis of experiments. Christine Klaus assisted the molecular cloning. Matteo Barberis (MB), Claudia Beck (CB), Christian Diener (CD) designed, programmed the stochastic model. MB, CB, CD and AA analyzed the results obtained from the simulations. Andreas Herrmann and Edda Klipp provided guidance and expertise.

- Description of the model

We focused on a reduced system that only considered the molecular abundances of Sic1, the Cdk-inhibitor, and Cdk1-Clb5,6, the activator of DNA replication. We addressed the influence of low *SIC1* mRNA copies in a cell on the Sic1 protein amount, on Sic1 protein noise and on the timing of the G1/S transition. This latter phenomenon is highly dependent on the inhibition of Sic1 via its interaction with Cdk1-Clb5,6.

The stochastic model of the G1/S transition has been implemented with Cain, a software built to simulate chemical model systems (http://cain.sourceforge.net/), by using mass action kinetics for all reactions (see section 3.2.5.1 in Material and Methods). The parameters $re1$ to $re7$ represent the degradation and production rates relative to Sic1 and Clb5,6 (Table 14 in RESULTS I). Numerical values of the constant parameters were taken from the literature. Rate constants for reactions $re3$ to $re6$ were taken from the G1/S network reported in the literature (Barberis et al., 2007) and translated into stochastic rate constants according to the procedure described by Gillespie (Gillespie, 1977). Consequently, $k3$ and $k5$ were taken directly having already the right dimension, $k4$ was divided by the volume of the cell and the Avogadro constant and $k6$ was multiplied by 1 ($k6a$), 10 ($k6b$) or 100 ($k6c$) *CLB5,6* mRNA molecules assuming a first-order reaction. Besides, parameters $k1$ and $k2$ were used to generate a specific *SIC1* mRNA amount. A volume of about 65 fl has been considered and divided into 25 fl and 40 fl for daughter and mother cells, respectively (Aldea et al., 2007) (http://bionumbers.hms.harvard.edu/bionumber.aspx?s=y&id=100452&ver=1&lnsh=1; http://bionumbers.hms.harvard.edu/bionumber.aspx?s=y&id=101794&ver=7&lnsh=1).

Initial molecule numbers for Sic1 protein and *SIC1* mRNA were taken from the literature (Di Talia et al., 2007) and divided between daughter and mother cells according to 25/65 and 40/65 ratios. We initiated the production of Clb5,6 after a characteristic time for G1 phase length (t_{G1}). The complete set of initial values is summarized in Table 15 for the case of a single daughter cell and in Table 16 for the case of a mother and daughter cells. We implemented this assumption in Cain by setting events and the first reaction method (Wilkinson, 2006). Moreover, we set $k6b$ = 3 min^{-1} and determined 10 trajectories for a time of 250 min. The number of frames was set to 125.

- Calculation of coefficients of variation for *SIC1* mRNA and protein levels

We compared the coefficient of variation of *SIC1* mRNA, CV_1, with the coefficient of variation of Sic1 protein, CV_2. Furthermore, we defined a ratio $Q = CV_2/CV_1$ as the percentage of how much larger is the noise of Sic1 protein compared to the noise of *SIC1* mRNA. In order to simulate a large number of trajectories for varying parameters (initial number of *SIC1* mRNAs, $k2$) we ported a fast implementation of the Gillespie algorithm (Mauch and Stalzer, 2011) to a Graphics Processing Unit (GPU) (for details of the algorithm for the GPU architecture see Supplementary Figure S 1 and Supplementary Figure S 2 in Appendix 1). Modifying some aspects of the algorithm in order to fully utilize the hardware of the GPU together with efficient memory management we ended up with an algorithm simulating more than 1,8 billion reactions per second. 100 000 trajectories were calculated for each simulation for a daughter cell, and mean and standard deviation were obtained at each time point. To estimate the value of Q and CV_2, the value corresponding to the first observed peak was always selected in the case of multiple local maxima.

- Implementation of cell growth.

The cell growth for both daughter and mother cells was implemented in the software Cain. The volume was not constant but time dependent therefore the second-order reaction $re4$, i.e. the complex formation of Sic1 with Clb5, was transformed manually. Indeed $re4$ resulted in the probability of the molecules to be in a reaction-distance and in a volume independent probability of interaction. For two molecules with independent and uniformly distributed positions in a sphere volume, the probability of both being in reaction-distance was inversely proportional to the volume (Wilkinson, 2006). The other reactions were not affected by the cell volume and were retained. Considering that the volume increases roughly linearly (Aldea et al., 2007) and doubles during the G1 phase, the following equation was derived for the volume $V(t)$ at the time point t_1:

$$V(t_1) = V_0 + t_1 \cdot \frac{V_0}{t_{G1}}$$

where t_{G1} was the duration of the G1 phase and V_0 the initial volume. Hence, the volume at t_{G1}, $V(t_{G1})$ was two times V_0. On this basis, the volume of the daughter cell at a time point t_1 was equal to:

$$V_D(t_1) = 25\,fl + t_1 \cdot 0.68\,fl \cdot \mathrm{min}^{-1}$$

and the volume of the mother cell was equal to:

$$V_M(t_1) = 40\,fl + t_1 \cdot 2.50\,fl \cdot \mathrm{min}^{-1}$$

Thus, the probability for $re4$ to occurred at the time point t_1 resulted in:

$$P(re_4, t_1) = Sic1 \cdot Clb5 \cdot \frac{k4}{V(t_1)}$$

Nevertheless, the probability for complex formation of Sic1 with Clb5,6 described as reaction $re4$ was very high because of the order of magnitude of volumes (denominator), hence the Sic1–Clb5,6 complex formed instantaneously.

3.2.5.2 Stochastic model of the G1/S transition focusing on *SIC1*, *CLN2* and *CLB5* and effect of hyperosmolarity

The following description of our second stochastic model is based on our manuscript (Amoussouvi et al., 2018):

Aouefa Amoussouvi, Lotte Teufel, Matthias Reis, Martin Seeger, Gabriele Schreiber, Andreas Herrmann, and Edda Klipp, Transcriptional timing and noise of yeast cell cycle regulators – a single cell approach (2018). npj Systems Biology and Applications. 4, 1, 1-36. DOI: 10.1038/s41540-018-0053-4

Contributions: Aouefa Amoussouvi (AA), Lotte Teufel (LT) and Gabriele Schreiber (GS) designed and conducted the experiments. AA, LT and Martin Seeger (MS) designed the microscopy image analysis workflow. MS programmed the microscopy image analysis workflow. Matthias Reis (MR) and AA designed the stochastic model for parameter estimation. MR programmed the stochastic model for parameter estimation. Edda Klipp (EK), Julia Katharina Schlichting (JKS), AA and LT designed the stochastic model for mRNA and protein simulations. EK and JKS programmed the stochastic model for mRNA and protein simulations. AA, LT, MR, JKS and EK analyzed the data. EK and AH provided guidance and expertise.

- Description of the model

This second stochastic model integrates the gene expression regulation of the three main regulators of the G1/S transition, namely *SIC1*, *CLN2* and *CLB5,* and their changes under hyperosmotic stress. Hyperosmotic stress activates Hog1, which stabilizes Sic1 via phosphorylation at a Threonine[173] and inhibits *CLN2* and *CLB5* transcription (Hohmann, 2002; Saito and Posas, 2012).

The reactions of the model are described in Table 17 in RESULTS II and have been stochastically simulated using the Gillespie algorithm (Gillespie, 1977). For simulation of mRNA time courses, 2000 cells have been simulated. For analysis of the full network, 100 cells have been simulated. In order to have comparable values at comparable time points, snapshots of the system have been taken every minute, i.e. the current molecule numbers at every full minute have been recorded. The resulting lists of 129 values for one cell cycle or 150 values for one simulation period (starting from Anaphase of one cell cycle to the T/C phase of the next cell cycle) have then been used to calculate means, standard deviations and coefficients of variation.

To analyze the general model behavior, we used the moment closure method (see Section D in Appendix 2) and derived expressions for mean values and variation of all model components. They have been used to determine time courses of noise of each model component.

- Parameter values

In the model, signals S_1 – S_3 indicate the periods of high expression of *SIC1* (S_1) as well as *CLN2* (S_2) and *CLB5* (S_3). The fitting of the experimental mRNA distributions obtained with RNA-FISH enabled to extract kinetic parameters of mRNA production rate ($k_{ih,l}$) in high (h) or low (l) expression phases, mRNA degradation rate (p_i) and timing of the beginning ($t_{Si,0}$) and the end ($t_{Si,e}$) of the high and low expression phases (see Appendix 2 Parameter estimation). More precisely the parameter values for rates and transcription start and stop times have been fitted to best reproduce (i) the time-resolved frequency distribution of *SIC1*, *CLN2*, and *CLB5* mRNA (Supplementary Table S3, Supplementary Table S9, Supplementary Table S15 in Appendix 4 and Figure 35, Figure 37B in RESULTS II)), (ii) the overall, non-time resolved distributions of these mRNAs (Figure 32B in RESULTS II), (iii) the normalized time courses of Sic1, Cln2, and Clb5 proteins as given in Adrover et al. (Adrover et al., 2011) and the average protein abundances of Sic1, Cln2, and Clb5 ((Ghaemmaghami et al., 2003): Sic1 768, Cln2 1270, Clb5 521 molecules per cell). The resulting parameter values are given in (Table 17 in RESULTS II).

Under hyperosmolarity the model assumed that the high-level transcription periods of *CLN2* and *CLB5* (mainly during late G1) were interrupted during the period of osmotic adaptation and resumed afterwards (Figure 44 in RESULTS II). Since all other model parameters were already fitted for the non-stress scenario, the remaining parameters to extract were the periods of transcriptional repression, t_d , from the experimental mRNA distributions and means for *CLN2* and *CLB5*, respectively. To determine these values, we tested 676 combinations of $t_{d,CLN2}$ and $t_{d,CLB5}$ ranging from 5 to 30 minutes for each gene. We run 200 simulations for 200 random stress time points for each combination and compared the simulated distributions 0, 15, 30, 45, 60 and 90 minutes after stress with our experimental data. The best combination of $t_{d,CLN2}$ and $t_{d,CLB5}$ minimized the total squared distance between simulated and experimental mRNA distributions during individual cell cycle phases and at different time points upon stress (Supplementary Figure S 11, Supplementary Figure S 12, Supplementary Figure S 13, Supplementary Figure S 14).

4. RESULTS I: VISUALIZING *SIC1* AND *CLN2* RNPs WITH MS2-CP SYSTEM AND STOCHASTIC MODELING OF G1/S TRANSITION CENTERED ON *SIC1*

In the first part of RESULTS I, I introduce the tagging of *SIC1* and the *CLN2* genes with the *in vivo* MS2-CP system (section 4.1). Single cell visualization of the MS2-CP-tagged *SIC1* and *CLN2* mRNA allowed us for qualitative analysis of their respective mRNA expression levels (section 4.2) and tracking of *SIC1* molecules (section 4.3) in an asynchronous cell population. The term of mRNA particles and RNP (Ribo-Nucleo-Protein complex), i.e. a complex of RNA(s) and protein(s), are used to refer to the fluorescent particles tagged with MS2-CP system. We employed the elutriation method to synchronize a cell culture in early G1 and monitored the dynamics of MS2-CP-GFP(x3) tagged *SIC1* mRNA particles level (section 4.4). In the last part of this chapter I describe the minimalistic stochastic model based on our experimental observations, which studies the influence of *SIC1* expression level on the timing of the G1/S transition (section 4.5). Parts of this chapter refers to our published article (Barberis et al., 2011):

Matteo Barberis, Claudia Beck, Aouefa Amoussouvi, Gabriele Schreiber, Christian Diener, Andreas Herrmann and Edda Klipp. A low number of *SIC1* mRNA molecules ensures a low noise level in cell cycle progression of budding yeast. *Mol. Biosyst.* **7,** 2804–12 (2011). doi: 10.1039/c1mb05073g

Contributions: Aouefa Amoussouvi (AA) and Gabriele Schreiber performed the molecular cloning, designed and conducted the experiments and analysis of experiments. Christine Klaus assisted the molecular cloning. Matteo Barberis (MB), Claudia Beck (CB), Christian Diener (CD) designed, programmed the stochastic model. MB, CB, CD and AA analyzed the results obtained from the simulations. Andreas Herrmann and Edda Klipp provided guidance and expertise.

4.1 Establishment of stable MS2-CP yeast strain constructs

To detect and track *SIC1* and *CLN2* mRNA molecules in single yeast cells we applied the *in vivo* MS2-CP mRNA tagging system. We used an established protocol for yeast to genomically incorporate twelve MS2 hairpin loops in the 3'UTR of *SIC1* and *CLN2* and observed their endogenous expressions (Haim-Vilmovsky and Gerst, 2009; Haim et al., 2007). To find the most appropriate setting for our biological question we established constructs with different fluorescent markers attached to the MS2-CP such as a triplet of GFPs (MS2-CP-GFP(3x)), YFP (MS2-CP-YFP) and the tetracystein system (MS2-CP-Tetracystein + FlashDye). In addition we also compared the GFP construct with and without Nuclear Localization Signal (NLS) (MS2-CP-GFP-NLS). The qualitative comparison of the advantages and disadvantages of the different constructs is summarized in Table 13.

Table 13. Comparison of the MS2-CP system constructs.

In the MS2-CP system, the mRNA is tagged with a series of hairpin loops, binding sites for MS2-CP. The MS2-CP is attached with a fluorescent label. The table shows the advantages and disadvantages of the constructs of MS2-CP system using different labels as fluorescent proteins (MS2-CP-GFP(3x), MS2-CP-YFP) or small fluorescent dyes (MS2-CP-Tetracystein + FlashDye). We also compared the GFP construct with and without NLS (Nuclear Localization Signal) (MS2-CP-GFP-NLS).

Constructs	MS2-CP-GFP(x3)	MS2-CP-GFP-NLS	MS2-CP-YFP	MS2-CP + Tetracystein System
Advantages	Strong and stable brightness	No background in the cytoplasm, no cytoplasmic aggregate	YFP is intrinsically monomeric, no polymerization, less aggregates	no aggregate
Disadvantages	High background, may tend to build aggregates	Nuclear signal very bright compared to the RNP signal. Analysis difficult	Bleaches fast, limited observation time	Requires additional incubation and washing steps, limited observation time due to the dilution of the fluorophores in the cell volume

Native GFP tends to dimerize at high concentration and to form aggregates (Yang et al., 1996). In order to control that we observed endogenous RNPs and no self-forming polymers of MS2-CPs, we compared the GFP(x3) constructs with the one with YFP, which is natively monomeric and for this reason does not form aggregates. We obtained similar patterns however the signal of the construct using YFP quickly bleached and was therefore not adapted for recording of microscopy images that required high and long illumination as it is the case in this study.

For the tetracystein system we exchanged the GFP(x3) against the small tetracysteine tag, which forms a three-dimensional structure. This structure has a high binding affinity for a specific FlashDye, a synthetic fluorescent probe, which needs to be incorporated into the cells. This system was not appropriate for our experiments as the long incubation (12 hours) and washing (1hour) times were comparable or longer to a full cell cycle. In addition the FlashDye fluorophores were diluted over time as the cells grew. This cellular dilution lead to uncertainty that all tetracystein binding sites were saturated with FlashDye probes. The tetracystein system resulted in low signal to background ratio and less RNP particles were observed than in the case of fluorescent protein (GFP(3x) and YFP).

The addition of a NLS in the GFP construct lead the unbound MS2-CP-GFP complexes to the nucleus and only the complexes attached to the hairpins of modified *SIC1* or *CLN2* mRNA could leave the nucleus and enter into cytoplasm. As a result we observed low fluorescent background signal in the cytoplasm and a high signal in the nucleus. The fluorescence of the nucleus was so bright that it blew out in the entire cell and we detected RNPs in rare cells. Therefore, we did not use the NLS further. As a consequence of the described advantages and disadvantages of each construct we employed in the following experiments the construct with trimer GFP without NLS (MS2-CP-GFP(x3)).

To test whether the genomic manipulation of the 3'UTR of *SIC1* and *CLN2* and the expression of the MS2-CP-GFP(x3) affected cell cycle progression, we measured the growth of wild type (WT) strain and strains modified with the MS2 system, e.g. genomic integration of the MS2 hairpins and transformation with the MS2-CP-GFP(x3) plasmid, in non-inducing (SD medium lacking histidine) and inducing (SD medium lacking histidine and methionine) conditions for the MS2-CP-GFP(x3) plasmid. Indeed MS2-CP-GFP(x3) plasmid has a histidine selection marker und the expression of MS2-CP-GFP(x3) is triggered by a methionine promoter. Similar growth curves were observed for the wild type and the modified strains. The growth of the three strains was slower in inducing medium (SD medium lacking histidine and methionine) than in non-inducing medium (SD medium lacking histidine) (Figure 21).

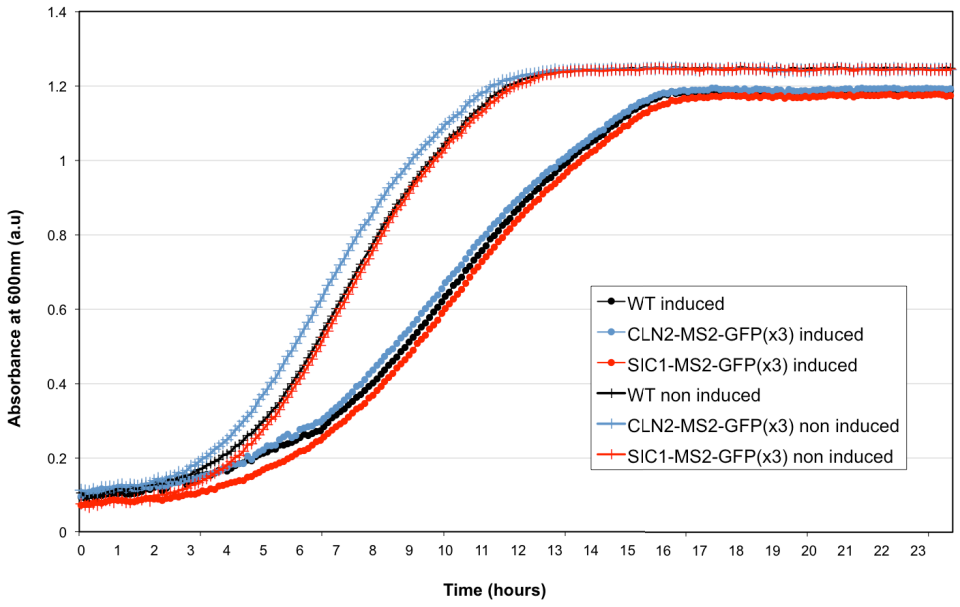

Figure 21. ***SIC1*** **and** ***CLN2*** **RNA tagging with MS2 system does not affect cell growth.**
Cell growth of the wild type (WT) and the mutant strains with MS2-CP system tagged *SIC1* and *CLN2* RNA were similar. The three strains grew slower in inducing medium (SD lacking histidine and methionine, crosses curves) than in non-inducing medium (SD lacking histidine, dotted curves). Cell growth was proportional to the absorbance at 600nm of the cell culture, which was measured by a plate reader at 30°C every 10 min for 24 hours.

4.2 Visualization of *SIC1* and *CLN2* RNPs with MS2-CP system revealed low expression levels

Since the fluorescent RNPs were scattered within the cellular lumen we acquired 3D z-stacks of images with an epi-fluorescence microscope and processed these stacks into 2D using a maximum intensity projection of each pixel along the z-axis. The wild type cell showed low signal due to auto-fluorescence (Figure 22A). The MS2-CP-GFP(x3) plasmid generated a fluorescent background within the transformed cells (Figure 22B). In contrast, in the modified cells with twelve MS2 hairpin-binding sites tagging *SIC1* or *CLN2* and the plasmid expressing MS2-CP-GFP(x3), we observed distinct fluorescent mRNA particles, which contrasted with the fluorescent background of the cells (Figure 22C to H).

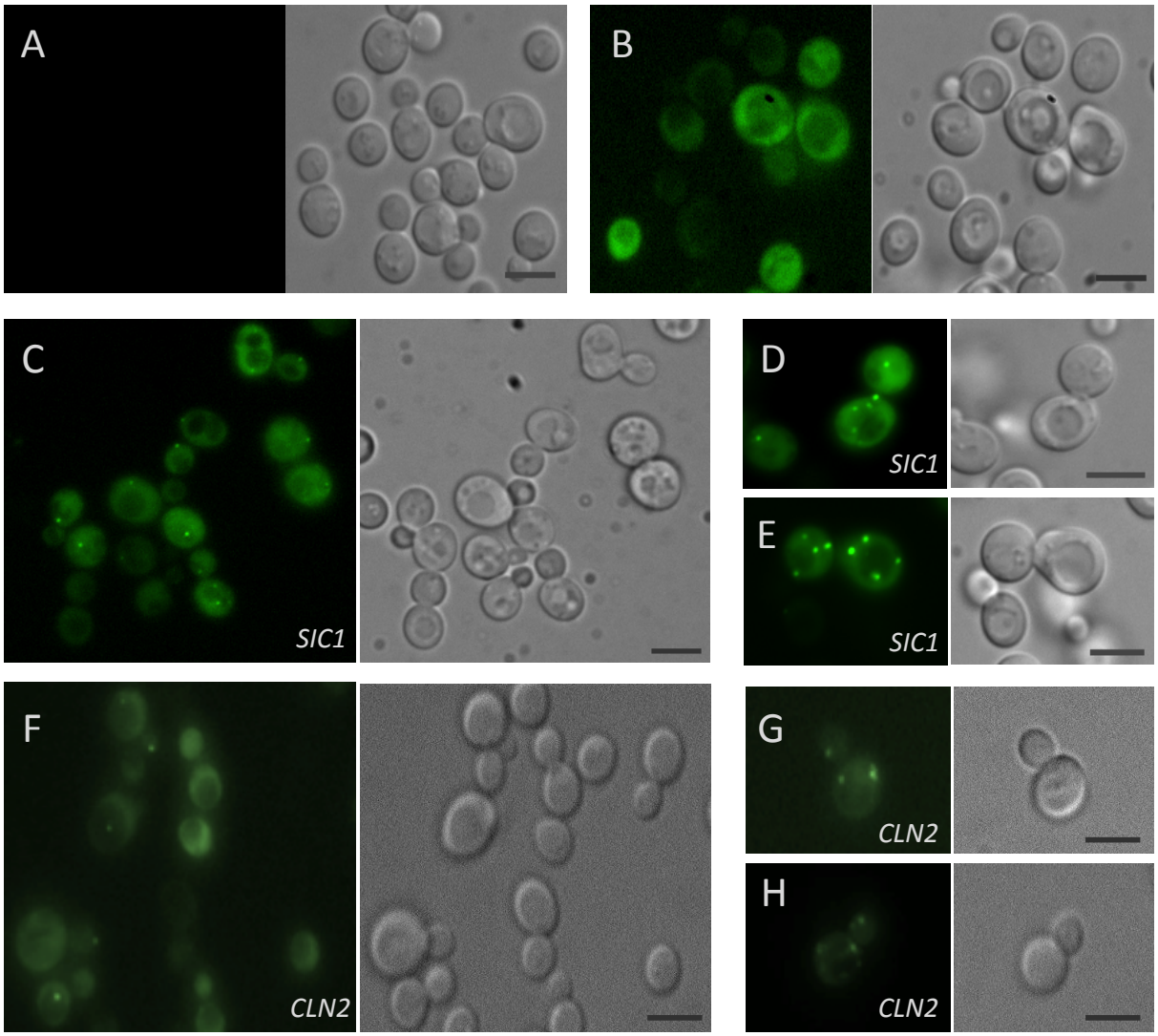

Figure 22. Visualization of *SIC1* and *CLN2* RNP molecules in single yeast cells.
For each set of image, fluorescence microscopic (left) and Differential Interference Contrast (DIC) (right) images of wild type cells and cells genetically modified with the MS2 system are shown. The cells were fixed in 4% paraformaldehyde to prevent the RNPs to move during the microscopy acquisition and therefore to prevent multiple imaging of the same RNPs. The fluorescence image was obtained by projecting the maximum intensity of a fluorescent image stack. (A and B) show negative controls of the specificity of the MS2-CP-GFP(x3). (A) Wild type cells show slight auto-fluorescence, whose signal was used as threshold. (B) Cells transformed with the MS2-CP-GFP(3x) plasmid showed GFP fluorescence. (C to H) Fluorescent granules of MS2-CP-GFP(3x) bound to the MS2 loop sequences of either *SIC1* (C to E) or *CLN2* (F to H) mRNAs. (C and F) show typical images where the majority of the cell population contained none or one *SIC1* or *CLN2* RNPs. (D, E, G and H) show few cells that contained several *SIC1* or *CLN2* RNPs. Scale bar represents 5 µm.

Populations of yeast cells mutated with the MS2 tagging system applied either on *SIC1* or *CLN2* mRNA were studied in the logarithmic growth phase. This asynchronous population contained individual cells at different stages of the cell cycle and the majority of cells contained either none or only one fluorescent RNP (Figure 22C and F). A small fraction of cells contained several fluorescent RNPs, up to 10 (Figure 22D, E, G and H). Qualitatively almost all cells had one *SIC1* RNP whereas in the case of *CLN2* a larger population contained no *CLN2* RNP. This indicated that *SIC1* had a basal presence throughout the cell cycle whereas *CLN2* expression was inactive in a large fraction of cells. The RNPs had heterogeneous fluorescence intensities and sizes therefore we assumed that the observed RNPs are not single mRNA but instead contained several mRNAs.

4.3 *SIC1* RNPs trajectory and localization studied with MS2-CP system

4.3.1 MS2-CP system enables visualization of *SIC1* RNPs localization and trajectory in living cells

We took advantage of the MS2 labeling method, which enables *in vivo* measurements, to assess the transport and localization of *SIC1* RNP. We monitored single *SIC1* RNPs in living cells for several minutes. We observed distinct categories of motions. A fraction of *SIC1* RNP particles were relatively static and their trajectories oscillated in a restricted volume. This is depicted by the *SIC1* RNP particle in the bud of the cell (Figure 23). A second category of *SIC1* RNP particles were more mobile and moved randomly in the entire cellular lumen without any clear trajectory, suggesting that diffusion drove of these moves. The *SIC1* RNP particle in the large mother cell in Figure 23 is an example of such undirected moves. To note, these movements were limited in the peripheries of the cell due to the presence of the vacuole (darker area in the center of the cell in Figure 23). Finally, we also observed some faster and more directed motions inside a cell as well from a mother cell into a daughter cell. One example of such directed motion is described in the following section.

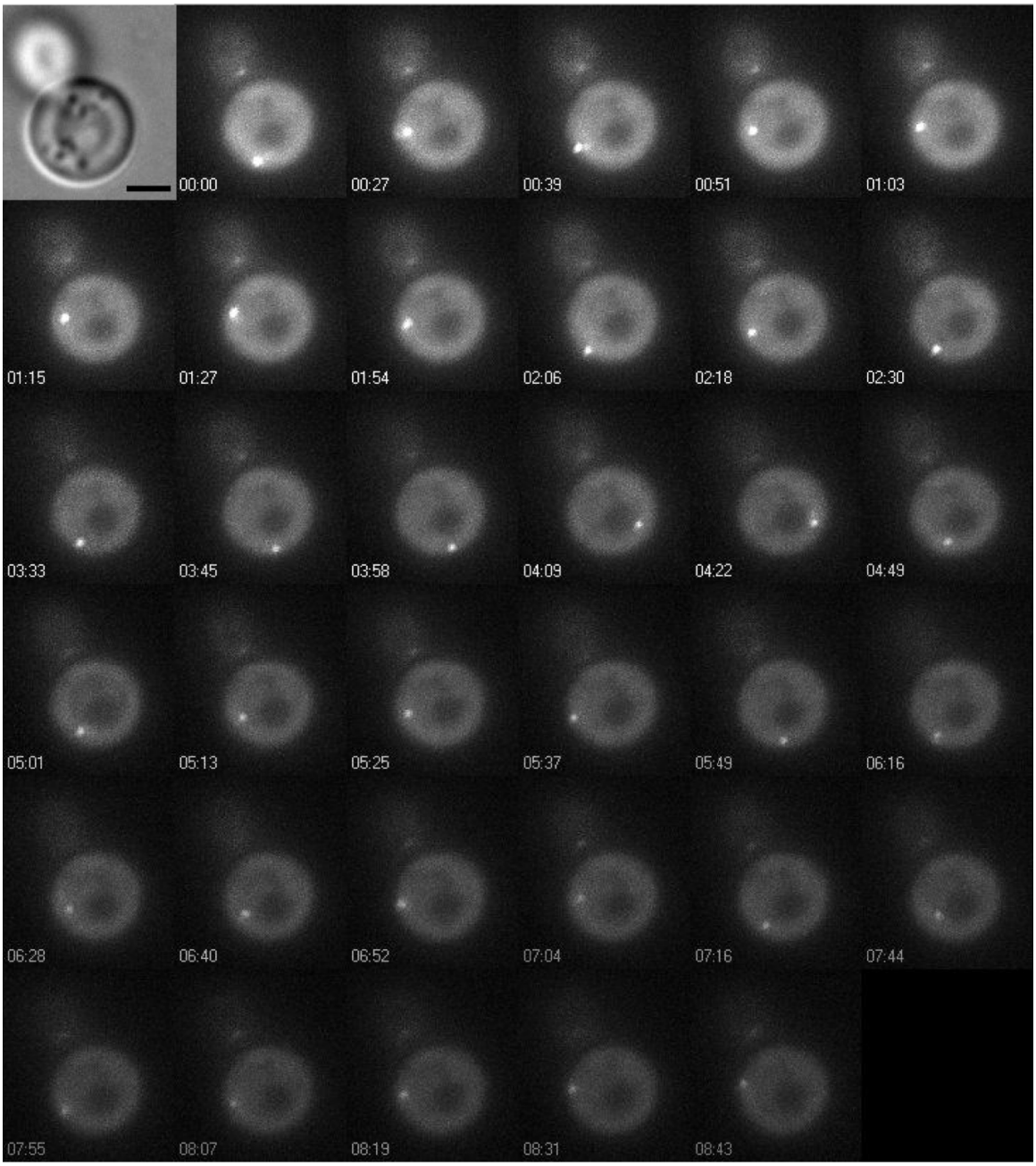

Figure 23. *SIC1* RNP granules showed different motion modes.

Sequence of 35 time frames of a single cell containing *SIC1* RNP fluorescent granules. The first frame refers to a DIC image, at 0 min. The 34 following frames are maximum projections of fluorescence intensity per pixel of a stack with 11 images for each time point. The step size separating the planes of the images was 0.2 µm. The number in the bottom left corner indicates the timing of the image acquisition. *SIC1* RNP fluorescent granule in the upper cell oscillated within a very restricted cellular volume whereas *SIC1* RNP fluorescent granule in the second cell exhibited random moves of broader distances within a larger volume. The dark round area in the larger cell represented the vacuole. Size bar represents 2 µm.

4.3.2 Transport of *SIC1* RNP from mother cell into bud

In few occasions, we observed a fast motion of *SIC1* RNP particle from the mother to the nascent daughter cell (Figure 24A,B). In the first 9 minutes of the tracking experiment, the *SIC1* messenger particle showed a random motion in the mother cytoplasm (Figure 24A,B). Forty five seconds later the *SIC1* RNP localized in the bud neck, and in the next image, 45 seconds later at 10 minutes 39 seconds, the *SIC1* RNP was in the bud. From this time point on until the end of the measurement, meaning a period of more than 11 minutes, the RNP remained in the daughter cell. Although the bud volume was quite narrow, the particle continued to randomly move in the bud. Unfortunately, after approximately 22 minutes, the fluorescence of the cell was bleached and did not permit any longer visualization of the *SIC1* RNP.

Our microscope monitoring focused on two single cells. Therefore, we fixed a population of cells with paraformaldehyde to facilitate the imaging of *SIC1* RNPs in several cells to test whether this kind of directed transport was a usual phenomenon. We observed the presence of *SIC1* RNPs in a significant portion of buds and daughter cells (Figure 24C). Some buds and daughter cells were too small to contain a nucleus yet and this implicated that the *SIC1* RNPs were produced in the mother cells, which contained a nucleus, and later transported from the mother to the bud or daughter cell probably with a similar kind of directed transport to the one in the previous live experiment (Figure 24A,B).

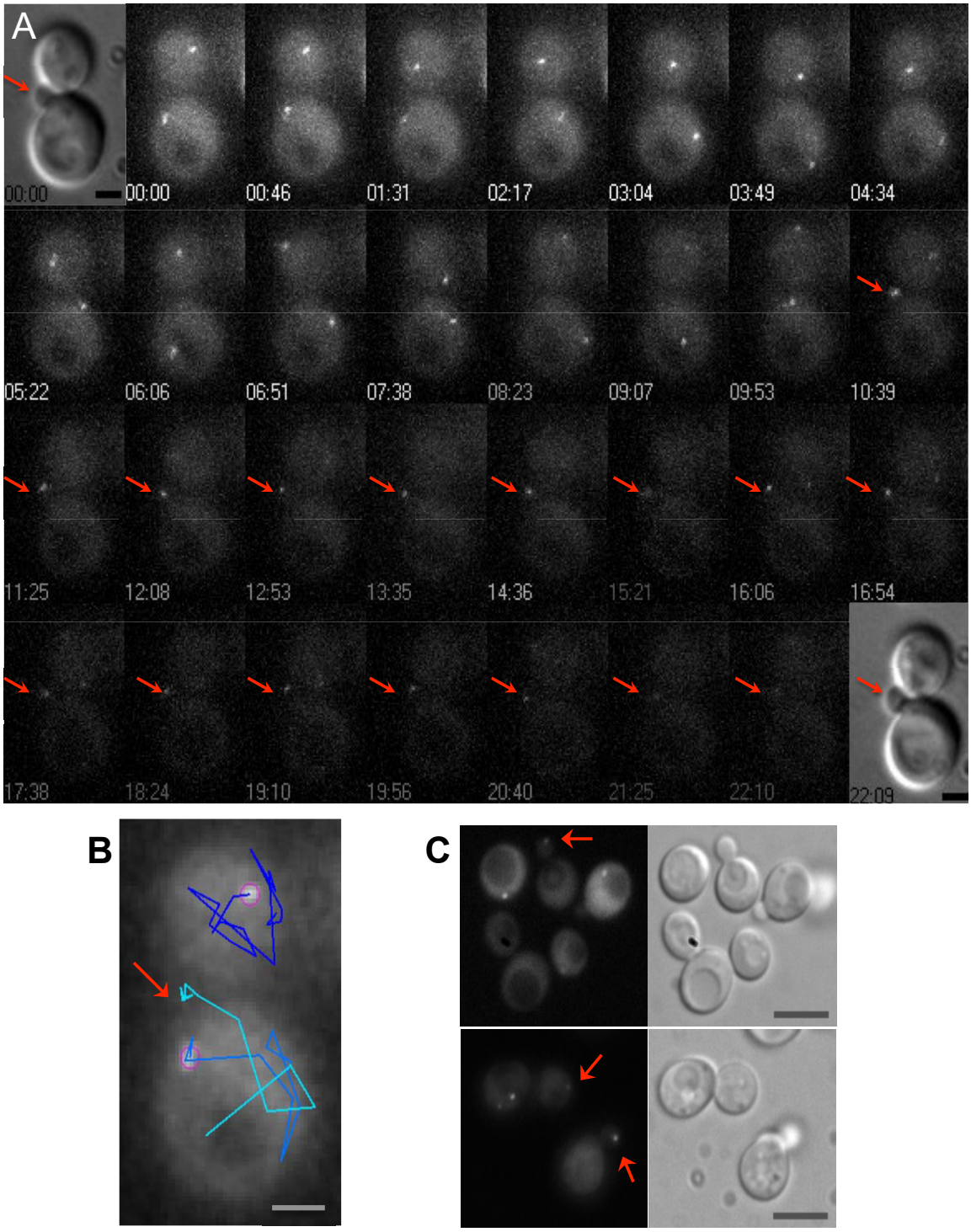

Figure 24. Transport of a *SIC1* RNP from a mother cell into its nascent daughter cell.

(A) Sequence of 30 frames of single cells containing *SIC1* mRNA fluorescent particles. Images were taken every 45 seconds. In all images the red arrows indicate the position of a bud. The first and the last frames refer to DIC images, at 0 min and at 22 min 9 seconds, respectively. The 28 other frames are maximum projections of fluorescence intensity per pixel of a stack of 11 images for each time point. The step size separating the planes of the images is 0.2 µm. (B) Trajectories of the *SIC1* RNP in the mother and bud cells of the image sequence in presented in (A). The pink circles indicate the start position. Size bars in (A) and (B) represent 2 µm. (C) Additional examples of buds and daughter cells containing *SIC1* RNP indicated by the red arrows. Size bars in (C) represent 5 µm.

4.4 Monitoring of a synchronized *SIC1*-MS2-GFP(x3) cell population provided timing of *SIC1* mRNA expression

To study the changes of *SIC1* transcript abundance over cell cycle we monitored a synchronized population of yeast cells modified with the MS2-CP system for tagging *SIC1*. The cell population was synchronized in early G1 via counterflow centrifugation elutriation. Elutriation is a non-chemical and non-invasive method of cells separation using weight and size difference. We cultivated this synchronized cell population for 250 min under optimal growth conditions and harvested samples every 2 min to monitor the level of *SIC1* RNPs tagged with MS2-CP-GFP(x3) via fluorescence microscopy (Figure 16 in Material and Methods). We also measured the fraction of budding cells, i.e. budding index, from bright field images to identify the timing of the G1/S transition.

We used SPOTALYZER, a customer written script, to process the microscopy images and to extract the number of *SIC1* fluorescent particles per cell (section 3.2.4.1 in Material and Methods). As observed in our previous experiment with an asynchronous population in section 4.2, we found that a majority of cells contained no or low number (< 10) of *SIC1* mRNA particles (Figure 25A). The overall population exhibited a peak of *SIC1* mRNA particles at 120 min after elutriation with a maximum of approximately 1.4 mRNA particle/cell on average (green curve in Figure 25A). Additionally the population showed a basal level of *SIC1* mRNA particles of approximately 0.1 mRNA particle/cells on average during the time course of the experiment.

The subpopulation of cells with one *SIC1* mRNA particle was the main contributor of this basal level observed in the overall population. Indeed, the dynamics of the average of *SIC1* mRNA particle considering only the fraction of cells with no or one single *SIC1* mRNA particle was similar to the basal level of the entire population, i.e of about 0.1 *SIC1* particle/cell and relatively constant level during the experiment (red curve in Figure 25A).

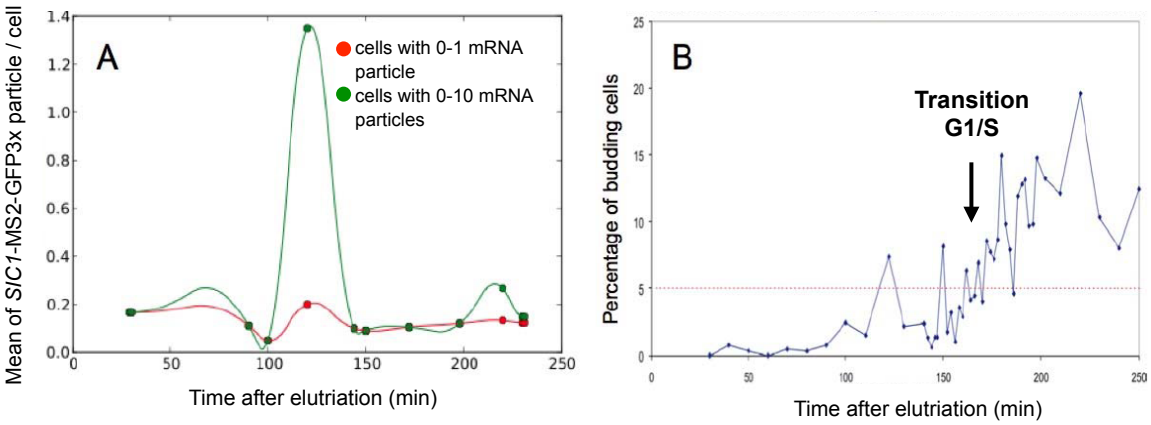

Figure 25. Level of *SIC1* mRNA particles tagged with MS2-CP-GFP(x3) peaked in G1 phase in cell population synchronized by elutriation.

Population of MS2-CP-GFP(x3) tagged *SIC1* cells was synchronized in early G1 via elutriation. (A) The average of *SIC1* mRNA particles/cell for the fraction of cells containing no or one single *SIC1* mRNA particle was constant during the time course of the 250 min measurement (red curve). The overall synchronized cells population exhibited basal level of *SIC1* mRNA and its average of *SIC1* mRNA particles/cell reached a maximum around 120 min after elutriation (green curve). (B) Budding index was measured from the bright field images. A fraction of 5% of budding cells was taken as the G1/S transition threshold and this transition occurred at approximately 160 min after elutriation (black arrow).

In order to correlate the increase of *SIC1* particles with the cell cycle progression, we compared the time-course of MS2-CP-GFP(x3) tagged *SIC1* particles with the time-course of the budding index. Indeed, budding is a morphological hallmark for G1/S transition and considering the value of 5% of budding cells as the threshold for when the synchronized population had entered into S phase (Labib et al., 1999). We found that the G1/S transition occurred at about 160 min after elutriation meaning that the observed maxima of MS2-CP-GFP(x3) tagged *SIC1* particles at 120 min was reached in the G1 phase, before the G1/S transition (Figure 25B).

The maximum of 20% of budding cells at about 220 min after elutriation revealed a partial synchrony of the cells. Indeed previous studies measured budding index oscillations of larger amplitudes with maxima up to roughly 100% for more homogenous population (Dirick et al., 1995; Gallego et al., 1997; Lengronne and Schwob, 2002). Thus this experiment provided information of *SIC1* expression timing as well as revealed the limitation of elutriation for synchronization and the need of additional markers to budding index to time the cell cycle events other than G1/S transition and follow the cell cycle progression.

4.5 Minimalistic stochastic model for G1/S transition centered on *SIC1* expression

Computational analysis and modeling were made in collaboration with the Theoretical Biophysics group of Prof. Edda Klipp. The models were developed within a constant exchange between the experimental and theoretical collaborators. As I represent the experimental team I will give here only a brief presentation of the computational strategies and models. Texts and images of this section refers to our published manuscript (Barberis et al., 2011):

Matteo Barberis, Claudia Beck, Aouefa Amoussouvi, Gabriele Schreiber, Christian Diener, Andreas Herrmann and Edda Klipp. A low number of *SIC1* mRNA molecules ensures a low noise level in cell cycle progression of budding yeast. *Mol. Biosyst.* **7,** 2804–12 (2011). doi: 10.1039/c1mb05073g

4.5.1 Description of our initial stochastic model centered on *SIC1*

One of the previously published models of the G1/S transition was based on a system of ordinary differential equations, considered 52 parameters to represent a large network of biochemical reactions (Barberis et al., 2007). Our experiments on *SIC1* and *CLN2* tagged with the MS2 system and previous published studies (Bon et al., 2006; Holstege et al., 1998; Zenklusen et al., 2008) showed that most of the regulated genes are expressed on average at only few mRNA copies per cell. Since transcription and translation are processes with stochastic characteristics, variability of such small molecules numbers is another important parameter to include in a model of the G1/S transition. On the basis of our experimental results with the MS2 system, we designed a stochastic model of the G1/S transition. Compared to other complex networks, we adopted the strategy to focus on a minimalistic system that considered only the molecular abundances of the Cdk inhibitor Sic1 and the activator of DNA replication Cdk1-Clb5,6 (Figure 26). We addressed the influence of low *SIC1* mRNA copies on the amount of protein noise and on the G1/S time resolution in a cell.

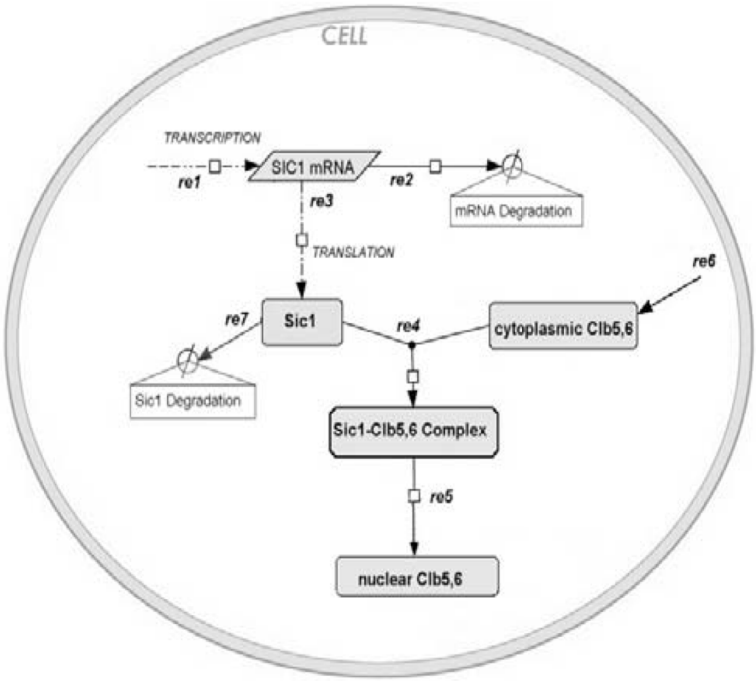

Figure 26. Biochemical reactions network of Sic1 and Clb5,6 used in the stochastic model of the G1/S transition.
This minimal network is centered on the Sic1 and its interaction with Clb5,6. Cdk1–Clb5,6 is here indicated as Clb5,6 for simplicity since Cdk1 is present during the whole cell cycle at a non-limiting level and is supposed to be always available. The parameters $re1$ to $re7$ represent several degradation and production rates relative to Sic1 and Clb5,6.

The stochastic model of the G1/S transition consists of six basic reactions (Figure 26, $re1$ to $re6$) and an additional degradation rate of Sic1 ($re7$) that is included and analyzed during later simulations. The reaction $re1$ describes the transcription process to produce *SIC1* mRNA and degradation of *SIC1* mRNA occurs in reaction $re2$. The reaction $re3$ describes the translation from *SIC1* mRNA to Sic1 protein. Furthermore, in reaction $re4$, Sic1 forms a protein complex with cytoplasmic Cdk1–Clb5,6 (here indicated as Clb5,6 for simplicity since Cdk1 is present during the whole cell cycle at a non-limiting level and, thus, is supposed to be always available). Sic1 binds to Cdk1–Clb5,6 and transports it from the cytosol to the nucleus (Rossi et al., 2005). The distinction between cytosolic and nuclear Clb5,6 is retained in this model, but transport over the nuclear membrane is surmised through the complex formation. Upon transport into the nucleus, the Sic1–Clb5,6 complex generates free nuclear Clb5,6 (reaction $re5$). The free nuclear Clb5,6 is able to initiate DNA replication. The cytoplasmic Clb5,6 is produced by reaction $re6$. The reaction $re7$ accounts for Cdk1-mediated degradation of Sic1 (Nash et al., 2001; Nasmyth, 1996). In the model, Sic1 is not recycled in the cytoplasm after titration into the Cdk1–Clb5,6 complex, hence we always refer to Sic1 as its cytoplasmic form. The best values for the parameters of reaction rates $re6$ and $re7$ to fit the Sic1/Clb5 intersection point are calculated in later simulations. The equations describing the stochastic model are listed in (Table 14).

Table 14. Chemical notations for the reactions of the G1/S stochastic model centered of *SIC1* transcription.

Reaction	ID (constant)	Chemical Notation
$re1$	Prod_mRNA ($k1$)	$\rightarrow$ mRNA_SIC1
$re2$	Deg_mRNA ($k2$)	mRNA_SIC1 $\rightarrow$
$re3$	Prod_Sic1 ($k3$)	mRNA_SIC1 $\rightarrow$ mRNA_SIC1 + Sic1
$re4$	Formation_of_Complex ($k4$)	Sic1 + Clb5 $\rightarrow$ Sic1Clb5
$re5$	Decay_of_Complex ($k5$)	Sic1Clb5 $\rightarrow$ Sic1 + Clb5_active
$re6(a,b,c)$	Prod_Clb5 ($k6a$; $k6b$; $k6c$)	$\rightarrow$ Clb5
$re7$	Deg_Sic1	Sic1 $\rightarrow$

4.5.2 Stochastic model generated detailed temporal dynamics of single trajectories and overall system behavior.

To address the dynamics at the G1/S transition, we examined the stochastic behavior of Sic1 and Clb5 for a single yeast daughter cell. As mentioned above, Sic1 was present at its maximum level at the beginning of the G1 phase, therefore in the model an initial value for *SIC1*/Sic1 had been set, whereas the other species involved were set to 0. The initial data and rate constants are presented in Table 15. Sic1 was initialized with 284 molecules, a value derived from its total number of molecules found in budding yeast (Ghaemmaghami et al., 2003) and recalculated for the size of a daughter cell (about 25 fl). Furthermore, the initial number of *SIC1* mRNA molecules was varied between 0 and 10 during later simulations, according to our experimental MS2-CP-GFP(3x) tagged *SIC1* observations (Figure 22). Clb5,6 production was included after 37 min, which represented the length of the G1 phase (t_{G1}) determined experimentally for newborn daughters (Di Talia et al., 2007).

Table 15. Initial conditions for a single daughter cell of the G1/S transition stochastic model centered of *SIC1* transcription.

Species ID	Amount of molecules	
mRNA_SIC1	varied between 0 and 12	
Sic1	738	
Sic1Clb5	0	
Clb5_active	0	
Clb5	0	
Reaction (constant)	Rate Constant Value (Deterministic)	Rate Constant Value (Stochastic)
$re1$ ($k1$)	0,1 min^{-1}	0,1 min^{-1}
$re2$ ($k2$)	varied between: 0,1 min^{-1}, 0,05 min^{-1}, 0,03333 min^{-1}, 0,025 min^{-1}, 0,02 min^{-1}, 0,01667 min^{-1}, 0,0143 min^{-1} and 0,0111 min^{-1}	varied between: 0,1 min^{-1}, 0,05 min^{-1}, 0,03333 min^{-1}, 0,025 min^{-1}, 0,02 min^{-1}, 0,01667 min^{-1}, 0,0143 min^{-1} and 0,0111 min^{-1}
$re3$ ($k3$)	0,32 min^{-1}	0,32 min^{-1}
$re4$ ($k4$)	84,6 $\mu M^{-1} * min^{-1}$	0,0056 min^{-1}
$re5$ ($k5$)	1 min^{-1}	1 min^{-1}
$re6$ ($k6b$)	0,3 min^{-1}	3 min^{-1} (assuming 10 *CLB5* mRNA molecules)

An advantage of stochastic modeling is to observe how potential behaviors result in differences in individual realizations and/or in the overall system. In order to investigate the variability in the system performance, we compared 10 exemplary trajectories of each species in the stochastic model during a simulation time of 250 min for one initial *SIC1* mRNA molecule and an average mRNA level equal to three, generated by the ratio between mRNA production ($k1$) and degradation ($k2$) rate constants (Figure 27A). The 10 curves showed a similar trend despite some variations between trajectories, which were described by mean (the similar trend) and standard deviation (the variations)(Figure 27B). The initial Sic1 amount (blue curve) decreased quickly after the production of nuclear Clb5,6 (pink curve), due to the increase of the Sic1–Clb5,6 complex formation. After about 170 min Sic1 converged to 0 because in the model Sic1 was not recycled in the cytoplasm after titration into the Cdk1–Clb5,6 complex; and cytoplasmic Clb5,6 (green curve) begun to accumulate. At the same time the slope of nuclear Clb5,6 gradually diminished, indicating that at this point Sic1 was the limiting factor for the appearance of nuclear Clb5,6. Figure 27C provides a detailed view of the *SIC1* mRNA performance (red curve). During the first 100 min of simulation, the trajectories split up from one initial molecule to a distribution between none and three molecules. Later, from 100 to 250 min, the distribution stabilized around a mean value of about three molecules, which is derived by the ratio $k1/k2 = 3$ (Figure 27C).

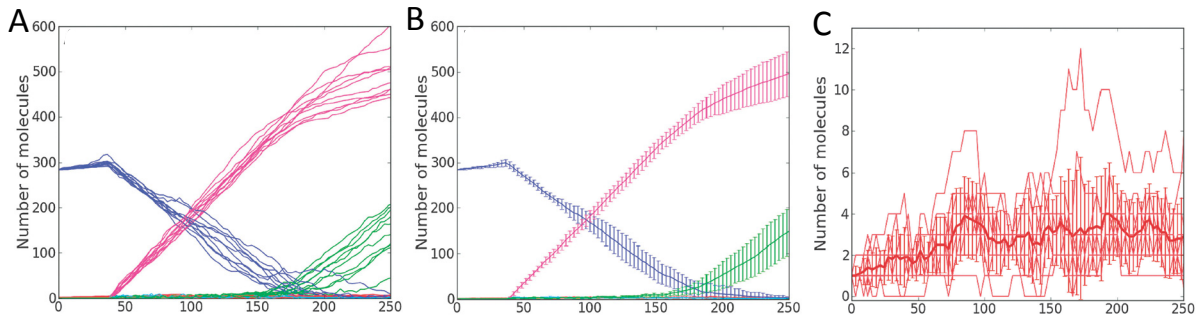

Figure 27. Simulated dynamics of the system generating 10 exemplary trajectories.
(A) *SIC1* dynamics resulting from the initial condition of 1 *SIC1* mRNA (red). Sic1 (blue) decreases after production of nuclear Clb5,6 (pink) and, when its level are close to 0, cytoplasmic Clb5,6 (green) accumulates. The crossing between blue and pink curves is the Sic1/Clb5 intersection point. (B) Mean ± standard deviation calculated from the 10 trajectories shown in panel (A). (C) Fluctuations (standard deviation) of *SIC1* mRNA molecules and mean (dark red). Zoom in from panel (A) and (B).

4.5.3 Stochastic model predicted that lower initial *SIC1* mRNA numbers ensure lower Sic1 protein noise and robust S phase onset.

The dynamics of protein interaction between Sic1 and Clb5,6 are critical for DNA replication onset. Therefore we employed our model to assess the effect of *SIC1* mRNA number fluctuations on Sic1 protein dynamics and related DNA replication timing. We calculated two coefficients of variation, CV_1 and CV_2, from the mean ($m; m \neq 0$) and standard deviation (s) values of *SIC1* mRNA and Sic1 protein. The coefficient of variation, $\mathrm{CV} = s/m$, also called weighted noise, is a measure to compare the degree of variation of data sets with drastically different means. In our case, CV_1 represents the noise of *SIC1* mRNA whereas CV_2 represents the noise of Sic1 protein. The ratio $Q = CV_2/CV_1$ was calculated to compare the noise of protein to the one of mRNA. The simulations were run each time by generating 100 000 trajectories during 800 min.

We first considered the situation of a $k1/k2$ ratio of *SIC1* mRNA equal to 3, varied the initial *SIC1* mRNA numbers from 0 to 10 and compared the simulated dynamics of Sic1, CV_2 and Q (Figure 28).

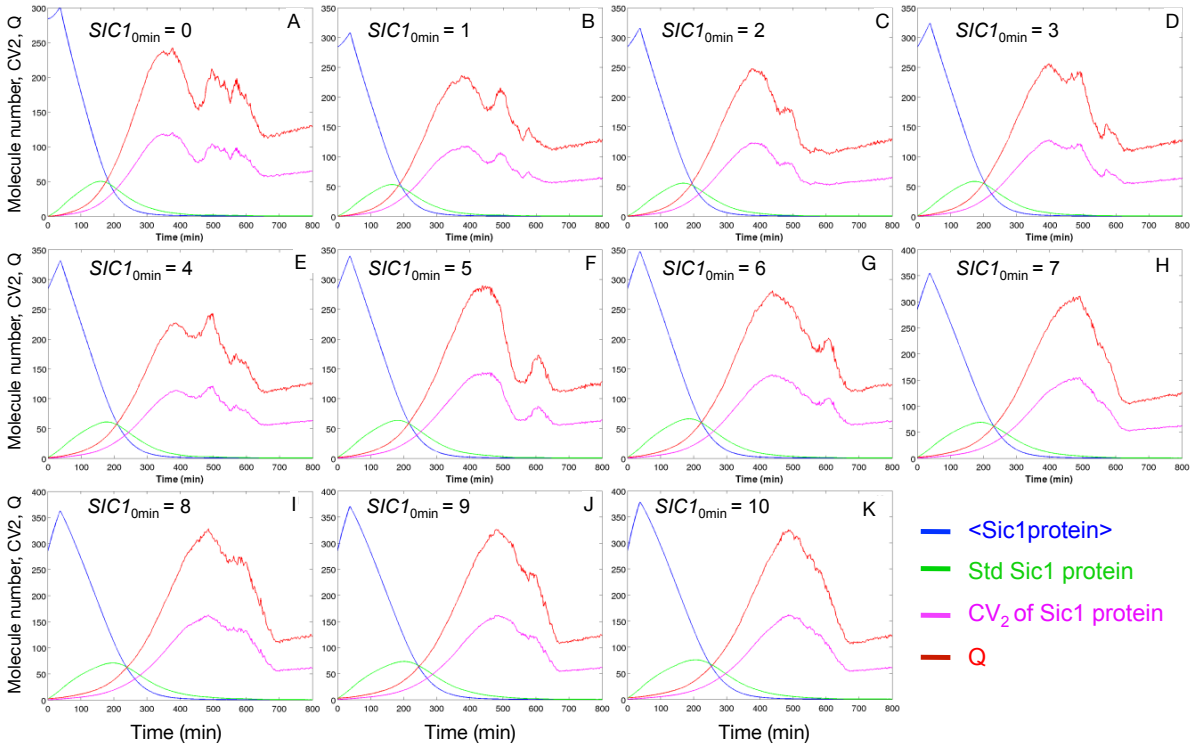

Figure 28. Influence of the initial *SIC1* mRNA copies number on the Sic1 protein dispersion and timing of the G1/S transition.

Simulated dynamics of mean (blue) and standard deviation (green) of Sic1 protein, of CV_2 of Sic1 protein (pink) and Q (red) for a range of 0 (A) to 10 (K) initial *SIC1* mRNA molecules. The curves of CV_2 of Sic1 protein and Q were multiplied by 50 for purpose of visualization. The maximum of the y-axis is 300, 350 or 400 depending of the graph.

During the simulations the mean of Sic1 increased until 37 min (t_{G1}), when nuclear Clb5,6 was produced; afterward Sic1 decreased and converged to zero. The standard deviation had a smoother dynamic than Sic1, maximized at a later timing, and also converged to zero. Sic1 protein noise, CV_2, and the noise ratio, Q, rose exponentially during this time and both curves reached a maximum when Sic1 was roughly zero. The profiles of CV_2 and Q were similar because CV_1 remained constant during the simulations due to the fact that *SIC1* mRNA was only affected by production ($k1$) and degradation ($k2$) rate constants. Moreover increasing the initial amount of *SIC1* transcripts lead to higher maximum values of Sic1 protein and elongated its presence and consequently the inhibition of the DNA replication. Higher initial *SIC1* mRNA amount also triggered a delay and higher levels of Sic1 protein noise and noise ratio, Q. For example maxima of Q were about 5.5 and 6.5 for 2 and 10 initial *SIC1* mRNAs, respectively (Figure 28C and K). Thus low level of initial *SIC1* mRNAs ensure a low Sic1 protein noise and a robust timing of the S-phase entrance.

We tested how the rates of production ($k1$) and degradation ($k2$) of *SIC1* mRNA influence Sic1 protein noise. To this purpose we varied the $k1/k2$ ratio and the *SIC1* initial mRNA number and compare the resulting maximum vales of Q (Figure 28).

As previously we observed an increase of Q maximal levels for higher initial *SIC1* mRNA number as well as an even more critical noise increase for higher $k1/k2$ ratios. Indeed noise, Q, increased from about 2 to 24 while $k1/k2$ ranged from 1 to 6. A higher *SIC1* mRNA level might increase the probability of the translation reaction for the *SIC1* gene and our results revealed that high *SIC1* mRNA levels lead to an amplified dispersion in the amount of the Sic1 protein. Translational activity depends generally on ribosome occupancy and ribosome density (Beyer et al., 2004). Nevertheless, from a stochastical point of view, the probability to produce Sic1 depends above all on the *SIC1* mRNA amount and on the rate constant of this reaction. Since the behavior of the system is time dependent, peaks of CV_2 and Q are shifted in time according to the initial conditions (Figure 28), hence Figure 29A does not refer to a specific time instant. Temporal profiles of CV_2 and Q peaks are reported in Supplementary Figure S 3A and B in Appendix 1. From Figure 29B, it is observed that the weighted noise of Sic1 protein ranges between 200 and 2400% of the SIC1 mRNAs weighted noise, which agrees with the indication of an amplified dispersion of the protein. Therefore, a low number of *SIC1* mRNA molecules ensure a low noise level, which is apparently more dependent on the production to degradation ratio of *SIC1* mRNA than on the initial *SIC1* mRNA number.

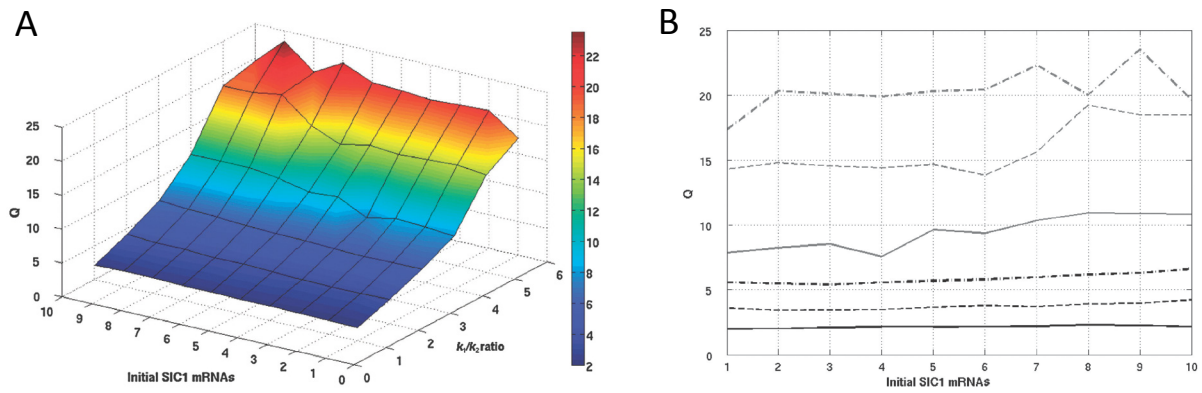

Figure 29. Relation between Q, the initial *SIC1* mRNA molecule number and different *SIC1* mRNA production to degradation (k1/k2) ratios.

Data shown with a three-dimensional representation (A) and a bi-dimensional representation (B). In panel B, dash-dotted, dashed and solid lines represent the ratios $k1/k2$ from 1 to 6 initial number of *SIC1* mRNAs (from lower to higher lines).

4.5.4 Interplay between Clb5 production and Sic1 degradation in setting S phase onset

In the second part of our analysis we used our stochastic model to estimate kinetic parameters for Clb5,6 production ($k6$) (Figure 30A to F) and Sic1 degradation ($k7$) (Figure 30G and H). To this purpose, we introduced cell growth for a daughter cell and a mother cell in our model. The initial volume was 25 fl and 40 fl for the daughter cell and the mother cell, respectively, and proportionally to the volume the initial *SIC1* and Sic1 amounts were larger in the mother cell than in the daughter cell (Aldea et al., 2007). As previously reported, we considered the duration of the G1 phase equal to t_{G1D} = 37 min for the daughter cell and to t_{G1M} = 15.6 min for the mother cells and for this reason in our simulation Clb5,6 production was initiated after t_{G1M} and t_{G1D} (Di Talia et al., 2007).

The initiation of the DNA duplication, which coincides with the G1/S transition, refers to the timing of the intersection point between Sic1 and free nuclear Clb5,6 and was previously experimentally measured at about 80 min after cell cycle begin (Barberis et al., 2007). Initial conditions and rate constants for both cells are listed in Table 16.

Table 16. Initial conditions for a mother and a daughter cell in the G1/S transition stochastic model centered of *SIC1* transcription.

Reaction	ID	Daughter cell	Mother cell
	(t_{G1}) time at the initiation of Clb5,6	37 min	15.6 min
	(V_0) cell volume	25 fl	40 fl
Initial molecule numbers			
	mRNA_SIC1	1	2
	Sic1	284	454
	Clb5	0	0
	Sic1Clb5	0	0
	Clb5_active	0	0
Recalculation of rate constants (min^{-1})			
$re1$	Prod_mRNA ($k1$)	0,1	0,1
$re2$	Deg_mRNA ($k2$)	0,03333	0,03333
$re3$	Prod_Sic1 ($k3$)	0,32	0,32
$re4$	Formation_of_Complex ($k4$)	0.0035	0.0056
$re5$	Decay_of_Complex ($k5$)	1	1
$re6a$	Prod_Clb5 ($k6a$ for ~ 1 CLB5 mRNAs)	0,3	0,3
$re6b$	Prod_Clb5 ($k6b$ for ~ 10 CLB5 mRNAs)	3	3
$re6c$	Prod_Clb5 ($k6c$ for ~ 100 CLB5 mRNAs)	30	30
$re7$	Deg_Sic1	-	-
Calculations for reaction re4			
	V_0/t_{G1}	0,68 fl min^{-1}	2,6 fl min^{-1}

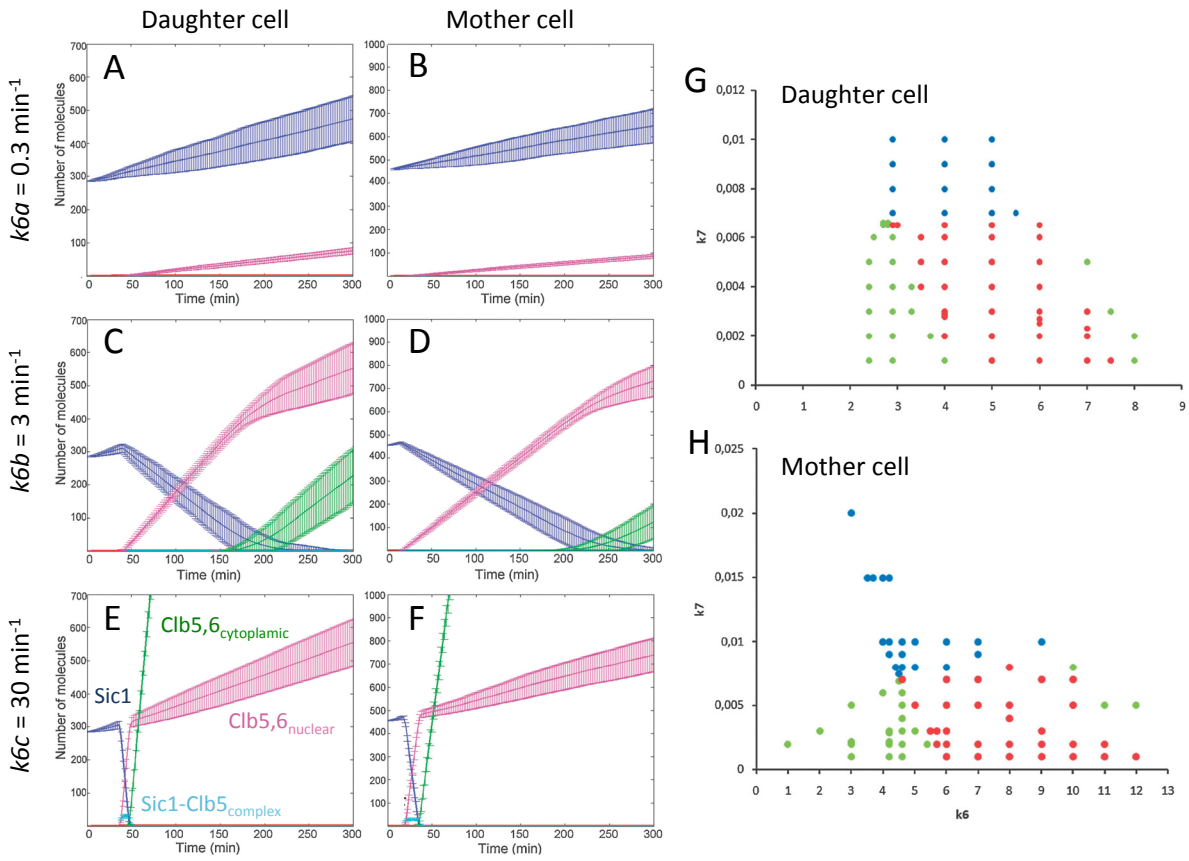

Figure 30. Stochastic model estimates kinetic parameters for Clb5,6 production and Sic1 degradation.
(A-F) Simulated dynamics of a daughter cell (left column) and a mother cell (right column) for different Clb5,6 production rate constants: $k6a$ =0.3 min^{-1} (A, B), $k6b$ =3 min^{-1} (C, D) and $k6c$ =30 min^{-1} (E, F). Sic1 (blue), cytoplasmic Clb5,6 (green), Sic1–Clb5 complex (light blue) and nuclear Clb5,6 (pink) are shown. Note the different scales of the y-axis for daughter and mother cells. Semi-log plots of (A-F) are shown in Supplementary Figure S 4. (G-H) Representation of combinations of Clb5,6 production ($k6$) and Sic1 degradation ($k7$) for daughter (G) and mother (H) cells. The red dots show possible combinations yielding the Sic1/Clb5 intersection point within the time window considered for the analysis and for possible Sic1 molecule numbers. The blue dots match with the time window and the green dots match with the Sic1 molecule numbers.

4.5.4.1 Estimation of Clb5 production rate.

We investigated to which extent the timing of initiation of DNA replication is influenced by Clb5,6 production by testing different Clb5,6 rate constant values: 0.3 min^{-1} ($k6a$), 3 min^{-1} ($k6b$) and 30 min^{-1} ($k6c$) for both daughter and mother cells that doubled their volume during the G1 phase (Alberghina and Porro, 1993). In our model, the total amount of Sic1 was the sum of free Sic1 and Sic1 in the Sic1–Clb5,6 complex, and no additional degradation was considered for Sic1.

For a low Clb5,6 production ($k6a$ =0.3 min^{-1}), the molecule number of Sic1 protein (blue curve) increased for both daughter (Figure 30A) and mother (Figure 30B) cells. This was reasonably due to the fact that formation of the Sic1–Clb5,6 complex was slower compared to Clb5,6 production and, therefore, there was no titration of Sic1 into the Cdk1–Clb5,6 complex in order to reduce Sic1 level. In our model Sic1 was solely consumed by complex titration without additional Sic1 degradation resulting in the increase of Sic1 levels, which is normally not observed in living cells. Since only a small part of

Sic1 was used to form the Sic1–Clb5,6 complex, and as well nuclear Clb5,6, there was no intersection point between Sic1 and Clb5 during this simulation time. It has to be emphasized that a value of 0.3 min^{-1} was used by Tyson's group because it generated the best fit to their experimental data (Barik et al., 2010).

By increasing the Clb5,6 production rate to $k6b$ = 3 min^{-1} and to $k6c$ = 30 min^{-1} (Figure 30C-F), Sic1 was titrated into the Cdk1–Clb5,6 complex and progressively down-regulated whereas cytosolic Clb5,6 could not be completely consumed anymore. Sic1 became a limiting factor of Sic1–Clb5,6 complex formation (reaction $re4$) and cytosolic Clb5,6 accumulated when Sic1 converged to 0. While converging to 0, Sic1 shows an exponential behavior, which was also observed by semi-log plots reported in Supplementary Figure S 4 in Appendix 1. Hence, when Sic1 decreased, the production rate of nuclear Clb5,6 diminished too (Fig. 6C–F). Therefore, to reach the Sic1/Clb5 intersection point for precise timing of the G1/S transition and the initiation of DNA replication, the Clb5,6 production rate should be between $k6b$ (3 min^{-1}) and $k6c$ (30 min^{-1}) for both daughter and mother cells, in the case that complexation with Clb5,6 was the only factor regulating Sic1 levels.

4.5.4.2 Estimation of Sic1 degradation rate.

In addition of complex formation with Clb5,6 other processes, such ubiquitination after Cln1,2-Cdk1 phosphorylation, influence the decrease of Sic1 during cell cycle progression (Nash et al., 2001; Verma, 1997). Accordingly we included an additional degradation rate for Sic1 (reaction $re7$) in our model. We estimated the best parameters combination for the rate of Clb5,6 production ($k6$) and the rate of Sic1 degradation ($k7$) to match a Sic1/Clb5 intersection point at about 80 min as measured in previous experiments (Barberis et al., 2007).

We started the simulation 20 min after the end of G1 (t_{G1D} = 37 min for the daughter cell, t_{G1M} = 15,6 min for the mother cell), which represented the middle point of the S phase where half of the maximal Clb5 level was reached, and ended after 20 min, to consider the duration of the S phase (typically of about 40 min) (Barberis et al., 2007). Thus, we searched for Sic1/Clb5 intersection points within a time window of 20 min for both mother and daughter cells. The result of multiple simulations is shown in Figure 30G,H and the red dots depict values of $k6$ and $k7$ for both daughter (Figure 30G) and mother (Figure 30H) cells that allowed an appropriate timing of the intersection point. From this analysis, we derived that the Sic1/Clb5 intersection point was reached for initial mRNA molecule numbers of *CLB5,6* equal to about 9 molecules for the daughter cell and about 15 molecules for the mother cell. These values agree with the ones computed from asynchronous populations of mother and daughter cells as recently published (Barik et al., 2010). Values of $k6$ = 2.9 min^{-1} and $k7$ = 0.0065 min^{-1} for the daughter cell and $k6$ = 4.6 min^{-1} and $k7$ = 0.007 min^{-1} for the mother cell ensured optimal intersection points. Therefore, we found that a Sic1 degradation rate of about 0.007 min^{-1} lead to the best parameter choice matching the timing of the Sic1/Clb5 intersection point for both daughter and mother cells. The similarity of the plots confirmed the previous experimental data, which show that daughter and mother cells are characterized by the same timing during the cell cycle, except for different growth rates and lengths of the G1 phase (Hatzis and Porro, 2006). In our case, differences in the G1 phase were balanced in the model by using distinct initial conditions (growth rates, volumes) as well as times of Clb5,6 initialization.

5. DISCUSSION I

5.1 MS2-CP system enables *in vivo* visualization of *SIC1* and *CLN2* mRNA particles.

In order to visualize *SIC1* and *CLN2* mRNAs we established stable yeast mutants in which these two genes were respectively tagged with the MS2-CP method. We compared several fluorophores and fluorescent proteins and found that the MS2-CP-GFP(x3) construct gave the most stable and brightest signal. *SIC1* and *CLN2* showed low expression in asynchronous population. Indeed many cells did not contain any or had one single RNP, whereas few cells had up to 10 RNPs. This low expression of *SIC1* or *CLN2* is similar to the one published in previous MS2 system studies on other genes involved in cell cycle progression (Bertrand et al., 1998), genes coding for peroxisomal proteins (Zipor et al., 2009) as well as genes regulating divers others functions in yeast (Gallardo et al., 2011; Thompson et al., 2010). Notably the trend for a unique or only few copies of mRNA fluorescent spots observed with the MS2 system for genes involved in so different functions is unexpected and raises multiple questions.

We observed that the mRNA particles had heterogeneous sizes and fluorescence intensities. This implicates that fluorescent granules may content different number of mRNA molecules as well as questions the full saturation of the MS2 hairpins by the MS2 coat proteins. Fusco and colleagues observed that the MS2 hairpin binding sites were not uniformly bound with MS2-GFP complexes and they quantified an average saturation rate of about 70% in COS cells (fibroblast-like cell lines derived from monkey kidney tissue) (Fusco et al., 2003). Consequently the measured *SIC1* and *CLN2* mRNA particle numbers might be an underestimation of their respective mRNA abundance. Heterogeneous sizes and fluorescent intensities may also be related to the aggregation of MS2 bound GFP(x3) as native GFP tends to dimerize at high concentration (Yang et al., 1996) and native MS2-CP contains a internal dimerization sequence (LeCuyer et al., 1995). Further efforts have been made in our lab to construct a mutant featuring MS2-CP linked to a triplet of monomeric GFP.

Normalization of the fluorescent signal could quantify the exact mRNA number present in each fluorescent spot. Such normalization is possible using, for example, a calibration curve of a serial dilution of known concentration of purified GFP in aqueous solution (Fusco et al., 2003; Hirschberg et al., 1998; Wells et al., 2007). Even better a calibration standard in living cells can be obtained with the JBY376 yeast strain, which expressed a well know number of lac repressor–binding sites (Lac-I) for Lac-I tagged GFP (Brickner et al., 2007; Haim-Vilmovsky and Gerst, 2009).

A novel system, PP7-CP, based on the PP7 bacteriophage protein binding hairpin loop showed higher saturation rate and therefore higher and more homogenous brightness then the MS2-CP system (Gandhi et al., 2011; Larson et al., 2011; Wu et al., 2012) and could be employed on *SIC1* and *CLN2*. Both PP7-CP and MS2-CP bind as dimers to their respective loops and this dimerization step is critical for binding sites occupancy and therefore quantitative analysis of the mRNA imaging. Wu and colleagues engineered single-chain tandem dimers of the MS2 and PP7 coat proteins (named tdMCP and tdPCP, respectively) (Wu et al., 2012). These improved systems eliminated the dimerization step and produced a uniform labeling and an increased signal to noise ratio of the tagged mRNA. Additionally MS2 and PP7 or tdMCP and tdPCP could be used in parallel within the same cells for

simultaneous imaging of those G1/S key players or of two other genes (Halstead et al., 2015; Hocine et al., 2013; Larson et al., 2011).

Comparing our MS2 results with those obtained with other experimental approaches may lead to a consensus on the transcription level. Indeed results from mRNA microarrays experiments (Bon et al., 2006; Holstege et al., 1998) and other genome wide experiments (Lipson et al., 2009; Miller et al., 2011; Miura et al., 2008), which quantified transcript levels in yeast cells, also revealed a general tendency for mRNAs to be present at only a few copies per cell. However re-analysis and re-normalization of these numbers with larger samples gave transcript averages approximately 4-folds higher than with smaller samples (Ball et al., 2013). These higher averages are consistent with recent works using single molecule RNA-FISH method on genes involved in cell cycle regulation, which measured that mRNA numbers in slightly broader ranges than 0-10 mRNAs/cell (Ball et al., 2013; Gandhi et al., 2011; Trcek et al., 2011). Although the ranges may vary it seems widely observed that transcription of cell cycle genes is rather low compare to the one of housekeeping genes, which are constantly expressed.

5.2 Monitoring of a synchronized *SIC1*-MS2-GFP(x3) cell population shows *SIC1* expression in G1 phase.

We followed a population of synchronized new-born cells selected via counter force elutriation and measured an increase of MS2-GFP(x3) tagged *SIC1* particles in G1. The duration of the G1 phase in our experiment was longer than the one previously measured in asynchronous populations (Di Talia et al., 2007; Trcek et al., 2011). Indeed the elutriation selects the smallest newborn early G1 cells, which need additional time to recover from the elutriation treatment (Futcher, 1999; Woldringh et al., 1995). In addition the younger and smaller cells have elongated G1 phase compare to the older and larger mother cells as they need to grow longer to reach a sufficient size for the entrance into S phase (about 17 and 37 min for mother and daughter cells, respectively, (Di Talia et al., 2007)).

SIC1 is an inhibitor of CDK and prevents G1 exit (Nash et al., 2001; Schwob, 1994). Accordingly the observed increase of *SIC1* in G1 may be related with additional *SIC1* mRNAs and Sic1 proteins needed by the small cells to stay longer in G1 and to continue growing until the required size for G1 exit. This agrees with previous studies that demonstrated that daughter cells produce *SIC1* in G1 due to activation of Ace2, a daughter specific *SIC1* transcriptional factor (Laabs et al., 2003; Di Talia et al., 2009; Toyn et al., 1997).

SIC1 was reported to be mainly expressed by Swi5 in late mitosis (Aerne et al., 1998; Knapp et al., 1996; Toyn et al., 1997). However our measurements did not show such peak of *SIC1* expression during the time course of the experiment and this discrepancy might be explained by the partial synchrony of the population at the end of our experiment. This loss of synchrony is observed by the low oscillations of the budding index. Asynchrony of the population flattens the oscillations of cell cycle regulators and this effect is more critical for *SIC1*, which has a narrow expression period in mitosis (Aerne et al., 1998; Knapp et al., 1996; Toyn et al., 1997).

Population synchronization via elutriation combined with the analysis of budding index were powerful to investigate early stages of the cell cycle, however, the approach showed limitations to study events occurring at later cell cycle phases. Combination of several cell cycle morphological markers would provide better time-resolution of the full cell cycle and therefore more accurate timings and amplitudes of the expression of cell cycle regulators.

5.3 *SIC1* RNPs exhibit different transport dynamics

Our tracking of *SIC1* tagged with MS2-CP-GFP(3x) in living cells revealed three categories of RNP motions. We observed *SIC1* mRNA particles that were almost static, others were randomly moving and finally, transport of some *SIC1* particles within the cell or from mother into the bud. The same observations were reported previously for mRNA of other genes. For example, the transport mode of *ARG3* transcript was recently studied using a double helix point spread function (DH-SPF) method (Thompson et al., 2010). This novel technique permits the three-dimensional tracking of single fluorescent particles with high spatial and time resolution (25 nm in the x and y dimensions and 50 nm in the z dimension). The analysis of the mRNA particles trajectory revealed a predominant Brownian motion of the *ARG3* mRNA molecules. Moreover, this diffusion transport was alternating with short periods of non-Brownian confined (or stationary) transport and of directed transport.

Few groups reported the directed motion of messenger particles from the mother into the bud or daughter cell. Bertrand and his coworkers observed the motion of MS2 tagged *ASH1* mRNA ending into the bud (Bertrand et al., 1998). They found that the velocity of *ASH1* mRNA of 200-400nm/sec coincided with the stepping rate of the octomyosin protein Myo4. These observations suggested that Myo4p actively transports *ASH1* mRNA along actin cables from the mother cell into the bud and *SIC1* may be as well transported through a similar process. In fixed cells 21 other genes were identified to localized in the bud using DNA microarray analysis (Shepard et al., 2003), several other genes coding for peroxisomal proteins were also detected in the bud using MS2 system (Zipor et al., 2009) and *CLB2*, involved in cell cycle regulation, was visualized in bud using RNA-FISH (Shepard et al., 2003; Trcek et al., 2011).

The consequences of the active transport and localization of the mRNA in the bud and daughter are still unknown. This phenomenon may serve to localize translation and therefore to polarize the cell. *CLB2* is another cell cycle gene that accumulates in the bud, and Spiesser and his colleagues suggested that this localization might serve as a bud sizer in G2. The localized production of Clb2 might be “measured” in the bud by the cell and served as a tracer to sense the translational capacity of the bud. Thus, entrance into mitosis would occur only once the bud/daughter is able to ensure sufficient biosynthesis capacity and therefore less dependence from the mother cell to produce proteins on its own (Spiesser et al., 2015). We observed a presence of *SIC1* in the bud and daughter cell as well as in the mother. Sic1 protein is also homogeneously distributed between mother and daughter cells (Rossi et al., 2005). Therefore, in the case of *SIC1*, transcript transport to the bud does not aim to create asymmetry in the cell but rather may provide an initial stock of *SIC1* mRNAs to the daughter cell to, for example, rapidly respond to stimuli (Shepard et al., 2003). A computational model of the G1/S transition including *SIC1* mRNA transport could provide insights on the functions or implications of such transport in context of a large molecular network.

To unravel the mechanisms of *SIC1* mRNA transport and its implications for cell cycle regulation, the three-dimensional rapid motion of the transcript should be more accurately tracked. In our experimental setup we were limited by the acquisition time of the wide-field microscope. Especially the mechanically change of the height between the images to acquire z-stacks were slow compare to the speed of *SIC1* mRNA moves. Our microscopy setting induced important photo-bleaching of the GFP fluorescence because a large portion of the sample received excitation light for every image taken of the z-stack. Microscopy technologies as double helix point spread function (Thompson et al., 2010), spinning disk confocal (Stehbens et al., 2012) or light sheet (Reynaud et al., 2008) allow high speed with low illumination therefore less photo-bleaching and could be employed on MS2-tagged samples for long-time experiments. We were also challenged by the quantitative analysis of the MS2-tagged samples microscopy images. Our current analysis protocol generated a two-dimensional trajectory of the *SIC1* mRNA transport. An improved analysis workflow could generate a three-dimensional trajectory of the *SIC1* mRNA transport within the cellular volume.

5.4 Stochastic model predicts that lower *SIC1* mRNA numbers ensure lower Sic1 protein noise and robust S phase onset. (modified from Barberis et al., 2011)

The single cells microscopy experiments of this chapter as well as of previously published studies showed that expression of a gene can vary among genetically identical cells because of stochastic fluctuations in transcription (Gandhi et al., 2011; Kærn et al., 2005; Kaufmann and van Oudenaarden, 2007; Thattai and Van Oudenaarden, 2004). Moreover, single cells microscopy also allowed to experimentally measure the noisiness of the G1/S transition in a population of budding yeast cells (Bean et al., 2006; Di Talia et al., 2007). Stochastic approaches are favorable to investigate the behavior of single cells and of cellular species present in low numbers, as it is the case for those involved in transcription (Paulsson, 2005; Wilkinson, 2009).

In this chapter, we employed computational modeling to assess the timing of the G1/S transition in regard to gene expression stochasticity of *SIC1*, one of the main G1/2 players. In the present model, our aim was to investigate and reproduce the essential dynamics of the G1/S transition by generating a stochastic model that considers only the balance between two key components: the cyclin-dependent inhibitor, Sic1, and the activator of DNA replication, Cdk1–Clb5,6 (referred to as Clb5,6 for simplicity). Our simulations revealed a critical effect of the *SIC1* mRNA molecule number on the Sic1/Clb5 intersection point and therefore, on the timing of the G1/S transition. In fact, high *SIC1* mRNA levels shifted the Sic1/Clb5 intersection point as well as complete extinction of Sic1 to a later time. In detail, high initial *SIC1* mRNA molecules as well as a high k1/k2 ratio, i.e production rate to degradation rate ratio, of *SIC1* mRNA lead to an amplified dispersion of the different trajectories for Sic1 (increasing weighted noise CV2 and Q), producing more Sic1 protein and Sic1–Clb5,6 complexes until the total amount of Sic1 became 0. Consequently, higher initial *SIC1* mRNA molecules influenced the onset into the S phase by delaying Sic1 production for the following cell cycle. Therefore, a low number of *SIC1* mRNA molecules ensure a low noise level providing a robust timing of cell cycle progression.

This result is supported by our experimental data of MS2-GFP(x3) tagged *SIC1*, which indicated a range of *SIC1* transcripts between 0 and 10. The timing of Sic1 extinction might be important to regulate its level during the next cell cycle, i.e. an earlier decrease of Sic1 might result in an additional time to produce more Sic1 protein. Consequently, the *SIC1* mRNA amount could influence the production of the next Sic1 wave. The potential regulatory mechanism through which Sic1 exploits this regulation could be by affecting its own transcription factor Swi5. Swi5 exploits its role at the exit from mitosis, where it promotes *SIC1* production in anaphase/telophase (Aerne et al., 1998; Barberis and Klipp, 2007; Toyn et al., 1997). This could be an interesting mechanism of a possible regulatory property of Sic1 that was not expected before.

Importantly, our simulation results revealed novel insights of the Sic1/Clb5 balance on the timing of S phase onset. To address this point, simulations of a daughter and a mother yeast cell were considered by including cell growth, appropriate volumes and cell cycle phase lengths as reported (Hatzis and Porro, 2006; Di Talia et al., 2007). From our findings, if Sic1 was only down-regulated by the available Clb5,6, the production rate of Clb5,6 would range between 3 and 30 min^{-1} for both daughter and mother cells. A value of 0.3 min^{-1} was used in the stochastic simulations of a recent cell cycle model from Tyson's group (Barik et al., 2010), whereas a value of 0.32 min^{-1} was introduced in a kinetic model of the G1/S network (Barberis et al., 2007). In the present work, the value of 0.3 min^{-1} was considered, which represented the production rate for 1 molecule of *CLB5* mRNA. Nevertheless, a value between 3 and 30 min^{-1} would imply that there must be between 10 and 100 *CLB5* mRNA molecules, which appears to be not realistic. Indeed, as known, Clb5 is not the only regulator of Sic1 down-regulation. Considering this fact, including an additional Sic1 degradation rate (a value adjusted to 0.007 min^{-1}) yielded best results by shifting the Sic1/Clb5 intersection point to a reasonable time together with Clb5,6 production rates of 2.9 min^{-1} and 4.6 min^{-1} for daughter and mother cells, respectively. It has to be emphasized that the optimal parameter for Sic1 degradation was similar for both daughter and mother cells, despite that the value for Clb5,6 production in the mother cell was larger compared to the one in the daughter cell. This finding agreed with recent sensitivity analyses showing that the rate of Sic1 degradation is a critical parameter that influences the setting of the critical cell size required at the G1/S transition and, therefore, starting of DNA replication (Barberis and Klipp, 2007; Palumbo et al., 2010).

In addition, with these parameter sets, we derived values for optimal *CLB5* mRNA molecule numbers necessary to reach the Sic1/Clb5 intersection point in both mother and daughter cells, which agreed with recent data obtained from more complex network of cell cycle regulation developed by Tyson's group (Barik et al., 2010). Although the stochastic model correctly reproduced the timing of S phase onset, it did not provide an explanation for dynamics of late cell cycle events. In fact, accumulation of Clb5,6 after decrease of Sic1 levels was not observed in yeast cells due to Clb5,6 down-regulation after the S phase by Cdk1–Clb complexes involved in G2/M regulation, which were not considered in the present model. This feature as well as further details, i.e. the mRNA amount for *CLB5* and *CLN2*, main regulators of Sic1 degradation (Hatzis and Porro, 2006; Nasmyth, 1996; Verma, 1997), will be introduced in the future to describe precise timing of the G1/S transition in a more detailed manner.

5.5 Conclusion of RESULTS I

In this chapter, single-cell fluorescence microscopy with MS2-CP system enabled us to visualize single RNPs of *SIC1* and *CLN2* in single cells, to obtain a qualitative estimation of their abundances and to record different types of transport for the *SIC1* RNPs within living cells. We combined this approach with counterflow elutriation and a morphological marker for the G1/S transition (budding) to monitor *SIC1* RNPs level in the early stages of the cell cycle. We developed a stochastic model to rationalize our experimental observation of low *SIC1* mRNA abundance with existing data and to investigate the influence of *SIC1* mRNA regulation on the timing of the G1/S. This minimal stochastic model allowed simulating time-courses of mRNAs, proteins and their related noise levels, estimating kinetic parameters and making predictions. Importantly, it revealed that a low mRNA level of the CKI prevents noise of CKI protein level and ensures a robust timing of the G1/S transition.

This chapter also revealed and discussed limitations of the MS2-CP system and elutriation previously. Therefore, improvements or alternative methods should be employed to provide absolute mRNA numbers throughout cell cycle, cell cycle timing and to characterize more accurately mRNA transport. Further research could, with such measurements and their integration in an extended model, better assess the role of transcriptional noise and mRNA transport in cell cycle regulation.

6. RESULTS II: SINGLE CELL, SINGLE MOLECULE ANALYSIS OF *SIC1*, *CLB5* AND *CLN2* UNDER OPTIMAL AND HYPEROSMOTIC GROWTH CONDITIONS WITH RNA-FISH AND STOCHASTIC MODELING

In the previous chapter our main focus was on the visualization of *SIC1* with the MS2-CP tagging method. In this chapter I described how we extended our study to the other two main players of the G1/S transition, the cyclins *CLN2* and *CLB5* and the cellular response to osmotic stress. Although the MS2-CP system is powerful for single cell mRNA detection, the tagging of the gene with the MS2 loops is challenging and time consuming and the quantitative analysis is difficult. In this current chapter we counted *SIC1*, *CLB5* and *CLN2* expression in single cells with the RNA-FISH method (sections 6.1, 6.2). We monitored their transcriptional levels over cell cycle phases employing cell cycle genetic and morphological markers (section 6.3). We challenged the robustness of gene expression applying osmotic stress to the cells and monitored the long-term response of cell cycle events (sections 6.5 & 6.5.2) as well as the transcriptional response of *SIC1*, *CLB5* and *CLN2* (sections 6.5.3 & 6.5.4). We employed stochastic modeling to extract kinetics parameters and to simulate the dynamics of the G1/S players at the RNA and protein levels throughout full cell cycle (section 6.4). Of note the model in the previous chapter (section 4.5) focused only on the beginning of the cell cycle, i.e the G1 and S phases. The model presented in this chapter also simulated the mRNA, protein and related noise levels of *SIC1*, *CLB5* and *CLN2* under hyperosmolarity (section 6.6). This chapter is based on our published article (Amoussouvi et al., 2018):

Transcriptional timing and noise of yeast cell cycle regulators – a single cell and single molecule approach. Amoussouvi A., Teufel L., Reis M., Seeger M., Schlichting J. K., Schreiber G., Herrmann A., Klipp E. (2018) *4, 1, 1-36*. *njp System Biology and Applications*. doi: 10.1038/s41540-018-0053-4 *

Contributions: Aouefa Amoussouvi (AA), Lotte Teufel (LT) and Gabriele Schreiber (GS) designed and conducted the experiments. AA, LT and Martin Seeger (MS) designed the microscopy image analysis workflow. MS programmed the microscopy image analysis workflow. Matthias Reis (MR) and AA designed the stochastic model for parameter estimation. MR programmed the stochastic model for parameter estimation. Edda Klipp (EK), Julia Katharina Schlichting (JKS), AA and LT designed the stochastic model for mRNA and protein simulations. EK and JKS programmed the stochastic model for mRNA and protein simulations. AA, LT, MR, JKS and EK analyzed the data. EK and Andreas Herrmann provided guidance and expertise.

* Note: This publication describes a version of the model for the transcription regulation of *SIC1*, *CLB5* and *CLN2* under optimal growth conditions and under osmotic stress whereas this chapter presents an extended version of the model involving mRNA and protein regulation under optimal growth conditions and under osmotic stress. The model for transcription regulation only is described in Appendix 5. The differences between the results of the models are discussed in section 7.6 of DISCUSSION II.

6.1 Establishment of single molecule resolution RNA-FISH method

RNA-Fluorescence *in situ* Hybridization (RNA-FISH) is a well-established method for single RNA molecule detection and absolute enumeration of transcripts in single cells and their transcriptional variability in populations (Ball et al., 2013; Femino et al., 1998; Raj et al., 2010; Taniguchi et al., 2010; Trcek et al., 2012; Vargas et al., 2011; Zenklusen et al., 2008). Indeed it was previously confirmed that the fluorescence of an RNA molecule tagged with RNA-FISH was proportional to the number of fluorescently labeled probes on it (Trcek et al., 2012).

We applied this method to *SIC1*, *CLN2* or *CLB5*. The RNA sequence of each gene of interest was hybridized by a set of about 35 DNA probes (Figure 17) (Raj et al., 2008). Each DNA probe was 20 nucleotides long and labeled on its 5' end with a fluorophore. We tested the specificity of the probe set for a single gene as *SIC1*, *CLN2* or *CLB5*, in performing RNA-FISH in knockout strains of those genes, *sic1Δ, cln2Δ, and clb5Δ*. We employed simultaneously two probe sets, one against the mRNAs of the deleted gene and one against a second expressed gene. The latter probe set permits to test the permeability of the cell. We observed no clear fluorescent particle for the deleted gene whereas distinct bright particles were visible for the second positive control gene. This proved that the cell preparation and hybridization were correctly executed, that the RNA-FISH probes were able to enter the cells, finally, that the RNA-FISH probes are highly specific (Figure 31).

We developed a semi-automatic analysis workflow combining existing analysis tools for cell segmentation, image stacks processing and fluorescent spot detection with newly written scripts to merge these pieces of information and performed quantitatively analysis, especially normalization of the fluorescent spot intensities and identification of transcription start sites (section 3.2.4.1 in Material and Methods). We normalized the intensity of fluorescent spots by the median fluorescence value of the spot population to estimate the number of mRNA per fluorescent spot (section 3.2.4.1 in Material and Methods). Nuclear spots containing at least three mRNA molecules indicate active transcription of the gene and were defined as transcription start sites (TSs) (Trcek et al., 2011). This workflow enabled us to speed up the processing of large set of microscopy stacks compared to a more manual workflow and to enhance the reproducibility of the image analysis.

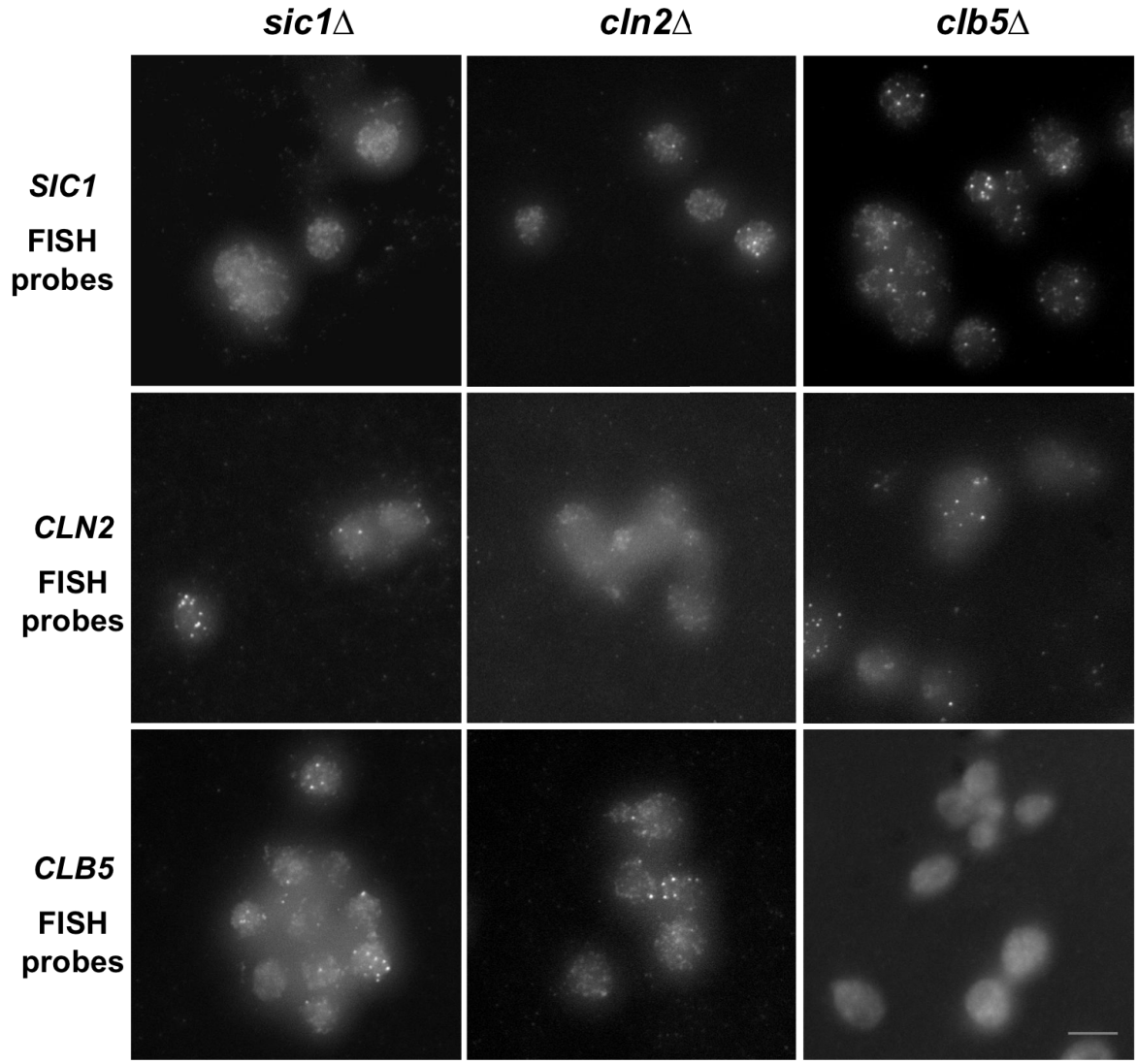

Figure 31. Specificity of the RNA-FISH probe sets for *SIC1*, *CLN2* and *CLB5*.

Specificity of a probe set for a single gene X was tested in performing RNA-FISH in a knockout strain of the specific gene X. A second set of RNA-FISH probe against a second expressed gene was used simultaneously in the same sample to test that the cell wall and membrane permeabilization and the hybridization worked well. Scale bar represents 5 μm.

6.2 Transcript distributions for *SIC1*, *CLN2* and *CLB5* in an asynchronous population.

We measured with RNA-FISH absolute transcript numbers of *SIC1*, *CLN2* and *CLB5* in single budding yeast cells of an asynchronous population (Figure 32A). We found that 96%, 92% and 88% of the spots for *SIC1*, *CLB5* and CLN2, respectively, contained one single mRNA molecule. We could also identify cell with TSs showing active transcriptional activity (Figure 32A).

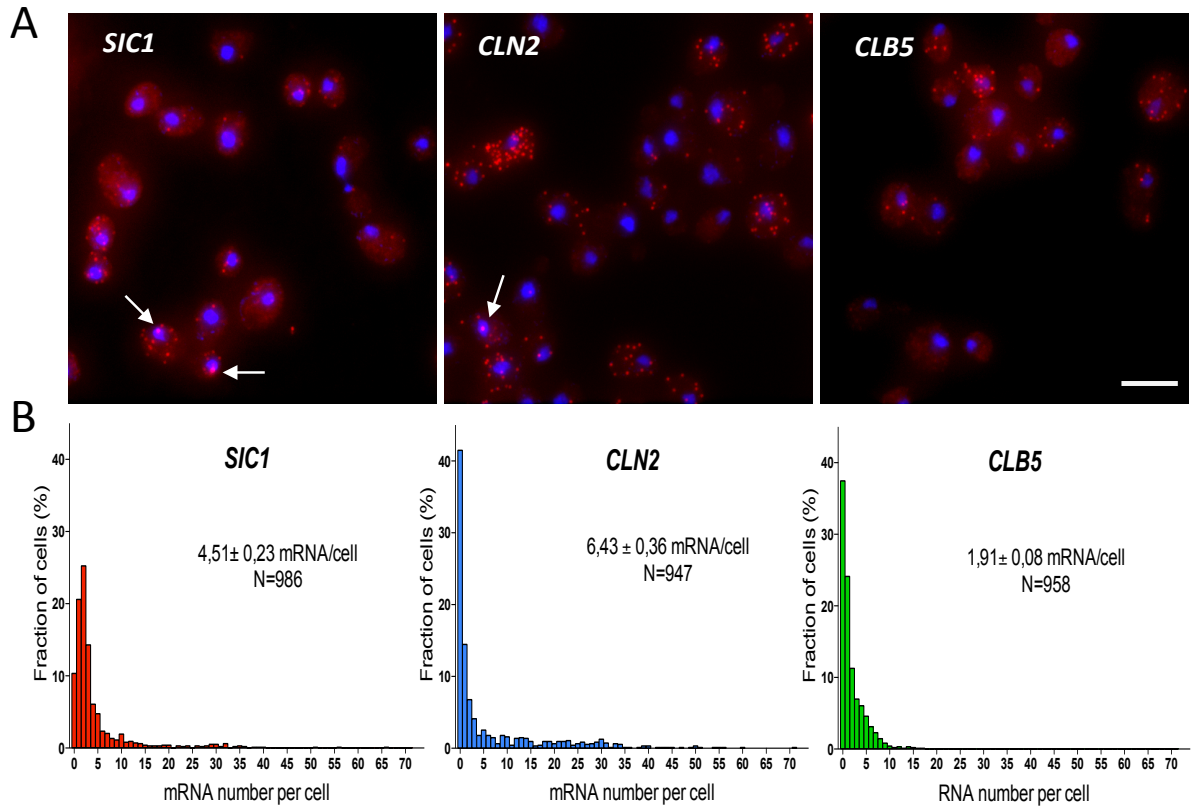

Figure 32. Images and quantitative analysis of single-cell gene expression for *SIC1*, *CLN2* and *CLB5* under optimal growth conditions in asynchronous cell population.

(A) Detection at a single molecule resolution of endogenous *SIC1*, *CLN2* and *CLB5* transcriptional expressions with RNA-FISH (mRNA molecules: red dots; DAPI-stained nucleus: blue). White arrows point towards transcription sites. Scale bar represents 5μm. (B) Experimental distribution of mRNA expression per cell for *SIC1*, *CLN2* and *CLB5* genes for the entire population. N>900 analyzed cells per gene (exact numbers in Supplementary Table S1). Full set of the numerical values for the mRNA distributions are shown in Supplementary Table S3, Supplementary Table S9 and Supplementary Table S15 in Appendix 3.

Microscopy images and frequency distributions of mRNA numbers per cell showed different patterns for the three genes with averages of 4,53, 6,46 and 1,93 and medians of 2, 1, and 1 mRNAs/cell for *SIC1*, *CLN2* and *CLB5,* respectively (Figure 32A,B). We analyzed more than 900 cells for each gene and full set of the numerical values for the mRNA distributions are shown in Supplementary Table S3, Supplementary Table S9 and Supplementary Table S15 in Appendix 3. These values were in the same order of magnitude as other RNA-FISH studies on budding yeast (Ball et al., 2013; Gandhi et al., 2011; Trcek et al., 2011) (Figure 33). 90% of the cells contained at least one *SIC1* mRNA indicating that its production is never turned completely off, whereas *CLN2* and *CLB5* mRNAs were absent from about 40% of the population (Figure 32B). A few cells showed very high mRNA abundances resulting in long tails in the distributions of *SIC1* and *CLN2* (Figure 32B). *CLN2* showed the higher fraction of cells with TSs (16,17%) compared to *SIC1* (3,31%) and *CLB5* (1,68%) (Figure 32A).

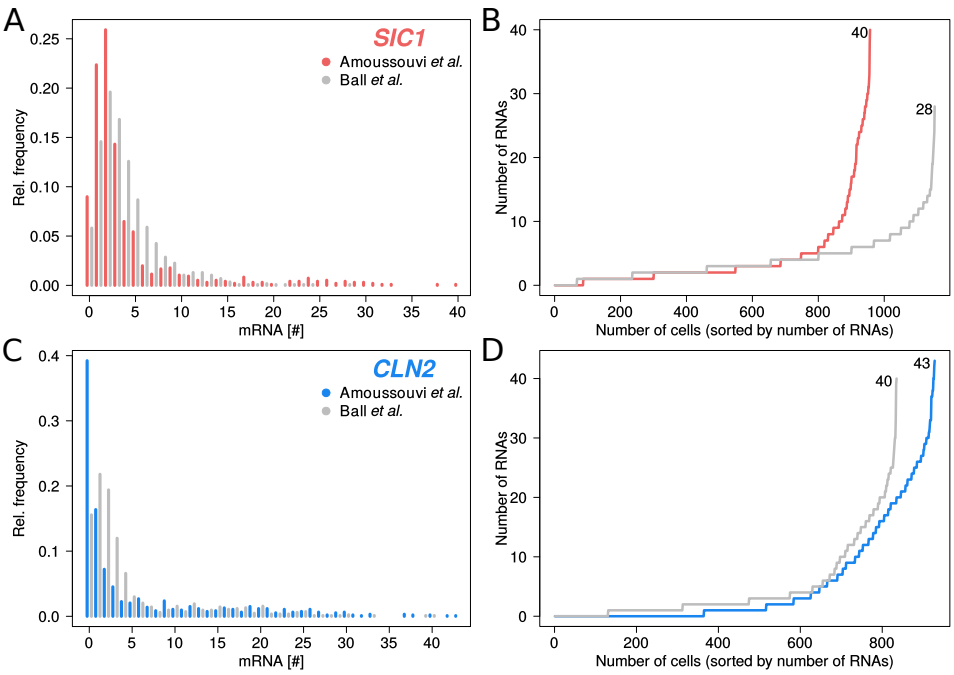

Figure 33. Comparison of this study with Ball *et al.* (2013) for mRNA distributions of *SIC1* and *CLN2*.
Comparisons for *SIC1* are given in (A)-(B) and for *CLN2* in (C)-(D). Data from this study are colored, whereas data from Ball *et al.* (2013) are gray. Data from this work correspond to number of detected fluorescent spots without normalization. (A) and (C) show histograms of relative frequencies of mRNA numbers over all cell cycle phases. (B) and (C) represent mRNA numbers per cell sorted by the number of mRNAs. The maximum number of mRNAs per cells is written close to the graphs. Means of mRNA per cell are in the same order of magnitude, i.e. for *SIC1* 4,11 in this study and 2,93 in Ball *et al.* as well as for *CLN2* 5,40 in this study and 4,24 in Ball *et al.* (discrepancies between single mRNA abundances can be partially attributed to systematic differences due to biological (yeast strain and culture media) and technical differences: we grew haploid BY4741 yeast strain in YPD while Ball and colleagues grew diploid BY4743 strain in SC medium).

6.3 Changes of *SIC1*, *CLB5* and *CLN2* transcriptional abundances over cell cycle progression

6.3.1 Genetic and morphological markers of cell cycle progression

To investigate changes of mRNA abundances over cell cycle we assigned each cell of an asynchronous cell culture to a cell cycle phase using genetic and morphological markers: presence and size of a bud, morphology of the DAPI-stained nucleus, number and localization of spindle pole body visualized by mTurquoise-labeled Spc42, and localization of TagGFP-labeled Whi5 (Trcek et al., 2011) (details in section 1.5.3 in Material and Methods). Whi5 is recruited to the nucleus between late M and early G1 and is cytoplasmic during the rest of the cycle (Costanzo et al., 2004). We distinguished seven phases, i.e. early G1, late G1, S, G2, prometa-/metaphase (P/M), anaphase (Ana) and telophase/cytokinesis (T/C) (Figure 34). Tagging of Whi5 and Spc42 did not alter cell cycle progression or gene expression as we obtained similar growth rates and mRNA distributions of *SIC1*, *CLN2* and *CLB5* in wild type and in the strain containing Whi5TagGFP and Spc42mTurquoise (Figure 13 in Material & Method). The culture doubling time was about 129 min in YPD at 30°C (124 min for wild type). Phase durations were determined as being proportional to the percentage of cells in each phase (Trcek et al., 2011) (Figure 34).

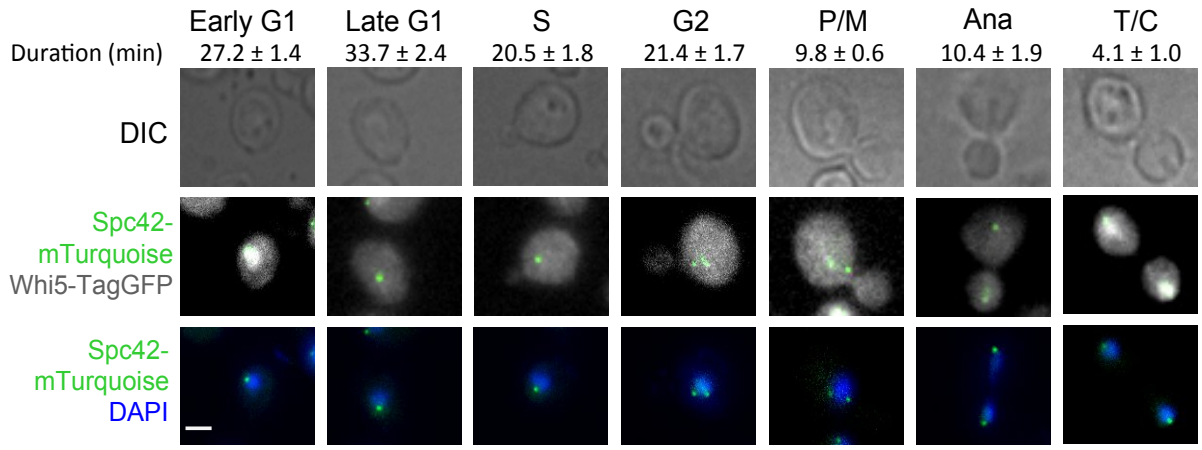

Figure 34. Morphological and genetic markers of cell cycle progression.

Morphological and genetic cell cycle progression markers allow discriminating seven different cell cycle phases (early G1, late G1, S, G2, P/M, Ana, T/C). Markers used were the presence and size of a bud (first line), the number and orientation of the spindle pole bodies (green spots in second and third lines), the localization of Whi5 (white in second line) and the shape and number of nuclei (blue in third line). Scale bar represents 5µm. The duration (mean ± SEM) of the phases has been determined according to the number of cells found in each phase (>2600 cells). Duration of a full cycle was 128.6 ± 10.7 min.

6.3.2 *SIC1* is present throughout cell cycle.

SIC1 transcript level was minimal between G1 and early mitosis, i.e. P/M, and sharply increased in anaphase from its basal level of about 2 mRNAs/cell to a maximum of about 25 mRNAs/cell in T/C, i.e. at the end of mitosis (Figure 35A). *SIC1* level dropped to about 4 mRNAs/cell when cells entered into next early G1 and further progressively decreased until S phase to its basal level. The *SIC1* mRNA expression peak maximum in T/C, i.e. late mitosis, is consistent with previous studies (Aerne et al., 1998; Knapp et al., 1996; Toyn et al., 1997). The fraction of cells with transcription sites showed a comparable dynamics reaching a maximum in anaphase and T/C phases (Figure 35A). To conclude basal *SIC1* presence was robust throughout cell cycle. Indeed, in S, G2, P/M, the phases of lowest *SIC1* expression, more than 80% of the cells contained at least one *SIC1* mRNA (Figure 35B).

6.3.3 *CLN2* and *CLB5* transcription shows enduring basal levels and rises in late mitosis.

As expected for genes of the G1 cluster, *CLN2* and *CLB5* showed transcription maxima in late G1 (Figure 35A). We observed an unexpected transcriptional increase during late mitosis with 60% and 80% of cells containing at least one mRNA of *CLN2* and *CLB5*, respectively, in T/C (Figure 35B). Since only about 3% of the cells were in T/C, we would need higher cell numbers to statically characterize this phenomenon. Transcript levels of *CLN2* and *CLB5* were low in early G1 and increased to a maximum of about 18 and 4 mRNAs/cell, respectively, in late G1. During late G1, 94% and 86% of cells contained at least one transcript of *CLN2* or *CLB5*, respectively (Figure 35B).

After G1/S transition transcript levels dropped. From G2 until mitosis, *CLN2* and *CLB5* levels were minimal, however, about 30% of cells contained at least one mRNA (Figure 35B). The dynamics of transcription sites resembled that of the mRNAs and displayed maxima in late G1 and T/C (Figure 35A).

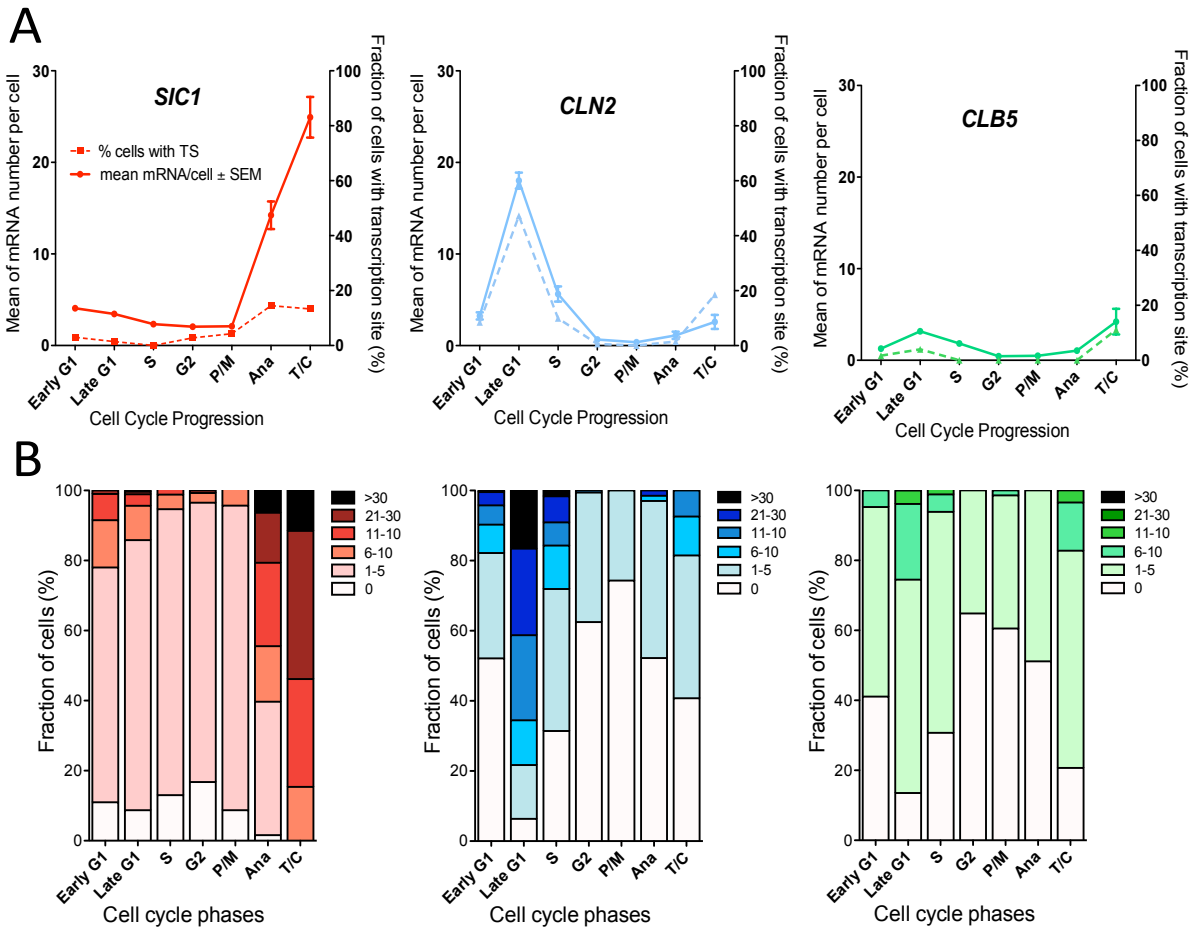

Figure 35. *SIC1*, *CLB5* And *CLN2* RNA abundances throughout cell cycle progression at native level.
(A) Abundances of mRNA (full lines) for *SIC1, CLB5* and *CLN2* and transcriptional activity (dotted lines) during the cell cycle progression. Lines between data points are for visualization only. Data shown are mean ± SEM. n > 900 (exact numbers in Supplementary Table S1). Full set of numerical data for mRNA means in Supplementary Table S2. (B) Distributions of mRNAs for each cell cycle phase grouped as follow 0, 1-5, 6-11, 12-20, 21-30, >30 mRNAs per cell.

6.4 Computational modeling for mRNA, protein and noise dynamics of *SIC1*, *CLN2* and *CLB5* - Rationalizing experimental data.

6.4.1 Description of the stochastic model including *SIC1, CLN2* and *CLB5* mRNA and protein expression and model parameterization.

Firstly, to understand mRNA dynamics based on static, but time-resolved, single cell RNA-FISH data we stochastically modeled transcription and degradation for each species. Secondly, to analyze the interplay of the three genes in G1/S transition regulation, we combined the model for transcription with the dynamics of the encoded proteins, i.e. Sic1, Cln2, Clb5 and complexes thereof as measured previously (Adrover et al., 2011). Cln2 and Clb5 bind the kinase Cdk1 to form active complexes. However, Sic1 binds to Clb5-Cdk1 thereby inhibiting it. The active kinase in complex with Cln2 phosphorylates Sic1 at multiple sites prompting it to degradation and release of active Clb5-Cdk1 (for details see Table 17). The network is shown in Figure 36A. For ease of reading figures, curves for *SIC1* and Sic1 are always in red, for *CLN2* and Cln2 in blue, and for *CLB5* and Clb5 in green.

Signals S_1 to S_3 indicate the up-regulation of transcription for *SIC1* (S_1), *CLN2* (S_2), and *CLB5* (S_3) (Figure 36). We assumed steady degradation rate constants (p_i) and different transcription rates (k_{ih} or k_{il}) in periods of either high (*h*) or low (*l*) expression, respectively (Figure 36B and C). Periods of high expression are defined by transcription start time ($t_{S_{i,0}}$) and transcription end time ($t_{S_{i,e}}$). The duration of one cell cycle is set to $t = 129\,\mathrm{min}$.

Because the mRNA numbers were measured as distributions per cell cycle phase, a specific approach in parameter estimation was required. Since the mRNAs for each gene evolved statistically independently, we could estimate parameter values for transcription and degradation rate constants and transcription start and end times separately. We used the analytical solution of the chemical master equation for monomolecular reactions with Poisson initial conditions. We obtained the best results with a local optimizer falling into the class of “line search” algorithms (see Appendix 2 Parameter estimation).

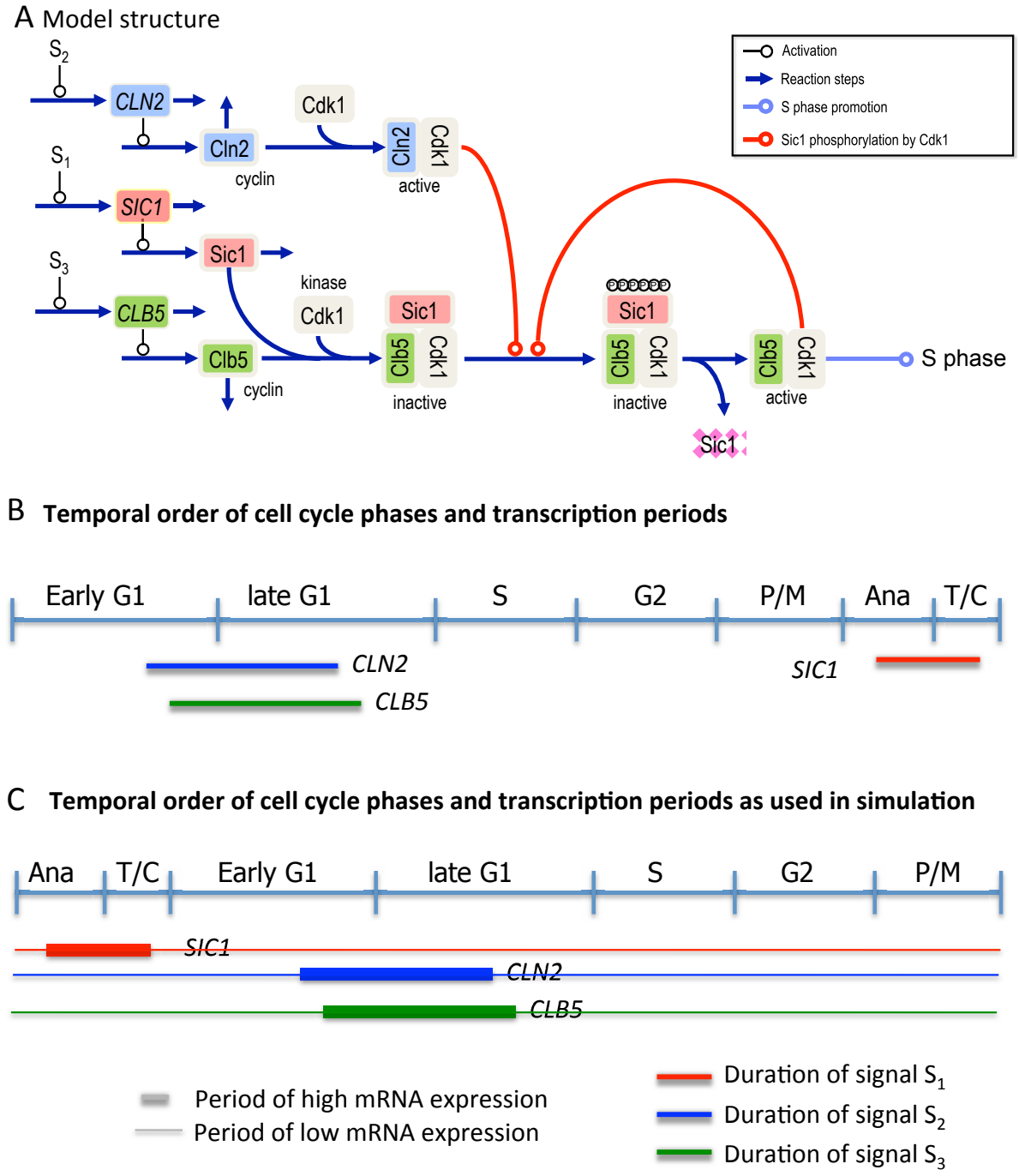

Figure 36. Molecular network and simulation rules for the model for G1/S transition controlled by *SIC1, CLN2* and *CLB5* under optimal growth conditions.

(A) Transcription of the genes *SIC1*, *CLN2*, and *CLB5* is regulated by the signals S_1, S_2, and S_3, respectively. The mRNAs, in turn, serve as templates for proteins Sic1, Cln2, and Clb5, respectively. The proteins bind the kinase Cdk1 (not accounted for in the model). Sic1 binds to Clb5 inhibiting it. Cln2-bound Cdk1 phosphorylates Sic1 prompting it for degradation. The released active Clb5-Cdk1 can also phosphorylate Sic1 and is also responsible for the transition into S phase. (B) Schematic of the temporal order of cell cycle phases and distinct active and inactive transcription periods of mRNA (due to S_1, S_2, or S_3 signals being on). (C) Simulations were started in anaphase of the previous cell cycle. In the model transcription activity switches between a high and a low state.

Table 17. Reactions of the G1/S transition network involving *SIC1*, *CLN2* and *CLB5* genes and their protein interactions.

This table lists all elementary processes and the respective reaction schemes. All reactions follow mass action kinetics. The rate expressions, i.e, transcription rates ($k_{ih,l}$) during high (h) or low (l) promoter activity and rates of mRNA degradation (p_i), are provided as well as the respective parameter values. The last column provides the times for beginning ($t_{Si,0}$) and end ($t_{Si,e}$) for high expression of the respective genes.

Process	Reaction scheme	Rate	Parameter values	Transcription times
SIC1 transcription	$\rightarrow SIC1$	$k_1 \cdot S_1$	$k_{1h} = 12{,}42\,\mathrm{min}^{-1}$ $k_{1l} = 1{,}097\,\mathrm{min}^{-1}$	$t_{S1,0} = 118\,\mathrm{min}$ $t_{S1,e} = 127{,}6\,\mathrm{min}$
SIC1 degradation	$SIC1 \rightarrow$	$p_1 \cdot SIC1$	$p_1 = 0{,}433\,\mathrm{min}^{-1}$	
Sic1 translation	$\rightarrow$ Sic1	$k_2 \cdot SIC1$	$k_2 = 15\,\mathrm{min}^{-1}$	
Sic1 degradation	Sic1 $\rightarrow$	$p_2 \cdot$ Sic1	$p_2 = 0.1\,\mathrm{min}^{-1}$	
CLN2 transcription	$\rightarrow CLN2$	$k_3 \cdot S_2$	$k_{3h} = 6{,}7\,\mathrm{min}^{-1}$ $k_{3l} = 0{,}15\,\mathrm{min}^{-1}$	$t_{S2,0} = 24\,\mathrm{min}$ $t_{S2,e} = 55\,\mathrm{min}$
CLN2 degradation	$CLN2 \rightarrow$	$p_3 \cdot CLN2$	$p_3 = 0{,}223\,\mathrm{min}^{-1}$	
Cln2 translation	$\rightarrow$ Cln2	$k_4 \cdot CLN2$	$k_4 = 25\,\mathrm{min}^{-1}$	
Cln2 degradation	Cln2 $\rightarrow$	$p_4 \cdot$ Cln2	$p_4 = 0.4\,\mathrm{min}^{-1}$	
CLB5 transcription	$\rightarrow CLB5$	$k_5 \cdot S_3$	$k_{5h} = 1{,}5\,\mathrm{min}^{-1}$ $k_{5l} = 0{,}17\,\mathrm{min}^{-1}$	$t_{S3,0} = 25\,\mathrm{min}$ $t_{S3,e} = 60\,\mathrm{min}$
CLB5 degradation	$CLB5 \rightarrow$	$p_5 \cdot CLB5$	$p_5 = 0{,}15\,\mathrm{min}^{-1}$	
Clb5 translation	$\rightarrow$ Clb5	$k_6 \cdot CLB5$	$k_6 = 25\,\mathrm{min}^{-1}$	
Clb5 degradation	Clb5 $\rightarrow$	$p_6 \cdot$ Clb5	$p_6 = 0.15\,\mathrm{min}^{-1}$	
Binding of Sic1 to Clb5	Sic1+Clb5 $\rightarrow$ Sic1Clb5	$k_7 \cdot$ Sic1 $\cdot$ Clb5	$k_7 = 2\,\mathrm{min}^{-1}$	
Phosphorylation of Sic1 by Cln2	Sic1Clb5 $\rightarrow$ P_Sic1Clb5	$k_8 \cdot$ Sic1Clb5 $\cdot$ Cln2	$k_8 = 2\,\mathrm{min}^{-1}$	
Degradation of P_Sic1	P_Sic1Clb5 $\rightarrow$ Clb5_*active*	$k_9 \cdot$ P_Sic1Clb5	$k_9 = 2\,\mathrm{min}^{-1}$	
Degradation of Clb5_*active*	Clb5_*active* $\rightarrow$	$p_{10} \cdot$ Clb5_*active*	$p_{10} = 0.2\,\mathrm{min}^{-1}$	
Phosphorylation of Sic1 by Clb5_*active*	Sic1Clb5 $\rightarrow$ P_Sic1Clb5	$k_{11} \cdot$ Sic1Clb5 $\cdot$ Clb5_*active*	$k_{11} = 3\,\mathrm{min}^{-1}$	

The rate constants and transcription start and stop times of the stochastic model for mRNA abundances were fitted (see Section D in Appendix 2 Parameter estimation) to best reproduce the experimental time-resolved frequency distributions of *SIC1*, *CLN2*, and *CLB5* mRNAs (Supplementary Table S3, Supplementary Table S9, Supplementary Table S15 and Supplementary Figure S 5) as well as their overall mRNA distributions (Figure 37A). For the combined stochastic model including the proteins and complexes thereof, those rate constants and transcription times were adjusted to take into account the normalized time courses of Sic1, Cln2, and Clb5 proteins (Adrover et al., 2011) and the average abundances of these proteins (768 Sic1, 1270 Cln2, 521 Clb5 molecules per cell (Ghaemmaghami et al., 2003)).

Expression dynamics could only be satisfactorily fitted to data by assuming low, but non-zero, transcription outside the main periods of high transcription with relative promoter activities of 8.8%, 2.2% or 7.7% for *SIC1*, *CLN2* and *CLB5*, respectively (Figure 36C). Table 17 provides the resulting parameter values.

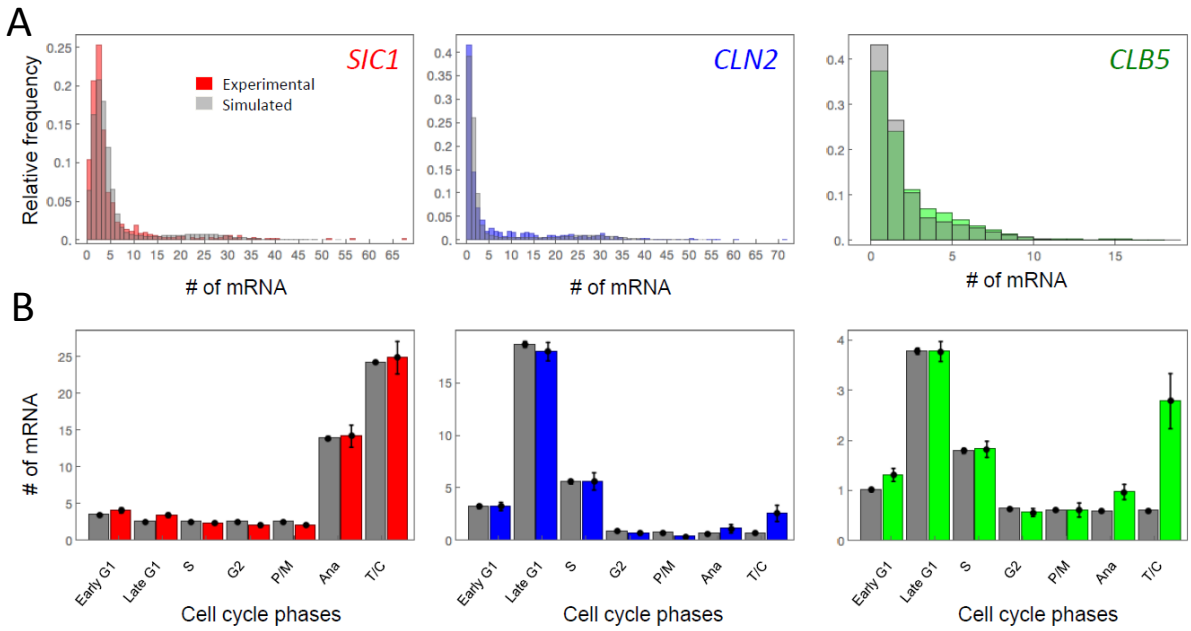

Figure 37. Stochastic model reproduces experimental *SIC1*, *CLN2* and *CLB5* expression under optimal growth conditions.

(A) Experimental (colored) and simulated (grey) distributions of mRNA numbers per cell for *SIC1*, *CLN2* and *CLB5* for the entire population. (B) Experimental (colored) and simulated (grey) mRNA average numbers for *SIC1, CLB5* and *CLN2* per cell cycle phases. Data shown are mean ± SEM. In (A) and (B) n>900 cells for experiments and n = 2000 cells for simulations. Experimental data in (A) and (B) are equivalent to the one presented in Figure 32B and Figure 35A.

6.4.2 Time courses of *SIC1*, *CLN2* and *CLB5* mRNA, protein and noise levels

6.4.2.1 *SIC1* mRNA level is less noisy than *CLN2* and *CLB5* and mRNA noise is lower in high expression phases than in low expression phases.

We analyzed the noise for experimental and simulated mRNA abundances of *SIC1*, *CLN2* and *CLB5* calculating the coefficient of variation (CV), i.e. ratio of standard deviation to mean (Figure 38,Supplementary Figure S 16A). Except of in late G1, *SIC1* transcript population had the lowest experimental CV values among the three genes and, therefore, the least degree of noise (Figure 38A).

A

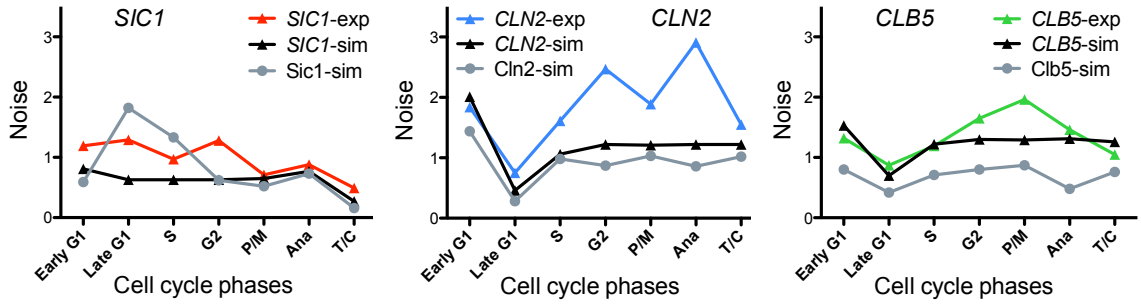

B

	high expression				low expression			
	RNA		Protein		RNA		Protein	
	Mean	Noise	Mean	Noise	Mean	Noise	Mean	Noise
SIC1	28.68	0.19	4302.54	0.09	2.53	0.63	380.02	0.31
CLN2	30.04	0.18	1877.80	0.25	0.67	1.22	42.04	1.64
CLB5	5.30	0.43	883.39	0.32	0.60	1.29	100.12	0.94

Figure 38. Noise of mRNA and protein.
Noise is calculated as CV, i.e. ratio of standard deviation to mean. (A) Experimental and simulated noise of mRNA and protein in cell cycle phases (experimental mRNA: triangles, colored lines; simulated mRNA: triangles, black lines; simulated proteins: circles, gray lines). Lines between data points are for visualization only. (B) Simulated noise in high and low periods of expression. Noise of mRNA has been determined from the RNA-FISH experimental data (A) (n>900 cells) or the stochastic simulations (n=2000 simulated cells) (A) and (B). Protein noise refers to the total of each protein species (i.e. including the complexes) and is calculated from the stochastic simulations (n=2000 simulated cells) in (A) and (B).

We simulated for each mRNA species (i) the time courses for a population of 2000 cells (Figure 39A), (ii) the noise for this population over time (Figure 39B), and (iii) the noise per cell during one cell cycle period (Supplementary Figure S 6. , Supplementary Figure S 7., Supplementary Figure S 8. and Supplementary Figure S 9.). Simulations were performed from anaphase until T/C phase of the next cell cycle, leading to a shift of 15 min between simulation time and cell cycle time. Our simulations satisfactorily reproduced the experimental data, i.e. distributions of mRNA per cell (Figure 37B), means per cell cycle phase and the distributions per cell cycle phase (Figure 37C, Supplementary Figure S 5) as well as mRNA noise (Figure 38). Noise calculated in periods of either high or low expression both from the parameter values and based on the simulated time courses (Figure 38B, Supplementary Figure S 7., Supplementary Figure S 8. and Supplementary Figure S 9.) revealed lower noise in high expression phases than in low expression phases.

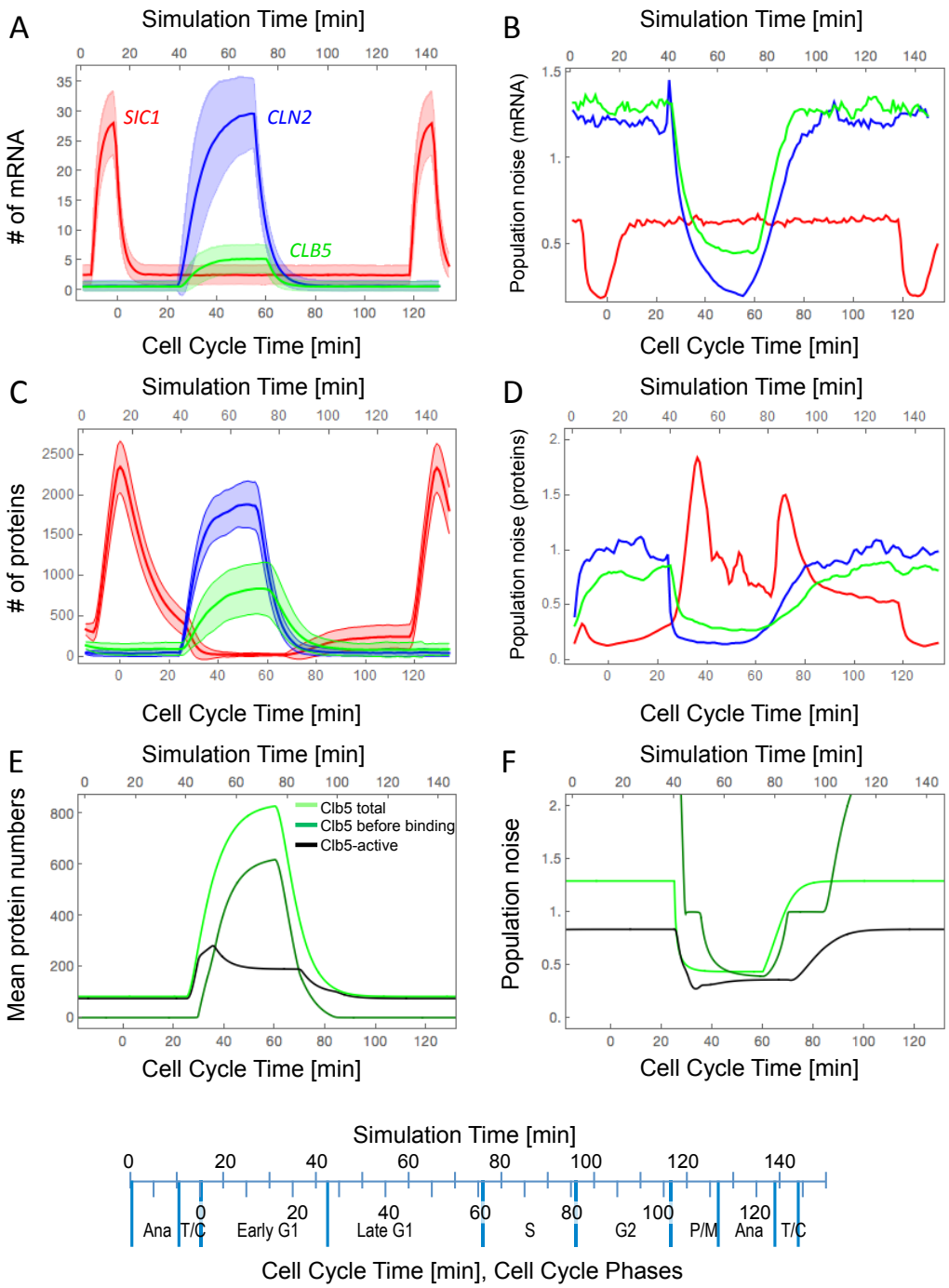

Figure 39. Simulated time-course of transcript, protein and molecular noise during cell cycle for *SIC1*, *CLN2* and *CLB5* under optimal conditions.

Simulations were performed with the Gillespie algorithm using the equations and parameter values provided in Table 1. 2000 cells were simulated. Time courses were simulated from anaphase until T/C phase of the next cell cycle, leading to a shift of 15 min between simulation time and cell cycle time. Transcript levels increase during periods of active signals S_1, S_2, or S_3 (see Figure 36A). (A) and (C) Time courses of mean values (thick lines) and standard deviations (shaded areas around thick lines) of mRNA and protein, respectively. (B) and (D) Time courses of noise measured over the whole population, i.e. standard deviation divided by mean of all 2000 cells at each time point. (E) and (F) represent the changes of molecule numbers and molecular noise of the different forms of Clb5 protein, e.g. total Clb5 (light green), Clb5 before binding with Sic1 (dark green) and active Clb5 released from Sic1 inhibition (black). Time courses in (E) and (F) were calculated with moment closure method.

6.4.2.2 Noise analysis for Sic1, Cln2 and Clb5 proteins

To investigate the noise of the protein level we estimated the parameters for protein translation, stochastically simulated protein levels for Sic1, Cln2 and Clb5 including active Clb5 and the complexes of Sic1 with Clb5 or phosphorylated Clb5 (Figure 39C: time courses of mean and standard deviation of total protein concentrations; Supplementary Figure S 10: single time courses for 2000 cells for each gene separately) and calculated the respective noise levels (Figure 39D). Especially interesting is the noise of total Clb5 and active Clb5 since the latter is critical for S phase transition (Figure 39E and F). The simulations revealed that (i) also protein noise is higher in low expression periods than during high expression (Figure 39D, Figure 38B), (ii) active Clb5, i.e. after release from Sic1, has the lowest noise levels (Figure 39F), especially in low transcription periods (Supplementary Figure S 9.).

6.4.3 Dependence of protein noise of single cells on their respective mRNA levels

We analyzed the dependence of protein noise of single cells on their respective mRNA levels over the cell cycle as well as for periods of either low or high expression based on our simulations (Figure 40). In case of low expression periods, low mRNA numbers are related to higher protein noise and *vice versa*. For high expression periods, this relation holds no longer true: protein noise is either independent of mRNA numbers for *CLB5*/Clb5 and *CLN2*/Cln2 or even increases with them for *SIC1*/Sic1. Noise of active Clb5 protein showed in high expression periods no clear correlation with neither the mean mRNA of *CLB5*, *CLN2* nor *SIC1* or Sic1. This indicates that high and sharp bursts may initiate more noise but also a further role of Sic1-Clb5 interaction and/or other post-translational processes in noise regulation.

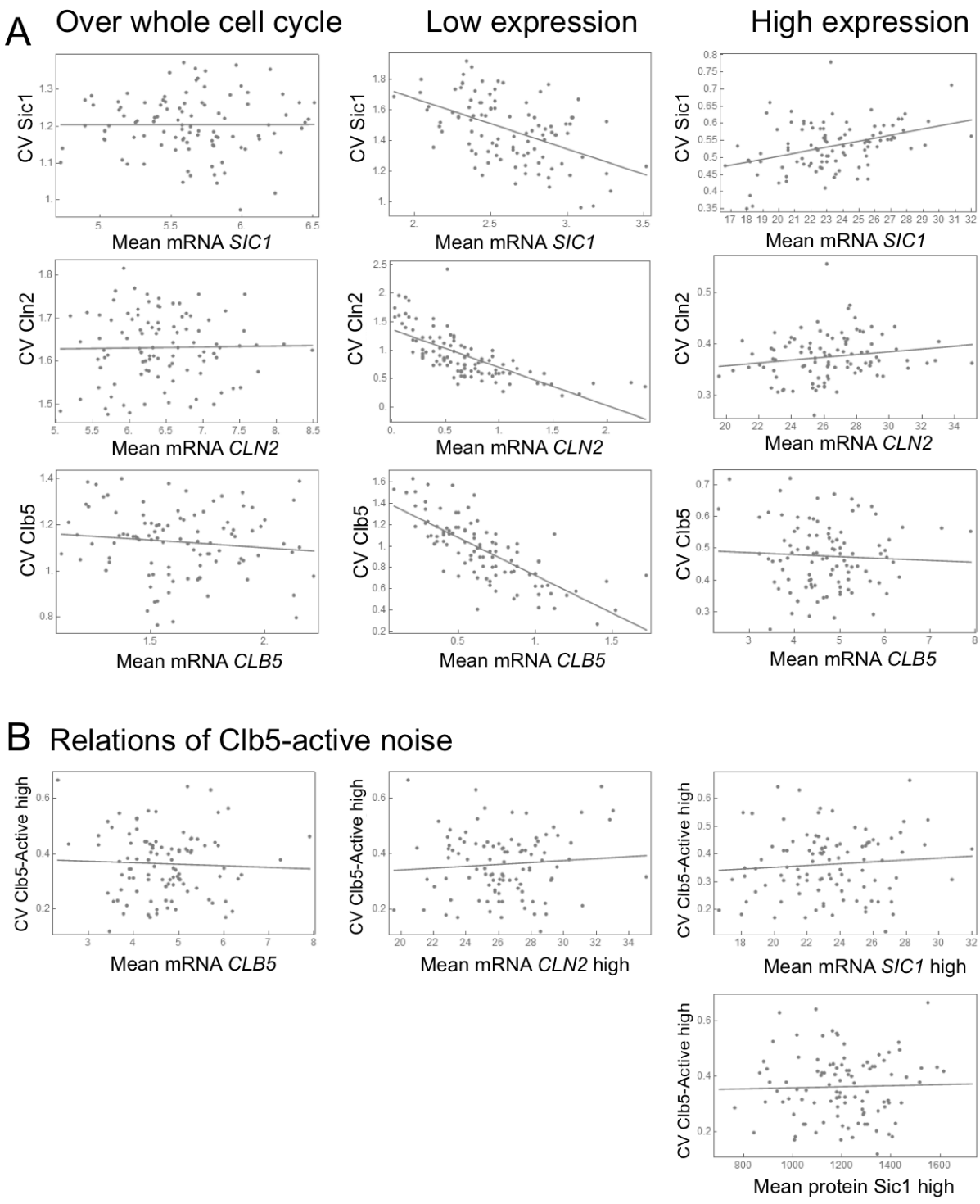

Figure 40. Relation of protein noise to abundances of other molecular species.

(A) Relation of protein noise to mean mRNA numbers. (B) Relations of noise of Clb5-active to mRNA abundances or amount of Sic1 protein in high expression phase. 200 cells were simulated. Lines represent linear fits.

6.5 Effects of hyperosmolarity on cell cycle progression and on *SIC1*, *CLB5* and *CLN2* transcription levels

6.5.1 Osmotic stress has short and long term impacts on the timing of cell cycle phases.

To test the robustness of G1/S transition with respect to perturbations, we exposed yeast cells to hyperosmolarity. Osmotic stress forces the cell to shrink within a few seconds, leads to activation of the stress-activated MAP kinase Hog1 and triggers a response program required for cell survival (Hohmann, 2002; Klipp et al., 2005; Saito and Posas, 2012). Dependently on the cell cycle phase cell, cell cycle progression is delayed to allow for stress adaptation. However the immediate influence of osmotic stress on transcription in unsynchronized cells and the long-term response remain elusive.

To monitor stress response we applied 0,4 M NaCl to a cell culture for 0, 15, 30, 45, 60 and 90 min, fixed the cells and assigned each cell to a cell cycle phase (Figure 41). Since cell population was not synchronized, the phase at which cells have been hit by stress could not be determined. While cell cycle duration without stress is known, the cell cycle phase lengths upon stress are affected to a so far unknown degree and the full cell cycle length upon stress remained undetermined. We found that the fraction of cells in each cell cycle phase, and hence the length of that phase, was affected differently and even 90 min under stress conditions the distribution of cells in each phase had not totally recovered to non-stress situation. Cells accumulated substantially in early G1 after 30 min and in G2 after 45 min of stress. The fraction of cells in both phases increased from 21.1% to 41.0 % for early G1 and from 16.6% to 19.8% for G2. Simultaneously, the fraction of cells in late G1, S, and in mitosis (P/M, Ana and T/C) decreased. Interestingly, the decrease of the mitosis fraction lasted longer than the one in late G1 and S phase fractions. Indeed, we observed that recovery of the mitosis fraction started after 60 min whereas those of the late G1 and S fractions already after 30 min. The measured results are largely in agreement with previous simulations obtained from modeling a cell population under osmotic stress (Spiesser et al., 2016).

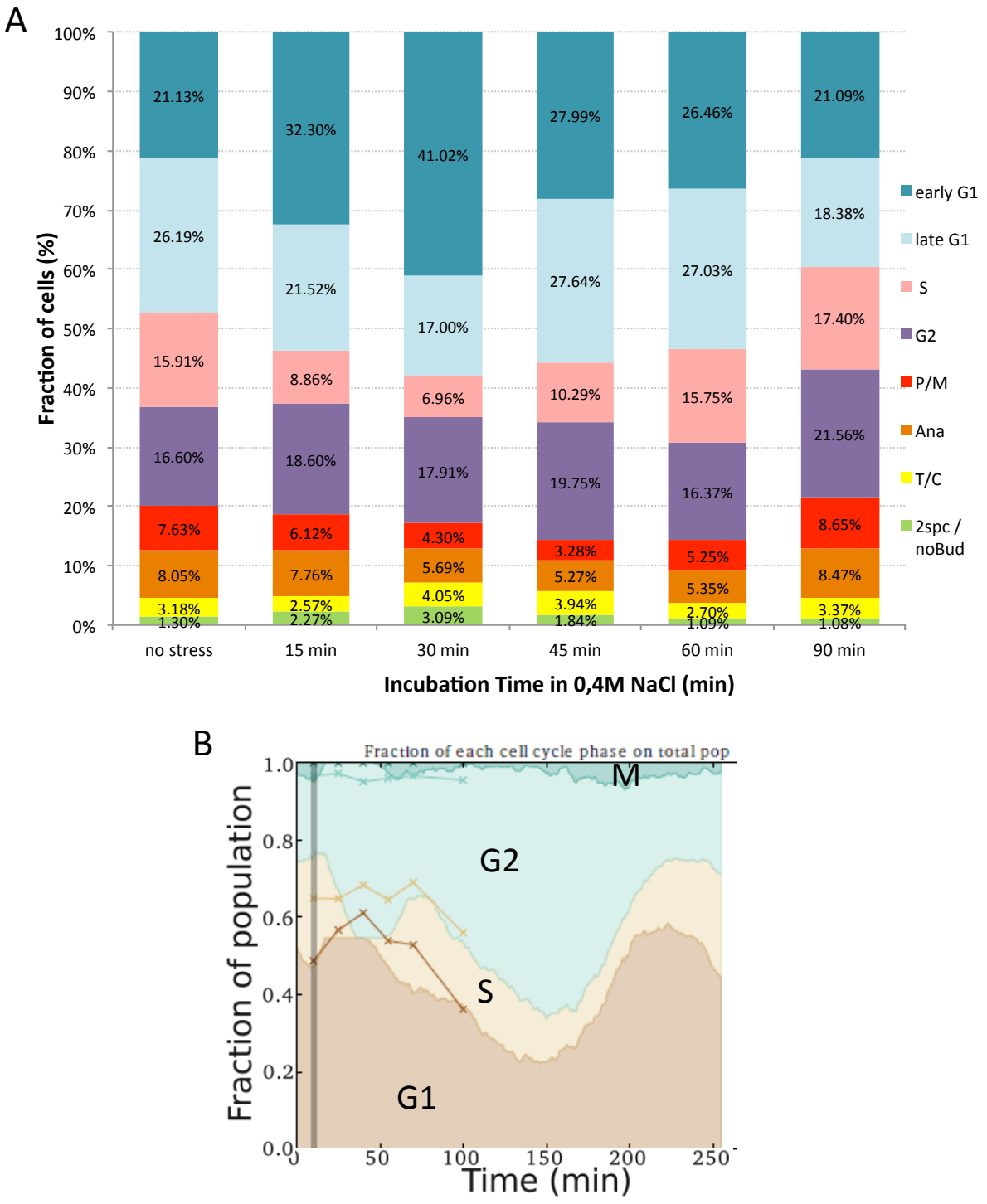

Figure 41. Hyperosmolarity affects cell cycle progression.

(A) Fraction of cells in each cell cycle phases under normal growth condition (no stress) and under exposure to hyperosmolarity for 15, 30, 45, 60 and 90 min. The cells were assigned to each phase using the markers previously described (>1500 cells per osmotic stress time point). (B) Comparison of experimental data in (A) with previous simulations obtained from modeling a cell population under osmotic stress (Spiesser et al., 2016). Crosses connected with lines are the experimental data in this study presented in (A).

6.5.2 Partial loss of synchrony between DNA replication and bud morphogenesis under osmotic stress.

Under normal growth conditions, budding and DNA duplication occur synchronously and are hallmarks of S phase entrance (Dirick et al., 1995; Schwob and Nasmyth, 1993; Stuart and Wittenberg, 1994). Under hyperosmotic conditions we observed a small fraction of cells with two spindle pole bodies but without bud, indicating loss of synchrony between bud morphogenesis and DNA duplication (Figure 42). Those cells represented 1.3% of the population under normal growth conditions and increased to a maximum of 3.1% after 30 min of osmotic stress, returning to 1.1% after 90 min (Figure 41).

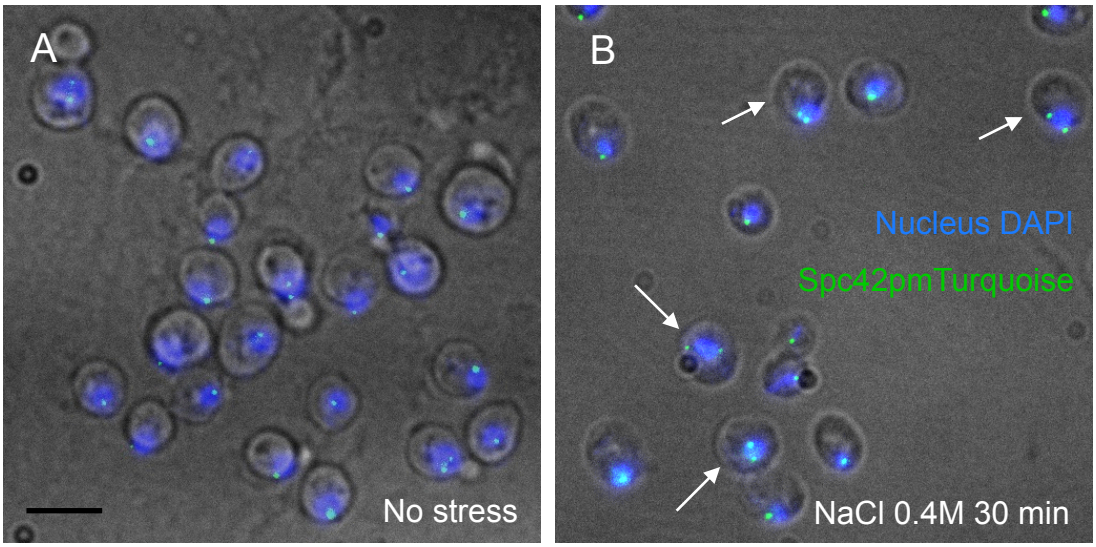

Figure 42. Hyperosmolarity causes an asynchrony between budding and DNA replication.
Fluorescence microscopy images depicting a fraction of cells under optimal growth conditions (A) and after 30 min under hyperosmolarity (B). In (B) white arrows point to cells containing two separated spindle pole bodies without bud, indicating a loss of synchrony between DNA replication and budding. Imagines are overlays of the images of bright field image, DAPI-stained nucleus (in blue) and mTurquoise tagged Spc42p part of the spindle pole body (in green). Scale bar represents 5μm.

6.5.3 Hyperosmolarity induces a transient inhibition of *CLN2* and *CLB5* and does not significantly affect *SIC1* level

Upon osmotic stress, *SIC1* mRNA levels and transcriptional dynamics were the least affected of the three genes (Figure 43, Supplementary Figure S 15). *SIC1* mRNA maximum remained at the end of mitosis in T/C and its basal level stayed robust from early G1 until the beginning of mitosis in P/M (Supplementary Figure S 15A, Figure 43C). The mean *SIC1* level of the asynchronous population slightly increased within the first 30 min upon stress (Figure 43AB) due to the increase of *SIC1* in T/C and anaphase at 15 and 30 min stress exposure (Figure 43C). The fraction of cells with *SIC1* transcription sites also showed a minor increase within the first 30 min upon stress (Figure 43A).

Contrarily, *CLN2* and *CLB5* mRNA levels declined within the first 15 min upon osmotic stress and showed distinct recovery patterns (Figure 43, Supplementary Figure S 15). Within the first 15 min *CLN2* and *CLB5* levels dropped from 6.4 to 2.0 and from 1.9 to 0.5 mRNA per cell, respectively, later

increased from 15 to 45 min. From 60 until 90 min of stress, *CLN2* mRNA levels recovered to unstressed transcription level, while *CLB5* levels at 90 min were still lower than before stress indicating only partial recovery within the cell population (Figure 43AB, Supplementary Figure S 15. The fraction of cells with transcription sites followed the behavior of their respective cyclin mRNA levels (Figure 43A).

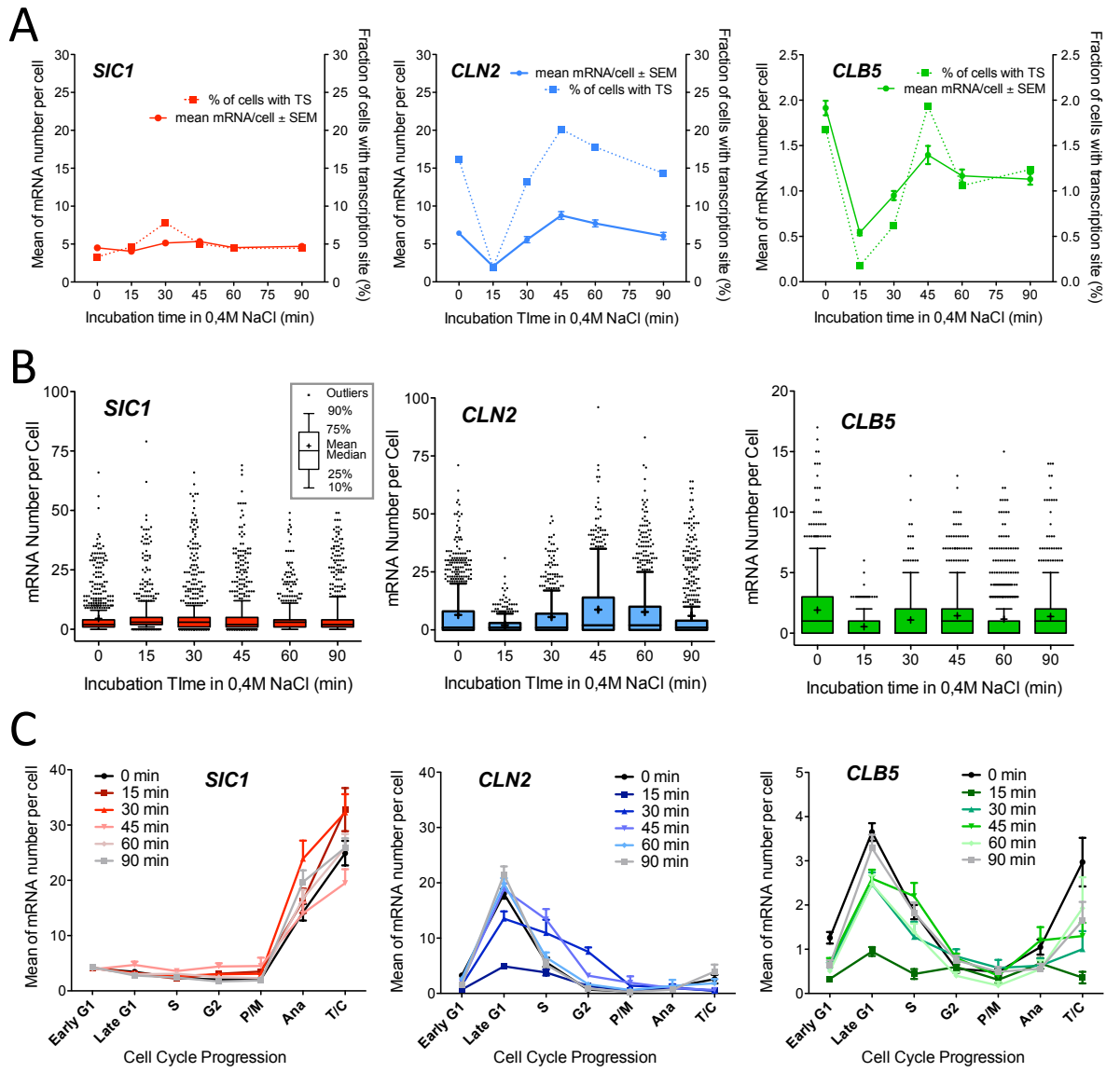

Figure 43. Hyperosmolarity affects *SIC1*, *CLB5* and *CLN2* transcription.

(A) Changes in mRNA levels shown as mean ± SEM (dots and full lines) and transcription activity represented by percentage of cells with a transcription site (TS) (squares and dotted lines). (B) Changes within the population. Lower and upper quartiles (75th and 25th percentiles) form boundaries of the boxes. Lines and crosses inside the boxes represent medians and mean values, respectively. Upper and lower whiskers limits represent 90th and 10th percentiles, respectively. Data points outside of the whiskers define single cell outliers. (C) Hyperosmolarity affects *CLB5* and *CLN2* transcription in cell cycle phase. Changes of mRNA level timing for *SIC1, CLN2* and *CLB5* in cell cycle phases under optimal growth conditions (0 min) and upon medium osmotic stress. Data shown are mean ± SEM. Black and grey curves correspond to data for 0 and 90 min, respectively. Darkest curves correspond to the shortest incubations in hyperosmotic medium. Between 400 and 1000 cells analyzed per gene and time point (exact numbers in Supplementary Table S1 in Appendix). Full set of the numerical values for the mRNA means is shown in Supplementary Table S2 and of the distributions is shown in Supplementary Table S3 to Supplementary Table S20 in Appendix 3.

6.5.4 Elongation of *CLN2* transcription to later cell cycle phases during recovery to osmotic stress.

We tested whether osmotic stress influences the transcription within individual cell cycle phases and found that *CLN2* and *CLB5* transcriptional timing and levels in cell cycle phases were perturbed (Figure 43C, Supplementary Figure S 15B,C,D). At 15 min of stress, the transcription of both cyclins was reduced. Both cyclin maxima in late G1 as well as their upshift in late mitosis reappeared after 30 min and after 90 min the *CLN2* peak was higher than before stress while the *CLB5* maximum was not totally recovered, yet (Figure 43C, Supplementary Figure S 15B,C).

Interestingly, we observed a broadening of the *CLN2* mRNA peak in late G1 into G2 and P/M phase after 30 and 45 min of osmotic stress, respectively (Figure 43C, Supplementary Figure S 15B). *CLB5* showed an extension of its transcription peak in late G1 into G2 at 45 min (Figure 43C, Supplementary Figure S 15C). *CLN2* and *CLB5* are transcribed synchronously under normal conditions and triggered by nuclear export of the inhibitor Whi5 ensuring simultaneously budding and DNA replication (Iyer et al., 2001; Koch et al., 1993; Schwob and Nasmyth, 1993; Stuart and Wittenberg, 1994), hence; the differences in expression profiles under osmotic stress indicate distinct osmo-regulation pathways. In order to calculate the duration of transcriptional inhibition for *CLN2* and *CLB5*, respectively, that best explained the single cell mRNA data we employed our computational model as explained below.

6.6 Computational modeling of mRNA, protein and noise levels under osmotic stress.

To simulate osmotic stress response of G1/S main regulators, our model integrated the stress-driven activation of the Hog1, which triggers of Sic1 stabilization (Escoté et al., 2004) and *CLN2* and *CLB5* transcription inhibition (Adrover et al., 2011; Zapater and Clotet, 2005) (Figure 44A). We assumed that high-level transcription of *CLN2* and *CLB5* (mainly during late G1) was interrupted during the period of osmotic adaptation and resumed afterwards (Figure 44B). Depending on the time point when osmotic stress hits the cell, the inhibitory effect on *CLN2* and *CLB5* transcription as well as the delay of following cell cycle phases are different (exemplary cases in Figure 44B). Since all other model parameters were fitted already for the non-stress scenario, the remaining parameters to extract were the periods, t_d, of transcriptional repression of the cyclins. Employing the experimental single-cell mRNA distributions and means, we obtained the values of $t_{d,CLN2}$ = 17 min for *CLN2* and $t_{d,CLB5}$ = 11 min for *CLB5*. These values were the best combination to minimize the total squared distance between simulated and experimental mRNA distributions during individual cell cycle phases and at different time points upon stress (Supplementary Figure S 11, Supplementary Figure S 12, Supplementary Figure S 13, Supplementary Figure S 14). The resulting time courses for mRNA, proteins and noise levels are shown in Figure 45.

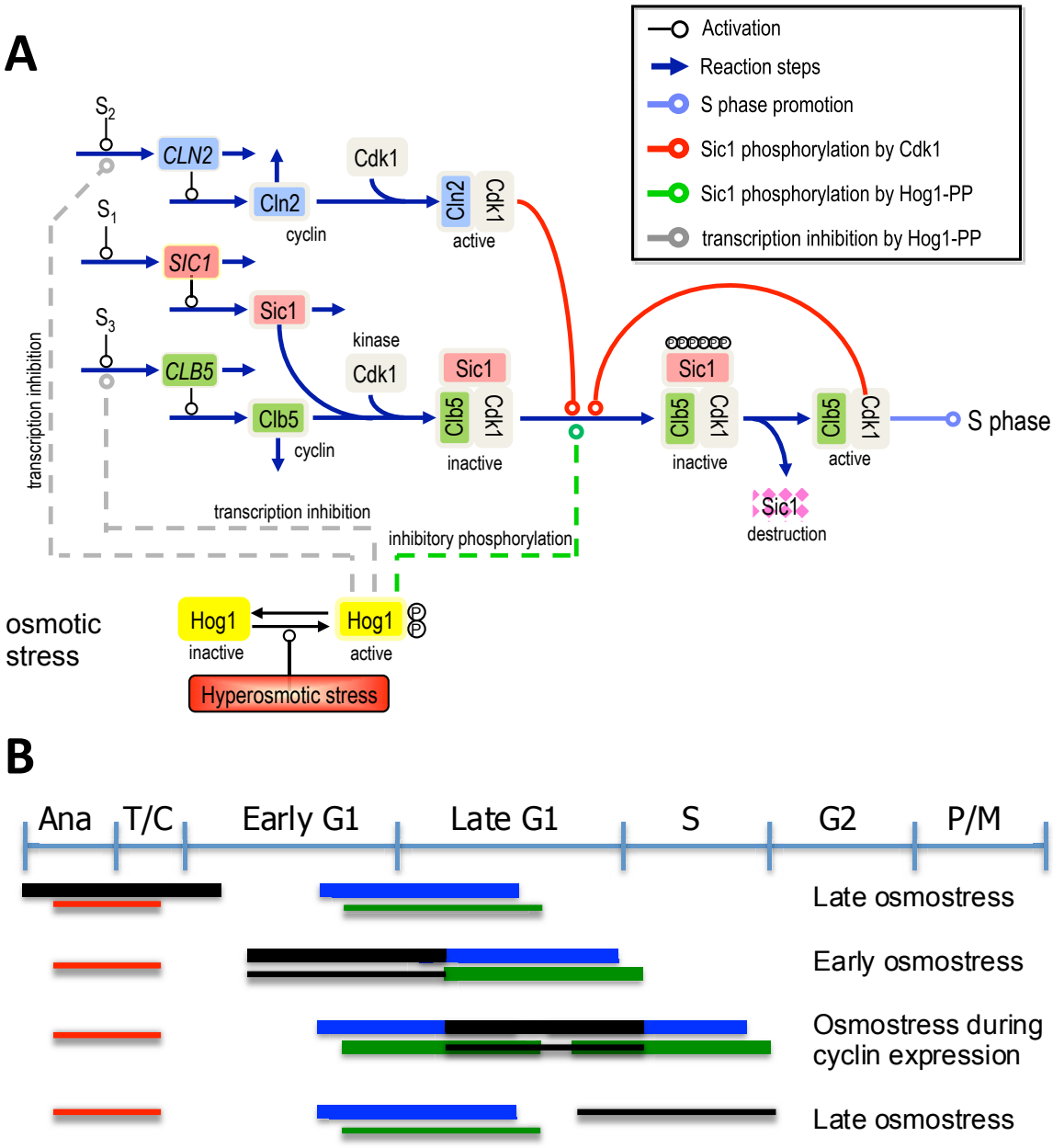

Figure 44. Molecular network and simulation rules of the G1/S transition controlled by *SIC1*, *CLN2* and *CLB5* under osmotic stress.

(A) Molecular network of the G1/S transition controlled by *SIC1*, *CLN2* and *CLB5* under osmotic stress. It is based on the model presented in Figure 36 including the gene expression of Sic1, Cln2 and Clb5 and their interactions between each other as well with Cdk1. Additionally it integrates the biochemical activity of Hog1, which is activated under hyperosmolarity. (B) Schematic of the temporal order of cell cycle phases and distinct active and inactive transcription periods of mRNA under osmotic stress. Active transcription periods for *SIC1*, *CLN2* and *CLB5* are represented by the red, blue and green bars, respectively. The black bars depict the delay in transcriptional activity due to osmotic stress.

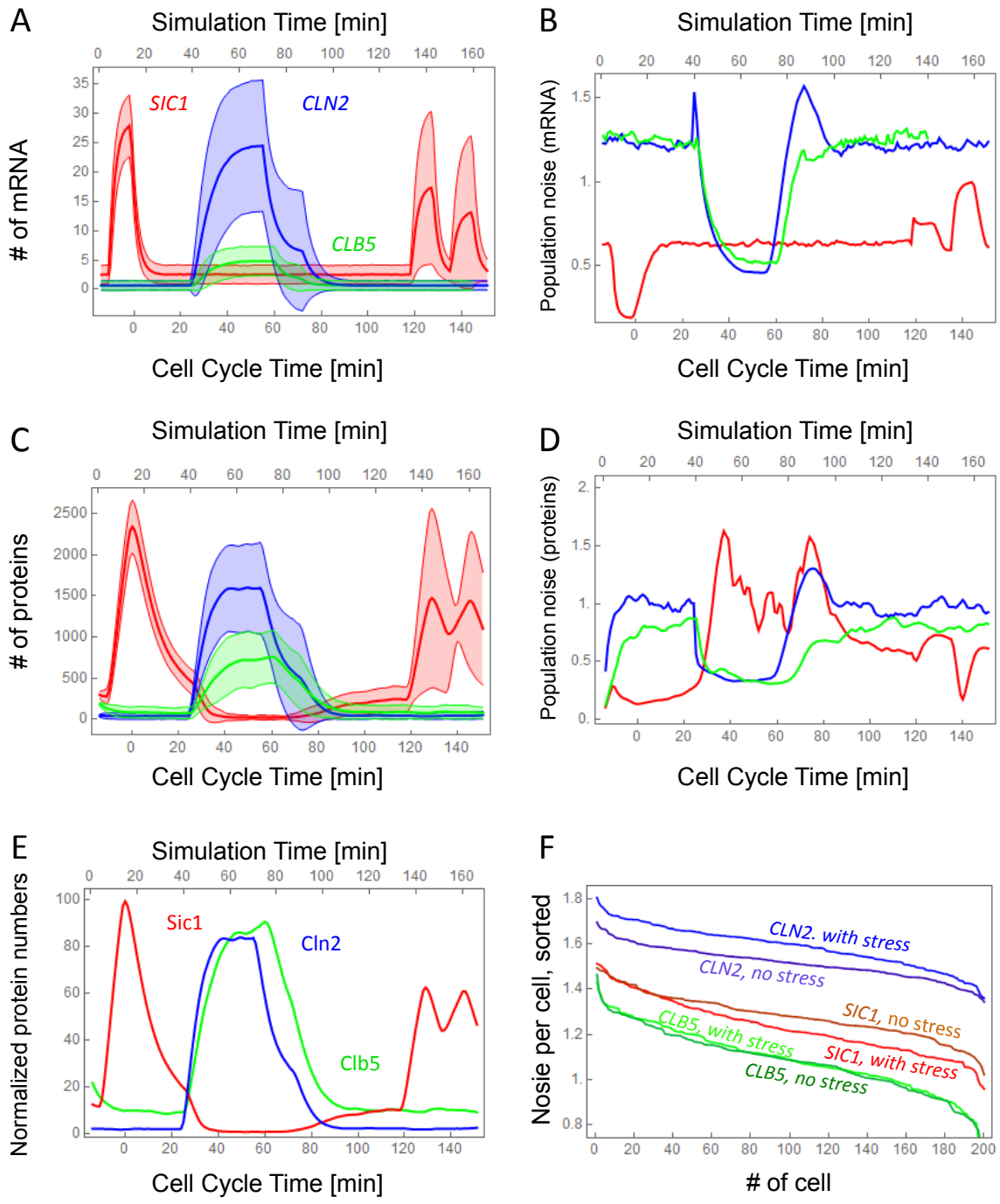

Figure 45. Simulated time courses of transcripts, proteins and molecular noise of *SIC1, CLN2* and *CLB5* during cell cycle under hyperosmolarity.

We simulated 200 cells and exposed them to osmotic stress starting at random time points leading to transcriptional repression (Figure 44C). (A) Time courses (mean ± SD) for mRNA numbers. (B) Time courses for mRNA noise. (C) Time courses for protein numbers (mean ± SD). (D) Time courses for protein noise. (E) Time courses of protein levels normalized with respect to the maximal values reached in no stress condition in Figure 39C. (F) Sorted protein noise of all 200 single cells measured for each cell individually over one cell cycle period. Different tones of each color represent conditions with (lighter tones) or without stress (darker tones). Data for *SIC1*/Sic1, *CLN2*/Cln2, and *CLB5*/Clb5 is shown in red, blue, and green, respectively..

As expected, levels of *SIC1* or Sic1 were only slightly affected by osmotic stress (Figure 45A,C,E, Supplementary Figure S 14B, Supplementary Figure S 15A and D). Simulated *SIC1* and Sic1 levels stayed low from early G1 to P/M and displayed high expression in Ana and T/C (Supplementary Figure S 14B). We observed a slightly broader and lower peak following osmotic stress (Figure 45E), resulting also in lower noise of Sic1 (Figure 45F). The broader peak is due to a loss of synchrony between the cells, some cells had been hit by osmotic shock during late G1 and, hence, experienced a cell cycle prolongation, while other cells hit earlier or later progressed with their cell cycle without extra time.

CLN2 and Cln2 expression were broader (Figure 45A and C, Supplementary Figure S 14B, Supplementary Figure S 14B and D) and showed higher noise levels compared to no stress condition in periods of high expression, i.e. late G1 and S phases (Figure 45B and D). Both *CLN2* and *CLB5* experienced severe transcriptional down-regulation (Figure 45A, Supplementary Figure S 14B and Supplementary Figure S 14B,C and D) resulted in lower Cln2 and Clb5 levels after stress (Figure 45C, E). Noise of Cln2 increased compared to the situation without stress, while Clb5 noise remained stable (Figure 45D, F).

7. DISCUSSION II:

7.1 Stochastic modeling simulates time-courses of mRNA, proteins, and their noise from static single cell RNA-FISH microscopy data

We applied single molecule resolution RNA-FISH to *SIC1*, *CLN2* and *CLB5*, which regulate G1/S transition in budding yeast, and used genetic and morphological markers to assign cells to cell cycle phases and thereby obtained absolute and cell cycle phase-resolved mRNA numbers in single cells. With this *in silico* synchronization approach, we avoided chemical or physical synchronization treatments. The average mRNA numbers were low, between 2 and 7 molecules/cell and in good agreement with previous studies in yeast (Ball et al., 2013; Gandhi et al., 2011; Silverman et al., 2010; Trcek et al., 2011). This shows the high quantitative consistency of RNA-FISH.

Based on our data and other published works, our stochastic modeling enabled estimation of transcription kinetics parameters (rate constants for transcription and degradation as well as high expression periods of each mRNA species), simulation of time courses of mRNA numbers, protein numbers, and their related noise and, eventually, to rationalize transcriptional responses and cell cycle timing upon external stress.

In the ideal case, we should experimentally follow the dynamics of mRNA numbers in the same cell over time in order to obtain an unbiased picture of gene expression regulation in cell cycle in unperturbed situations and during stress. This is currently technically very challenging. To overcome this limitation, we used static single cell data and performed an *in silico* synchronization. This approach revealed detailed quantitative insights into transcriptional regulation and profiles with and without stress that were not available from studies with synchronized cells, since all available synchronization methods have adverse side effects and only limited duration of synchrony.

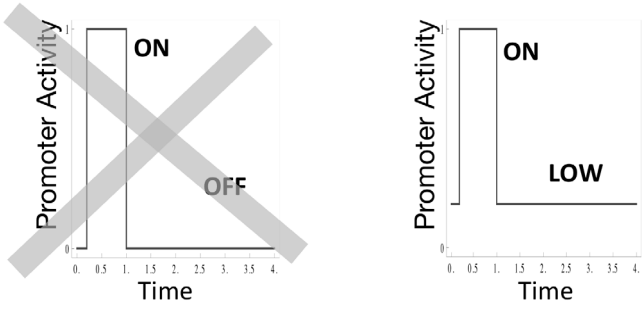

Figure 46. Our results advocate for a "leaky" promoter activity.

Single cell mRNA microscopy and stochastic model suggest a switch between an active, ON, and a non-zero, LOW, state of transcription.

The three genes showed experimentally enduring basal levels of expression, but highest for *SIC1*. Our model reproduced the experimental mRNA distributions best when considering low, non-zero, expression outside the high expression phase Figure 46. The model, revealed – as expected – lower noise during periods of high transcription than during low transcription for each mRNA species.

However, we found lower noise for *SIC1* than for *CLN2* or *CLB5* in both high and low expression periods. During low expression periods, protein noise displayed a negative correlation with mRNA levels (higher protein noise for lower mRNA numbers), while this pattern did not hold true for high expression periods. Here, protein noise showed no statistically relevant dependency on mRNA levels or even increased with increasing mRNA abundances. This may indicate that sharp expression bursts result in noisier, i.e. unpredictable, cellular behavior (Raj and van Oudenaarden, 2008; Di Talia et al., 2007).

7.2 Basal *SIC1* mRNA level might prevent noise in expression and cell cycle timing

A potential consequence of the basal level of *SIC1* may be to prevent strong transcriptional bursts and, thus, higher transcript noise (Raj et al., 2006; Taniguchi et al., 2010) as well as cell cycle timing noise (Barberis et al., 2012; Costanzo et al., 2004; Di Talia et al., 2007). FRET measurements revealed that Sic1 binds to Clb2, Clb3 and Clb5 suggesting a role for Sic1 in different phases and not restricted to G1/S transition (Schreiber et al., 2012). Indeed, these cyclins lost their oscillation-like periodicities in cells lacking Sic1 (Barberis, 2012). As sole CKI of B-type cyclins, Sic1 is therefore important to act as cell cycle timer under normal conditions, but as brake under stress. We suggest that the basal transcription of *SIC1* might be an advantage to enable smoother and less burst-like expression peaks as well as to provide basal Sic1 protein levels in case the cell cycle must suddenly be arrested.

Which regulatory processes may be responsible for *SIC1* mRNA basal levels? *SIC1* transcription is activated by Swi5 in late mitosis and, in daughter cells only, by Ace2 in early G1 (Aerne et al., 1998; Knapp et al., 1996; Toyn et al., 1997). Strains lacking *SWI5* or *ACE2* showed a basal level of *SIC1* over the cell cycle similar to wild type (Knapp et al., 1996), suggesting that *SIC1* basal levels are not regulated by these transcription factors but by some yet unknown factors or mechanisms.

7.3 Single mRNA FISH and *in sicilo* synchronization revealed precise quantification and timing of gene expression

We experimentally measured a sharper peak of *SIC1* in late mitosis (Ana and T/C) dropping in early G1. In comparison, previous works using population assays reported that *SIC1* mRNA and Sic1 protein levels remain high until S phase entrance (Archambault et al., 2003; Coccetti et al., 2004). This expanded expression of *SIC1* might be due to the limitations of synchronization to resolve the short phases of mitosis. In addition previous studies differed on the initiation of *SIC1* main transcription in or after anaphase (Aerne et al., 1998; Knapp et al., 1996; Toyn et al., 1997). We could show that the *SIC1* peak in mitosis starts during anaphase.

CLN2 and *CLB5* exhibited both an enduring basal levels and a main expression peak in late G1. Basal expression was observed previously for *CLN2* using α-factor synchronization (Ball et al., 2013). Regulation of *CLN2* and *CLB5* promoter activity by stably expressed *BCK2* may explain the cyclin basal levels (Di Como et al., 1995; Epstein and Cross, 1994).

CLN2 and *CLB5* mRNA maxima in late G1 agree with previous reports for population studies using ?-factor or elutriation for synchronization in G1 for *CLN2* (Dirick and Nasmyth, 1991; Ogas et al., 1991) and for *CLB5* (Epstein and Cross, 1994; Schwob and Nasmyth, 1993), but timing of cell cycle phases differs between synchronized cultures and non-synchronized cultures, due to the shortened cell cycle length of chemically synchronized cells, which keep gaining size without cell cycle progression. *CLB5* mRNA level was found to decay after exit from S phase leading to minimal levels of *CLB5* mRNA (Jacobson et al., 2000; Shirayama et al., 1999) and Clb5 protein (Yaakov et al., 2009) from S throughout M until G1. The *CLN2* maximum was 4-fold higher than that of *CLB5* as previously observed for mRNA (Bon et al., 2006; Holstege et al., 1998) and protein levels (Ghaemmaghami et al., 2003). This might be due to a positive feedback loop of Cln2 triggering its own expression (Cross and Tinkelenberg, 1991; Dirick and Nasmyth, 1991; Skotheim et al., 2008). Cln2 and Clb5 elicit budding and DNA replication, respectively (Knapp et al., 1996; Schwob and Nasmyth, 1993; Spellman et al., 1998; Stuart and Wittenberg, 1994), and the differences in abundance may indicate a higher sensitivity of DNA replication to Clb5 than of budding to Cln2.

The unexpected transcription upshift in late mitosis of both cyclins might have been overlooked in previous studies due to the loss of synchrony at later cell cycle phases in populations synchronized in (Ball et al., 2013; Dirick and Nasmyth, 1991; Epstein and Cross, 1994; Schwob and Nasmyth, 1993). A potential explanation for the mitotic transcription may be related to transcription factor complexes SBF (SCB-binding factor) and MBF (MCB-binding factor), which induce *CLN2* and *CLB5* transcription, respectively, in late G1 (Harris et al., 2013; Iyer et al., 2001; Koch et al., 1993). In mitosis, SBF is repressed by binding of mitotic B-type cyclins (Amon et al., 1993) and of nuclear Whi5 (de Bruin et al., 2004; Costanzo et al., 2004). The Zinc finger protein Rme1, which has maximum expression at M/G1, induces promoter activity at *CLN2* loci (Toone et al., 1995). However, MBF is inhibited by Nrm1 outside G1 (de Bruin et al., 2006) but is degraded at the exit of mitosis (Ostapenko and Solomon, 2011). As a result, there may be a short time window allowing transcription of cyclins when SBF and MBF are bound to the promoters and not yet inhibited.

We are not aware of any evidences of higher Cln2 or Clb5 protein levels or additional waves of budding or DNA replication in late mitosis. Furthermore if those mRNAs were translated into functional proteins, their stoichiometric levels would have to be higher than the one of Sic1 in order to trigger budding and DNA replication as referring to the titration model of Sic1 by the B-type cyclins (Cross et al., 2007). *SIC1* mRNA and protein levels are maximal in late mitosis (this study, (Aerne et al., 1998; Knapp et al., 1996; Toyn et al., 1997) and higher than the ones of Cln2 and Clb5. Therefore Sic1 proteins may inhibit eventual Cln2 and Clb5 proteins present at late mitosis. Direct comparison of protein levels in late cell cycle phases still may be complicated since they either require time-resolved single cell measurements or precise synchronization until this period of cell cycle.

7.4 Cell cycle progression under osmotic stress: Slow-down or make compromise! - Osmotic stress induces arrests in early G1 as well as in G2 and long-term effects.

We placed special emphasis on the effect of stress – here osmotic stress – on gene expression. While most previous studies focused on the initial phase of adaptation using synchronization methods, we also investigated long-term effects of hyperosmolarity on cell cycle progression. Measuring the fraction of cells per cell cycle phase at different times of stress we observed an effect on cell cycle

progression throughout the single cell cycle phases. Even after 90 min the initial subdivision of the population into cell cycle phases was not fully restored, consistent with previously reported two hours for recovery (Macia et al., 2009). Cells accumulated in gap phases, early G1 and G2, with a preference for early G1. This may indicate that arrest in early G1 before START, which prevents DNA replication, may be more important than arrest in G2, which delays nuclear division and allows for DNA repair. Consequently, the fractions of cells decreased in late G1, S and mitosis. Previous studies showed that S phase is delayed and elongated upon osmotic stress to ensure genomic integrity by preventing collisions between the replication and transcription machineries due to transcriptional bursts of stress-induced genes (Duch et al., 2013b; Yaakov et al., 2009). Indeed to delay origin firing and slow-down replication complex progression Hog1 phosphorylates Mrc1, which is part of the replication complex and couples DNA helicase and DNA polymerase during replication. We could not observe S phase elongation because, although some individual cells may have had longer S phases, the overall S phase group decreased as cells arrested in early G1.

Intriguingly, after osmotic stress we observed cells having two spindle pole bodies but no bud, exhibiting a loss of synchrony between DNA replication and budding. This fraction of cells reached a maximum after 30 min of stress. This specific state may be related to the independent regulation of *CLN2* and *CLB5* upon stress and it is unclear whether it is simply transient or has severe consequences (Figure 47). A comparable phenomenon was observed when osmotic stress was applied close to or after START (Adrover et al., 2011). Adrover and colleagues suggested that after START cells lost the ability to arrest in G1 in response to stress and initiated DNA replication whereas budding was delayed by about 30 min. The loss of coordination between DNA replication and budding decreased the cellular fitness but was not reported to be lethal (González-Novo et al., 2015). We conducted preliminary long-term microscopy monitoring of living cells under osmotic stress and observed no cell division of these specific cells during the 5 hours of the experiment (data not shown).

Since osmotic stress hits cells at arbitrary cell cycle phase and affects all phases, measuring osmo-adaptation in single living cells using e.g. microfluidic devices, cell cycle markers and MS2-tagging system would provide deeper insight into the exact timing of cell cycle progression and gene expression under stress conditions.

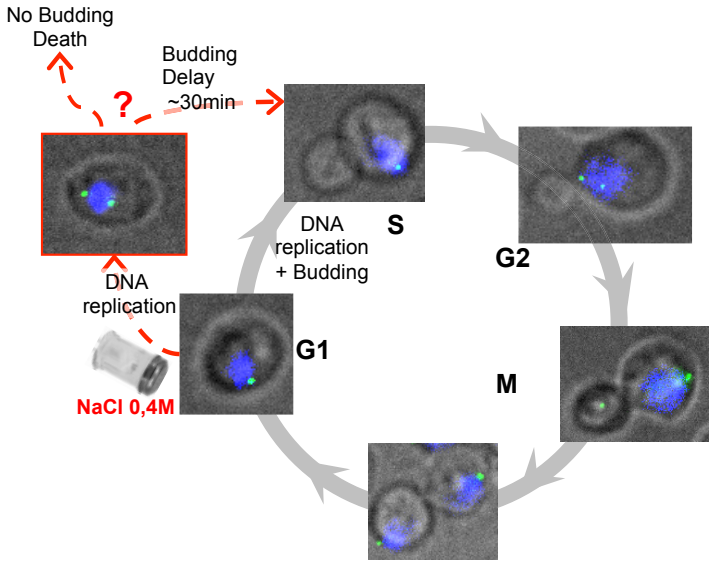

Figure 47. Lack of synchrony of budding and DNA replication under hyperosmolarity.
Cell cycle morphological markers enables the observation of cell cycle events and progression. In the overlay images nucleus is stained with DAPI (blue), spindle pole body is tagged with Spc42-mTurquoise (green). Under optimal growth conditions bud and DNA replication are simultaneously initiated in late G1 leading to the presence of a bud and two spindle pole bodies in the following phases. Under hyperosmolarity a fraction of cells contain two spindle pole bodies and no bud suggesting a lack of synchrony between initiation of budding and DNA replication. After adaptation to hyperosmolarity the faith of these cells is unknown.

7.5 Distinct pathways regulate *CLN2* and *CLB5* inhibition under osmotic stress

Our single cell experiments and model measured different inhibition duration and recovery patterns for *CLN2* and *CLB5* indicating distinct osmoregulation mechanisms of these cyclins. In unstressed cells their transcription is triggered synchronously (Dirick et al., 1995; Koch et al., 1993) ensuring simultaneous budding and DNA replication. However, upon osmotic stress Hog1 appears to down-regulate *CLN2* and *CLB5* expressions independently and for different periods. Whereas Hog1 is specifically recruited to the *CLB5* promoter inhibiting its transcription (Adrover et al., 2011), Hog1 targets Whi5 and other factors to indirectly down-regulate *CLN2* (González-Novo et al., 2015). Indeed upon stress, Hog1 phosphorylation of Whi5, Msa1 and MSa2 binds to and prevents *CLN2* transcription (González-Novo et al., 2015). Additionally *CLN2* inhibition under stress has been also related to Cip1, a new discovered CKI, which targets Cdk1–Cln3 complex to prevent Whi5 phosphorylation and therefore inhibits *CLN2* transcription (Chang et al., 2017). This inhibitory mechanism is amplified under osmotic stress by Hog1, which phosphorylates Cip1 and thereby may reinforce the interaction of Cip1 with Cdk1-G1 cyclin complexes.

In contrast to the transient inhibition of *CLN2* and *CLB5* transcription, *SIC1* expression was less affected upon hyperosmolarity. The differential behavior of *SIC1* and the cyclins is reflected by their different roles in cell cycle progression and stress response. Sic1 as inhibitor of Cdk1-cyclin complex (Rossi et al., 2005; Schwob, 1994) and, hence, inhibitor of cell cycle progression may be crucial to control the delay of cell cycle events required under stress. In contrast, Cln2 and Clb5 are activators of the G1/S transition.

7.6 Revised stochastic model for *SIC1*, *CLN2* and *CLB5* transcription under normal growth conditions and under osmotic stress.

Since the current model assumed only one high expression phase it did not fit the second mitotic upshift of expression of the two cyclins. In a revised version of the model focusing only on transcription regulation of *SIC1*, *CLN2* and *CLB5*, we assumed two periods of high transcription for *CLN2* and *CLB5*, labeled as $first$ and sec (Appendix 5). The resulting simulations are shown in Supplementary Figure S 18- Supplementary Figure S 23 in Appendix 5. The model extracted the relative promoter activities of 7.7%, 0.4% and 15% for *SIC1*, *CLN2* and *CLB5*, respectively, outside the main transcription periods (compared to 8.8%, 2.2% or 7.7% for *SIC1*, *CLN2* and *CLB5*, respectively, with the model in RESULTS II with only one single high phase of transcription and translation regulation). According to the Akaike criterion (AIC), the fits improved when allowing for two periods of high promoter activity for *CLN2* and *CLB5*.

The fitting by the revised model extracted of the mRNA data under osmotic stress provided new periods of transcription inhibition $t_{d,CLN2}$=28 min for *CLN2* and $t_{d,CLB5}$=12 min for *CLB5*. The

difference between these two values is larger than the difference between the periods of transcription inhibition for the two cyclins from the initial model in RESULTS II (values from the model presented in RESULTS II: $t_{d,CLN2}$ = 17 min for *CLN2* and $t_{d,CLB5}$ = 11 min for *CLB5*). Hence the new values reinforced the hypothesis that *CLN2* and *CLB5* have distinct osmo-regulations. The revised model was published in (Amoussouvi et al., 2018)

7.7 Conclusion of RESULTS II

Combination of single molecule RNA-FISH and microscopy with a mathematical model revealed detailed and quantitative regulatory patterns in gene expression of three well-known G1/S regulators. Detection of a ubiquitous basal expression level, an unexpected mitotic expression, the determination of molecular noise as well as dynamics of transcription recovery upon hyperosmolarity required a quantitative single cell resolution method. Furthermore, the use of morphological cell cycle markers can avoid adverse side effects and the averaging effect of synchronized population assays. Our mathematical model enabled computational cell cycle synchronization and to rationalize the experimental data. Future investigations could address the question whether these patterns are specific to *SIC1*, *CLN2* and *CLB5* or general to other cell cycle regulators in yeast or to homologous genes in other organisms.

8. GENERAL DISCUSSION

8.1 Background and Objective of the project

This thesis explored the interplay between eukaryotic cell division cycle, stochastic gene expression and cell signaling. Cell survival requires precise oscillations of expression and activity of the cell cycle regulators as well as a precise cellular response including gene expression reprogramming and cell cycle response to adapt to stress. Importantly, in this study, we provided experimental single cell mRNA abundances, which were lacking to develop stochastic models. Finally, we assessed the regulation of eukaryotic cell cycle in context of stochastic gene expression resulting in low molecule numbers and cell-to-cell variability of cell cycle regulator genes as well as in context of response to external stimuli.

8.2 Main topics of research projects and methodology

We focused on *SIC1*, *CLN2* and *CLB5*, the main regulators of the G1/S transition in *S. cerevisiae*. We combined single-cell fluorescence microscopy, cell synchronization and computational approaches to:

(1) Develop protocols and tools for single cell microscopy and image analysis.

(2) Measure absolute numbers of single cell gene expression and noise level of these three genes.

(3) Measure timing of gene expression of these three genes over a full cell cycle.

(4) Assess the propagation between gene expression noise from mRNA to protein level and on the cell cycle timing.

(5) Assess the gene expression regulation of these genes under osmotic stress.

(6) Assess the regulation of cell cycle events under osmotic stress.

8.3 Main achievements and findings

In the first part of this thesis, I described how we visualized *SIC1* and *CLN2* mRNA particles with the MS2-CP tagging method in fixed and living cells, we synchronized cells with counterflow centrifugation elutriation and, finally, studied the influence of *SIC1* mRNA number on the timing of G1/S transition with stochastic modeling. Our main achievements and findings in this chapter were:

- Engineering of stable yeast mutant strains with MS2-CP-GFP(x3) tagged *SIC1* and *CLN2* mRNA, respectively.
- Viualization of single *SIC1* and *CLN2* mRNA particles in fixed cells: most of the cells contained only 0 or 1 MS2 tagged *SIC1* and *CLN2* mRNA particle.
- Monitoring of *SIC1* mRNA particles in living cells: *SIC1* mRNA particles exhibited different types of transport.
- Development of a stochastic model of G1/S transition focused on *SIC1*.
- Lower initial *SIC1* mRNA numbers ensured lower Sic1 protein noise and robust S phase onset.
- A low *SIC1* mRNA number and its related low noise level were apparently more dependent on the production to degradation ratio of *SIC1* mRNA than on the initial *SIC1* mRNA number.
- S phase onset was set by a balance between Clb5 protein production and Sic1 protein degradation and we estimated these kinetic parameters.

In the second part of this thesis, I explained how we employed the RNA-FISH method and genetic and morphological markers to monitor *SIC1*, *CLN2* and *CLB5* mRNA numbers throughout cell cycle and upon osmotic stress. An extended stochastic model enabled to extract kinetic parameters and o simulate time courses of mRNA, protein and noise levels. Our main achievements and findings in this part were:

- Development of protocols and semi-automatic microscopic analysis tools for RNA-FISH and *in silico* synchronization.
- Visualization of single molecules of *SIC1*, *CLN2* and *CLB5*.
- Dataset of mRNA numbers per single cells and related noise in each cell cycle phase under optimal growth conditions and under osmotic stress.
- Development of an extended stochastic model that simulated the dynamics of *SIC1*, *CLN2* and *CLB5*, their proteins and noises throughout cell cycle and their osmoregulation.
- The three genes showed basal level and the cyclins showed upshift of expression in mitosis
- Stochastic modeling suggested switch between periods of high and low expression.
- The CKI, *SIC1*, showed less noise than the cyclins maybe because of higher *SIC1* basal level.
- *CLN2* and *CLB5* had distinct osmo-regulatory pathways and this may cause the observed loss of synchrony between DNA duplication and budding in a fraction of cells under hyperosmolarity.
- Osmotic stress had long-term effects on cell cycle progression and cells preferentially arrested in Gap phases.

8.4 Interactive combination of experimental and computational approaches:

This project used an interactive combination of experimental, especially single cell microscopy, and computational approaches. In this work, experimental data were not "simply" fitted by a model but regular exchanges between the collaborators enabled to establish a recurrent loop for design of the experiments and computational models and for implementations of the results of one approach into the other. Such collaboration is challenging in term of communication and required the standardization of names, data formats and data exchange. Since more and more projects are interdisciplinary, (at least basic) knowledge of experiment conduction and of computational model development are valuable for experimentalists and theoreticians to better understand each other and to recognize the constraints and limitations of the different methods.

8.5 Single cell mRNA methods are required to quantify absolute expression noise level within a cell population

8.5.1 Comparison of the MS2-CP system and RNA-FISH as single mRNA visualization approaches

We employed the MS2 tagging system and RNA-FISH to visualize mRNAs in single living and fixed cells, respectively, via fluorescent microscopy. Table 18 displays the comparison between the two methods. An important part of this thesis was dedicated to the establishment or improvement of protocols for tagging, microscopy acquisition and microscopy image analysis necessary to perform these two single cell resolution methods.

Technically, we found challenging to tag the mRNA sequence with the MS2 hairpin loops, once this steps was achieved we obtained stable cell lines, which could be easily combined with different types of fluorescently labeled MS2-CP containing plasmids. Prior to an experiment, cells only had to be grown overnight in medium lacking methionine for induction of the MS2–CP fused to GFP (3x) complexes. In comparison, the preparation for RNA-FISH did not required molecular cloning but several hours of cell labeling and washing treatments. Importantly, the RNA-FISH samples were stable for several months, which enabled to perform the microscopy acquisition of large samples from the same experiment over several days.

Notably, we obtained different patterns of *SIC1* mRNA particle localization and abundance with the two labeling methods (Table 18). With the MS2 system we measured only few fluorescent mRNA particles (up to 10 for *SIC1*) of heterogeneous intensity and, therefore, did not derive absolute quantification of mRNA numbers from these presumable mRNA aggregates. Most of the cells contained no or one MS2-CP-GFP(x3) tagged *SIC1* mRNA particle. In contrast with the RNA-FISH method, we detected larger numbers of mRNA particles per cell and assumed that the mRNA particles were mostly single mRNA molecules based on the homogeneity of the fluorescence intensity of the cytoplasmic mRNA particles and published studies (Ball et al., 2013; Raj et al., 2008; Trcek et al., 2012). After normalization of the mRNA fluorescent particles we observed that most of the cells contained less than 10 *SIC1* mRNA however some cells contained up to 80 *SIC1* mRNAs after normalization. These high mRNA numbers were mostly due to the presence of nuclear transcriptional start sites, which appeared as bright fluorescent spots containing several mRNAs. In conclusion RNA-FISH was a

more efficient tool to quantify mRNA level in single fixed cells and to investigate transcriptional noise within a cell population. Importantly the full dataset of single cell mRNA abundances are available to the science community and provide a basis for future studies on these specific three genes or on other cell cycle genes in yeast.

Table 18. Comparison of the MS2-CP system and RNA-FISH methods.

	MS2-CP	RNA-FISH
Microscopy Image	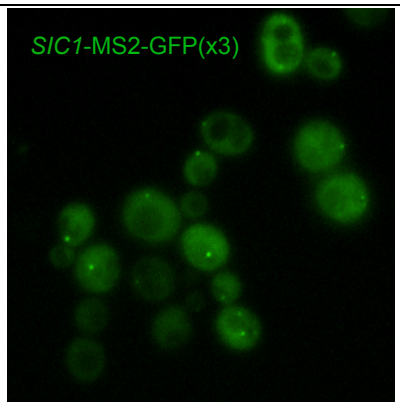	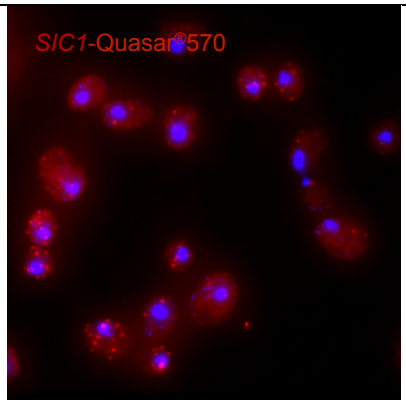
Living cell	yes	no
Endogenous expression	yes	yes
Tagging method	Molecular cloning /Genomic tagging	*in situ* hybridization
Tagging molecule in this study	Fluorescent proteins GFP(x3)[a]	Chemical fluorophores Quasar®570, CAL Fluor Red®610
Single RNA molecule resolution	not confirmed	yes
Number of observed mRNA particles for *SIC1*	0-10	0-80 (after normalization)
Number of genes simultaneously detected in literature	2 when combined with PP7 (Hocine et al., 2013; Larson et al., 2011)	7 with reiterative hybridization after photobleaching (Gandhi et al., 2011; Silverman et al., 2010; Xiao and Guo, 2015)
Advantages	Stable MS2 mutant strain, Spatio-temporal tracking, live monitoring of transcription elongation and production (with fluorescence correlation and/or FRAP analysis)	Single molecule resolution, absolute mRNA quantification, high photo-stability; high stability of the samples (several months at -20°C)
Disadvantages	Photobleaching, mRNA tracking required fast microscopy setup and 3D analysis tools, difficulty to calculate single mRNA numbers, challenging genomic tagging	Fixed cells, time consuming preparation of the cells and probe hybridization

[a] We tested different constructs and employed a construct with a triplet of GFP in our final experiments.

Many cell cycle regulators have localized functions therefore mRNA transport is a critical step to enable localized translation and ensure the right amount of proteins at the right place and right time (Chartrand et al., 2001; Rodriguez et al., 2007; Shepard et al., 2003). RNA-FISH was used to assess mRNA localization within fixed cells (Ben-Ari et al., 2010; Bertrand et al., 1998); however, in comparison MS2-CP system had the great advantage to enable mRNA particles tracking in single living cells. We tracked MS2-CP-GFP(x3) tagged *SIC1* mRNA particles for up to 22 min and observed different types of movement: diffusion, static with slight oscillations and directed movement. Further investigations could assess the interplay between cell cycle progression and *SIC1* transport/distribution between mother and daughter cells. We were unfortunately limited by the microscope setup and photo-bleaching of the probes that prevented for longer monitoring and spatially more accurate measurements. These limitations could be reduced or overcome with fastest and more precise microscopy setups (Reynaud et al., 2008; Stehbens et al., 2012; Thompson et al., 2010). The 3D analysis of the mRNA moves was also challenging and would require more specific quantitative tools for tracking analysis. For long microscopy measurements, the use of a microfluidic device would ensure that the cells are continuously in fresh growth medium and therefore have optimal growth conditions (Uhlendorf et al., 2012).

The discrepancy of expression patterns for *SIC1* obtained with these two single-cell labeling techniques (Table 18) raised questions about how the methods may create artifacts and influence mRNA processing. With the RNA-FISH method the cells are fixed prior to the hybridization therefore RNA-FISH probes should not influence the mRNA processing. As discussed in DISCUSSION I (sections 5.1 and 5.3), we assumed that this version of the MS2-CP system, i.e. 24 MS2 hairpins coupled with MS2-CP-GFP(x3), might trigger the formation of mRNA aggregates. Some studies reported that the MS2-CP tagging could affect mRNA processing, especially transport, and may inhibit mRNA degradation (Garcia and Parker, 2015; Heinrich et al., 2017; Tutucci et al., 2018). Indeed MS2-hairpins are introduced in the 3'-UTR, which usually contains cis-acting localization elements, also referred to as zipcodes, controlling mRNA localization (Kislauskis et al., 1994). These concerns motivated several research groups to develop new versions of the hairpin tag, for example the PP7 hairpin tag (Gandhi et al., 2011; Larson et al., 2011; Tutucci et al., 2018; Wu et al., 2012), and to employ different fluorescent tags than GFP to prevent or at least reduce clustering and the influence on mRNA localization and processing (Wu et al., 2012). Because of these improvements the MS2-CP system and its variations stay a powerful method for mRNA visualization in single living cells. Also few groups successfully employed the MS2-CP system for other purposes than mRNA tracking, for instance real time measurement of transcription kinetics at transcription sites with FRAP or fluctuation analysis (Ben-Ari et al., 2010; Larson et al., 2011; Querido et al., 2011; Yunger et al., 2010). Importantly MS2-CP system and RNA-FISH can be employed simultaneously within the same cells either with RNA-FISH probes homologous to the MS2 hairpins or with RNA-FISH probes homologous to the RNA gene sequence and MS2 hairpins available to MS2-CP-GFP(x3) (Ben-Ari et al., 2010; Bertrand et al., 1998; Querido et al., 2011; Yunger et al., 2010)(see Material and Methods for example of the appropriate FISH probe for MS2 hairpin). Both RNA-FISH and MS2-CP system have become well-established methods over the last decade and their usages and applications are still growing within the mRNA research community.

8.5.2 Future perspectives: addressing the regulatory transcription in *S. cerevisiae* with multi-color RNA-FISH and pairwise correlation analysis.

In order to study transcription of two genes or large network of molecules, RNA-FISH can be simultaneously applied on multiple genes within the same cell by using two or multiple sets of RNA-FISH probes labeled with different fluorophores (Gandhi et al., 2011; Silverman et al., 2010; Xiao and Guo, 2015). This technique had the advantage that the genes are expressed within a similar cellular environment and can thereby give information about co-localization of simultaneously expressed genes. Multi-color RNA-FISH reduces the time needed for preparation of the cells, microscopy acquisition and analysis of the microscopy images, compared to an experiment where the genes would be independently measured in different samples. Pairwise correlation analysis between transcripts provides understanding of some common properties between the gene expression regulations of those genes, i.e. timing of expression, inter-regulation or sensibility to the same stimulus (Munsky et al., 2012).

We performed an experiment of simultaneous RNA-FISH tagging of *SIC1* and *CLB5* with the fluorophores Quasar570® and Red610®, respectively (Figure 48A). The microscopy images showed a tendency for the cells to either contain a large amount of *SIC1* or *CLB5* mRNAs. 2D plotting of *SIC1* distribution against the one of *CLB5* confirmed the low or no correlation between the two genes when expressed under optimal growth conditions (Figure 48B). Additionally the use of genetic and morphological markers allowed assessing the correlation between the two genes in each cell cycle phase (Figure 48B). The calculation of the correlation coefficients would allow to quantitatively compare different gene pairs and/or conditions (Gandhi et al., 2011; Silverman et al., 2010). Through reiterative cycles of hybridization, imaging and photo-bleaching, the number of detected genes in the same sample is not restricted to the number of filter channels in the microscope setting and can theoretically be unlimited (Xiao and Guo, 2015).

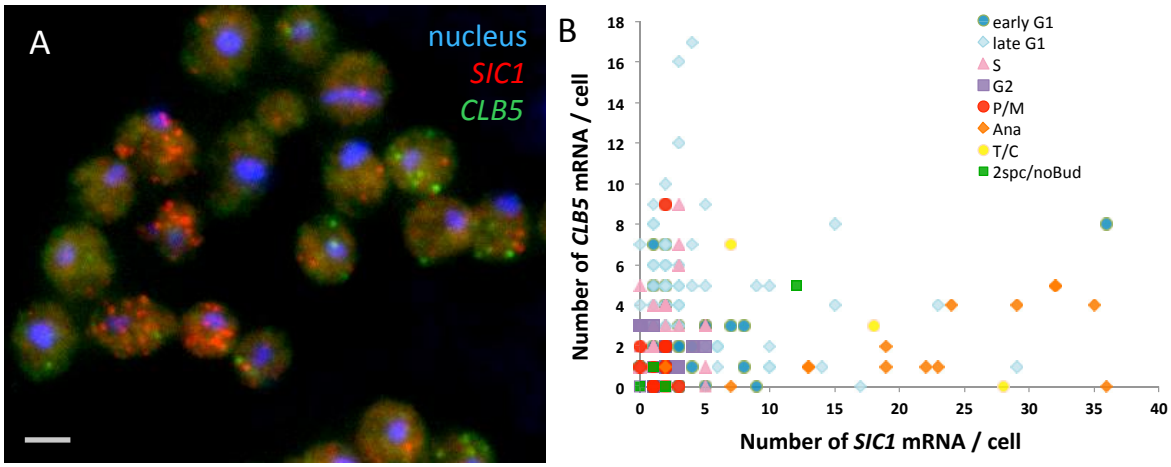

Figure 48. Multi-color RNA-FISH for simultaneous detection of multiple genes.
(A) Simultaneous detection of *SIC1* and *CLB5* with RNA-FISH probes labeled with Quasar570® fluorophore (*SIC1* in red) and Red610® fluorophores (*CLB5* in green), respectively. Cell nuclei are stained with DAPI (in blue). Scale bar represents 5µM. (B) Correlation between *SIC1* and *CLB5* under normal growth conditions. Abundance of *SIC1* plotted against the one of *CLB5* obtained from simultaneous tagging with RNA-FISH within the same cell population (n = 258 cells). Cells were assigned to cell cycle phases using genetic and morphological markers. We observed low or no correlation between the genes.

8.5.3 Future perspectives: simultaneous counting of transcriptional and translational level in single cells

In this project we employed computational modeling to simulate protein level and protein noise changes from our measured transcript levels and published data (Adrover et al., 2011; Ghaemmaghami et al., 2003). Direct measurement of mRNA and protein and their related noise levels within the same population are important to accurately study the regulation at mRNA and protein level and the translation from mRNA to protein. Indeed this strategy would prevent the artifacts linked with the possible differences of yeast strains, growth conditions, data measurement and normalization between the mRNA and protein levels obtained from different sources. Our group is currently running quantitative Western-Blot assays to quantify the protein levels of Sic1, Cln2 and Clb5 simultaneously within the same population. For single cell resolution, microscopy immunofluorescence was previously successfully combined with RNA-FISH (Garí et al., 2001). Additionally RNA-FISH and MS2-CP methods were also combined with a fluorescent protein reporter sequence to tag the related protein of a given gene (Haim-Vilmovsky et al., 2011; Taniguchi et al., 2010).

Different approaches have been used to quantify mRNA and protein levels in single cells, for example, Taniguchi and colleagues combined a YFP coding sequence and a Atto594 fluorophore labeled RNA-FISH probe homologous to the YFP sequence to tag the protein and its related transcript, respectively, in individual fixed cells (Taniguchi et al., 2010). Interestingly, Taniguchi and colleagues quantified the proteome and transcriptome of *E. coli* and found that protein and mRNA numbers of any given gene in a single cell are uncorrelated in bacteria. A similar approach could be applied in yeast. Haim-Vilmovsky and colleagues simultaneously visualized endogenous mRNAs and proteins in living yeast (Haim-Vilmovsky et al., 2011). In addition to the mRNA tagging with the MS2 hairpin loops and the transformation of the cell with a plasmid expressing MS2-CP-GFP(x3), Haim-Vilmovsky and colleagues genomically introduced a sequence coding for mCherry, a red fluorescent protein, between the ORF and the 3' UTR of the gene of interest. They studied the (co-)localization of the tagged mRNA via GFP fluorescence and its translated protein via mCherry fluorescence and suggested that this method can also be employed for quantitative studies.

The endogenous protein levels of cell cycle genes are usually difficult to detect by microscopy because of their low abundances, leading to low signal to noise ratio, and to the challenge of converting fluorescence intensity of fluorescently labeled proteins into molecule number or molecule concentration. We conducted preliminary experiments employing the Number and Brightness (N&B) analysis, which provides absolute quantification of protein numbers and concentration in living cells (Digman et al., 2008, 2009; Ferguson et al., 2011). N&B employs the mean and variance of the fluorescence of a microscopy image stack to calculate the number and brightness of fluorescent molecules present in each pixel. The required excitation light is very low compare to traditional microscopy, which prevents photo-bleaching and photo-toxicity. The processing of the image stack enables to eliminate noise signal and therefore enhances the detection of low protein abundances. With this method we were able to monitor GFP-tagged-*Clb2* and GFP-tagged-*Cln2* mutant cells for 405 min with no significant photo-bleaching (complete study in Meyer, 2012).

8.6 Monitoring cell cycle progression

Monitoring cell cycle progression is challenging as many chemical cell synchronization methods affect cellular biochemical pathways (Breeden, 1997; Futcher, 1999; Hur et al., 2011). Therefore, we chose two synchronization methods with minimal influence on the cell growth: counterflow centrifugation elutriation (in short elutriation) and *in silico* synchronization with genetic and morphological cell cycle markers (Table 19) (Futcher, 1999; Trcek et al., 2011; Walker, 2011; Woldringh et al., 1995).

Table 19. Comparison of the counterflow centrifugation elutriation and *in silico* synchronization with cell cycle markers as cell cycle synchronization methods.

	Counterflow centrifugation elutriation	*in sicilo* with genetic and morphological cell cycle markers
Advantages	- Cell samples can be spilt to be employed with different techniques in parallel - Population can be followed for several generations - Homogeneity of the cell size and age - Robust to study early cell cycle phases, especially G1.	- Calculation of the phase durations - Single cell resolution: each cell is individually sorted into a phase - Resolution throughout the full cell cycle, especially important for late cell cycle phases.
Disadvantages	- Cost of the centrifuge and elutriation equipment - Cells are all daughters and not representative of mixed population with all ages and sizes, mother and daughter cells - Low cells number (5% of initial population) - Low resolution of the late cell cycle events	- Time consuming sorting, partly automatized partly manually - Dissection of “one” single cell cycle (no possibility of study several generations) - Progression within the phase can not be monitored (or only with further markers or computational modeling)

Elutriation selects G1 newborn cells using physical forces and therefore yields to a population of living cells homogenous in size and age ages (Brewer et al., 1984). We recorded the timing of the G1/S transition using budding index. We found *SIC1* expression in G1 phase, which is known to be specific to daughter cells (Laabs et al., 2003; Di Talia et al., 2009; Toyn et al., 1997), therefore this expression timing is not representative of the behavior in a mixed population, i.e. with all cell sizes and ages (Brewer et al., 1984). Consequently synchronization via elutriation may introduce an artifact (or an advantage) if the studied biological process is different for daughters and mothers or age dependent. Elutriation was well adapted to study early stages of the cell cycle, especially G1. G1 is the longest phase (this study, Cooper, 2000; Di Talia et al., 2009) and elutriation allowed in other studies

to resolve sub-phases and events in G1, which were not discerned in α-factor and cdc15-2 synchronized populations (Futcher, 1999). Theoretically, elutriated population could be followed for several generations/cycles however we observed a rapid loss of synchrony of the elutriated population already within the first cell cycle leading to low resolution of the latest cell cycle phases, which are also the shortest phases (this study, Cooper, 2000; Di Talia et al., 2009). One advantage of elutriation is the possibility to split the cell samples and to apply the cells in parallel to different techniques, e.g. FACS, immunolabeling, RNA-FISH. Furthermore synchrony of elutriated populations might be increased with improved protocols and cell cycle progression may be more accurately monitored with additional cell cycle markers.

The second synchronization method we employed was genetic and morphological markers with subsequent *in silico* synchronization, which successfully enabled us to monitor the entire cell cycle and, especially, to resolve latest cell cycle phases. This was especially important since *SIC1* main expression period is in mitosis (Aerne et al., 1998; Knapp et al., 1996; Toyn et al., 1997). Importantly, using this synchronization method combined with RNA-FISH we monitored *SIC1*, *CLN2* and *CLB5* expression throughout a full cell cycle and resolved specific expression profiles, e.g. basal levels for *SIC1*, expression upshift in later phases for *CLN2* and *CLB5*, which might be unclear or undetectable with other synchronization or bulk scale measurement methods. Each cell was assigned to a cell cycle phase and from the fraction of cells in phase we estimated the duration of each cell cycle phase. Phase durations were essential to determine transcription kinetics parameters in our stochastic models. We also monitored the changes of cell fraction in each phase under normal growth conditions and osmotic stress for up to 90 min. Such measurements would have been highly challenging with elutriation or other population synchronization methods. Indeed osmotic stress differently affects all cell cycle phases (Alexander et al., 2001; Clotet et al., 2006; Duch et al., 2013b; Yaakov et al., 2009), therefore, one would need to apply osmotic stress at different cell cycle times in distinct synchronized population samples and would still not cover all possibilities of the cell cycle progression (Adrover et al., 2011). Under hyperosmolarity cell cycle markers enabled us to resolve a fraction of cells with two spindle pole bodies and no bud, indicating a loss of synchrony between the initiations of DNA replication and budding. As downsides, the cell cycle markers and *in silico* synchronization method allowed to monitor only “one” cell cycle and the microscopy image analysis and cell sorting were highly time consuming due to partly manual sorting of the cells. Additionally, the time resolution was limited to the cell phases defined by the chosen cell cycle markers and did not make distinction between the intermediate states within each phase, e.g. early and late S phase. Notably, intermediate states were assessed in the simulated time courses and higher resolution with the markers could be obtained with more markers or deeper analysis of the current markers, e.g. distance of the spindle pole bodies, ratio of daughter/bud to mother size or fluorescent intensity of the nucleus.

For instance, we manually detected the presence of a bud as hallmark of the S phase entry. Bud initiation is a slight morphological change and could be better distinguished by fluorescently tagged Cdc20 or Cdc10. Indeed Cdc20 and Cdc10 are proteins accumulating in a cluster on the cell wall, where budding is initiated, and later forming the bud neck (Bean et al., 2006; Charvin et al., 2008). Additionally, disappearance of the Cdc10/Cdc20 ring is hallmark for mitotic cell division. The accumulation of Cdc10 and Cdc20 generates a bright fluorescent spot and its disappearance, could be easily detected by our current analysis tool. An upgraded workflow is under development to automatically sort the cells using more quantitative information. This improvement would be extremely valuable since it could considerably accelerate the image processing and enable to define

new sub-phases of the cell cycle. Analysis of the cell size could also enable to estimate the molecule concentration in each cell and assess the influence of size distribution on molecular noise.

Importantly in our study, since the use of genetic and morphological markers with subsequent *in silico* synchronization was combined with RNA-FISH, cells were fixed, however, this synchronization technique can be similarly employed in living cells (Bean et al., 2006; Charvin et al., 2008). Microfluidic device would also be an advantage as it would enable to follow the cells over several generations (Uhlendorf et al., 2012).

8.7 Stochastic modeling enables to address changes of discrete molecule numbers and cell-to-cell variability.

The yeast cell cycle has been extensively investigated at protein level with deterministic modeling (Adrover et al., 2011; Barberis and Klipp, 2007; Barik et al., 2010). In this study, we focused on the transcription process of cell cycle regulators resulting in small and discrete numbers of mRNA and transcriptional noise, which are poorly represented by mean and variance only (Reis et al., 2018). Therefore, we developed stochastic models to assess the gene expression of *SIC1*, *CLN2* and *CLB5* based on our experimental mRNA microscopy measurements and published data (Ghaemmaghami et al., 2003). The first model was centered on *SIC1* and its interaction with Cdk1-Clb5,6 while the second model additionally integrated the regulations of the two cyclins and the osmotic stress response of *SIC1*, *CLN2* and *CLB5*. In this latter case, we also developed a specific approach for the fitting of the cell cycle phase resolved RNA-FISH distributions (Appendix 2 Parameter estimation). Our stochastic models simulated time courses for mRNA, protein, and molecular noise levels from static mRNA data. Importantly, we could estimate kinetic parameters and simulate different molecule species, which were not experimentally measured, for example Sic1 alone, in complex with Clb5 or phosphorylated in complex with Clb5.

Our first stochastic model revealed that lower initial *SIC1* mRNA numbers prevented high Sic1 protein noise and ensured robust S phase onset (Barberis et al., 2011). Additionally, the model showed that low *SIC1* mRNA number and the related low noise level were more dependent on the production to degradation ratio of *SIC1* mRNA than on the initial *SIC1* mRNA number. Our second model revealed that *SIC1*, *CLN2* and *CLB5* had basal levels throughout cell cycle enlightening that transcription was not divided in on and off but rather in high and low phases (Amoussouvi et al., 2018). Interestingly, Corrigan and colleagues also proposed based on single living mammalian cell microscopy and stochastic modeling that transcription of the actin gene occurs “across a spectrum of activity” with the gene switching between a range of intermediate states between on and off (Corrigan et al., 2016). Therefore, this continuum model of transcription may be generalized to other genes and organisms.

It is a common practice to disturb a system and study its recovery to equilibrium in order to learn about its regulation we therefore applied osmotic stress to a cell population and assess its recovery behavior. In contrast to most studies focusing on the immediate and short term adaptation to osmotic stress (Adrover et al., 2011; Neuert et al., 2013), we made an emphasis in this project on the middle and long-term response. With our second model we extracted different expression inhibition durations for *CLN2* and *CLB5* upon osmotic stress suggesting independent regulation under stress conditions.

The two models were kept minimalistic therefore we chose to ignore some biological processes, which are discussed below and could be integrated in the future.

8.7.1 Gene dosage

The gene dosage, i.e. copy number of a particular gene in the genome, may be important to consider when comparing the transcription rates of different genes or the transcription rates of the same gene at different cell cycle phases. During S phase the DNA replication results in a duplicated genome and, consequently, in the double gene dosage and double capacity for transcription events to occur from S until the end of cell division (Alberts et al., 2002). Hence, the apparent transcription rate (and mRNA amount) of a gene in late S, G2 and mitosis is the summation of two transcription rates (and mRNAs amount produced) from a double gene dosage within a cell (Bar-Ziv et al., 2016; O Skinner et al., 2016; Voichek et al., 2016). Our second model revealed that *SIC1* had the highest transcription rate in period of high expression compared to *CLB5* and *CLN2* (transcription rates from our second model in high expression periods (min^{-1}): *SIC1*: 12,4; *CLB5*: 1,5; *CLN2*: 6,7). Notably, *SIC1* is mainly expressed in late mitosis when its production occurs from a double gene dosage (Aerne et al., 1998; Knapp et al., 1996; Toyn et al., 1997) whereas *CLB5* and *CLN2* are mainly expressed in late G1 from one single genome (Dirick et al., 1995; Epstein and Cross, 1994; Ogas et al., 1991; Schwob and Nasmyth, 1993). Interestingly, because of these two genomes, the cell is also able to contain multiple transcription sites of a gene in late cell cycle phases.

8.7.2 Cellular growth and distinction between mother and daughter cells

Cellular growth and the distinction between mother and daughter cells were only considered in our first model centered on *Sic1* and its interaction with Cdk1-Clb5,6. Cellular growth in the first model was employed to calculate the probability of complexation of Sic1 with Cdk1-Clb5,6. When the cell was larger the probability for Sic1 and Cdk1-Clb5,6 to interact declined. All other parameters of the system did not depend on the cell growth. Growth and gene expression noise are interconnected and this interconnection could be assessed if cell growth and size were considered in the second model for the three G1/S regulators (Gomez et al., 2014; Kiviet et al., 2014; Shahrezaei and Marguerat, 2015). Larger cells are expected to have more molecules than the smaller cells so the concentration of molecules in each cell could be compared within the population instead of the number of molecules in each cell within the population. Furthermore, the distribution of cell size could be compared with the gene expression noise within a population. With RNA-FISH and cell cycle markers we observed an upshift of transcription for *CLN2* and *CLB5* in late mitosis, which may be partially due to cell growth and larger cell size at cell division than at the beginning of the cell cycle.

Related to this question of size the distinction between mother and daughter cells, which could also be considered in the model. Indeed mother and daughter cells differ in size (about 40 and 25 fl for mother and daughter, respectively (Aldea et al., 2007)), length of the G1 (about 37 and 17 min ratio for mother and daughter, respectively (Brewer et al., 1984; Di Talia et al., 2007)) and also biological processes, e.g. daughter cells have a specific *SIC1* expression in early G1 induced by Ace2 (Aerne et al., 1998; Colman-Lerner et al., 2001; Knapp et al., 1996; Toyn et al., 1997).

Also daughter cells are smaller and therefore have lower molecule abundances than mother cells. A future model could investigate whether daughter cells, because of their smaller sizes and molecule abundances, are more sensitive to noise and/or to external stresses and which mechanisms may exist to protect daughter cells from noise.

8.7.3 Oscillating transcription and degradation rate constants

In both models we employed a single rate constant for the mRNA degradation. The mRNA production rate constants oscillate between high and low values throughout the cell cycle and previous works suggested that the mRNA degradation rate constants similarly oscillate over time to ensure rapid mRNA decay and sharp mRNA peaks (Cacace et al., 2012; Eser et al., 2013; Trcek et al., 2011). In our case, we tested our second model for *SIC1*, *CLN2* and *CLB5* with two degradation rates and as a result, the identifiability of the parameter values was lost. This loss of identifiability was especially significant for the cyclins. We considered a different model than, for example, Eser and colleagues who nicely discussed the implications of two degradation rates on the shape of the mRNA peak (Eser et al., 2013). We estimated instead the period of high transcription and decided to work with one degradation rate to keep the model simple and identifiable. Since we had no strong evidence for different mRNA degradation mechanisms with and without stress, we also assumed the same rate constants for unstressed and osmotic stressed conditions. This allowed us to estimate the duration of transcriptional inhibition of each cyclin under osmotic stress.

Importantly, the findings and predictions of the models could serve as a basis for experimental design. Also the models can be integrated in a larger model for more complex system as for example the long-term project of Prof. Edda Klipp's group on Whole Cell Modeling.

8.8 Implications for other genes and higher eukaryotes

8.8.1 Implications for other cell cycle genes in yeast and higher eukaryotes

In this work, we focused on the main players of G1/S transition in *S. cerevisiae* cell cycle. *S. cerevisiae* expresses seven other cyclins interacting with Cdk1 (Morgan, 1995) and our method could be applied to these genes to assess whether the findings presented in this thesis are common to other cyclins or cell cycle related genes. For example, we observed basal transcription for our three cell cycle regulators throughout the cell cycle. Interestingly basal level was also detected for at least Clb1-Cdk1 and Clb2-Cdk1 protein levels (Grandin and Reed, 1993) and via Northern Blot for *CLB1* and *CLB2* mRNA levels (Richardson et al., 1992). Beside Cdk1, Pho85 is another Cdk in *S. cerevisiae* and a binding target for 10 specific cyclins, named Pcls (Espinoza et al., 1994; Huang et al., 2007; Lenburg and O'Shea, 2001; Morgan, 1997). Pho85 regulon is less known than Cdk1 and our lab has started investigating *PCL1* and *PCL9* with RNA-FISH.

The architecture of the cell cycle regulation as well as the function of its regulators are highly conserved among eukaryotes (Foury, 1997; Harashima et al., 2013). Our genes of interest, i.e. *SIC1*, *CLN2* and *CLB5*, are functionally homologous in mammalian cells to $p27^{Kip1}$, cyclin A and cyclin E, respectively (Barberis et al., 2005; Hwang and Clurman, 2005). Also Hog1 the MAPK initiating the

response to osmotic stress is homologue to mammalian p38 MAPK and the downstream molecular network of both MAPK is also well conserved between yeast and higher eukaryotes (Duch et al., 2012; Han et al., 1994). Therefore, our study suggests gene expression patterns, e.g basal level, transcription activation during mitosis for the cyclins, and osmo-response dynamics that could be tested in higher eukaryotes cells.

8.8.2 Implications for cancers and other cell cycle related diseases

Since dysfunctional cell cycle regulation has been related to cancers, diabetes and neurodegenerative and cardiovascular diseases (Boehm and Nabel, 2003; Currais et al., 2009; Zhivotovsky and Orrenius, 2010), one may ask whether and how this study has any implications for diagnosis or treatments development for such diseases.

Importantly, the mammalian homologues of *SIC1*, *CLN2* and *CLB5* have been related to cancer (Barberis et al., 2005; Foury, 1997; Harashima et al., 2013; Hwang and Clurman, 2005; Zhivotovsky and Orrenius, 2010). Sic1 mammalian homologue, $p27^{Kip1}$, is a tumor repressor, i.e. inhibits cell growth, cell proliferation and tumor development. Cln2 and Clb5 mammalian homologues, cyclin A and cyclin E, respectively, are onco-proteins, i.e. promote cell proliferation and their mutations and/or overexpression of them can cause cancer.

Notably, cancer development and diseases in higher organisms are usually not caused by a single mutation or a single dysfunctional protein but by a deregulation within a regulatory pathway (Hwang and Clurman, 2005; Pereira et al., 2012; Zhivotovsky and Orrenius, 2010). Indeed, many cell cycle regulating proteins have homologues or genes with redundant functions, which overcome or compensate a gene deletion or a dysfunctional gene. In yeast many genes also have redundant functions, for example *CLN1* and *CLN2* or *CLB5* and *CLB6* (Dirick et al., 1995; Schwob and Nasmyth, 1993). Additionally, other mechanisms such as post-transcription, post-translation, protein modifications, transport and feedback loops further enable to regulate protein activity and maintain robustness within cell cycle progression (Barik et al., 2010; Becskei et al., 2004; Finley et al., 2012; Jensen et al., 2006; Kõivomägi et al., 2011; Zhang et al., 2011). Therefore, it is difficult to find a direct cause-effect relationship between a (mutated) protein and a disease. In this study, computational modeling enabled an integrative approach that not only assesses the regulation of a single gene but also of the interplay of genes within a molecular network. Indeed, computational modeling was essential to rationalize data from divers sources and to investigate the dynamics of the chosen molecular pathway. We provided a set of quantitative data and gene expression regulation dynamics that can be used as basis for other genes. In this regard, the identification of gene expression signatures can reveal a normal or abnormal regulation and, therefore, be used as biomarkers of diseases. Hence, our approach opened a path toward medical and pharmaceutical system biology that aims at the integrative studies of biological entities in context of whole cells or subsystems.

For example, overexpression of cyclin E (mammalian homologue of *CLB5*) mRNA and protein was detected in various cancer cells (Hwang and Clurman, 2005; Tissier et al., 2004). Cyclin E belongs to the retinoblastoma (Rb) pathway (homologue to the Whi5 pathway in yeast (Foury, 1997; Harashima et al., 2013)) and cyclin E overexpression was found not to be the direct cause of cancer but to be hallmark of mutations and dysfunctions in the Rb pathway including among others cyclin E,

cyclin D, p16, Rb and E2F (Hwang and Clurman, 2005). Interestingly, cyclin E was not effective as therapeutic target however high cyclin E level was an effective biomarker for breast cancer diagnosis (Hwang and Clurman, 2005). Therefore, studies on *CLB5* in yeast bring useful insights on the regulation of *CLB5*, the Whi5 pathway and new hypotheses that can be further tested for cyclin E.

Interestingly, low expression as well as mislocalization of $p27^{Kip1}$ (mammalian homologue of Sic1) were observed in several cancer cells (Besson et al., 2004; Catzavelos et al., 1997; Slingerland and Pagano, 2000). Low $p27^{Kip1}$ level promotes premature cell cycle progression and also increases sensitivity to chemical carcinogens and radiation (Catzavelos et al., 1997; Fero et al., 1996, 1998; Nakayama et al., 1996). Elevated cytoplasmic localization was linked with tumorigenesis and is thought to increase cancer cells motility (Besson et al., 2004; Blain et al., 2003; Denicourt et al., 2007; Slingerland and Pagano, 2000). Here, we presented two microscopy methods that can be not only quantify mRNA levels but also enable quantitative measurement of cellular localization and, in the case of the MS2-CP system, live mRNA tracking. Additionally, one could adapt our experiments with osmotic stress to study the effects of chemical carcinogens or radiation on yeast cell cycle progression and gene expression of chosen genes.

In this work, we worked with 'healthy' wild type yeast cells and genes with wild type behaviors. In the future, our methodology could be applied to mutated genes or deletion strains to investigate the effect of a specific feature on gene expression, cell cycle and/or stress response ability. This is especially interesting in the case of features that may be related to dysfunctional cell cycle progression and diseases.

8.9 Budding yeast as eukaryotic model organism

Our interest lay on the eukaryotic cell cycle and we took advantage of the budding yeast as a model organism for eukaryotes. Because of its fast growth, easy manipulation, numerous published mutant libraries and established tools for genetic manipulation, *S. cerevisiae* is a powerful model organism (Baker Brachmann et al., 1998; Ghaemmaghami et al., 2003; Hinnen et al., 1978; Lundblad and Struhl, 2008). The gene functions of *SIC1*, *CLN2* and *CLB5* are conserved among eukaryotes and their properties may be predictive of the ones of their homologous in higher eukaryotes (Foury, 1997; Harashima et al., 2013). Interestingly, if a gene does not have homologous in *S. cerevisiae*, it can be cloned in a yeast vector to construct a "humanized yeast" (Pereira et al., 2012). Within this method the study of the heterologous expression of the gene in yeast lead to information about the gene function and the discoveries can then later be tested in a higher model organism. This was successfully done, for example for the tumor repressor p53 (Coutinho et al., 2009; Pereira et al., 2012) or the different isoforms of the protein kinase C (PKC) involved in regulation of cell proliferation and apoptosis (Pereira et al., 2012; Saraiva et al., 2004). Yeast cell as a unicellular eukaryote model organism still has major limitations, for example, it is not possible to assess mechanisms resulting in diseases that rely on cell-cell interaction or multi-cellularity.

9. CONCLUDING REMARKS

Although cell cycle has been extensively investigated, we aimed in this project to assess cell cycle regulation in regards to gene expression stochasticity and cell signaling. We required a single cell quantitative approach and applied single cell RNA microscopy, cell cycle synchronization and stochastic modeling to the three main G1/S regulators in *S. cerevisiae*.

We provided a large quantitative data set on single-cell absolute mRNA numbers and molecular noise throughout the cell cycle under optimal growth conditions as well as in response to osmotic stress. Single cell resolution and the use of morphological and genetic markers enabled us to resolve detailed patterns in the transcription profiles, such as basal levels, mitotic upshift of expression, which might be overlooked or cannot be detected with population assays. We disturbed the cells with hyperosmolarity and assessed how osmotic stress, especially on a long term, differently affected gene expression of cell cycle regulator genes and perturbed progression of cell cycle events. Additionally, we also monitored live mRNA transport of the CKI within single cells.

Mathematical modeling extracted kinetic parameters for gene expression from the experimental mRNA distribution as well expanded the static mRNA data to dynamics time-courses for mRNA, protein and related noise levels. Therefore mathematic modeling allowed for an integrative and systematic analyze of the experimental data since the three genes were assessed within their molecular network and in context of previously published information. In the future our stochastic models could be adapted as module or expanded for other cell cycle phases.

Importantly, regulation mechanisms specific to the three yeast genes may be generalized to others genes of other cell cycle phases as well as to other organisms. This is especially interesting in the case of the mammalian homologues of *SIC1*, *CLN2* and *CLB5*, which are directly related to cancer development and whose transcriptional patterns may be employed as biomarkers for disease diagnosis. Hence, this project with its integrative strategy and results provided a basis for integrative and systemic studies as the long-term project of Prof. Edda Klipp on Whole Cell Modeling, and paved the way for improvements of biotechnological approaches and developments of new biomedical applications.

Appendix

- Appendix 1 – Details of the algorithm for the GPU architecture of the model in centered on *SIC1.*
- Appendix 2 – Parameter estimation
- Appendix 3 – Supplementary Figures
- Appendix 4 – Supplementary Tables
- Appendix 5 – Revised stochastic model for *SIC1*, *CLN2* and *CLB5* transcription under normal growth conditions and under osmotic stress.

Appendix 1: Details of the algorithm for the GPU architecture of the model in centered on *SIC1.*

This section presents the details of the algorithm for the GPU architecture of the model in centered on *SIC1* in RESULTS II. This algorithm was developed in the Theoretical Biophysics group (Humboldt University Berlin) and was published in (Barberis et al., 2011).

- Algorithm

The algorithm for the GPU architecture was adapted from the Gillespie implementation of Mauch et. al. which is, to our knowledge, the fastest single core implementation available (Mauch and Stalzer, 2011). The major differences of the algorithm are the utilization of the ziggurat method to generate the exponential deviates combined with a 2D search on the propensities and continuous updating.

The ziggurat implementation was taken from the original publication with the minor difference that we did not use the proposed SHR3 generator but rather a concatenated multiply-with-carry generator (MWC) with random seeding which passes the DIEHARD tests for randomness (Marsaglia, 2003; Marsaglia and Tsang, 2000). This has virtually no impact on the speed of the random number generation. The 2D search is implemented as in the Mauch version. The propensities are stored in a matrix with row and column size equal to the smallest integer larger than the square root of the reaction count. For each row we also store the row sum of propensities. The uniform variate used for the search is also generated from the MWC. The 2D search first identifies the row of the corresponding propensity row sum and than looks within the row for the corresponding propensity. After identifying the next reaction updates are only executed for propensities influenced by the executed reaction. This is achieved by automatic computation of a dependency list prior to the simulation from the stoichiometry of the model. The propensity function itself is compiled together with the simulator. For a schematic view of the algorithm also see Supplementary Figure S 1.

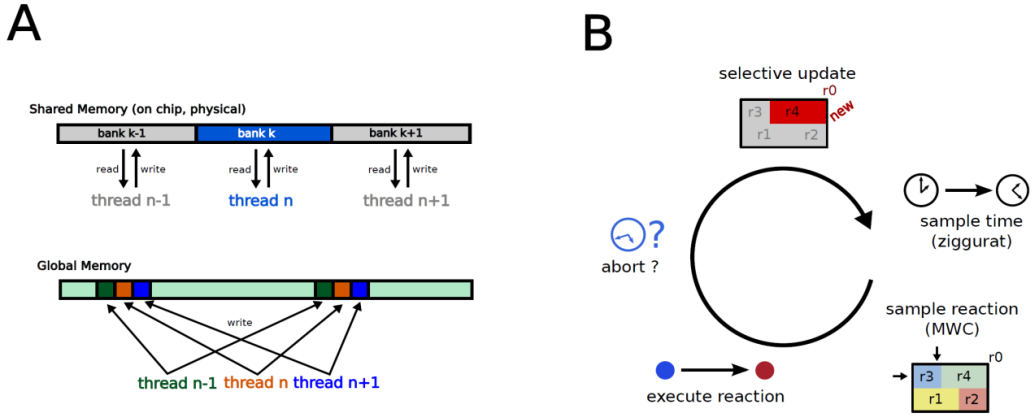

Supplementary Figure S 1. Schematic view of the memory management (A) and the implemented algorithm (B).

APPENDIX 1: Details of the algorithm for the GPU architecture of the model in centered on *SIC1*.

- Parallelization and memory management

In order to efficiently parallelize the algorithm we adapted the memory accesses in the model to comply with NVIDIA hardware. All matrix data structures used during the simulation are linearized first to meet alignment constraints and access patterns have been optimized. The data structures used during the simulation (dependencies, stoichiometry, propensities and state) are kept within shared memory, which is on chip and can be accessed two orders of magnitude faster than global memory. Every single thread will now simulate a single trajectory. Additionally, every single thread will only access a single memory bank in shared memory, thus minimizing the number of bank conflicts. In particular, there will be no bank conflicts at all if the number of threads is equal or less to the number of banks (32 for devices of compute capability 2.x). Recording in the state is done in global memory with a maximum amount of coalescing and caching. As such, recording of the state can be bundled into one write operation for several threads (also see Supplementary Figure S 1A). The tables for the exponential random number generation are kept within constant memory, and are, thus, always cached.

As random number generation using the described methods is rapid on the GPU and since the propensity calculation uses only simple float operations simulation speed is mostly bandwidth-limited. Thus, we chose the thread number as a compromise between a relatively low thread number (to avoid bank conflicts) and maximum occupancy.

- Benchmark

The algorithm was benchmarked on a NVIDIA Geforce 480GTX. The chosen thread number per block was 192, which resulted in occupancy of 75%. The benchmark model was the Decaying Dimerization model, which comprises the following reactions ri:

$$r1: S1 \rightarrow 0 \qquad r2: S1 + S1 \rightarrow S2 \qquad r3: S2 \rightarrow S1 + S1 \qquad r4: S2 \rightarrow S3$$

with corresponding parameters $k1 = 1.0$, $k2 = 0.002$, $k3 = 0.5$ and $k4 = 0.04$.

The average simulation time per reaction for our method and tow other implementations is shown in Supplementary Figure S 2. For implementations other than our own the average time per reaction has been calculated from the mean and the extreme values for the number of reactions per trajectory. The mean, minimum and maximum numbers of reactions were calculated from a set of 20 million trajectories. The CPU times have been generated with Cain on Dual Core Intel processor (blue line). This corresponds perfectly to the minimal single core CPU simulation time of about 105 ns for a single reaction. The green lines denote a GPU implementation of (Hong Li and Petzold, 2010). The observed jump of simulation is likely to be caused by a switch in the thread number, which increases occupancy of the GPU. However, since their simulation times come from NVIDA GeForce 8800GTX which has a different hardware setup as well as a different compute capability we cannot say what exactly causes the speed up of our implementation compared to theirs. The red line denotes our own implementation, which always shows the fastest simulation times, which peak at a maximum speed of 0.53 ns per reaction (more than 1.8 billion reactions per second). A simulation speed of around 0.6 ns per reaction is achieved from 10,000 trajectories on and thus makes it applicable for a large variety of tasks. Additionally, recording of several time steps only mildly affects simulation times.

APPENDIX 1: Details of the algorithm for the GPU architecture of the model in centered on *SIC1*.

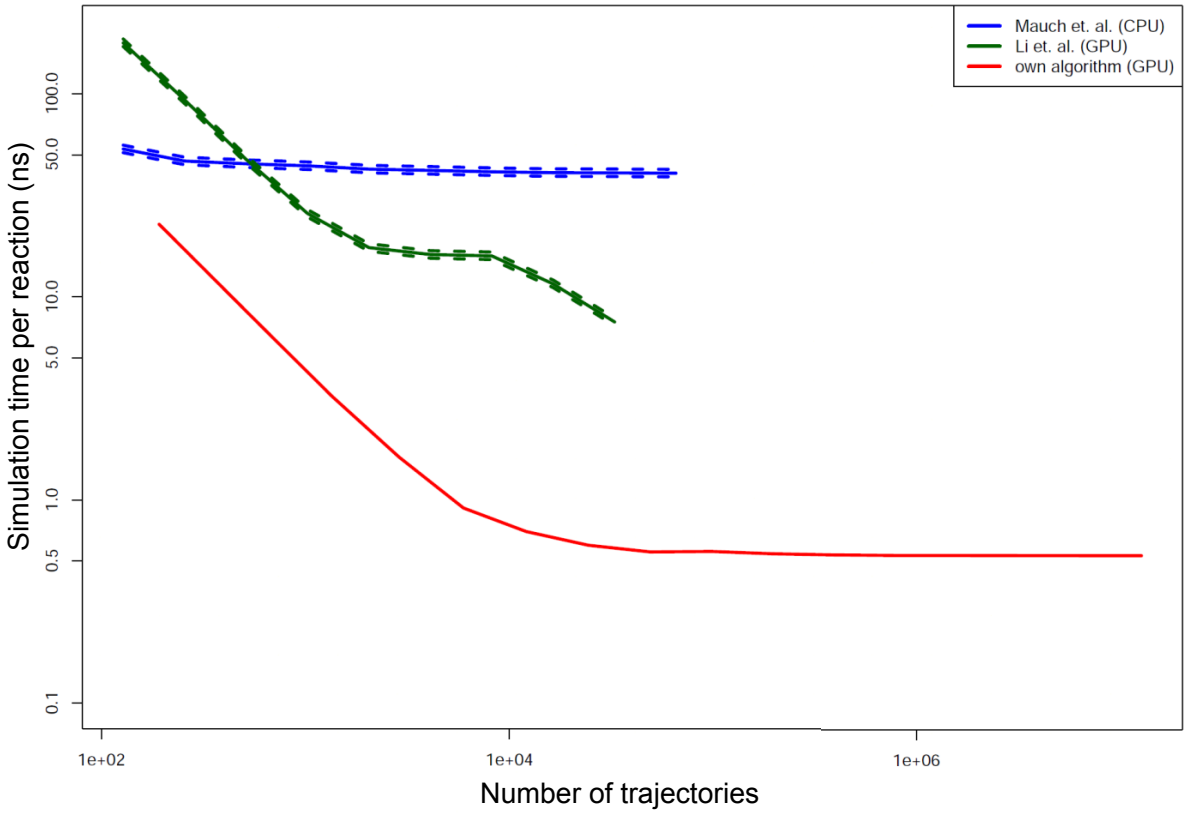

Supplementary Figure S 2. Comparison of simulation times per reaction for the Decaying Dimerization model.
The CPU used was a Intel Core 2 Duo 3.16 GHz. The GPUs used were a NVIDIA GeForce 8800 GTX (Hong Li and Petzold, 2010) and a NVIDIA GeForce 480 GTX (this study, i.e. Barberis et al., 2011). The dashed lines correspond to minimum and maximum approximations.

Appendix 2: Parameter estimation for transcriptional activity of *SIC1*, *CLN2*, and *CLB5* from the experimental mRNA distributions obtained with RNA-FISH

A. Description of the model for parameter estimation

The basic structure of the model is shown in Figure 36A. Considering that the number of mRNA molecules in the measurements was small (between 0 and 71 molecules per cell) and available in distribution form, we chose a stochastic modeling approach. We only considered the transcription part of the model for parameter estimation, since the transcription evolved statistically independent from the rest of the reaction network. For the same reason we were able to treat each gene separately. Consequently the following reactions, i.e. mRNA production and mRNA degradation, were considered for parameter estimation:

$$\emptyset \xrightarrow{k(t)} mRNA$$

$$mRNA \xrightarrow{p} \emptyset$$

Transcription with a rate k_{1h} was started at a time $t_{S,0}$ and stopped at time $t_{S,e}$. (Signal S_i present, $k(t) = k_{1h}, \forall t_{S,0} \leq t \leq t_{S,e}$).

Since all promoters exhibited a basal activity (especially *SIC1*) we considered a transcription rate k_{1l} at all other times of the cell cycle. (Signal S_i absent, $k(t) = k_{1l}, \forall t < t_{S,0}, t > t_{S,e}$).

We implemented the stochastic part of the model using the exact solution of the master equation for monomolecular reaction networks (Jahnke and Huisinga, 2006). In our case, the reaction system only consisted of one species, namely the number of mRNA molecules, $n(t)$. The solution of the master equation was then a matrix $P(n, t|n_0, t_0)$ that described the probability of a transition between n_0 molecules at a time t_0 and n molecules at time t. Note that the definition of a monomolecular reaction according to (Jahnke and Huisinga, 2006) (p. 4) included only conversion, production from source or degradation, but neither (auto)catalytic nor splitting reactions. The form of the solution of the chemical master equation yielding this matrix depended on the type of initial conditions, which will be discussed in the following paragraph.

Since our experiments did not reveal information about the past of a given cell. The number of molecules, n_0, at the beginning of the cell cycle, t_0, was assumed to be distributed according to a Poisson distribution rather than to take a discrete value. This distribution was chosen because the measurements of $n(t)$ can be considered statistically independent of each other. In other words the number of mRNA molecules $n(t)$ of a given cell does not depend on whether another cell with $n_0(t)$ molecules was measured before.

As already noted by (Gardiner, 2009) (p. 269), proposition 2 in (Jahnke and Huisinga, 2006) state that the solution of the monomolecular master equation for a Poissonian initial distribution is a Poisson distribution. The parameter set of the latter distribution is given by the solution of the traditional reaction rate equations. For our system consisting of only one random variable $n(t)$, i.e. the mRNA number, only one reaction rate equation needed to be solved, namely:

$$\frac{d\langle n(t)\rangle}{dt} = k(t) - p\langle n(t)\rangle$$

Equation 1

$\langle n(t_0)\rangle$ was the initial value used for numerical solution of the equation 1, which was also the parameter for the initial distribution. The mentioned proposition was also valid in the case of time dependent reaction rates such as our $k(t)$. Note that under the Poissonian initial condition

$$P(n_0, t_0) = e^{-\langle n(t_0)\rangle} \frac{\langle n(t_0)\rangle^{n(t_0)}}{n(t_0)!},$$

the matrix $P(n, t|n_0, t_0)$ had identical row entries. Therefore the solution could be represented by a vector or a histogram, i.e a mRNA distribution, per time point.

One last step was missing to simulate a histogram for parameter fitting as depicted in Supplementary Figure S 5 . The cells in our experiments were measured not at a certain time point during the cell cycle but were assigned to a certain stage of the cell cycle using the described *in silico* synchronization approach (see Figure 34 in RESULTS II and Section 3.2.1.5 Genetic and morphological markers for in silico synchronization). Consequently, we averaged the mRNA distributions for all time points between the start and the end of a given cell cycle phase. This allowed for comparison of the simulated mRNA distributions with the experimental data.

This semi-analytical approach enabled us to estimate the parameters $k_{1h}, k_{1l}, t_{S,0}, t_{S,e}$ and p of the model in about the same computation time an exclusively deterministic ordinary differential equation approach would take. The algorithm used for parameter estimation is described in the following Section B. Calculation of likelihood for parameter estimation.

B. Calculation of likelihood for parameter estimation

Since the experimental mRNA distributions were given in the form of discrete histograms and the number of cells in each bin of the histograms (between 0 and 71) was small, a χ^2 test could not be applied (Baker and Cousins, 1984). The reason was that a χ^2 test, here in Neyman's form

$$\chi^2 = \sum_{i=1}^{n} \frac{(m_i - y_i)^2}{n_i},$$

where m_i is the number of events (cells) in histogram bin i and y_i is the prediction of the model in histogram bin i, amounts to the implicit assumption of a Gaussian error distribution.

Thus, the conditional probability of observing m_i given y_i could be written as

$$\log L_{\text{Normal}} = \log \prod_{i=1}^{n} P(m_i|y_i) = \sum_{i=1}^{n} \left(-\frac{1}{2}\log(2\,\pi\,m_i) - \frac{(m_i - y_i)^2}{m_i}\right),$$

Equation 2

where y_i is the mean and and $m_i/\sqrt{2}$ is the variance of the Gaussian. Since the logarithm is a strictly increasing function, the maximum of the likelihood in a numerically is obtained in a more convenient form by optimizing in the log domain. The additive term, $-\log(2\,\pi\,m_i)$, does not play a role when maximizing the likelihood. We now see that the minimization of χ^2 is equivalent to the maximization of L_{Normal}.

There are two intuitive reasons why the Gaussian distribution could not describe the statistics of the measurement. Firstly, a Gaussian error distribution would assign a non-vanishing probability density to negative values of m_i, which was unphysical since counting a negative number of cells is impossible. Secondly, the Gaussian distribution is a distribution describing continuous random variables, but in the case of this study we counted a discrete number of cells.

As an alternative approach we chose a Poissonian error model assuming that the single cells in each bin were measured independently of each other. The likelihood of a histogram given a model y_i was therefore given by

$$L = \prod_{i=1}^{n} e^{-y_i} \frac{(y_i)^{y_i}}{m_i!}.$$

Equation 3

As described in the following section C.Description of the algorithm to calculate likelihood for parameter estimation the model y_i was normalized to conserve the area, which was the total number of cells in the histogram, for the measurement. This guaranteed that data bins that contained a low number of cells were considered to have a larger "measurement noise" than bins with a high number of cells. To understand this, it is instructive to consider that for a Poisson distribution the variance is equal to the mean, so the standard deviation $\sqrt{y_i}$, here interpreted as "measurement noise", decreases comparably for larger mean y_i. Put in other words, the more cells we counted for a given bin i, the higher the information we had about the system is.

C. Description of the algorithm to calculate likelihood for parameter estimation

The objective function (likelihood) was calculated by the following algorithm:

1. Calculate $\langle n(t) \rangle$ by solving Equation 1 numerically.

2. Since the ODE-solver algorithm used to obtain $\langle n(t) \rangle$ returns the function at non-equidistant time points, these are interpolated to obtain m equally spaced samples. This is necessary because the integration over each cell cycle phase (step 4) would otherwise yield incorrect results. Consequently the cell cycle average distribution would depend on the sampling density defined by the ODE solver.

3. For each sampling point $t_i \in t_1, \dots, t_n$ (with $t_0 = 0$ and $t_n = 129$ min), store a Poisson distribution with mean $\langle n(t_i) \rangle$.

4. For every cell cycle phase $j = 0, \dots, 6$, starting at t_j and t_{j+1} (except $j = 6$), sum up all histograms between t_j and t_{j+1}.

5. Normalize each histogram to reach the same number of mRNAs as in the experiments.

6. Calculate the likelihood function with Equation 3.

The described likelihood was then maximized with respect to the model parameters $k_{1h}, k_{1l}, p, t_{S,0}$ and $t_{S,e}$.

D. Moment closure method for calculation of the time courses of mean and variance protein numbers.

For the calculation of the time courses of mean and variance protein numbers, we used the moment closure method (Matis and Guardiola, 2010). Moment closure allows to simulate nonlinear stochastic compartmental models by a set of ordinary differential equations much more quickly than by Monte-Carlo methods such as Gillespie's algorithm. The difference is that while Gillespie's algorithm allows for the simulation of the full stochastic dynamics, the moment closure method we used approximates the system by the dynamics of the first two cumulants of the system. The exact set of differential equations needed for the simulation of the cumulants is infinite for general second order reaction networks and we therefore needed to neglect the cumulants above some order. Since the full stochastic dynamics simulated using Gillespie's algorithm showed small differences compared to the simulation of the first two cumulants corresponding to mean and (co-)variance, we neglected cumulants of order higher than two. The basic procedure of the Mathematica Package (Matis and Guardiola, 2010) we used was the following:

1. Set up the stoichiometric matrix and initial conditions of the model.

2. The partial differential equation for the cumulant generating function $K(\xi, t) := \log(\sum_{i=1}^{\infty} \exp(\xi\, n)\, P(n, t|n_0, t_0))$ corresponding to the chemical master equation is created and stored. Here, $\xi = (\xi_1, \xi_2, \dots, \xi_m)^T$ is a vector of positive real numbers and $n = (n_1, n_2, \dots, n_m)^T$ is the number of molecules of all m species.

3. Since the first two cumulants (mean and (co-)variance) are given by the first two coefficients of the cumulant generating function, the partial derivatives of $K(\xi, t)$ are expanded up to second order in ξ about the origin and the resulting ODEs are obtained.

4. The ODEs are solved numerically using the Mathematica function NDSolve and the desired time courses for mean and (co-)variance are obtained.

Appendix 3: Supplementary Tables

Supplementary Table S1. Numbers of analyzed cells per gene and per time point under normal growth conditions and under osmotic stress for the RNA-FISH experiments of RESULTS II.

0 min is equivalent to normal growth conditions.

TOTAL NUMBER OF ANALYZED CELLS			
Minutes under stress	*SIC1*	*CLN2*	*CLB5*
0 (no stress)	972	940	950
15	623	518	573
30	665	502	486
45	915	690	724
60	654	798	755
90	807	684	647

Supplementary Table S2. Experimental mean values of of *SIC1*, *CLN2* and *CLB5* mRNAs per cell in each cell cycle phase under normal growth conditions and under osmotic stress.

0 min is equivalent to normal growth conditions. This data set represents the numerical values for Figure 35 and Figure 43 for the RNA-FISH experiments of RESULTS II.

SIC1									
	early G1	late G1	S	G2	P/M	Ana	T/C	2spc / no bud	Full cell cycle
0 min	4,08	3,45	2,34	2,06	2,10	14,23	24,93	4,07	4,51
15 min	4,11	3,07	2,19	3,12	3,53	16,34	32,75	3,26	4,05
30 min	4,25	3,23	2,66	3,01	3,07	23,89	32,35	5,83	5,14
45 min	3,90	4,73	3,64	4,42	4,54	13,96	19,46	2,59	5.34
60 min	4,09	3,01	3,09	2,52	2,32	16,67	25,88	3,11	4.54
90 min	4,28	2,83	2,43	1,68	1,92	19,66	25,95	6,00	4.70

CLN2									
	early G1	late G1	S	G2	P/M	Ana	T/C	2spc / no bud	Full cell cycle
0 min	3,25	18,02	5,64	0,67	0,36	1,12	2,59	8,33	6,43
15 min	0,71	4,89	3,78	1,34	0,53	0,96	0,50	1,44	2,04
30 min	1,49	13,53	10,93	7,53	1,39	1,13	0,48	10,17	5,56
45 min	2,00	18,82	13,38	3,21	1,95	0,97	0,64	5,14	8,76
60 min	2,68	19,83	6,52	1,65	0,60	1,36	1,84	1,43	7,71
90 min	1,50	21,52	5,18	0,85	0,28	0,67	3,94	1,33	6,06

CLB5									
	early G1	late G1	S	G2	P/M	Ana	T/C	2spc / no bud	Full cell cycle
0 min	1,32	3,78	1,83	0,57	0,62	0,98	2,79	0,91	1,91
15 min	0,34	0,94	0,45	0,54	0,20	0,70	0,36	0,55	0.54
30 min	0,62	2,48	1,33	0,86	0,32	0,65	1,00	1,10	0.95
45 min	0,70	2,56	2,18	0,68	0,22	1,15	1,26	1,24	1,40
60 min	0,51	2,53	1,44	0,35	0,11	0,55	1,93	0,33	1.17
90 min	0,65	3,40	1,82	0,74	0,27	0,57	1,65	0,25	1,13

The following Supplementary Table S3 to Supplementary Table S20 are the experimental distributions of mRNA numbers for *SIC1*, *CLN2* and *CLB5* per cell in each cell cycle phase under normal growth conditions (equivalent to 0 min) and under osmotic stress for the RNA-FISH experiments of RESULTS II.

Supplementary Table S3. Experimental distributions of mRNA numbers for *SIC1* per cell in each cell cycle phase under normal growth conditions (equivalent to 0 min under osmotic stress or no stress).

SIC1 no stress									
# RNA/cell	# of cells	early G1	late G1	S	G2	P/M	Ana	T/C	2spc / noBud
0	102	22	24	22	24	6	1	0	3
1	200	35	53	41	45	22	1	0	3
2	245	48	74	54	36	20	10	0	3
3	139	30	52	22	19	10	6	0	0
4	58	10	19	9	10	6	4	0	0
5	47	11	14	12	4	2	3	0	1
6	23	3	10	2	0	2	3	1	2
7	20	5	6	2	1	1	3	1	1
8	13	7	2	0	1	0	2	1	0
9	10	4	3	0	1	0	2	0	0
10	19	8	6	3	1	0	0	1	0
11	8	4	2	0	0	0	2	0	0
12	9	5	2	0	0	0	1	0	1
13	7	1	1	1	0	0	3	1	0
14	6	4	1	0	0	0	1	0	0
15	4	1	2	0	0	0	1	0	0
16	3	0	0	1	0	0	1	0	1
17	3	0	1	0	0	0	1	1	0
18	3	0	0	0	0	0	0	3	0
19	4	0	0	0	0	0	2	2	0
20	4	0	0	0	0	0	3	1	0
22	2	0	0	0	0	0	1	1	0
23	2	0	1	0	0	0	1	0	0
24	3	0	0	0	0	0	1	2	0
26	3	0	0	0	1	0	0	2	0
27	2	1	0	0	0	0	0	1	0
28	3	0	0	0	0	0	1	2	0
29	5	1	1	0	0	0	3	0	0
30	5	0	0	0	0	0	2	3	0
31	2	0	0	0	0	0	0	2	0
32	6	0	1	0	0	0	4	1	0
34	2	0	0	0	0	0	1	1	0
35	3	0	0	0	0	0	2	1	0
36	2	1	0	0	0	0	1	0	0
38	1	0	0	0	0	0	1	0	0
39	0	0	0	0	0	0	0	0	0
40	1	0	1	0	0	0	0	0	0
51	1	0	0	0	0	0	0	1	0
56	1	0	0	0	0	0	1	0	0
66	1	0	0	0	0	0	0	1	0
Total # of cells	**972**	**201**	**276**	**169**	**143**	**69**	**69**	**30**	**15**

Supplementary Table S4. : Experimental distributions of mRNA numbers for *SIC1* per cell in each cell cycle phase for 15 min under osmotic stress.

SIC1 15 min									
# RNA/cell	# of cells	early G1	late G1	S	G2	P/M	Ana	T/C	2spc / noBud
0	36	14	8	6	7	1	0	0	0
1	94	26	25	15	20	2	1	0	5
2	148	53	40	12	29	7	2	0	5
3	116	36	25	15	30	5	2	1	2
4	70	17	13	6	20	8	2	0	4
5	30	11	4	2	8	3	1	0	1
6	22	8	2	0	6	2	4	0	0
7	19	8	2	1	2	1	4	0	1
8	13	7	2	0	1	0	3	0	0
9	8	2	3	0	2	1	0	0	0
10	7	2	1	0	2	0	2	0	0
11	3	1	1	0	0	0	1	0	0
12	4	4	0	0	0	0	0	0	0
13	3	2	0	0	0	0	0	0	1
14	4	0	1	0	0	0	2	1	0
15	5	2	0	0	1	0	1	1	0
16	3	1	0	0	0	0	2	0	0
17	2	1	0	0	0	0	1	0	0
18	1	1	0	0	0	0	0	0	0
19	5	2	1	0	0	0	0	2	0
20	1	0	0	0	0	0	1	0	0
21	1	0	1	0	0	0	0	0	0
24	1	0	0	0	0	0	1	0	0
25	2	0	0	0	0	0	2	0	0
26	1	1	0	0	0	0	0	0	0
29	1	0	0	0	0	0	1	0	0
30	1	0	0	0	0	0	1	0	0
31	3	1	0	0	0	0	0	2	0
32	0	0	0	0	0	0	0	0	0
33	1	0	0	0	0	0	0	1	0
36	3	0	0	0	0	0	2	1	0
37	2	0	0	0	0	0	1	1	0
38	2	0	0	0	0	0	1	1	0
39	1	0	0	0	0	0	0	1	0
40	1	0	0	0	0	0	0	1	0
42	3	0	0	0	0	0	1	2	0
43	2	0	0	0	0	0	1	1	0
46	1	0	0	0	0	0	0	1	0
48	1	0	0	0	0	0	0	1	0
62	1	0	0	0	0	0	1	0	0
79	1	0	0	0	0	0	0	1	0
Total # of cells	**623**	**200**	**129**	**57**	**128**	**30**	**41**	**19**	**19**

Supplementary Table S5. : Experimental distributions of mRNA numbers for *SIC1* per cell in each cell cycle phase for 30 min under osmotic stress.

SIC1 30 min									
# RNA/cell	# of cells	early G1	late G1	S	G2	P/M	Ana	T/C	2spc / noBud
0	37	20	7	5	3	2	0	0	0
1	114	62	20	11	18	3	0	0	0
2	122	54	22	12	27	6	0	0	1
3	131	49	20	15	29	7	3	1	7
4	73	26	14	8	17	5	1	0	2
5	49	25	4	4	13	2	1	0	0
6	22	8	3	1	7	1	1	1	0
7	14	8	1	0	1	2	0	1	1
8	15	8	2	2	1	0	1	1	0
9	7	7	0	0	0	0	0	0	0
10	7	7	0	0	0	0	0	0	0
11	9	8	1	0	0	0	0	0	0
12	1	1	0	0	0	0	0	0	0
13	2	1	0	0	0	0	1	0	0
14	3	2	0	0	0	0	0	1	0
15	2	2	0	0	0	0	0	0	0
16	5	2	0	0	0	0	2	1	0
17	5	3	0	0	0	0	2	0	0
18	1	0	0	0	0	0	1	0	0
19	3	2	0	0	0	0	1	0	0
20	3	1	0	0	0	0	1	1	0
21	2	1	0	0	0	0	0	1	0
23	2	0	1	0	0	0	1	0	0
24	6	2	0	0	0	0	4	0	0
25	1	1	0	0	0	0	0	0	0
26	2	1	0	0	0	0	0	1	0
27	1	0	0	0	0	0	0	1	0
29	1	0	0	0	0	0	0	1	0
30	1	0	0	0	0	0	1	0	0
31	1	0	0	0	0	0	0	1	0
32	1	0	0	0	0	0	0	0	1
34	3	0	0	0	0	0	0	3	0
35	1	0	1	0	0	0	0	0	0
36	2	0	0	0	0	0	0	2	0
37	0	0	0	0	0	0	0	0	0
38	0	0	0	0	0	0	0	0	0
39	0	0	0	0	0	0	0	0	0
40	0	0	0	0	0	0	0	0	0
41	0	0	0	0	0	0	0	0	0
42	2	0	0	0	0	0	1	1	0
43	2	0	0	0	0	0	2	0	0
44	0	0	0	0	0	0	0	0	0
45	2	0	0	0	0	0	1	1	0
46	2	0	0	0	0	0	0	2	0
48	0	0	0	0	0	0	0	0	0
49	0	0	0	0	0	0	0	0	0
51	1	0	0	0	0	0	0	1	0
54	1	0	0	0	0	0	0	1	0
56	1	0	0	0	0	0	1	0	0
57	3	0	0	0	0	0	1	2	0
61	1	0	0	0	0	0	0	1	0
66	1	0	0	0	0	0	1	0	0
Total # of cells	**665**	**301**	**96**	**58**	**116**	**28**	**28**	**26**	**12**

Supplementary Table S6. : Experimental distributions of mRNA numbers for *SIC1* per cell in each cell cycle phase for 45 min under osmotic stress.

SIC1 45 min									
# RNA/cell	# of cells	early G1	late G1	S	G2	P/M	Ana	T/C	2spc / noBud
0	82	27	16	8	23	3	2	2	1
1	183	58	41	19	45	7	4	4	5
2	190	64	48	17	45	5	9	0	2
3	141	34	48	22	26	2	2	3	4
4	80	23	22	6	19	2	4	1	3
5	57	18	18	6	9	0	4	1	1
6	36	6	16	1	6	2	3	1	1
7	17	6	3	2	4	1	1	0	0
8	11	4	1	0	3	1	1	1	0
9	5	4	0	0	0	0	1	0	0
10	11	5	1	0	1	2	2	0	0
11	5	2	1	1	1	0	0	0	0
12	7	2	1	0	3	0	1	0	0
13	2	1	0	0	0	0	0	1	0
14	4	3	0	1	0	0	0	0	0
15	3	2	0	0	0	0	0	1	0
16	8	5	1	0	1	0	1	0	0
17	1	0	0	0	1	0	0	0	0
18	3	0	1	1	0	0	1	0	0
19	3	1	1	1	0	0	0	0	0
20	5	0	0	1	2	0	0	2	0
21	3	0	0	1	0	0	1	1	0
22	2	1	0	0	0	0	1	0	0
23	1	0	0	0	0	0	1	0	0
24	4	0	1	1	0	0	2	0	0
25	3	1	0	0	0	0	1	1	0
26	3	1	0	0	0	0	2	0	0
27	2	0	0	0	0	0	0	2	0
28	4	0	0	0	0	0	1	3	0
29	2	0	0	0	0	0	0	2	0
30	2	0	0	0	0	0	0	2	0
31	3	1	1	0	0	0	1	0	0
32	4	0	0	0	2	0	0	2	0
33	4	0	3	0	1	0	0	0	0
34	4	0	2	0	0	0	1	1	0
36	2	0	0	0	0	0	2	0	0
39	1	0	0	0	0	0	1	0	0
40	2	0	0	0	0	1	0	1	0
41	1	0	0	0	0	0	0	1	0
43	2	0	0	0	0	0	1	1	0
44	1	0	0	0	0	0	1	0	0
47	1	0	0	0	0	0	1	0	0
48	1	0	0	0	1	0	0	0	0
50	1	0	0	0	1	0	0	0	0
53	4	1	0	0	1	0	1	1	0
58	1	0	1	0	0	0	0	0	0
65	1	0	1	0	0	0	0	0	0
67	1	0	0	0	1	0	0	0	0
69	1	0	1	0	0	0	0	0	0
Total # of cells	**915**	**270**	**229**	**88**	**196**	**26**	**54**	**35**	**17**

Supplementary Table S7. : Experimental distributions of mRNA numbers for *SIC1* per cell in each cell cycle phase for 60 min under osmotic stress.

SIC1 60 min									
# RNA/cell	# of cells	early G1	late G1	S	G2	P/M	Ana	T/C	2spc / noBud
0	69	23	13	13	18	1	1	0	0
1	114	37	28	19	21	7	0	0	2
2	119	35	32	26	19	5	0	0	2
3	129	32	42	26	20	5	3	0	1
4	72	12	27	18	10	1	3	0	1
5	41	8	15	5	4	3	3	0	3
6	16	4	4	3	4	0	1	0	0
7	11	4	2	3	0	0	2	0	0
8	8	7	0	1	0	0	0	0	0
9	6	1	1	2	0	0	1	1	0
10	3	3	0	0	0	0	0	0	0
11	7	6	0	1	0	0	0	0	0
12	7	5	0	0	0	0	1	1	0
13	3	2	0	0	0	0	1	0	0
14	5	4	0	1	0	0	0	0	0
15	3	2	0	0	0	0	1	0	0
16	2	0	0	1	0	0	0	1	0
17	1	0	0	0	0	0	1	0	0
18	1	0	0	0	0	0	1	0	0
19	5	2	0	1	0	0	1	1	0
20	5	1	0	0	0	0	2	2	0
21	2	1	0	0	0	0	1	0	0
22	2	1	0	0	0	0	0	1	0
23	3	0	1	0	0	0	1	1	0
24	3	0	0	0	0	0	0	3	0
25	1	0	0	0	0	0	1	0	0
26	1	0	0	0	0	0	1	0	0
27	1	0	0	0	0	0	1	0	0
28	3	0	1	0	0	0	1	1	0
33	3	0	0	0	0	0	2	1	0
37	1	0	0	0	0	0	0	1	0
40	1	0	0	0	0	0	0	1	0
41	1	0	0	0	1	0	0	0	0
42	1	0	0	0	0	0	1	0	0
43	1	0	0	0	0	0	0	1	0
44	1	0	0	0	0	0	1	0	0
46	1	0	0	0	0	0	0	1	0
49	1	0	0	0	0	0	1	0	0
Total # of cells	**654**	**190**	**166**	**120**	**97**	**22**	**33**	**17**	**9**

Supplementary Table S8. : Experimental distributions of mRNA numbers for *SIC1* per cell in each cell cycle phase for 90 min under osmotic stress.

SIC1 90 min									
# RNA/cell	# of cells	early G1	late G1	S	G2	P/M	Ana	T/C	2spc / noBud
0	111	25	13	23	39	10	1	0	0
1	180	43	21	40	53	15	4	0	4
2	154	33	29	34	42	11	4	0	1
3	112	24	28	25	23	6	5	1	0
4	58	14	15	10	10	5	2	0	2
5	39	11	10	8	6	2	1	1	0
6	15	7	1	2	1	1	3	0	0
7	8	4	1	1	0	1	1	0	0
8	17	11	1	0	0	0	2	3	0
9	14	6	3	2	0	0	1	1	1
10	4	3	0	0	0	0	1	0	0
11	4	2	0	0	0	0	2	0	0
12	9	7	0	0	1	0	1	0	0
13	2	2	0	0	0	0	0	0	0
14	6	5	1	0	0	0	0	0	0
15	1	0	0	0	0	0	1	0	0
16	2	0	1	1	0	0	0	0	0
17	4	2	0	0	0	0	1	1	0
18	4	2	0	0	0	0	2	0	0
19	3	0	0	1	0	0	0	2	0
21	3	2	0	0	0	0	1	0	0
22	1	0	0	0	0	0	0	1	0
23	1	0	0	0	0	0	0	1	0
24	5	0	0	1	0	0	2	2	0
25	3	0	0	0	0	0	1	2	0
26	5	1	0	0	0	0	1	3	0
27	2	0	0	0	0	0	1	1	0
28	1	0	0	0	0	0	0	1	0
29	5	0	0	0	0	0	1	4	0
30	1	0	0	0	0	0	1	0	0
31	3	0	0	0	0	0	0	2	1
32	2	0	0	0	0	0	1	1	0
33	2	0	0	0	0	0	1	1	0
34	4	0	0	0	0	0	3	1	0
35	3	0	0	0	0	0	1	2	0
36	1	0	0	0	0	0	1	0	0
37	2	0	0	0	0	0	1	1	0
38	3	0	0	0	0	0	2	1	0
39	1	0	0	0	0	0	0	1	0
40	1	0	0	0	0	0	1	0	0
41	2	0	0	0	0	0	1	1	0
42	2	0	0	0	0	0	2	0	0
43	2	0	0	0	0	0	0	2	0
46	3	0	0	0	0	0	3	0	0
49	2	0	0	0	0	0	2	0	0
Total # of cells	**807**	**204**	**124**	**148**	**175**	**51**	**59**	**37**	**9**

Supplementary Table S9. : Experimental distributions of mRNA numbers for *CLN2* per cell in each cell cycle phase under normal growth conditions (equivalent to 0 min under osmotic stress or no stress).

CLN2 no stress									
# RNA/cell	# of cells	early G1	late G1	S	G2	P/M	Ana	T/C	2spc / noBud
0	388	123	15	38	105	55	35	11	6
1	136	27	8	22	37	12	23	6	1
2	64	11	11	9	20	6	3	3	1
3	39	12	7	12	4	1	2	1	0
4	17	10	2	2	1	0	2	0	0
5	24	11	8	4	0	0	0	1	0
6	17	6	6	2	0	0	1	2	0
7	14	5	7	2	0	0	0	0	0
8	6	2	2	2	0	0	0	0	0
9	17	4	7	5	0	0	0	0	1
10	15	2	8	4	0	0	0	1	0
11	4	0	4	0	0	0	0	0	0
12	13	3	8	2	0	0	0	0	0
13	14	0	10	2	0	0	0	1	1
14	12	1	11	0	0	0	0	0	0
15	9	4	4	0	0	0	0	1	0
16	3	0	3	0	0	0	0	0	0
17	4	1	3	0	0	0	0	0	0
18	9	2	7	0	0	0	0	0	0
19	9	1	5	1	1	0	0	0	1
20	6	1	2	3	0	0	0	0	0
21	9	1	8	0	0	0	0	0	0
22	9	3	5	1	0	0	0	0	0
23	10	2	7	1	0	0	0	0	0
24	4	0	3	1	0	0	0	0	0
25	6	1	4	1	0	0	0	0	0
26	8	1	5	1	0	0	1	0	0
27	5	0	4	1	0	0	0	0	0
28	6	1	5	0	0	0	0	0	0
29	8	0	7	1	0	0	0	0	0
30	12	0	10	2	0	0	0	0	0
31	7	1	6	0	0	0	0	0	0
32	1	0	1	0	0	0	0	0	0
33	6	0	5	1	0	0	0	0	0
34	5	0	5	0	0	0	0	0	0
35	1	0	1	0	0	0	0	0	0
36	1	0	1	0	0	0	0	0	0
38	1	0	1	0	0	0	0	0	0
39	3	0	3	0	0	0	0	0	0
40	3	0	3	0	0	0	0	0	0
42	1	0	1	0	0	0	0	0	0
43	1	0	1	0	0	0	0	0	0
44	1	0	1	0	0	0	0	0	0
45	1	0	1	0	0	0	0	0	0
47	1	0	1	0	0	0	0	0	0
49	1	0	1	0	0	0	0	0	0
50	3	0	3	0	0	0	0	0	0
51	1	0	1	0	0	0	0	0	0
54	1	0	0	1	0	0	0	0	0
55	1	0	1	0	0	0	0	0	0
56	1	0	0	0	0	0	0	0	1
60	1	0	1	0	0	0	0	0	0
71	1	0	1	0	0	0	0	0	0
Total # of cells	**940**	**236**	**235**	**121**	**168**	**74**	**67**	**27**	**12**

Supplementary Table S10. : Experimental distributions of mRNA numbers for *CLN2* per cell in each cell cycle phase for 15 min under osmotic stress.

CLN2 15 min									
# RNA/cell	# of cells	early G1	late G1	S	G2	P/M	Ana	T/C	2spc / noBud
0	256	120	29	8	31	25	34	5	4
1	85	23	14	9	21	4	6	5	3
2	43	8	5	8	14	3	5	0	0
3	31	5	4	6	13	1	1	0	1
4	26	6	11	4	4	0	1	0	0
5	12	0	7	2	2	1	0	0	0
6	12	1	9	2	0	0	0	0	0
7	9	1	2	5	0	0	0	0	1
8	15	1	12	2	0	0	0	0	0
9	5	1	3	1	0	0	0	0	0
10	3	0	2	1	0	0	0	0	0
11	8	1	5	2	0	0	0	0	0
12	2	0	2	0	0	0	0	0	0
13	3	0	3	0	0	0	0	0	0
14	1	0	1	0	0	0	0	0	0
15	1	0	1	0	0	0	0	0	0
17	1	0	1	0	0	0	0	0	0
18	2	0	2	0	0	0	0	0	0
20	1	0	0	1	0	0	0	0	0
23	1	0	0	0	0	0	1	0	0
31	1	0	1	0	0	0	0	0	0
Total # of cells	**518**	**167**	**114**	**51**	**85**	**34**	**48**	**10**	**9**

Supplementary Table S11. : Experimental distributions of mRNA numbers for *CLN2* per cell in each cell cycle phase for 30 min under osmotic stress.

CLN2 30 min									
# RNA/cell	# of cells	early G1	late G1	S	G2	P/M	Ana	T/C	2spc / noBud
0	221	134	15	6	9	7	29	18	3
1	64	20	5	4	15	6	5	5	4
2	21	6	4	1	7	1	1	1	0
3	24	7	1	4	8	2	2	0	0
4	12	4	5	0	3	0	0	0	0
5	13	3	3	0	4	1	1	1	0
6	15	4	3	0	5	1	0	0	2
7	13	2	1	1	7	0	1	0	1
8	7	0	4	1	1	0	0	0	1
9	10	2	4	2	2	0	0	0	0
10	7	1	1	2	3	0	0	0	0
11	8	2	3	0	3	0	0	0	0
12	7	1	2	0	2	0	0	0	2
13	6	0	3	0	1	0	0	0	2
14	1	0	0	0	1	0	0	0	0
15	2	0	1	0	0	0	0	0	1
16	7	2	3	1	1	0	0	0	0
17	6	0	3	0	3	0	0	0	0
18	6	0	1	0	5	0	0	0	0
19	5	1	1	0	3	0	0	0	0
20	3	0	1	1	0	0	1	0	0
21	3	1	0	1	1	0	0	0	0
22	3	0	2	1	0	0	0	0	0
23	6	0	4	1	1	0	0	0	0
24	4	0	3	0	1	0	0	0	0
25	1	0	1	0	0	0	0	0	0
27	1	0	0	0	1	0	0	0	0
28	5	1	3	0	1	0	0	0	0
29	2	0	1	0	1	0	0	0	0
30	1	0	1	0	0	0	0	0	0
31	1	0	1	0	0	0	0	0	0
32	2	0	2	0	0	0	0	0	0
34	4	0	2	2	0	0	0	0	0
35	2	0	2	0	0	0	0	0	0
37	2	0	2	0	0	0	0	0	0
38	1	0	0	1	0	0	0	0	0
40	2	0	1	0	0	0	0	0	1
41	1	0	1	0	0	0	0	0	0
46	1	0	1	0	0	0	0	0	0
47	1	0	0	0	0	0	0	0	1
49	1	0	0	1	0	0	0	0	0
Total # of cells	**502**	**191**	**91**	**30**	**89**	**18**	**40**	**25**	**18**

Supplementary Table S12. : Experimental distributions of mRNA numbers for *CLN2* per cell in each cell cycle phase for 45 min under osmotic stress.

CLN2 45 min									
# RNA/cell	# of cells	early G1	late G1	S	G2	P/M	Ana	T/C	2spc / noBud
0	246	112	21	11	47	12	24	17	2
1	74	15	12	4	21	4	10	5	3
2	56	12	9	6	23	2	1	0	3
3	32	7	6	2	13	1	2	1	0
4	26	5	7	3	7	0	0	2	2
5	20	3	8	4	3	1	1	0	0
6	9	2	0	1	4	0	0	0	2
7	6	2	2	0	2	0	0	0	0
8	9	3	4	1	1	0	0	0	0
9	11	0	9	1	1	0	0	0	0
10	6	1	4	1	0	0	0	0	0
11	6	2	3	1	0	0	0	0	0
12	10	2	4	2	2	0	0	0	0
13	7	1	5	1	0	0	0	0	0
14	10	2	5	2	1	0	0	0	0
15	12	0	7	2	2	0	1	0	0
16	12	0	5	3	3	0	0	0	1
17	3	0	2	1	0	0	0	0	0
18	9	0	9	0	0	0	0	0	0
19	7	0	5	1	1	0	0	0	0
20	9	0	7	2	0	0	0	0	0
21	6	0	4	0	2	0	0	0	0
22	6	1	3	2	0	0	0	0	0
24	5	1	3	1	0	0	0	0	0
25	8	0	5	1	1	1	0	0	0
26	3	0	3	0	0	0	0	0	0
27	7	0	6	0	0	0	0	0	1
28	5	0	4	0	1	0	0	0	0
29	12	2	9	1	0	0	0	0	0
30	3	0	2	1	0	0	0	0	0
31	1	0	1	0	0	0	0	0	0
32	5	0	4	1	0	0	0	0	0
34	2	0	2	0	0	0	0	0	0
35	3	0	2	1	0	0	0	0	0
36	4	0	4	0	0	0	0	0	0
37	3	0	2	1	0	0	0	0	0
38	3	0	2	1	0	0	0	0	0
39	3	0	3	0	0	0	0	0	0
40	3	0	2	1	0	0	0	0	0
41	6	0	6	0	0	0	0	0	0
42	1	0	1	0	0	0	0	0	0
43	6	0	4	2	0	0	0	0	0
44	2	0	2	0	0	0	0	0	0
45	1	0	1	0	0	0	0	0	0
48	2	0	1	1	0	0	0	0	0
49	1	0	1	0	0	0	0	0	0
52	2	0	2	0	0	0	0	0	0
53	1	0	1	0	0	0	0	0	0
55	0	0	0	0	0	0	0	0	0
57	1	0	1	0	0	0	0	0	0
64	1	0	1	0	0	0	0	0	0
66	1	0	1	0	0	0	0	0	0
69	1	0	1	0	0	0	0	0	0
71	1	0	0	1	0	0	0	0	0
96	1	0	1	0	0	0	0	0	0
Total # of cells	**690**	**173**	**219**	**64**	**135**	**21**	**39**	**25**	**14**

Supplementary Table S13. : Experimental distributions of mRNA numbers for *CLN2* per cell in each cell cycle phase for 60 min under osmotic stress.

CLN2 60 min									
# RNA/cell	# of cells	early G1	late G1	S	G2	P/M	Ana	T/C	2spc / noBud
0	300	123	8	23	66	31	34	14	1
1	94	26	6	10	30	8	5	6	3
2	68	11	8	16	23	6	1	1	2
3	32	4	5	10	7	3	1	1	1
4	21	4	7	7	3	0	0	0	0
5	19	4	9	5	1	0	0	0	0
6	9	1	3	4	1	0	0	0	0
7	16	2	13	0	1	0	0	0	0
8	8	1	5	1	1	0	0	0	0
9	15	4	9	2	0	0	0	0	0
10	19	2	11	4	1	0	0	1	0
11	10	0	6	2	2	0	0	0	0
12	12	2	9	0	0	0	0	1	0
13	11	3	7	0	0	0	0	1	0
14	12	1	6	5	0	0	0	0	0
15	8	2	3	3	0	0	0	0	0
16	14	1	5	4	4	0	0	0	0
17	6	1	5	0	0	0	0	0	0
18	3	1	2	0	0	0	0	0	0
19	1	0	1	0	0	0	0	0	0
20	8	1	6	1	0	0	0	0	0
21	9	0	8	1	0	0	0	0	0
22	4	0	4	0	0	0	0	0	0
23	8	0	8	0	0	0	0	0	0
24	4	0	3	1	0	0	0	0	0
25	5	0	4	1	0	0	0	0	0
26	4	0	3	1	0	0	0	0	0
27	3	0	3	0	0	0	0	0	0
28	2	0	2	0	0	0	0	0	0
29	5	1	3	1	0	0	0	0	0
30	5	0	5	0	0	0	0	0	0
31	6	0	5	1	0	0	0	0	0
32	3	0	3	0	0	0	0	0	0
33	5	0	5	0	0	0	0	0	0
34	2	0	2	0	0	0	0	0	0
36	6	0	6	0	0	0	0	0	0
37	2	0	2	0	0	0	0	0	0
38	4	0	4	0	0	0	0	0	0
39	2	0	2	0	0	0	0	0	0
40	3	0	3	0	0	0	0	0	0
41	2	1	0	1	0	0	0	0	0
42	3	0	3	0	0	0	0	0	0
43	3	0	3	0	0	0	0	0	0
45	4	0	4	0	0	0	0	0	0
46	1	0	1	0	0	0	0	0	0
47	2	0	1	0	0	0	1	0	0
48	1	1	0	0	0	0	0	0	0
49	1	0	1	0	0	0	0	0	0
51	2	0	2	0	0	0	0	0	0
52	1	0	0	1	0	0	0	0	0
53	1	0	1	0	0	0	0	0	0
54	1	1	0	0	0	0	0	0	0
55	1	0	1	0	0	0	0	0	0
56	2	0	2	0	0	0	0	0	0
60	1	0	1	0	0	0	0	0	0
65	1	0	1	0	0	0	0	0	0
70	1	0	1	0	0	0	0	0	0
71	1	0	1	0	0	0	0	0	0
83	1	0	1	0	0	0	0	0	0
Total # of cells	**798**	**198**	**233**	**105**	**140**	**48**	**42**	**25**	**7**

Supplementary Table S14. : Experimental distributions of mRNA numbers for *CLN2* per cell in each cell cycle phase for 90 min under osmotic stress.

CLN2 90 min									
# RNA/cell	# of cells	early G1	late G1	S	G2	P/M	Ana	T/C	2spc / noBud
0	320	79	18	35	75	56	47	6	4
1	97	14	4	21	36	12	8	2	0
2	61	12	6	11	19	4	5	3	1
3	24	3	7	6	8	0	0	0	0
4	15	4	3	6	0	0	1	1	0
5	16	4	4	3	2	0	1	2	0
6	11	0	2	5	2	0	1	0	1
7	8	0	2	5	0	0	0	1	0
8	6	1	2	3	0	0	0	0	0
9	3	0	3	0	0	0	0	0	0
10	7	2	2	0	0	0	1	2	0
11	2	0	1	1	0	0	0	0	0
12	6	1	2	3	0	0	0	0	0
13	5	0	3	2	0	0	0	0	0
14	1	1	0	0	0	0	0	0	0
15	6	0	4	2	0	0	0	0	0
16	1	0	1	0	0	0	0	0	0
17	3	0	2	1	0	0	0	0	0
18	5	1	3	1	0	0	0	0	0
19	1	0	1	0	0	0	0	0	0
20	4	0	4	0	0	0	0	0	0
21	3	0	2	1	0	0	0	0	0
22	4	0	3	0	0	0	0	1	0
23	2	0	2	0	0	0	0	0	0
24	1	0	1	0	0	0	0	0	0
25	2	0	1	1	0	0	0	0	0
26	3	0	3	0	0	0	0	0	0
27	6	0	6	0	0	0	0	0	0
28	2	0	2	0	0	0	0	0	0
29	1	0	1	0	0	0	0	0	0
30	5	1	4	0	0	0	0	0	0
31	5	0	5	0	0	0	0	0	0
32	3	0	3	0	0	0	0	0	0
33	3	0	2	1	0	0	0	0	0
34	5	0	3	2	0	0	0	0	0
35	2	0	2	0	0	0	0	0	0
36	3	0	3	0	0	0	0	0	0
38	2	0	2	0	0	0	0	0	0
39	3	0	3	0	0	0	0	0	0
40	2	0	2	0	0	0	0	0	0
41	2	0	2	0	0	0	0	0	0
43	1	0	1	0	0	0	0	0	0
44	2	0	2	0	0	0	0	0	0
45	1	0	0	1	0	0	0	0	0
46	6	0	6	0	0	0	0	0	0
48	2	0	2	0	0	0	0	0	0
49	1	0	1	0	0	0	0	0	0
51	1	0	1	0	0	0	0	0	0
52	1	0	1	0	0	0	0	0	0
53	1	0	1	0	0	0	0	0	0
56	2	0	2	0	0	0	0	0	0
59	1	0	1	0	0	0	0	0	0
61	2	0	1	1	0	0	0	0	0
64	2	0	2	0	0	0	0	0	0
Total # of cells	**684**	**123**	**147**	**112**	**142**	**72**	**64**	**18**	**6**

Supplementary Table S15. : Experimental distributions of mRNA numbers for *CLB5* per cell in each cell cycle phase under normal growth conditions (equivalent to 0 min under osmotic stress or no stress).

CLB5 no stress									
# RNA/cell	# of cells	early G1	late G1	S	G2	P/M	Ana	T/C	2spc / noBud
0	353	69	35	55	94	43	45	6	6
1	229	46	47	47	31	19	26	10	3
2	108	27	27	27	12	8	5	1	1
3	67	10	25	22	5	0	3	2	0
4	58	4	32	12	3	0	4	3	0
5	44	4	27	5	0	0	5	2	1
6	30	2	22	6	0	0	0	0	0
7	22	4	15	1	0	0	0	2	0
8	14	2	9	1	0	0	0	2	0
9	8	0	6	1	0	1	0	0	0
10	4	0	4	0	0	0	0	0	0
11	2	0	1	0	0	0	0	1	0
12	3	0	3	0	0	0	0	0	0
13	1	0	0	1	0	0	0	0	0
14	3	0	2	1	0	0	0	0	0
15	2	0	2	0	0	0	0	0	0
16	1	0	1	0	0	0	0	0	0
17	1	0	1	0	0	0	0	0	0
Total # of cells	**950**	**168**	**259**	**179**	**145**	**71**	**88**	**29**	**11**

Supplementary Table S16. : Experimental distributions of mRNA numbers for *CLB5* per cell in each cell cycle phase for 15 min under osmotic stress.

CLB5 15 min									
# RNA/cell	# of cells	early G1	late G1	S	G2	P/M	Ana	T/C	2spc / noBud
0	360	135	57	29	67	35	22	9	6
1	145	43	39	11	25	4	14	5	4
2	47	7	17	3	10	2	7	0	1
3	18	2	10	1	4	0	1	0	0
4	1	0	1	0	0	0	0	0	0
5	1	0	1	0	0	0	0	0	0
6	1	0	1	0	0	0	0	0	0
Total # of cells	**573**	**187**	**126**	**44**	**106**	**41**	**44**	**14**	**11**

Supplementary Table S17. : Experimental distributions of mRNA numbers for *CLB5* per cell in each cell cycle phase for 30 min under osmotic stress.

CLB5 30 min									
# RNA/cell	# of cells	early G1	late G1	S	G2	P/M	Ana	T/C	2spc / noBud
0	257	119	20	14	52	18	14	9	11
1	107	38	22	3	23	6	8	4	3
2	53	18	19	4	6	1	3	0	2
3	32	8	12	2	3	0	1	2	4
4	12	0	5	2	4	0	0	0	1
5	8	2	4	1	1	0	0	0	0
6	7	0	4	1	1	0	0	1	0
7	3	1	1	0	1	0	0	0	0
8	3	0	3	0	0	0	0	0	0
9	2	0	2	0	0	0	0	0	0
10	0	0	0	0	0	0	0	0	0
11	1	0	1	0	0	0	0	0	0
13	1	0	1	0	0	0	0	0	0
Total # of cells	**486**	**186**	**94**	**27**	**91**	**25**	**26**	**16**	**21**

Supplementary Table S18. : Experimental distributions of mRNA numbers for *CLB5* per cell in each cell cycle phase for 45 min under osmotic stress.

CLB5 45 min									
# RNA/cell	# of cells	early G1	late G1	S	G2	P/M	Ana	T/C	2spc / noBud
0	339	137	57	27	69	18	11	11	9
1	153	45	38	19	28	5	9	7	2
2	85	18	28	16	13	0	3	5	2
3	48	7	29	6	0	0	1	3	2
4	31	5	15	6	4	0	0	0	1
5	23	2	16	3	0	0	1	0	1
6	10	2	7	1	0	0	0	0	0
7	15	0	10	4	0	0	1	0	0
8	10	1	6	1	1	0	0	1	0
9	4	0	2	2	0	0	0	0	0
10	4	0	3	1	0	0	0	0	0
12	1	0	0	1	0	0	0	0	0
13	1	0	1	0	0	0	0	0	0
Total # of cells	**724**	**217**	**212**	**87**	**115**	**23**	**26**	**27**	**17**

Supplementary Table S19. : Experimental distributions of mRNA numbers for *CLB5* per cell in each cell cycle phase for 60 min under osmotic stress.

CLB5 60 min									
# RNA/cell	# of cells	early G1	late G1	S	G2	P/M	Ana	T/C	2spc / noBud
0	425	143	52	54	93	43	30	4	6
1	150	42	44	26	21	1	8	5	3
2	66	9	37	13	4	0	1	2	0
3	39	4	21	9	2	0	2	1	0
4	20	1	11	5	2	1	0	0	0
5	13	2	7	3	0	0	0	1	0
6	10	2	6	2	0	0	0	0	0
7	13	1	9	2	0	0	1	0	0
8	5	0	4	1	0	0	0	0	0
9	2	0	2	0	0	0	0	0	0
10	5	0	2	2	0	0	0	1	0
11	4	0	4	0	0	0	0	0	0
12	2	0	2	0	0	0	0	0	0
15	1	0	1	0	0	0	0	0	0
Total # of cells	**755**	**204**	**202**	**117**	**122**	**45**	**42**	**14**	**9**

Supplementary Table S20. : Experimental distributions of mRNA numbers for *CLB5* per cell in each cell cycle phase for 90 min under osmotic stress.

CLB5 90 min									
# RNA/cell	# of cells	early G1	late G1	S	G2	P/M	Ana	T/C	2spc / noBud
0	308	76	20	36	80	51	34	5	6
1	156	30	25	32	35	8	18	6	2
2	73	9	18	19	21	1	4	1	0
3	40	7	12	11	5	1	1	3	0
4	21	1	12	5	1	1	1	0	0
5	11	0	9	0	1	0	0	1	0
6	11	0	7	2	1	0	0	1	0
7	9	0	7	2	0	0	0	0	0
8	4	1	2	1	0	0	0	0	0
9	1	0	1	0	0	0	0	0	0
10	1	0	1	0	0	0	0	0	0
11	6	0	3	3	0	0	0	0	0
12	1	0	1	0	0	0	0	0	0
13	2	0	2	0	0	0	0	0	0
14	3	0	2	1	0	0	0	0	0
Total # of cells	**647**	**124**	**122**	**112**	**144**	**62**	**58**	**17**	**8**

Appendix 4: Supplementary Figures

- Supplementary Figure S 3 and Supplementary Figure S 4 are linked to the RESULTS I.
- Supplementary Figure S 5 to Supplementary Figure S 23 are linked to RESULTS II.

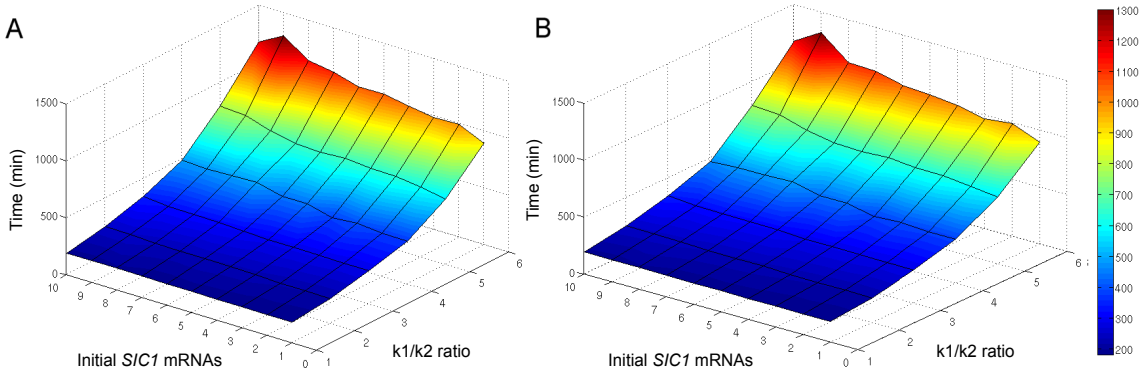

Supplementary Figure S 3. Relation between the time of peaks for Q (A) and CV2 (B), the initial *SIC1* mRNA molecule number and different k1/k2 ratios of *SIC1* mRNA shown with a three-dimensional representation.

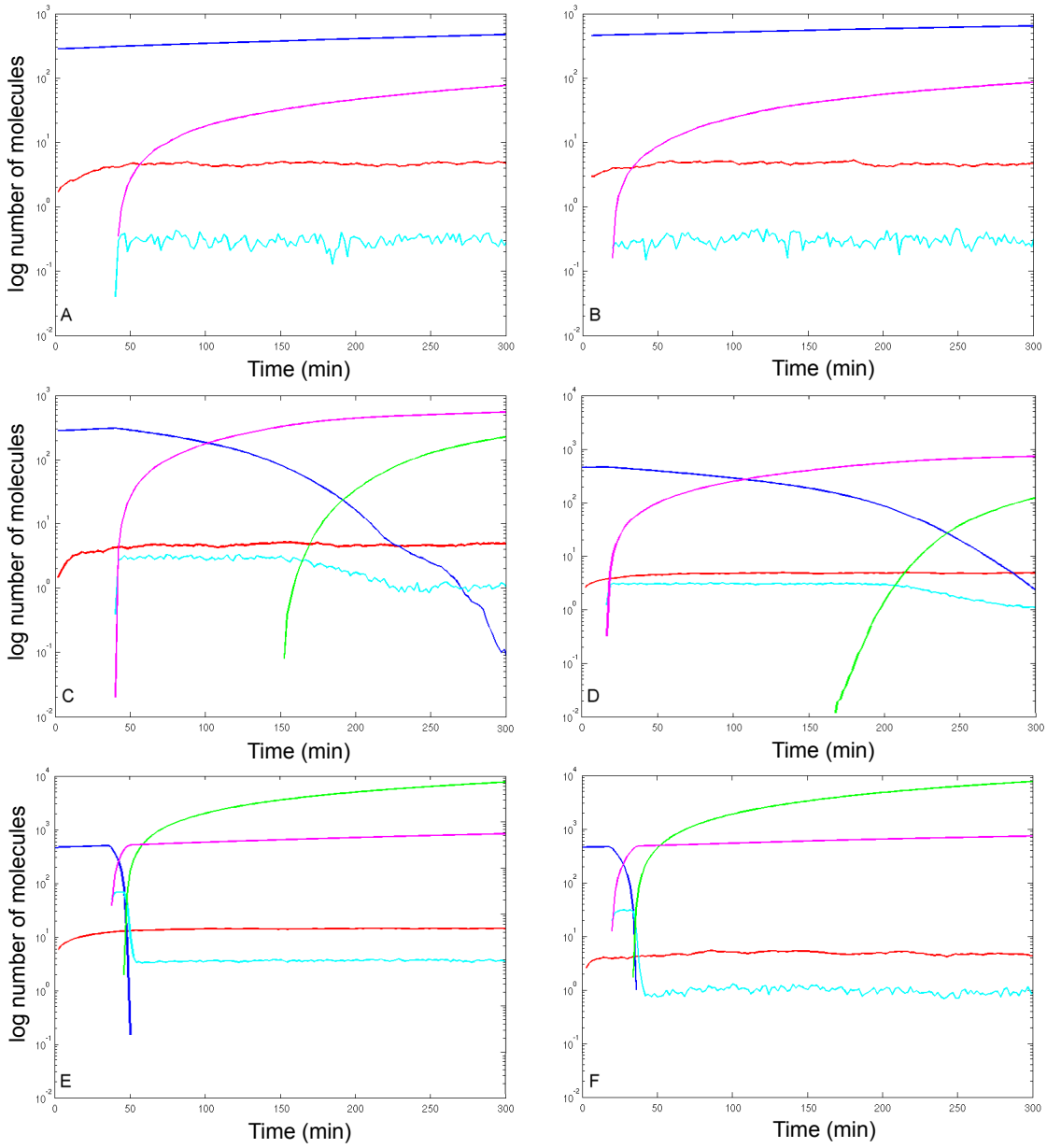

Supplementary Figure S 4. Semi-log plots of data shown in Figure 30**.**

Simulated dynamics of a daughter cell (left column) and a mother cell (right column) for different Clb5,6 production rate constants: *k*6a (A, B), *k*6b (C, D) and *k*6c (E, F). Sic1 (blue), cytoplasmic Clb5,6 (green), Sic1-Clb5 complex (light blue), nuclear Clb5,6 (pink) and *SIC1* mRNA (red) are shown.

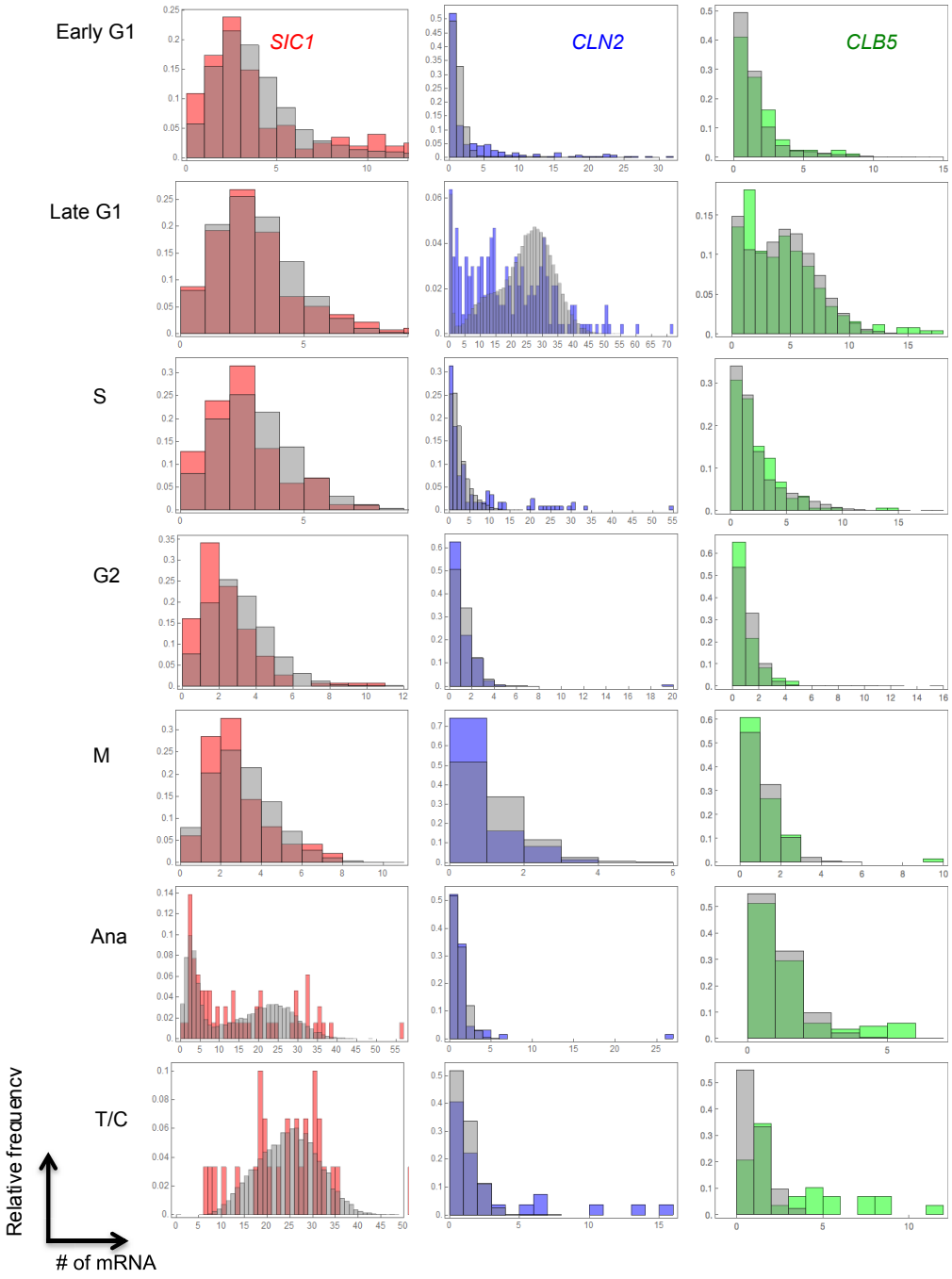

Supplementary Figure S 5 Distributions of *SIC1*, *CLN2* and *CLB5* mRNA in each cell cycle phase.

Data for *SIC1*, *CLN2* and *CLB5* are shown in left, middle and right columns, respectively. Histograms of relative frequency of mRNA numbers were obtained experimentally from RNA-FISH assays (colors) and from computational simulations (grey). Numerical values for *SIC1*, *CLN2* and *CLB5* are shown in Supplementary Table S3, Supplementary Table S9 and Supplementary Table S15, respectively.

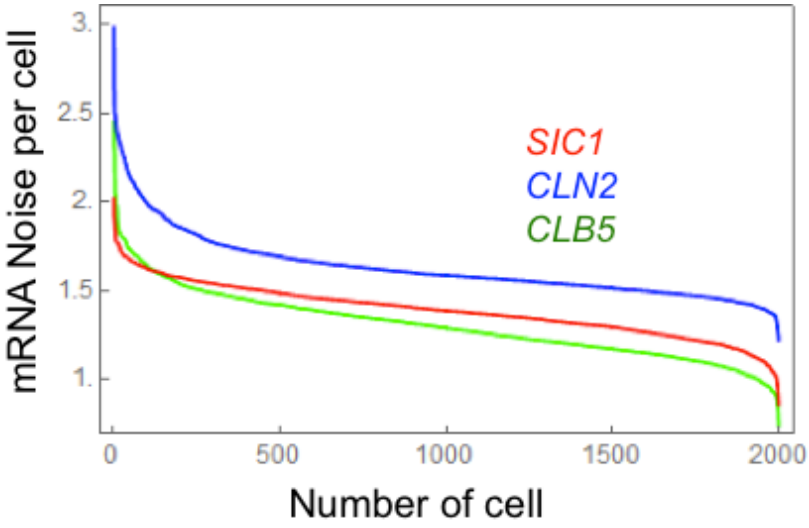

Supplementary Figure S 6. Sorted noise of all 2000 single cells measured for each cell individually over one cell cycle period for *SIC1* in red, *CLN2* in blue, *CLB5* in green.

Simulations were performed with the Gillespie algorithm using the equations and parameter values provided in Table 17.

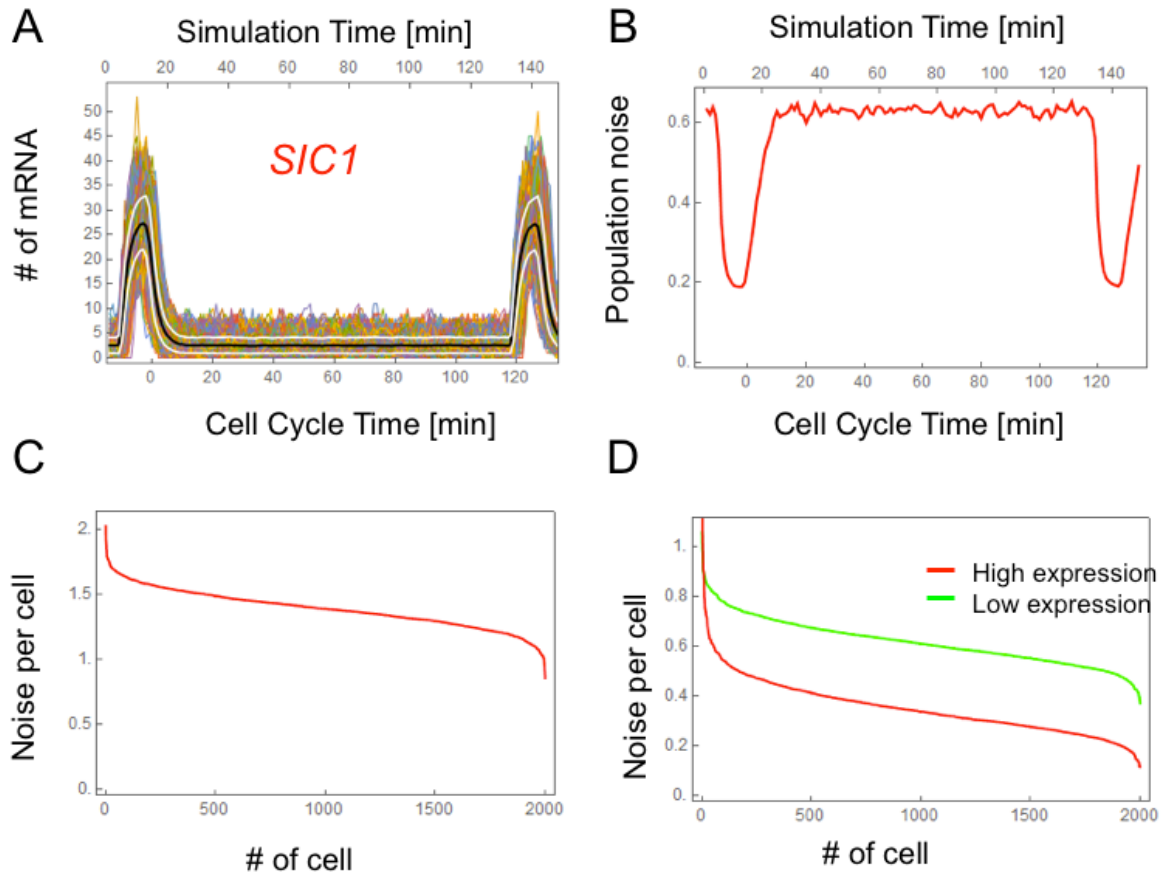

Supplementary Figure S 7. Characterization of *SIC1* mRNA simulated dynamics.

(A) Time course of *SIC1*. Shown are all individual traces for 2000 simulated cells as well as their mean (black curve) and their mean ± SD (white curves). Since simulations start in anaphase and last until T/C phase of the next cell cycle, the simulation time (upper axis) is shifted by 15 min compared to the cell cycle time (lower axis). (B) Time courses of noise measured over the whole population, i.e. standard deviation divided by mean of all cells at each time point. (C) Sorted noise of all single cells measured for each cell individually over one cell cycle period. (D) Sorted noise of all single cells measured for each cell individually over one cell cycle period in high (red) and low expression (green) periods.

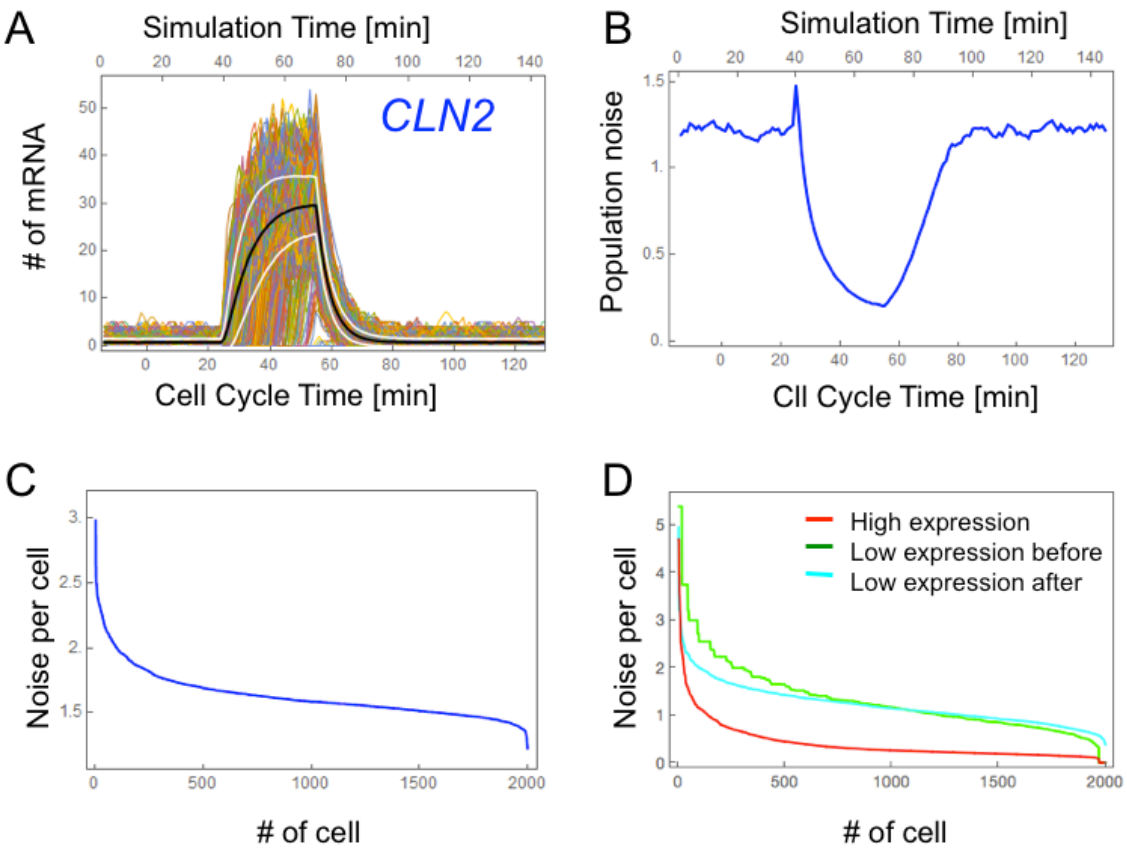

Supplementary Figure S 8. Characterization of *CLN2* mRNA simulated dynamics.

(A) Time course of *CLN2*. Shown are all individual traces for 2000 simulated cells as well as their mean (black curve) and their mean ± SD (white curves). Since simulations start in anaphase and last until T/C phase of the next cell cycle, the simulation time (upper axis) is shifted by 15 min compared to the cell cycle timing (lower axis). (B) Time courses of noise measured over the whole population, i.e. standard deviation divided by mean of all cells at each time point. (C) Sorted noise of all single cells measured for each cell individually over one cell cycle period. (D) Sorted noise of all single cells measured for each cell individually over one cell cycle period in high (red), low expression before high expression (green) and low expression after high expression (bright blue) periods.

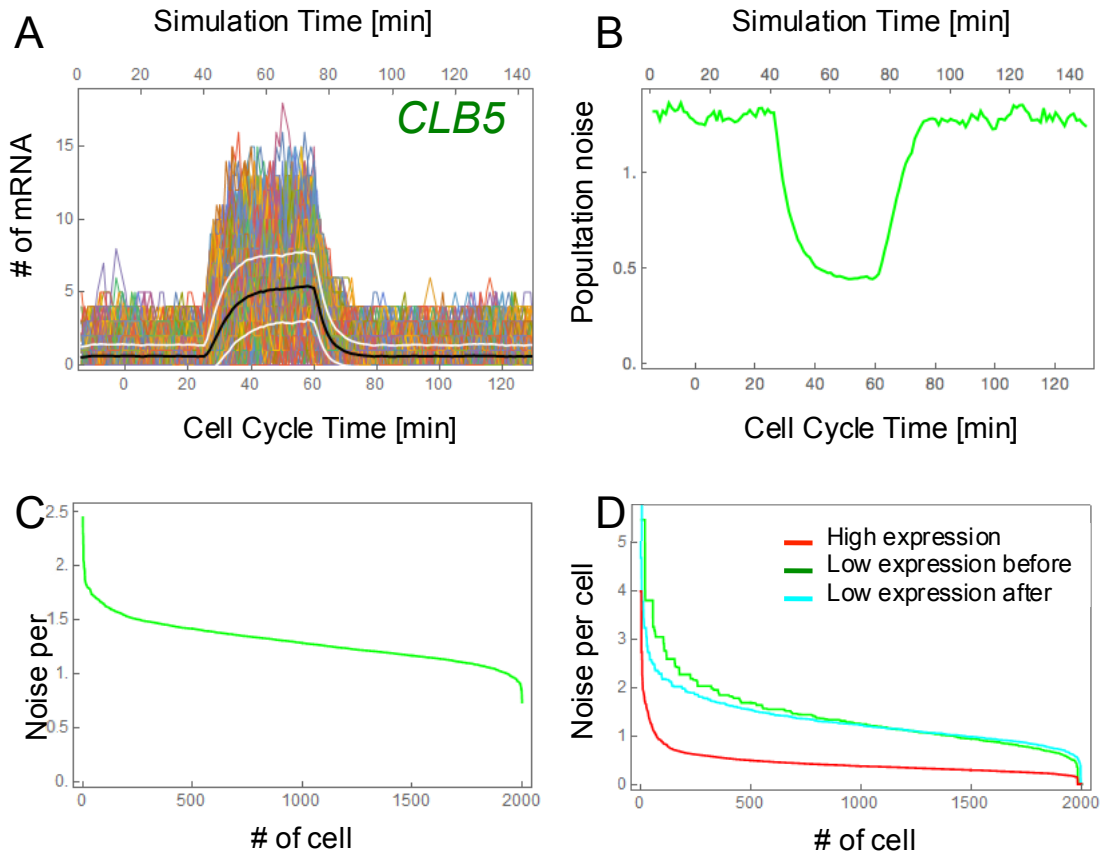

Supplementary Figure S 9. Characterization of *CLB5* mRNA simulated dynamics.
(A) Time course of *CLB5*. Shown are all individual traces for 2000 simulated cells as well as their mean (black curve) and their mean ± SD (white curves). Since simulations start in anaphase and last until T/C phase of the next cell cycle, the simulation time (upper axis) is shifted by 15 min compared to the cell cycle timing (lower axis). (B) Time courses of noise measured over the whole population, i.e. standard deviation divided by mean of all cells at each time point. (C) Sorted noise of all single cells measured for each cell individually over one cell cycle period. (D) Sorted noise of all single cells measured for each cell individually over one cell cycle period in high (red) and low expression before high expression (green) and low expression after high expression (bright blue) periods.

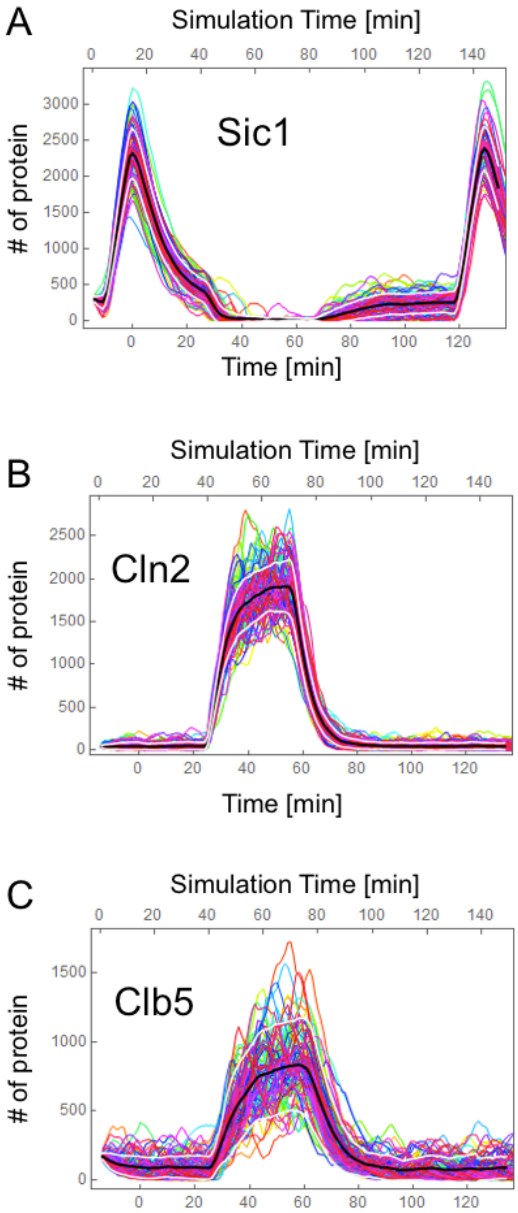

Supplementary Figure S 10. Time course of the protein for Sic1, Cln2 and Clb5.
Data for Sic1, Cln2 and Clb5 are shown in A, B and C, respectively. Trajectories are all individual traces for 2000 simulated cells as well as their mean (black curve) and their mean ± SD (white curves).

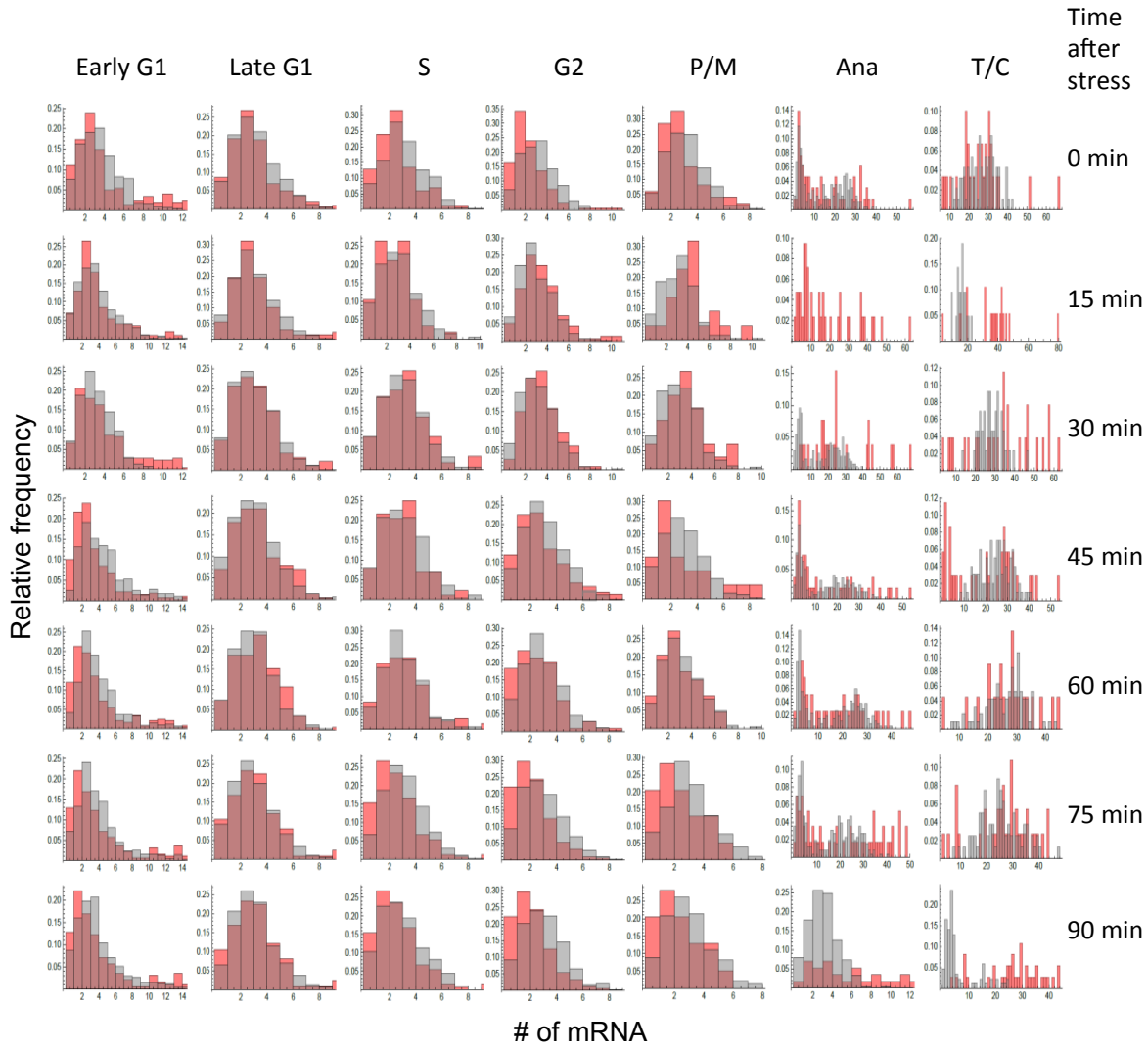

Supplementary Figure S 11. Distributions of *SIC1* mRNA in each cell cycle phase under osmotic stress. Histograms of relative frequency of mRNA numbers were experimentally obtained from RNA-FISH assays (red) and from computational simulations (grey). Osmotic stress was applied for 0 (no stress), 15, 30, 45, 60 and 90 min. Numerical values in Supplementary Table S3 in Appendix.

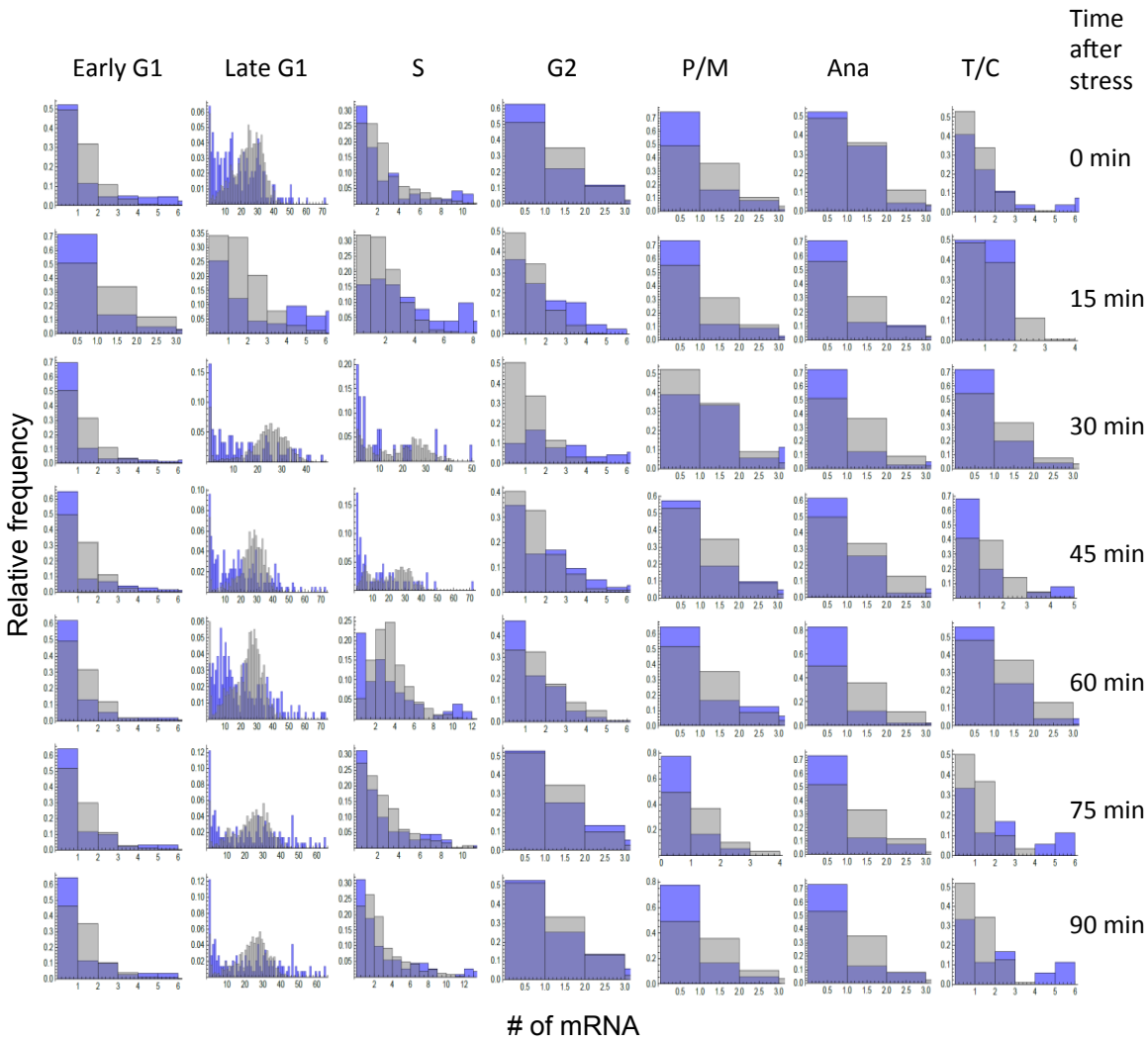

Supplementary Figure S 12. Distributions of *CLN2* mRNA in each cell cycle phase under osmotic stress. Histograms of relative frequency of mRNA numbers were experimentally obtained from RNA-FISH assays (red) and from computational simulations (grey). Osmotic stress was applied for 0 (no stress), 15, 30, 45, 60 and 90 min. Numerical values in Supplementary Table S9 in Appendix.

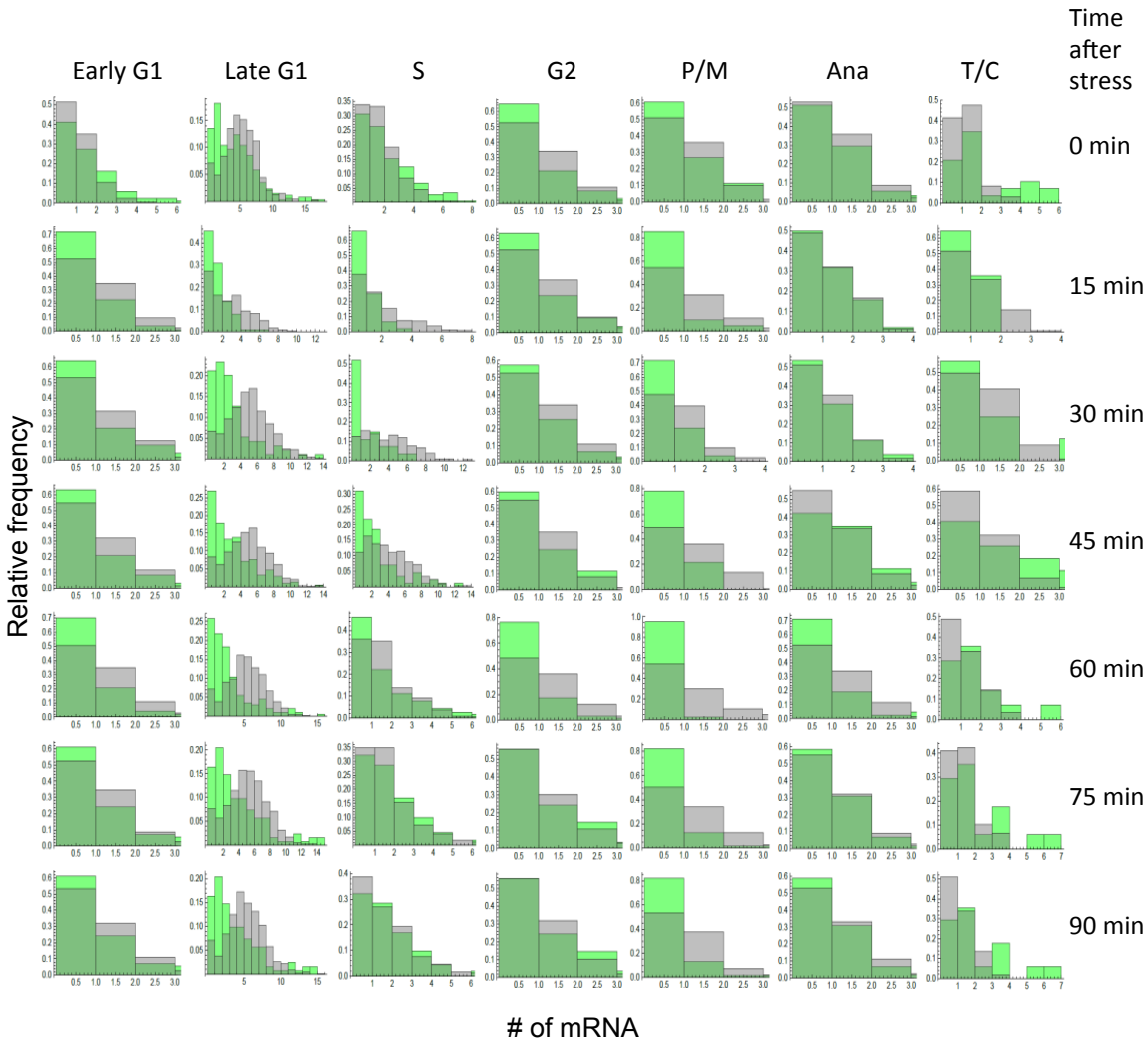

Supplementary Figure S 13. Distributions of *CLB5* mRNA in each cell cycle phase under osmotic stress. Histograms of relative frequency of mRNA numbers were experimentally obtained from RNA-FISH assays (red) and from computational simulations (grey). Osmotic stress was applied for 0 (no stress), 15, 30, 45, 60 and 90 min. Numerical values in Supplementary Table S15 in Appendix.

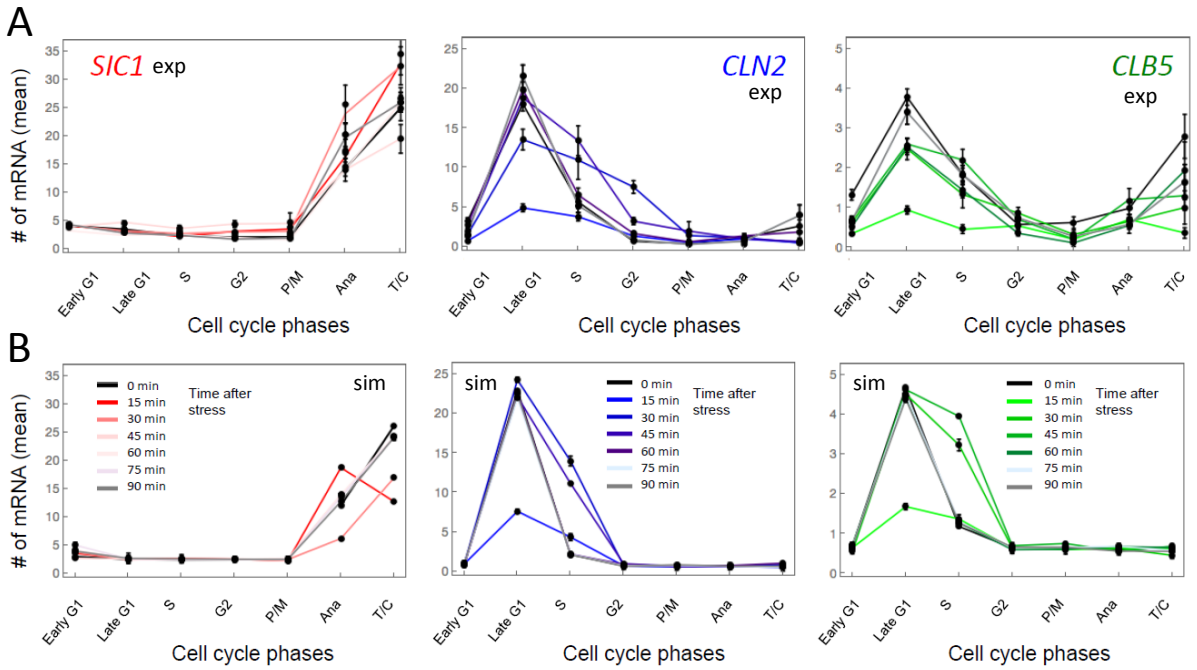

Supplementary Figure S 14. Medium osmotic stress affects cell cycle progression and transcription.

(A) Changes of mRNA abundances for *SIC1, CLN2* and *CLB5* during the cell cycle upon medium osmotic stress. Data shown are mean ± SEM. Darkest curves correspond to the shortest incubations in hyperosmotic medium. Exact numbers of analyzed cells are presented in Supplementary Table S1 and numerical values in Supplementary Table S2 in Appendix. (B) Simulated changes of timing of mRNA abundances for *SIC1, CLB5* and *CLN2* during the cell cycle progression upon medium osmotic stress. Data shown are mean ± SEM. In (A) and (B) 0min are equivalent to no stress conditions (Figure 35 and Figure 37). (A) is equivalent to Figure 43C.

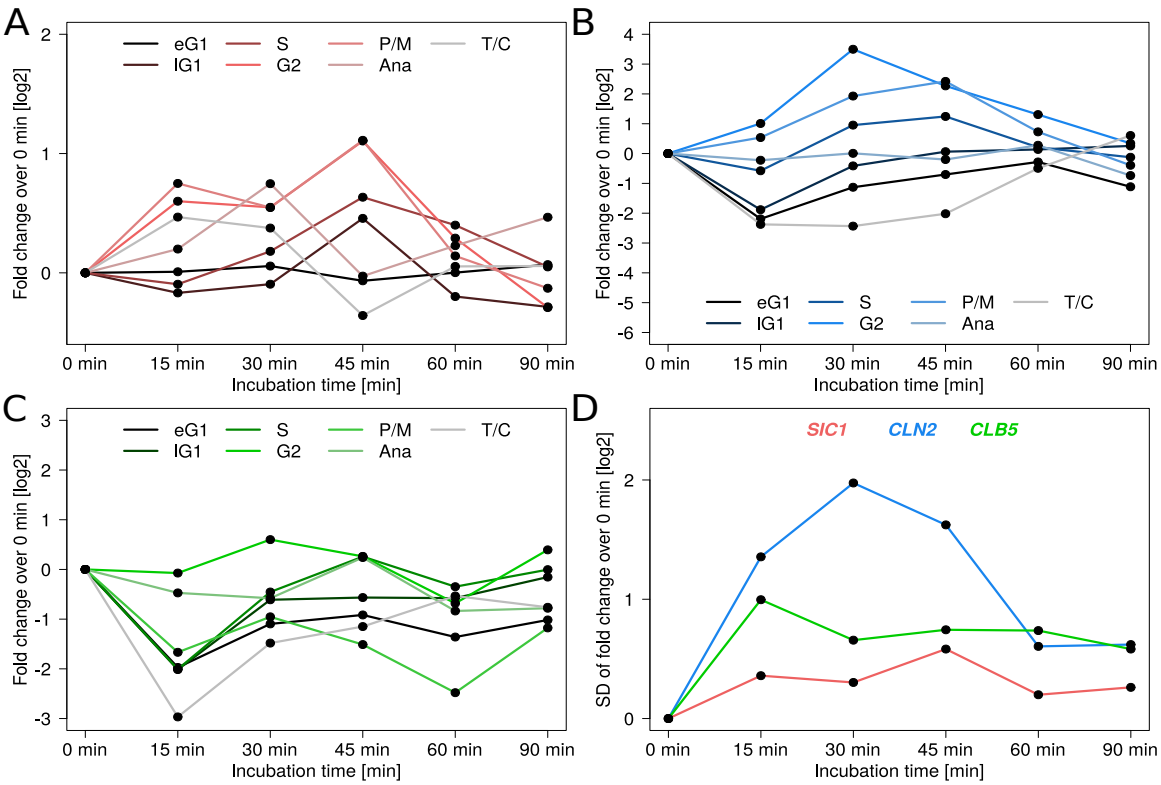

Supplementary Figure S 15. Osmotic stress response presented as fold changes over no stress condition.
(A), (B) and (C) show fold changes over 0 minutes osmotic stress (no stress condition) for *SIC1* (red), *CLN2* (blue) and *CLB5* (green), respectively. Fold changes are expressed in $\log_2$ and calculated from the mean values per cell cycle phase. Fold changes are plotted for each stress time (0, 15, 30, 45, 60 and 90 minutes) and each cell cycle phase, whereby cell cycle phases are given as colored lines. (D) Standard deviation of fold changes per stress time and gene are depicted. Lines between data points in (A)-(D) are for visualization only.

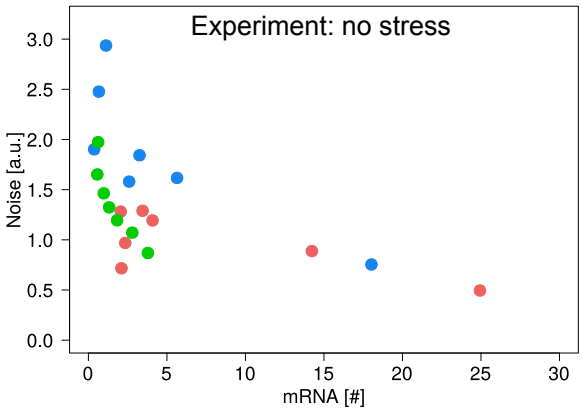

Supplementary Figure S 16. Relationship between expression level and noise.
The mean value of noise is plotted against the mean number of mRNAs for *SIC1*, *CLN2* and *CLB5* in each cell cycle phase. Correlation coefficients for the experimental data under no stress condition are r_{SIC1} = -0.71, r_{CLN2} = -0.80, r_{CLB5} = -0.90 and r_{all} = -0.56, where r_{all} correspond to the correlation coefficient over all genes. Correlation coefficients indicate strong correlations, means lower mRNA levels have higher noise levels. *SIC1* and *CLN2* show significantly different noise levels in the experiment ($p_{SIC1\text{-}CLN2}$ = 0.01, $p_{CLN2\text{-}CLB5}$ = 0.16, $p_{CLB5\text{-}SIC1}$ = 0.07). p values are calculated from with the Wilcoxon-Mann-Whitney test.

Appendix 5: Revised stochastic model for *SIC1*, *CLN2* and *CLB5* transcription under normal growth conditions and under osmotic stress.

This revised stochastic model focuses on transcription regulation only and employs the static, time-resolved, single cell RNA-FISH data of RESULTS II to stochastically modeled transcription and degradation for each species. The model was published in (Amoussouvi et al., 2018). In the model, signals S_1 to S_3 indicate the up-regulation of transcription for *SIC1* (S_1), *CLN2* (S_2), and *CLB5* (S_3) (Supplementary Figure S 17). We assumed equal degradation rate constants ($\boldsymbol{p_i}$) and different transcription ($\boldsymbol{k_{ih}}$ or $\boldsymbol{k_{il}}$) rate constants in periods of either high (*h*) or low (*l*) expression, respectively. Periods of high expression are defined by transcription start time ($\boldsymbol{t_{S_{i,0}}}$) and transcription end time ($\boldsymbol{t_{S_{i,e}}}$). We assumed a second period of high transcription for *CLN2* and *CLB5*, labeled as $\boldsymbol{first}$ and $\boldsymbol{sec}$. The duration of one cell cycle is set to $t = 129\,\mathrm{min}$. All reactions and parameters values are shown in Supplementary Table S 21.

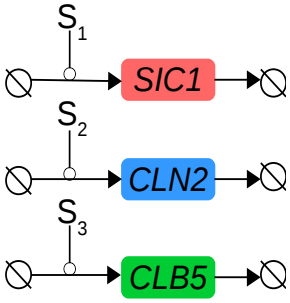

Supplementary Figure S 17. Sketch of the stochastic model for *SIC1*, *CLN2* and *CLB5* transcription and degradation.
S_1, S_2, and S_3 denote signals for transcription up-regulation in the model.

The model extracted the relative promoter activities of 7.7%, 0.4% and 15% for *SIC1*, *CLN2* and *CLB5*, respectively, outside the main transcription periods (compared to 8.8%, 2.2% or 7.7% for *SIC1*, *CLN2* and *CLB5*, respectively, with the model with only one single high phase of transcription in RESULTS II). According to the Akaike criterion (AIC), the fits improved when allowing for two periods of high promoter activity for *CLN2* and *CLB5*. Comparison of the experimental and simulated distributions of mRNA number per cell for an asynchronous population (Supplementary Figure S 18A), per cell cycle phase (Supplementary Figure S 18B) and time-courses of mRNA and related noise level (Supplementary Figure S 19A and C) and relationship between mRNA expression level and noise (Supplementary Figure S 23AB) for optimal growth conditions are shown below.

To simulate osmotic stress response of G1/S main regulators, we assumed that high-level transcription of *CLN2* and *CLB5* (mainly during late G1) was interrupted during the period of osmotic adaptation and resumed afterwards. Depending on the time point when osmotic stress hits the cell, the inhibitory effect on *CLN2* and *CLB5* transcription as well as the delay of following cell cycle phases is different (for case-by-case analysis see Supplementary Figure S 20).

The fitting by the revised model extracted of the mRNA data under osmotic stress provided new periods of transcription inhibition $t_{d,CLN2}$=28 min for *CLN2* and $t_{d,CLB5}$=12 min for *CLB5* (values with the model presented in this chapter: $t_{d,CLN2}$ = 17 min for *CLN2* and $t_{d,CLB5}$ = 11 min for *CLB5*). These new values reinforce the hypothesis that *CLN2* and *CLB5* have distinct osmoregulation. Comparison of the experimental and simulated distributions of mRNA number per cell per cell cycle phase (Supplementary Figure S 21 and details in Supplementary Figure S 22), time-courses of mRNA and related noise level (Supplementary Figure S 19B and D) and and relationship between mRNA expression level and noise (Supplementary Figure S 23C) for osmotic stress conditions are shown below.

Supplementary Table S 21. Table of the reactions and parameters values of the revised model for *SIC1*, *CLN2* and *CLB5* transcription under normal growth conditions and under osmotic stress.

This table lists all elementary processes and the respective reaction schemes as shown in (A). All reactions follow mass action kinetics. The rate expressions are provided as well as the respective parameter values. The last column provides the start and end times for high expression of the respective genes.

Process	Reaction scheme	Rate	Parameter values [min^{-1}]	Transcription times [min]
SIC1 transcription	$\rightarrow SIC1$	$k_1 \cdot S_1$	$k_{1h} = 22.15$ $k_{1l} = 1.72$	$t_{S_{1,0}} = 118.09$ $t_{S_{1,e}} = 124.05$
SIC1 degradation	$SIC1 \rightarrow$	$p_1 \cdot SIC1$	$p_1 = 0.56$	
CLN2 transcription	$\rightarrow CLN2$	$k_3 \cdot S_2$	$k_{3h} = 4.4$ $k_{3l} = 0.02$	$t_{S_{2,0,first}} = 20.57$ $t_{S_{2,e,first}} = 39.83$ $t_{S_{2,0,sec}} = 119.01$ $t_{S_{2,e,sec}} = 124.05$
CLN2 degradation	$CLN2 \rightarrow$	$p_3 \cdot CLN2$	$p_3 = 0.09$	
CLB5 transcription	$\rightarrow CLB5$	$k_5 \cdot S_3$	$k_{5h} = 3.05$ $k_{5l} = 0.46$	$t_{S_{3,0,first}} = 40.16$ $t_{S_{3,e,first}} = 62.59$ $t_{S_{3,0,sec}} = 120.26$ $t_{S_{3,e,sec}} = 124.35$
CLB5 degradation	$CLB5 \rightarrow$	$p_5 \cdot CLB5$	$p_5 = 0.51$	

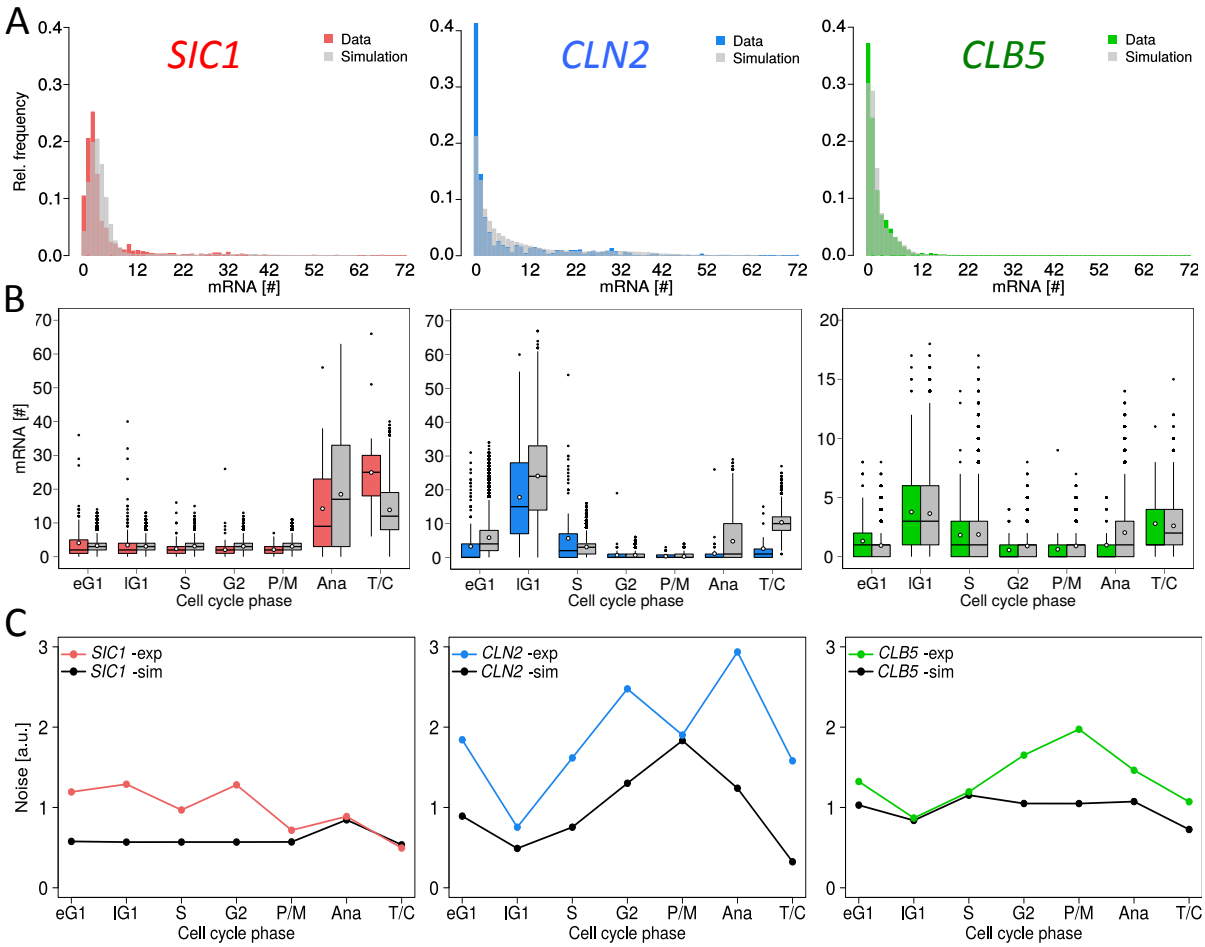

Supplementary Figure S 18. Quantitative analysis of single-cell transcription for *SIC1*, *CLN2* and *CLB5* under optimal growth conditions in an asynchronous cell population.

(A) Experimental and simulated distributions of mRNA number per cell for *SIC1*, *CLN2* and *CLB5*. (B) Measured and simulated mRNA distributions for each cell cycle phase. Lower and upper quartiles form boundaries of the boxes. Lines and white dots insight the boxes represent medians and mean values, respectively. Whiskers are given by 1.5 x IQR (interquartile range). Data points outside of the IQR define outliers. For better overview early G1 and late G1 are abbreviated to eG1 and lG1, respectively. (C) Noise is calculated as ratio of standard deviation to mean. Noise of mRNA numbers for *SIC1*, *CLN2* and *CLB5* has been determined either from the RNA-FISH experimental data (n>900 cells per gene) or from the stochastic simulations (n=2000 simulated cells). Lines between data points are for visualization only.

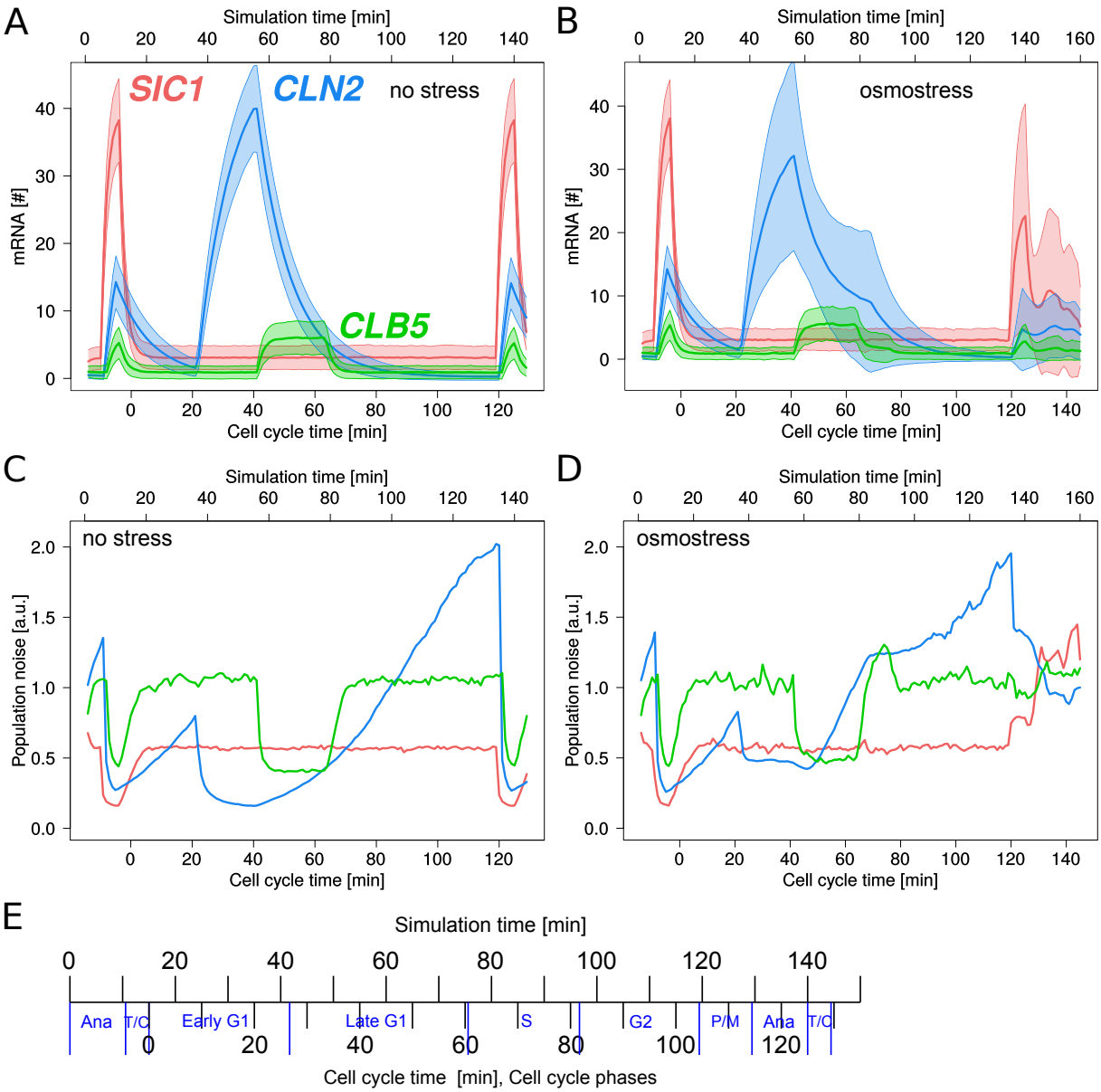

Supplementary Figure S 19. Simulated time-courses of transcript numbers and molecular noise during cell cycle for *SIC1*, *CLN2* and *CLB5* under optimal conditions and under osmotic stress.

Simulations were performed with the Gillespie algorithm using the equations and parameter values provided in Table 1. 2000 cells were simulated from anaphase until T/C phase of the next cell cycle, leading to a shift of 15 min between simulation time and cell cycle time. Transcript levels increase during periods of active signals S_1, S_2, or S_3 (see Figure 1B). (A) and (B) Time-courses of mean values (thick lines) and standard deviations (shaded areas around thick lines) of mRNA under optimal conditions and under osmotic stress, respectively. (C) and (D) Time-courses of noise measured over the whole population, i.e. standard deviation divided by mean of all 2000 cells at each time point. (E) Relation between cell cycle and simulation time.

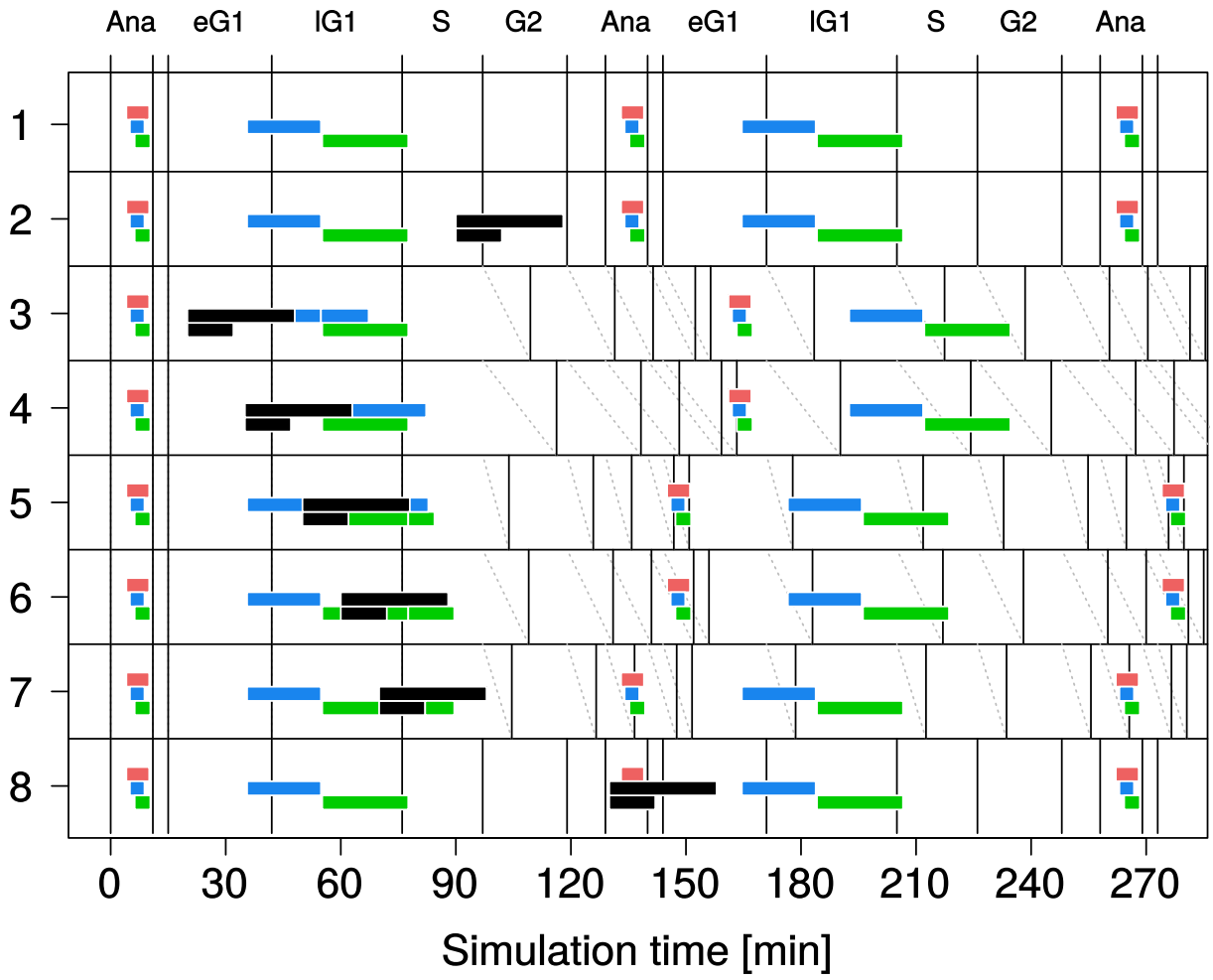

Supplementary Figure S 20. Schematic of the temporal order of cell cycle phases and distinct active and inactive transcription periods of mRNA under osmotic stress.

Active transcription periods for *SIC1*, *CLN2* and *CLB5* are represented by red, blue and green bars, respectively. The delay in transcriptional activity due to osmotic stress is depicted by black bars. The unnamed phases around Ana correspond to P/M and T/C. 1: No osmotic stress; no phase shifts. 2: Osmotic stress has no effect on high expression regions; no phase shifts. 3: Osmotic stress hits *CLN2* at the beginning of the high expression region; phases are shifted by the overlap between osmotic stress and the high transcription region of *CLN2*. 4. Osmotic stress overlaps the high transcription region of *CLN2*; phases are shifted by the stress duration of *CLN2*. 5. Osmotic stress cuts high transcription region of *CLN2* and hits *CLB5* at the beginning of its high transcription region; phases are shifted by the larger overlap between osmotic stress and the high transcription regions of *CLN2* or *CLB5*. 6. Osmotic stress is located insight high transcription region of *CLB5*; phases are shifted by the stress duration of *CLB5*. 7. Osmotic stress cuts high transcription region of *CLB5*; phases are shifted by the overlap between osmotic stress and the high transcription region of *CLB5*. 8. Osmotic stress has no effect on high transcription region of *SIC1* and second expression peaks of *CLN2* and *CLB5* aren't made up after being hit by osmotic stress; no phase shifts.

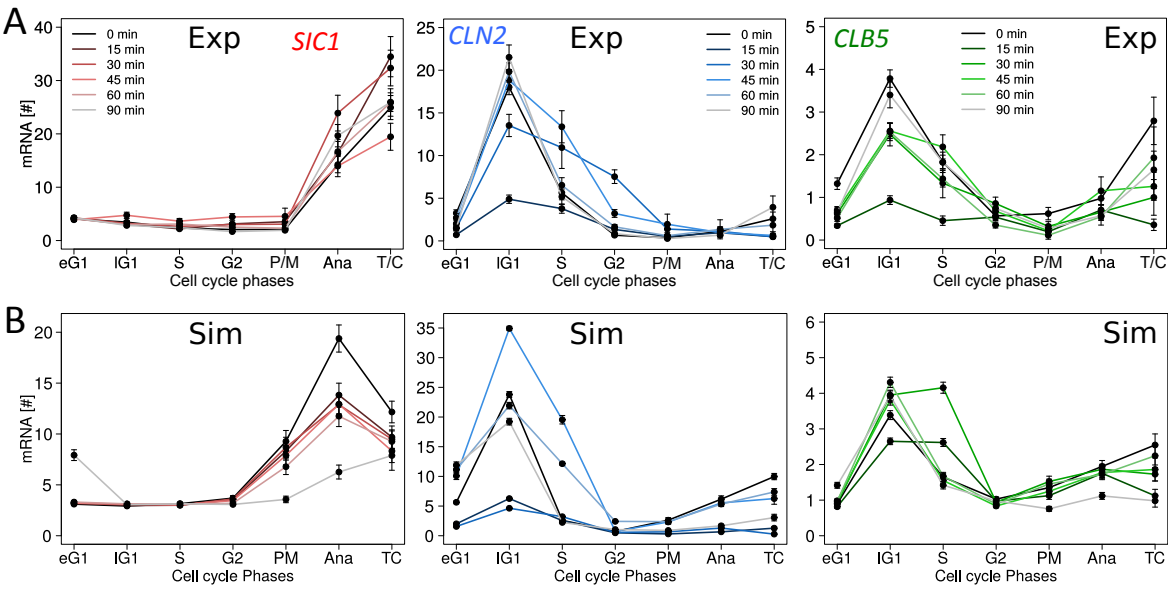

Supplementary Figure S 21. Medium osmotic stress affects timing of mRNA abundances for *SIC1, CLN2* and *CLB5* during the cell cycle.

Data shown are mean ± SEM. Darkest curves correspond to the shortest incubations in hyperosmotic medium. (A) Experimental and (B) Simulated changes of timing of mRNA abundances for *SIC1* (red), *CLN2* (blue) and *CLB5* (green) during the cell cycle progression upon osmotic stress. n> 400 cells per genes and time points for experimental values in (A). n=2000 cells per simulations in (B). Details of (A) and (E) depicted in Supplementary Figure S 22. In (A) and (B) 0 min is equivalent to no stress conditions. Lines between data points in (A) and (B) are for visualization only.

A: experiments

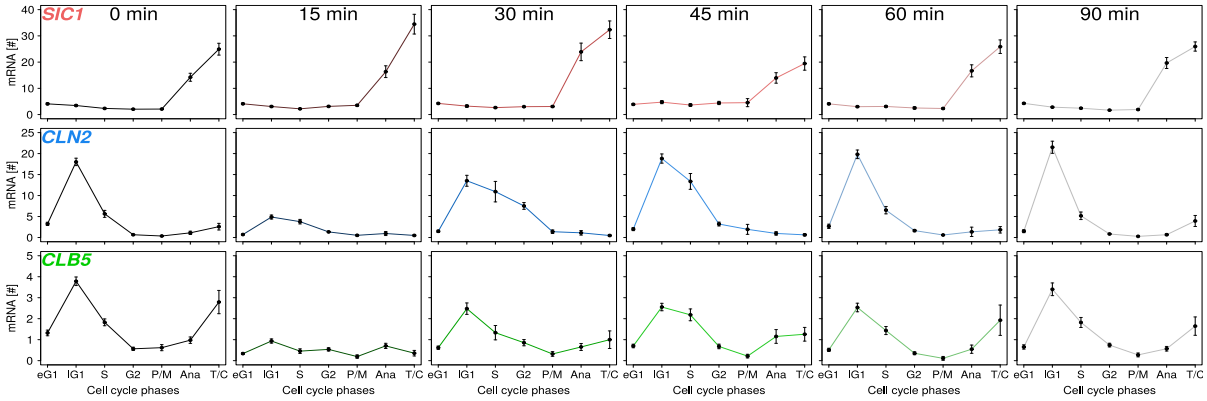

B: simulations

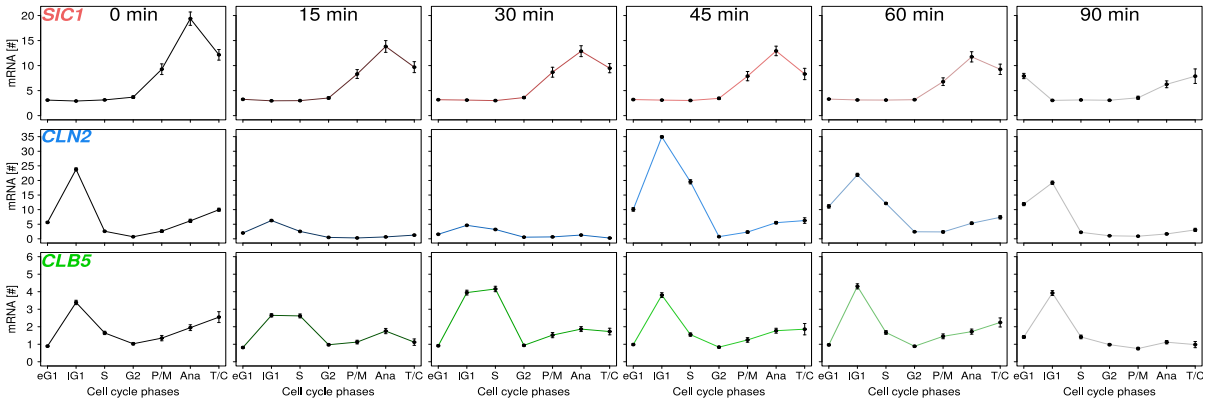

Supplementary Figure S 22. Influence of osmotic stress on timing of mRNA abundances for *SIC1*, *CLN2* and *CLB5*. Individual plots for experimental (A) and simulated (B) Abundances of mRNA per cell cycle phase shown Supplementary Figure S 21. Genes are presented in rows and stress times in columns. Data shown are mean ± SEM. Lines between data points in (A) and (B) are for visualization only.

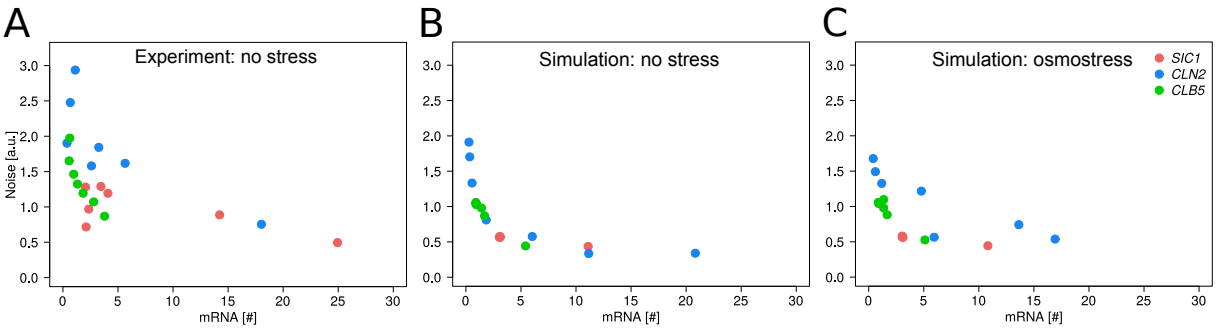

Supplementary Figure S 23. Relationship between mRNA expression level and noise.

In each diagram, the mean value of noise is plotted against the mean number of mRNAs for *SIC1*, *CLN2* and *CLB5* in each cell cycle phase. (a) Correlation coefficients for the experimental data under no stress condition are r_{SIC1} = -0.71, r_{CLN2} = -0.80, r_{CLB5} = -0.90 and r_{all} = -0.56, where r_{all} correspond to the correlation coefficient over all genes. (b) Simulations under no stress condition result in correlation coefficients r_{SIC1} = -1, r_{CLN2} = -0.78, r_{CLB5} = -0.99 and r_{all} = -0.62, and (c) correlation coefficients for simulations with osmotic stress are r_{SIC1} = -0.99, r_{CLN2} = -0.84, r_{CLB5} = -0.97 and r_{all} = -0.51. Correlation coefficients indicate strong correlations; means lower mRNA levels have higher noise levels. *SIC1* and *CLN2* show significantly different noise levels in the experiment ($p_{SIC1\text{-}CLN2}$ = 0.01, $p_{CLN2\text{-}CLB5}$ = 0.16, $p_{CLB5\text{-}SIC1}$ = 0.07), whereas *SIC1* and *CLB5* show significant differences in simulations with ($p_{SIC1\text{-}CLN2}$ = 0.20, $p_{CLN2\text{-}CLB5}$ = 0.90, $p_{CLB5\text{-}SIC1}$ = 0.02) and without osmotic stress ($p_{SIC1\text{-}CLN2}$ = 0.10, $p_{CLN2\text{-}CLB5}$ = 0.46, $p_{CLB5\text{-}SIC1}$ = 0.02). Only CLN2 has similar noise levels for the experiment and data under no stress condition (p_{SIC1} = 0.02, p_{CLN2} = 0.07, p_{CLB5} = 0.02). p values are calculated from with the Wilcoxon-Mann-Whitney test.

Selbständigkeitserklärung

Hiermit erkläre ich, die Dissertation selbstständig und nur unter Verwendung der angegebenen Hilfen und Hilfsmittel angefertigt zu haben.

Ich habe mich anderwärts nicht um einen Doktorgrad beworben und besitze keinen entsprechenden Doktorgrad.

Ich erkläre, dass ich die Dissertation oder Teile davon nicht bereits bei einer anderen wissenschaftlichen Einrichtung eingereicht habe und dass sie dort weder angenommen noch abgelehnt wurde.

Ich erkläre die Kenntnisnahme der dem Verfahren zugrunde liegenden Promotionsordnung der Mathematisch-Naturwissenschaftlichen Fakultät I der Humboldt-Universität zu Berlin vom 6. Juli 2009.

Weiterhin erkläre ich, dass keine Zusammenarbeit mit gewerblichen Promotionsberaterinnen/Promotionsberatern stattgefunden hat und dass die Grundsätze der Humboldt-Universität zu Berlin zur Sicherung guter wissenschaftlicher Praxis eingehalten wurden.

Berlin, den 1. November 2018

Aouefa Amoussouvi

Acknowledgement

Many people contributed to this project and I want thank few of them here. This PhD has been a deep journey of professional and personal growth. I learned scientific thinking and several methods, as well was lucky enough to be introduced to inspiring scientists through collaborations and attending conferences in Berlin and around the world.

First, I want to thank Prof. Andreas Herrmann for opening me his lab, where I conducted my Master Thesis and later my PhD Thesis. I am grateful for his guidance. I have been inspired by his ability to create research network and his global vision to expand research into society.

The topic of this PhD project was an initial idea of Prof. Edda Klipp and I am thankful for her supervision, time over the years as well as her commitment in adjusting her computational models to my experimental data. I will remember her expert and personal leadership.

I conducted the experiments of this project in the Molecular Biophysics Lab of Prof. Andreas Herrman and I thank all the lab members, who introduced me to molecular biology/cloning assays and fluorescence spectroscopy and microscopy as well as helping me to practice German and to get a glimpse of Berlin and the German culture. I'm especially grateful to Gabriele Schreiber, who taught me almost everything to know about yeast, bacteria and molecular cloning. I am also deeply thankful to Lotte Teufel, who I spent long hours designing, conducting and analyzing experiments and hanging out to forget the failed experiments.

A PhD is full of high and low moments and I had great colleagues to share the successes and the frustration of the scientific research. Caroline Mair, Joanna Ziomkowska, Santiago Di Lella, Andrea Gramatica, Chris Höfer, Roland Schwarzer... I have a deep gratitude for your feedbacks to my conference abstracts and talk presentations, our daily laughers in the lab, weekends and holiday trips, bike tours, dancing nights… I am deeply grateful to Caro and Joanna for our girls climbing evenings and our friendships. In the last year in the lab, I really enjoyed sharing the same room with Chris Höfer and I am thankful for her motivation and company while analyzing my last experiments.

Since my project involved a strong theoretical and mathematical part, I spent a lot of time in the Theoretical Biophysics Group of Edda Klipp and I thank the entire group for their cookies breaks and insights in computational biology. In this lab, I am particularly thankful to Matthias Reis for our long hours of discussions. Additionally, I thank Martin Seeger, Matteo Barberis, Julia Katharina Schlichting and Szymon Stoma for their contribution to this project.

I am grateful for the technical support of Thomas Korte, Christine Klause, Christine Müller, Gudrun Habermann, Sabine Schiller and Ivo Maintz and for the helpful work of student assistants: Roman Scholz, Katrina Meyer, Dominique Sydow, Claudia Beck. I also thank Angela Piater and Sabine Wagnitz for taking care of the administrative questions.

I had the chance to learn the RNA-FISH method during a stay in Daniel Larson's Lab in NIH in Bethesda and I thank him and his team for their warm welcome and teaching.

I am deeply grateful to all my friends in Berlin for their support, patience, and motivation. It has been great to discover this vibrant city together. You made me survive the cold and dark winters here: Giulia Molinengo, Ann-Sofie Paternoster, Tanja Peuker, Benni Apitius, Martin Michette, Ryszard Auksztulewicz, Matthieu Lalane, Lucile Bouvard, Thomas Ritschel, Zsuzsa Pavelka, Ylva Köhncke, Maggie Krarsch, Tinka Knoll, Philipp Schläger, Maria R. Ponce, Malte Wittenberg, Sebastian Jobst, Rachel Quigley, Suse Bachinger…

Although we were separated by geographic distance I thank my French and "abroad" friends for visiting me and for holding our friendships: Marianne Buclet, Mauro Haldner, Marielle Pottier, Romain Chassefière, Mai Diep, Cecilia Petiperez, Alice Malice, Sayonne Hay, Amandine Lions, Liz Brunk, Cécile Fessler, Oscar Herdandez...

Finalement, je remercie ma famille pour leur soutien et amour: Françoise Bartoli, François Amoussouvi, Andrée Toussaint, Nicolas Amoussouvi, Christophe Amoussouvi, Anne Bartoli, Jean-Baptiste Bartoli, Danielle Gobbert, Salomé Gaba, Eric Pablo and Christel Daudé.

Publications

Peer reviewed articles

Amoussouvi A, Teufel L., Reis M., Schreiber G, Beck C, Seeger M, Herrmann A., Klipp E. Single cell fluorescence imaging with FISH allows for quantitative characterization of transcription regulation of cell cycle in *S. cerevisiea*. *npj System Biology and Applications* (2018) 4:17 DOI:10.1038/s41540-018-0053-4

Wietek J, Haralampiev I, **Amoussouvi A**, Herrmann A and Stöckl M Membrane bound α-synuclein is fully embedded in the lipid bilayer while loci with higher flexibility remain. *FEBS Lett*. 587 (2013) 2572–2577 journal DOI: 10.1016/j.febslet.2013.06.034

Barberis M, Beck C, **Amoussouvi A**, Schreiber G, Diener C, Herrmann A and Klipp E (2011) Low number of *SIC1* mRNA molecules ensures low noise level in cell cycle progression of budding yeast, *Mol. BioSyst*, (2011) 7,2804–2812 DOI: 10.1039/C1MB05073G

Oral presentations

56th Biophysical Society Meeting,
San Diego, USA – Feb 25. - 29. 2012
Transcriptional dynamics at single cell level of G1/S phase transition regulating genes in S.cerevisiae.

4th Berlin Summer Meeting – Experimental & Computational Molecular Biology Meet, From RNA to Protein and Beyond
Berlin, Germany – June 23. - 25. 2011
Counting of SIC1 mRNA molecules in single budding yeast cells to investigate how transcription variability influences timing of G1/S transition

EMBO Workshop & Conference, RNA Control of Cell Dynamics
Kibbutz Ein-Gedhi, Israel –Nov 15. - 18. 2010 - **Travel Grant**
Detection of SIC1 and CLN2 mRNA molecules in individual cells during the yeast cell cycle

Poster presentations

8th Berlin Summer Meeting - Experimental & Computational Molecular Biology Meet, Localization Of Cellular Processes
Berlin, Germany – June 4. - 6. 2015 – **Poster Award**
Single cell fluorescence imaging with MS2-CP and RNA-FISH allows RNA localization and quantitative characterization of transcription regulation in S. cerevisiae

DAAD Science Tour 2014, Modeling the Future – Understanding Global Challenges through Computer-Based Modeling and Simulation
Berlin, Germany - Dec 5. 2014
Single cell fluorescence imaging with FISH allows for quantitative characterization of transcription regulation of cell cycle in S. cerevisiae

2nd Sign Gene – IRI / German-Israeli Symposium, Quantitative Approaches in Cell Biology
Berlin, Germany - Aug 31. - Sept 2. 2014
Single cell fluorescence imaging with FISH allows for quantitative characterization of transcription regulation of cell cycle in S. cerevisiae

7th Berlin Summer Meeting - Experimental & Computational Molecular Biology Meet, From Systems Biology to Systems Medicine,
Berlin, Germany - June 12.-13. 2014
Single cell fluorescence imaging with FISH allows for quantitative characterization of transcription regulation of cell cycle in S. cerevisiae

1st Sign Gene German-Israeli Symposium,
Berlin, Germany - June 12.-13. 2014
Single cell fluorescence imaging with FISH allows for quantitative characterization of transcription regulation of cell cycle in S. cerevisiae

EMBO Conference, Gene Transcription in Yeast**,**
Gerona, Spain – June 16. - 21. 2012 - **Travel Grant**
Single cell fluorescence imaging with FISH allows for quantitative characterization of transcription regulation of cell cycle in S. cerevisiae

International Conference on System Biology (ICSB) 2011
Heidelberg/Mannheim, Germany - Aug 28. - Sept 1. 2011
Experimental and stochastic model analysis of the influence of SIC1 transcriptional noise on the G1/S transition in S. cerevisiae cell cycle

55th Biophysical Society Meeting
Baltimore, USA - March 5. – 9. 2011
Counting of single SIC1 mRNA molecules to investigate how transcription variability influences timing of G1/S transition

3rd Berlin Summer Meeting - Experimental & Computational Molecular Biology Meet
Berlin, Germany - 24th – 26th June 2010
Detection of single CLN2 and SIC1 mRNA molecules in living yeast cells using MS2-CP-GFP method

Bibliography

Adrover, M.À., Zi, Z., Duch, A., Schaber, J., González-Novo, A., Jimenez, J., Nadal-Ribelles, M., Clotet, J., Klipp, E., and Posas, F. (2011). Time-dependent quantitative multicomponent control of the G1-S network by the stress-activated protein kinase Hog1 upon osmostress. Sci. Signal. *4*, ra63.

Aerne, B.L., Johnson, A.L., Toyn, J.H., and Johnston, L.H. (1998). Swi5 controls a novel wave of cyclin synthesis in late mitosis. Mol. Biol. Cell *9*, 945–956.

Alberghina, L., and Porro, D. (1993). Quantitative flow cytometry: analysis of protein distributions in budding yeast. A mini-review. Yeast *9*, 815–823.

Alberts, B., Johnson, A., Lewis, J., Raff, M., Roberts, K., and Walter, P. (2002). Molecular Biology of the Cell (New York: Garland Science).

Aldea, M., Garí, E., and Colomina, N. (2007). Control of cell cycle and cell growth by molecular chaperones. Cell Cycle *6*, 2599–2603.

Alexander, M.R., Tyers, M., Perret, M., Craig, B.M., Fang, K.S., and Gustin, M.C. (2001). Regulation of cell cycle progression by Swe1p and Hog1p following hypertonic stress. Mol. Biol. Cell *12*, 53–62.

Amon, A., Tyers, M., Futcher, B., and Nasmyth, K. (1993). Mechanisms that help the yeast cell cycle clock tick: G2 cyclins transcriptionally activate G2 cyclins and repress G1 cyclins. Cell *74*, 993–1007.

Amoussouvi, A., Teufel, L., Reis, M., Seeger, M., Schlichting, J.K., Schreiber, G., Herrmann, A., and Klipp, E. (2018). Transcriptional timing and noise of yeast cell cycle regulators—a single cell and single molecule approach. Npj Syst. Biol. Appl. *4*, 17.

Andrews, B.J., and Mason, S.W. (1993). Gene expression and the cell cycle: a family affair. Science *261*, 1543–1544.

Archambault, V., Li, C.X., Tackett, A.J., Wasch, R., Chait, B.T., Rout, M.P., and Cross, F.R. (2003). Genetic and biochemical evaluation of the importance of Cdc6 in regulating mitotic exit. Mol. Biol. Cell *14*, 4592–4604.

Bachere, E., Chagot, D., and Grizel, H. (1988). Cell separation by centrifugal elutriation. Am. Fish. Soc. … *18*, 281–285.

Baker, S., and Cousins, R.D. (1984). Clarification of the use of CHI-square and likelihood functions in fits to histograms. Nucl. Instruments Methods Phys. Res. *221*, 437–442.

Baker Brachmann, C., Davies, A., Cost, G.J., Caputo, E., Li, J., Hieter, P., and Boeke, J.D. (1998). Designer deletion strains derived fromSaccharomyces cerevisiae S288C: A useful set of strains and plasmids for PCR-mediated gene disruption and other applications. Yeast *14*, 115–132.

Ball, D. a, Marchand, J., Poulet, M., Baumann, W.T., Chen, K.C., Tyson, J.J., and Peccoud, J. (2011). Oscillatory dynamics of cell cycle proteins in single yeast cells analyzed by imaging cytometry. PLoS One *6*, e26272.

Ball, D.A., Adames, N.R., Reischmann, N., Barik, D., Franck, C.T., Tyson, J.J., and Peccoud, J. (2013). Measurement and modeling of transcriptional noise in the cell cycle regulatory network. Cell Cycle *12*, 3203–3218.

Banfalvi, G. (2008). Cell cycle synchronization of animal cells and nuclei by centrifugal elutriation. Nat. Protoc. *3*, 663–673.

Bar-Ziv, R., Voichek, Y., and Barkai, N. (2016). Dealing with Gene-Dosage Imbalance during S Phase. Trends Genet. *32*, 717–723.

Barberis, M. (2012). Sic1 as a timer of Clb cyclin waves in the yeast cell cycle - design principle of not just an inhibitor. FEBS J. *279*, 1–25.

Barberis, M., and Klipp, E. (2007). Insights into the network controlling the G1/S transition in budding yeast. Genome Inform. *18*, 85–99.

Barberis, M., De Gioia, L., Ruzzene, M., Sarno, S., Coccetti, P., Fantucci, P., Vanoni, M., and Alberghina, L. (2005). The yeast cyclin-dependent kinase inhibitor Sic1 and mammalian p27Kip1 are functional homologues with a structurally conserved inhibitory domain. Biochem. J. *387*, 639–647.

Barberis, M., Klipp, E., Vanoni, M., and Alberghina, L. (2007). Cell size at S phase initiation: an emergent property of the G1/S network. PLoS Comput. Biol. *3*, e64.

Barberis, M., Beck, C., Amoussouvi, A., Schreiber, G., Diener, C., Herrmann, A., and Klipp, E. (2011). A low number of SIC1 mRNA molecules ensures a low noise level in cell cycle progression of budding yeast. Mol. Biosyst. *7*, 2804–2812.

Barberis, M., Linke, C., Adrover, M.À., González-Novo, A., Lehrach, H., Krobitsch, S., Posas, F., and Klipp, E. (2012). Sic1 plays a role in timing and oscillatory behaviour of B-type cyclins. Biotechnol. Adv. *30*, 108–130.

Barik, D., Baumann, W.T., Paul, M.R., Novak, B., and Tyson, J.J. (2010). A model of yeast cell-cycle regulation based on multisite phosphorylation. Mol. Syst. Biol. *6*, 405.

Bean, J.M., Siggia, E.D., and Cross, F.R. (2006). Coherence and timing of cell cycle start examined at single-cell resolution. Mol. Cell *21*, 3–14.

Becskei, A., Boselli, M.G., and van Oudenaarden, A. (2004). Amplitude control of cell-cycle waves by nuclear import. Nat. Cell Biol. *6*, 451–457.

Bellí, G., Garí, E., Aldea, M., and Herrero, E. (2001). Osmotic stress causes a G1 cell cycle delay and downregulation of Cln3/Cdc28 activity in Saccharomyces cerevisiae. Mol. Microbiol. *39*, 1022–1035.

Ben-Ari, Y., Brody, Y., Kinor, N., Mor, A., Tsukamoto, T., Spector, D.L., Singer, R.H., and Shav-Tal, Y. (2010). The life of an mRNA in space and time. J. Cell Sci. *123*, 1761–1774.

Berset, C., Griac, P., Tempel, R., La Rue, J., Wittenberg, C., and Lanker, S. (2002). Transferable domain in the G(1) cyclin Cln2 sufficient to switch degradation of Sic1 from the E3 ubiquitin ligase SCF(Cdc4) to SCF(Grr1). Mol. Cell. Biol. *22*, 4463–4476.

Bertrand, E., Chartrand, P., Schaefer, M., Shenoy, S.M., Singer, R.H., and Long, R.M. (1998). Localization of ASH1 mRNA particles in living yeast. Mol. Cell *2*, 437–445.

Besson, A., Assoian, R.K., and Roberts, J.M. (2004). Regulation of the cytoskeleton: an oncogenic function for cdk inhibitors? Nat. Rev. Cancer *4*, 948–955.

Beyer, A., Hollunder, J., Nasheuer, H.-P., and Wilhelm, T. (2004). Post-transcriptional expression regulation in the yeast Saccharomyces cerevisiae on a genomic scale. Mol. Cell. Proteomics *3*, 1083–1092.

Blain, S.W., Scher, H.I., Cordon-Cardo, C., and Koff, A. (2003). p27 as a target for cancer therapeutics. Cancer Cell *3*, 111–115.

Boehm, M., and Nabel, E.G. (2003). The cell cycle and cardiovascular diseases. Prog. Cell Cycle Res. *5*, 19–30.

Bon, M., McGowan, S.J., and Cook, P.R. (2006). Many expressed genes in bacteria and yeast are transcribed only once per cell cycle. FASEB J. *20*, 1721–1723.

Breeden, L.L. (1997). Alpha-factor synchronization of budding yeast. Methods Enzymol. *283*, 332–341.

Brewer, B.J., Chlebowicz-Sledziewska, E., and Fangman, W.L. (1984). Cell cycle phases in the unequal mother/daughter cell cycles of Saccharomyces cerevisiae. Mol. Cell. Biol. *4*, 2529–2531.

Brickner, D.G., Cajigas, I., Fondufe-Mittendorf, Y., Ahmed, S., Lee, P.-C., Widom, J., and Brickner, J.H. (2007). H2A.Z-mediated localization of genes at the nuclear periphery confers epigenetic memory of previous transcriptional state. PLoS Biol. *5*, e81.

de Bruin, R.A.M., McDonald, W.H., Kalashnikova, T.I., Yates, J., and Wittenberg, C. (2004). Cln3 activates G1-specific transcription via phosphorylation of the SBF bound repressor Whi5. Cell *117*, 887–898.

de Bruin, R.A.M., Kalashnikova, T.I., Chahwan, C., McDonald, W.H., Wohlschlegel, J., Yates, J., Russell, P., and Wittenberg, C. (2006). Constraining G1-Specific Transcription to Late G1 Phase: The MBF-Associated Corepressor Nrm1 Acts via Negative Feedback. Mol. Cell *23*, 483–496.

Cacace, F., Paci, P., Cusimano, V., Germani, A., and Farina, L. (2012). Stochastic Modeling of Expression Kinetics Identifies Messenger Half-Lives and Reveals Sequential Waves of Co-ordinated Transcription and Decay. PLoS Comput. Biol. *8*, e1002772.

Cağatay, T., Turcotte, M., Elowitz, M.B., Garcia-Ojalvo, J., and Süel, G.M. (2009). Architecture-dependent noise discriminates functionally analogous differentiation circuits. Cell *139*, 512–522.

Catzavelos, C., Bhattacharya, N., Ung, Y.C., Wilson, J.A., Roncari, L., Sandhu, C., Shaw, P., Yeger, H., Morava-Protzner, I., Kapusta, L., et al. (1997). Decreased levels of the cell-cycle inhibitor p27Kip1 protein: prognostic implications in primary breast cancer. Nat. Med. *3*, 227–230.

Chang, Y.-L., Tseng, S.-F., Huang, Y.-C., Shen, Z.-J., Hsu, P.-H., Hsieh, M.-H., Yang, C.-W., Tognetti, S., Canal, B., Subirana, L., et al. (2017). Yeast Cip1 is activated by environmental stress to inhibit Cdk1–G1 cyclins via Mcm1 and Msn2/4. Nat. Commun. *8*, 56.

Chartrand, P., Singer, R.H., and Long, R.M. (2001). RNP localization and transport in yeast. Annu. Rev. Cell Dev. Biol. *17*, 297–310.

Charvin, G., Cross, F.R., and Siggia, E.D. (2008). A microfluidic device for temporally controlled gene expression and long-term fluorescent imaging in unperturbed dividing yeast cells. PLoS One *3*, e1468.

Chernomoretz, A., Bush, A., Yu, R., Gordon, A., and Colman-Lerner, A. (2008). Using Cell-ID 1.4 with R for microscope-based cytometry. Curr. Protoc. Mol. Biol. *Chapter 14*.

Choi, P.J., Xie, S.X., and Shakhnovich, E.I. (2010). Stochastic switching in gene networks can occur by a single-molecule event or many molecular steps. J. Mol. Biol. *396*, 230–244.

Chubb, J.R., Trcek, T., Shenoy, S.M., and Singer, R.H. (2006). Transcriptional pulsing of a developmental gene. Curr. Biol. *16*, 1018–1025.

Chymkowitch, P., and Enserink, J.M. (2013). The cell cycle rallies the transcription cycle: Cdc28/Cdk1 is a cell cycle-regulated transcriptional CDK. Transcription *4*, 3–6.

Ciemerych, M.A., and Sicinski, P. (2005). Cell cycle in mouse development. Oncogene *24*, 2877–2898.

Clotet, J., Escoté, X., Adrover, M.À., Yaakov, G., Garí, E., Aldea, M., de Nadal, E., and Posas, F. (2006). Phosphorylation of Hsl1 by Hog1 leads to a G2 arrest essential for cell survival at high osmolarity. EMBO J. *25*, 2338–2346.

Coccetti, P., Rossi, R.L., Sternleri, F., Porro, D., Russo, G.L., Fonzo, A. Di, Magni, F., Vanoni, M., and Alberghina, L. (2004). Mutations of the CK2 phosphorylation site of Sic1 affect cell size and S-Cdk kinase activity in Saccharomyces cerevisiae. Mol. Microbiol. *51*, 447–460.

Colman-Lerner, A., Chin, T.E., and Brent, R. (2001). Yeast Cbk1 and Mob2 activate daughter-specific genetic programs to induce asymmetric cell fates. Cell *107*, 739–750.

Colman-Lerner, A., Gordon, A., Serra, E., Chin, T., Resnekov, O., Endy, D., Pesce, C.G., and Brent, R. (2005). Regulated cell-to-cell variation in a cell-fate decision system. Nature *437*, 699–706.

Di Como, C.J., Chang, H., and Arndt, K.T. (1995). Activation of CLN1 and CLN2 G1 cyclin gene expression by BCK2. Mol. Cell. Biol. *15*, 1835–1846.

Cooper, G.M. (2000). The Cell: A Molecular Approach. (Sinauer Associates).

Cooper, S. (2004). Rejoinder: whole-culture synchronization cannot, and does not, synchronize cells. Trends Biotechnol. *22*, 274–276.

Corrigan, A.M., Tunnacliffe, E., Cannon, D., and Chubb, J.R. (2016). A continuum model of transcriptional bursting. Elife *5*, e13051.

Costanzo, M., Nishikawa, J.L., Tang, X., Millman, J.S., Schub, O., Breitkreuz, K., Dewar, D., Rupes, I., Andrews, B., and Tyers, M. (2004). CDK activity antagonizes Whi5, an inhibitor of G1/S transcription in yeast. Cell *117*, 899–913.

Coulon, A., Chow, C.C., Singer, R.H., and Larson, D.R. (2013). Eukaryotic transcriptional dynamics: from single molecules to cell populations. Nat. Rev. Genet. *14*, 572–584.

Coutinho, I., Pereira, G., Leão, M., Gonçalves, J., Côrte-Real, M., and Saraiva, L. (2009). Differential regulation of p53 function by protein kinase C isoforms revealed by a yeast cell system. FEBS Lett. *583*, 3582–3588.

Cross, F.R., and Tinkelenberg, A.H. (1991). A potential positive feedback loop controlling CLN1 and CLN2 gene expression at the start of the yeast cell cycle. Cell *65*, 875–883.

Cross, F.R., Schroeder, L., and Bean, J.M. (2007). Phosphorylation of the Sic1 inhibitor of B-type cyclins in Saccharomyces cerevisiae is not essential but contributes to cell cycle robustness. Genetics *176*, 1541–1555.

Currais, A., Hortobágyi, T., and Soriano, S. (2009). The neuronal cell cycle as a mechanism of pathogenesis in Alzheimer's disease. Aging (Albany, NY. Online) *1*, 363–371.

Day, A., Schneider, C., and Schneider, B. (2004). Yeast cell synchronization. Cell Cycle Checkp. Control … *241*, 55–76.

Denicourt, C., Saenz, C.C., Datnow, B., Cui, X.-S., and Dowdy, S.F. (2007). Relocalized p27Kip1 tumor suppressor functions as a cytoplasmic metastatic oncogene in melanoma. Cancer Res. *67*, 9238–9243.

Digman, M.A., Dalal, R., Horwitz, A.F., and Gratton, E. (2008). Mapping the number of molecules and brightness in the laser scanning microscope. Biophys. J. *94*, 2320–2332.

Digman, M.A., Wiseman, P.W., Choi, C., Horwitz, A.R., and Gratton, E. (2009). Stoichiometry of molecular complexes at adhesions in living cells. Proc. Natl. Acad. Sci. *106*, 2170–2175.

Dirick, L., and Nasmyth, K. (1991). Positive feedback in the activation of Gl cyclins in yeast. Nature *351*, 754–757.

Dirick, L., Böhm, T., and Nasmyth, K. (1995). Roles and regulation of Cln-Cdc28 kinases at the start of the cell cycle of Saccharomyces cerevisiae. EMBO J. *14*, 4803–4813.

Donovan, J.D., Toyn, J.H., Johnson, A.L., and Johnston, L.H. (1994). P40SDB25, a putative CDK inhibitor, has a role in the M/G1 transition in Saccharomyces cerevisiae. Genes Dev. *8*, 1640–1653.

Duch, A., de Nadal, E., and Posas, F. (2012). The p38 and Hog1 SAPKs control cell cycle progression in response to environmental stresses. FEBS Lett. *586*, 2925–2931.

Duch, A., de Nadal, E., and Posas, F. (2013a). Dealing with transcriptional outbursts during S phase to protect genomic integrity. J. Mol. Biol. *425*, 4745–4755.

Duch, A., Felipe-Abrio, I., Barroso, S., Yaakov, G., García-Rubio, M., Aguilera, A., de Nadal, E., and Posas, F. (2013b). Coordinated control of replication and transcription by a SAPK protects genomic integrity. Nature *493*, 116–119.

Elowitz, M.B., Levine, A.J., Siggia, E.D., and Swain, P.S. (2002). Stochastic gene expression in a single cell. Science *297*, 1183–1186.

Epstein, C.B., and Cross, F.R. (1994). Genes that can bypass the CLN requirement for Saccharomyces cerevisiae cell cycle START. Mol. Cell. Biol. *14*, 2041–2047.

Escoté, X., Zapater, M., Clotet, J., and Posas, F. (2004). Hog1 mediates cell-cycle arrest in G1 phase by the dual targeting of Sic1. Nat. Cell Biol. *6*, 997–1002.

Eser, P., Demel, C., Maier, K.C., Schwalb, B., Pirkl, N., Martin, D.E., Cramer, P., and Tresch, A. (2013). Periodic mRNA synthesis and degradation co-operate during cell cycle gene expression. Mol. Syst. Biol. *10*, 717.

Espinoza, F.H., Ogas, J., Herskowitz, I., and Morgan, D.O. (1994). Cell cycle control by a complex of the cyclin HCS26 (PCL1) and the kinase PHO85. Science *266*, 1388–1391.

Femino, A.M. (1998). Visualization of Single RNA Transcripts in Situ. Science (80-.). *280*, 585–590.

Ferguson, M.L., Coq, D., Jules, M., and Aymerich, S. (2011). Absolute Quantification of Gene Expression in Individual Bacterial Cells Using Two Photon Fluctuation Microscopy. Analytical *419*, 250–259.

Fero, M.L., Rivkin, M., Tasch, M., Porter, P., Carow, C.E., Firpo, E., Polyak, K., Tsai, L.-H., Broudy, V., Perlmutter, R.M., et al. (1996). A Syndrome of Multiorgan Hyperplasia with Features of Gigantism, Tumorigenesis, and Female Sterility in p27Kip1-Deficient Mice. Cell *85*, 733–744.

Fero, M.L., Randel, E., Gurley, K.E., Roberts, J.M., and Kemp, C.J. (1998). The murine gene p27 Kip1 is haplo-insufficient for tumour suppression. Nature *396*, 177–180.

Finley, D., Ulrich, H.D., Sommer, T., and Kaiser, P. (2012). The ubiquitin-proteasome system of Saccharomyces cerevisiae. Genetics *192*, 319–360.

Foury, F. (1997). Human genetic diseases: a cross-talk between man and yeast. Gene *195*, 1–10.

Fujii-Yamamoto, H., Kim, J.M., Arai, K., and Masai, H. (2005). Cell cycle and developmental regulations of replication factors in mouse embryonic stem cells. J. Biol. Chem. *280*, 12976–12987.

Fusco, D., Accornero, N., Lavoie, B., Shenoy, S.M., Blanchard, J., Singer, R.H., and Bertrand, E. (2003). Single mRNA Molecules Demonstrate Probabilistic Movement in Living Mammalian Cells. Curr. Biol. *13*, 161–167.

Futcher, B. (1999). Cell cycle synchronization. Methods Cell Sci. *21*, 79–86.

Gallardo, F., Laterreur, N., Cusanelli, E., Ouenzar, F., Querido, E., Wellinger, R.J., and Chartrand, P. (2011). Live cell imaging of telomerase RNA dynamics reveals cell cycle-dependent clustering of telomerase at elongating telomeres. Mol. Cell *44*, 819–827.

Gallego, C., Garí, E., Colomina, N., Herrero, E., and Aldea, M. (1997). The Cln3 cyclin is down-regulated by translational repression and degradation during the G1 arrest caused by nitrogen deprivation in budding yeast. EMBO J. *16*, 7196–7206.

Gandhi, S.J., Zenklusen, D., Lionnet, T., and Singer, R.H. (2011). Transcription of functionally related constitutive genes is not coordinated. Nat. Struct. Mol. Biol. *18*, 27–34.

Garcia, J.F., and Parker, R. (2015). MS2 coat proteins bound to yeast mRNAs block 5' to 3' degradation and trap mRNA decay products: implications for the localization of mRNAs by MS2-MCP system. RNA *21*, 1393–1395.

Gardiner, C. (2009). Stochastic Methods: A Handbook for the Natural and Social Sciences (Springer Berlin Heidelberg).

Garí, E., Volpe, T., Wang, H., Gallego, C., Futcher, B., and Aldea, M. (2001). Whi3 binds the mRNA of the G1 cyclin CLN3 to modulate cell fate in budding yeast. Genes Dev. *15*, 2803–2808.

Geijer, C., Medrala-Klein, D., Petelenz-Kurdziel, E., Ericsson, A., Smedh, M., Andersson, M., Goksör, M., Nadal-Ribelles, M., Posas, F., Krantz, M., et al. (2013). Initiation of the transcriptional response to hyperosmotic shock correlates with the potential for volume recovery. FEBS J. *280*, 3854–3867.

Ghaemmaghami, S., Huh, W.-K., Bower, K., Howson, R.W., Belle, A., Dephoure, N., O'Shea, E.K., and Weissman, J.S. (2003). Global analysis of protein expression in yeast. Nature *425*, 737–741.

Ghosh, S., Marchand, V., Gáspár, I., and Ephrussi, A. (2012). Control of RNP motility and localization by a splicing-dependent structure in oskar mRNA. Nat. Struct. Mol. Biol. *19*, 441–449.

Gillespie, D.T. (1977). Exact stochastic simulation of coupled chemical reactions. J. Phys. Chem. *81*, 2340–2361.

Goffeau, A., Barrell, B.G., Bussey, H., Davis, R.W., Dujon, B., Feldmann, H., Galibert, F., Hoheisel, J.D., Jacq, C., Johnston, M., et al. (1996). Life with 6000 genes. Science *274*, 546, 563–567.

Golding, I., and Cox, E.C. (2004). RNA dynamics in live Escherichia coli cells. Proc. Natl. Acad. Sci. U. S. A. *101*, 11310–11315.

Golldack, D., Li, C., Mohan, H., and Probst, N. (2014). Tolerance to drought and salt stress in plants: Unraveling the signaling networks. Front. Plant Sci. *5*, 151.

Gomez, D., Marathe, R., Bierbaum, V., and Klumpp, S. (2014). Modeling stochastic gene expression in growing cells. J. Theor. Biol. *348*, 1–11.

González-Novo, A., Jiménez, J., Clotet, J., Nadal-Ribelles, M., Cavero, S., de Nadal, E., and Posas, F. (2015). Hog1 Targets Whi5 and Msa1 Transcription Factors To Downregulate Cyclin Expression upon Stress. Mol. Cell. Biol. *35*, 1606–1618.

Grandin, N., and Reed, S.I. (1993). Differential function and expression of Saccharomyces cerevisiae B-type cyclins in mitosis and meiosis. Mol. Cell. Biol. *13*, 2113–2125.

Haim, L., Zipor, G., Aronov, S., and Gerst, J.E. (2007). A genomic integration method to visualize localization of endogenous mRNAs in living yeast. Nat. Methods *4*, 409–412.

Haim-Vilmovsky, L., and Gerst, J.E. (2009). m-TAG: a PCR-based genomic integration method to visualize the localization of specific endogenous mRNAs in vivo in yeast. Nat. Protoc. *4*, 1274–1284.

Haim-Vilmovsky, L., Gadir, N., Herbst, R.H., and Gerst, J.E. (2011). A genomic integration method for the simultaneous visualization of endogenous mRNAs and their translation products in living yeast. RNA *17*, 2249–2255.

Halstead, J.M., Lionnet, T., Wilbertz, J.H., Wippich, F., Ephrussi, A., Singer, R.H., and Chao, J.A. (2015). An RNA biosensor for imaging the first round of translation from single cells to living animals. Science (80-.). *347*, 1367–1671.

Han, J., Lee, J.D., Bibbs, L., and Ulevitch, R.J. (1994). A MAP kinase targeted by endotoxin and hyperosmolarity in mammalian cells. Science *265*, 808–811.

Harashima, H., Dissmeyer, N., and Schnittger, A. (2013). Cell cycle control across the eukaryotic kingdom. Trends Cell Biol. *23*, 345–356.

Harris, M.R., Lee, D., Farmer, S., Lowndes, N.F., and de Bruin, R.A.M. (2013). Binding specificity of the G1/S transcriptional regulators in budding yeast. PLoS One *8*, e61059.

Hartwell, L.H., and Weinert, T. a (1989). Checkpoints: controls that ensure the order of cell cycle events. Science *246*, 629–634.

Hatzis, C., and Porro, D. (2006). Morphologically-structured models of growing budding yeast populations. J. Biotechnol. *124*, 420–438.

Heinrich, S., Sidler, C.L., Azzalin, C.M., and Weis, K. (2017). Stem–loop RNA labeling can affect nuclear and cytoplasmic mRNA processing. RNA *23*, 134–141.

Hinnen, A., Hicks, J.B., and Fink, G.R. (1978). Transformation of yeast. Proc. Natl. Acad. Sci. U. S. A. *75*, 1929–1933.

Hirschberg, K., Miller, C.M., Ellenberg, J., Presley, J.F., Siggia, E.D., Phair, R.D., and Lippincott-Schwartz, J. (1998). Kinetic analysis of secretory protein traffic and characterization of golgi to plasma membrane transport intermediates in living cells. J. Cell Biol. *143*, 1485–1503.

Hocine, S., Raymond, P., Zenklusen, D., Chao, J.A., and Singer, R.H. (2013). Single-molecule analysis of gene expression using two-color RNA labeling in live yeast. Nat. Methods *10*, 119–121.

Hohmann, S. (2002). Osmotic stress signaling and osmoadaptation in yeasts. Microbiol. Mol. Biol. Rev. *66*, 300–372.

Holstege, F.C.P., Jennings, E.G., Wyrick, J.J., Lee, T.I., Hengartner, C.J., Green, M.R., Golub, T.R., Lander, E.S., and Young, R.A. (1998). Dissecting the Regulatory Circuitry of a Eukaryotic Genome. Cell *95*, 717–728.

Hong Li, and Petzold, L. (2010). Efficient Parallelization of the Stochastic Simulation Algorithm for Chemically Reacting Systems On the Graphics Processing Unit. Int. J. High Perform. Comput. Appl. *24*, 107–116.

Horn, W.T., Tars, K., Grahn, E., Helgstrand, C., Baron, A.J., Lago, H., Adams, C.J., Peabody, D.S., Phillips, S.E. V, Stonehouse, N.J., et al. (2006). Structural basis of RNA binding discrimination between bacteriophages Qβ and MS2. Structure *14*, 487–495.

Huang, D., Friesen, H., and Andrews, B. (2007). Pho85, a multifunctional cyclin-dependent protein kinase in budding yeast. Mol. Microbiol. *66*, 303–314.

Hur, J.Y., Park, M.C., Suh, K.-Y., and Park, S.-H. (2011). Synchronization of cell cycle of Saccharomyces cerevisiae by using a cell chip platform. Mol. Cells *32*, 483–488.

Hwang, H.C., and Clurman, B.E. (2005). Cyclin E in normal and neoplastic cell cycles. Oncogene *24*, 2776–2786.

Iyer, V.R., Horak, C.E., Scafe, C.S., Botstein, D., Snyder, M., and Brown, P.O. (2001). Genomic binding sites of the yeast cell-cycle transcription factors SBF and MBF. Nature *409*, 533–538.

Jacobson, M.D., Gray, S., Yuste-Rojas, M., and Cross, F.R. (2000). Testing cyclin specificity in the exit from mitosis. Mol. Cell. Biol. *20*, 4483–4493.

Jahnke, T., and Huisinga, W. (2006). Solving the chemical master equation for monomolecular reaction systems analytically. J. Math. Biol. *54*, 1–26.

Jensen, L.J., Jensen, T.S., de Lichtenberg, U., Brunak, S., and Bork, P. (2006). Co-evolution of transcriptional and post-translational cell-cycle regulation. Nature *443*, 594–597.

Kærn, M., Elston, T.C., Blake, W.J., and Collins, J.J. (2005). Stochasticity in gene expression: from theories to phenotypes. Nat. Rev. Genet. *6*, 451–464.

Kar, S., Baumann, W.T., Paul, M.R., and Tyson, J.J. (2009). Exploring the roles of noise in the eukaryotic cell cycle. Proc. Natl. Acad. Sci. U. S. A. *106*, 6471–6476.

Kaufmann, B.B., and van Oudenaarden, A. (2007). Stochastic gene expression: from single molecules to the proteome. Curr. Opin. Genet. Dev. *17*, 107–112.

Kislauskis, E.H., Zhu, X., and Singer, R.H. (1994). Sequences responsible for intracellular localization of β-actin messenger RNA also affect cell phenotype. J. Cell Biol. *127*, 441–451.

Kiviet, D.J., Nghe, P., Walker, N., Boulineau, S., Sunderlikova, V., and Tans, S.J. (2014). Stochasticity of metabolism and growth at the single-cell level. Nature *514*, 376–379.

Klipp, E., Nordlander, B., Krüger, R., Gennemark, P., and Hohmann, S. (2005). Integrative model of the response of yeast to osmotic shock. Nat. Biotechnol. *23*, 975–982.

Knapp, D., Bhoite, L., Stillman, D.J., and Nasmyth, K. (1996). The transcription factor Swi5 regulates expression of the cyclin kinase inhibitor p40SIC1. Mol. Cell. Biol. *16*, 5701–5707.

Ko, M.S. (1991). A stochastic model for gene induction. J. Theor. Biol. *153*, 181–194.

Koch, C., Moll, T., Neuberg, M., Ahorn, H., and Nasmyth, K. (1993). A role for the transcription factors Mbp1 and Swi4 in progression from G1 to S phase. Science *261*, 1551–1557.

Kõivomägi, M., Valk, E., Venta, R., Iofik, A., Lepiku, M., Balog, E.R.M., Rubin, S.M., Morgan, D.O., and Loog, M. (2011). Cascades of multisite phosphorylation control Sic1 destruction at the onset of S phase. Nature *480*, 128–131.

Laabs, T.L., Markwardt, D.D., Slattery, M.G., Newcomb, L.L., Stillman, D.J., and Heideman, W. (2003). ACE2 is required for daughter cell-specific G1 delay in Saccharomyces cerevisiae. Proc. Natl. Acad. Sci. U. S. A. *100*, 10275–10280.

Labib, K., Diffley, J.F., and Kearsey, S.E. (1999). G1-phase and B-type cyclins exclude the DNA-replication factor Mcm4 from the nucleus. Nat. Cell Biol. *1*, 415–422.

Ladbury, J.E., and Arold, S.T. (2012). Noise in cellular signaling pathways: causes and effects. Trends Biochem. Sci. *37*, 173–178.

Larson, D.R., Singer, R.H., and Zenklusen, D. (2009). A single molecule view of gene expression. Trends Cell Biol. *19*, 630–637.

Larson, D.R., Zenklusen, D., Wu, B., Chao, J. a, and Singer, R.H. (2011). Real-time observation of transcription initiation and elongation on an endogenous yeast gene. Science *332*, 475–478.

LeCuyer, K.A., Behlen, L.S., and Uhlenbeck, O.C. (1995). Mutants of the bacteriophage MS2 coat protein that alter its cooperative binding to RNA. Biochemistry *34*, 10600–10606.

Lenburg, M.E., and O'Shea, E.K. (2001). Genetic evidence for a morphogenetic function of the Saccharomyces cerevisiae Pho85 cyclin-dependent kinase. Genetics *157*, 39–51.

Lengronne, A., and Schwob, E. (2002). The Yeast CDK Inhibitor Sic1 Prevents Genomic Instability by Promoting Replication Origin Licensing in Late G1. Mol. Cell *9*, 1067–1078.

Lipson, D., Raz, T., Kieu, A., Jones, D.R., Giladi, E., Thayer, E., Thompson, J.F., Letovsky, S., Milos, P., and Causey, M. (2009). Quantification of the yeast transcriptome by single-molecule sequencing. Nat. Biotechnol. *27*, 652–658.

López-Avilés, S., Kapuy, O., Novák, B., and Uhlmann, F. (2009). Irreversibility of mitotic exit is the consequence of systems-level feedback. Nature *459*, 592–595.

Lundblad, V., and Struhl, K. (2008). Yeast. In Current Protocols in Molecular Biology, (Hoboken, NJ, USA: John Wiley & Sons, Inc.),.

Macia, J., Regot, S., Peeters, T., Conde, N., Solé, R., and Posas, F. (2009). Dynamic signaling in the Hog1 MAPK pathway relies on high basal signal transduction. Sci. Signal. *2*, ra13.

Marsaglia, G. (2003). Xorshift RNGs. J. Stat. Softw. *8*, 1–6.

Marsaglia, G., and Tsang, W.W. (2000). The Ziggurat Method for Generating Random Variables. J. Stat. Softw. *5*, 1–7.

Matis, T., and Guardiola, I. (2010). Achieving Moment Closure through Cumulant Neglect. Math. J. *12*.

Mauch, S., and Stalzer, M. (2011). Efficient Formulations for Exact Stochastic Simulation of Chemical Systems. IEEE/ACM Trans. Comput. Biol. Bioinforma. *8*, 27–35.

Meetoo, D. (2008). Chronic diseases: the silent global epidemic. Br. J. Nurs. *17*, 1320–1325.

Mettetal, J.T., Muzzey, D., Oudenaarden, A. Van, Gómez-Uribe, C., and van Oudenaarden, A. (2008). The frequency dependence of osmo-adaptation in Saccharomyces cerevisiae. Science *319*, 482–484.

Meyer, K. (2012). Zellzyklus in Hefe unter Osmostress.

Miller, C., Schwalb, B., Maier, K., Schulz, D., Dümcke, S., Zacher, B., Mayer, A., Sydow, J., Marcinowski, L., Dölken, L., et al. (2011). Dynamic transcriptome analysis measures rates of mRNA synthesis and decay in yeast. Mol. Syst. Biol. *7*, 458.

Miura, F., Kawaguchi, N., Yoshida, M., Uematsu, C., Kito, K., Sakaki, Y., and Ito, T. (2008). Absolute quantification of the budding yeast transcriptome by means of competitive PCR between genomic and complementary DNAs. BMC Genomics *9*, 574.

Molin, C., Jauhiainen, A., Warringer, J., Nerman, O., and Sunnerhagen, P. (2009). mRNA stability changes precede changes in steady-state mRNA amounts during hyperosmotic stress. RNA *15*, 600–614.

Morgan, D.O. (1995). Principles of CDK regulation. Nature *374*, 131–134.

Morgan, D.O. (1997). CYCLIN-DEPENDENT KINASES: Engines, Clocks, and Microprocessors. Annu. Rev. Cell Dev. Biol. *13*, 261–291.

Munsky, B., Neuert, G., and van Oudenaarden, A. (2012). Using gene expression noise to understand gene regulation. Science *336*, 183–187.

Muzzey, D., Gómez-Uribe, C.A., Mettetal, J.T., and van Oudenaarden, A. (2009). A systems-level analysis of perfect adaptation in yeast osmoregulation. Cell *138*, 160–171.

Nadal-Ribelles, M., Conde, N., Flores, O., González-Vallinas, J., Eyras, E., Orozco, M., de Nadal, E., and Posas, F. (2012). Hog1 bypasses stress-mediated down-regulation of transcription by RNA polymerase II redistribution and chromatin remodeling. Genome Biol. *13*, R106.

de Nadal, E., Ammerer, G., and Posas, F. (2011). Controlling gene expression in response to stress. Nat. Rev. Genet. *12*, 833–845.

Nagy, Z. (2007). The dysregulation of the cell cycle and the diagnosis of Alzheimer's disease. Biochim. Biophys. Acta *1772*, 402–408.

Nakayama, K., Ishida, N., Shirane, M., Inomata, A., Inoue, T., Shishido, N., Horii, I., Loh, D.Y., and Nakayama, K. (1996). Mice Lacking p27Kip1 Display Increased Body Size, Multiple Organ Hyperplasia, Retinal Dysplasia, and Pituitary Tumors. Cell *85*, 707–720.

Nash, P., Tang, X., Orlicky, S., Chen, Q., Gertler, F.B., Mendenhall, M.D., Sicheri, F., Pawson, T., and Tyers, M. (2001). Multisite phosphorylation of a CDK inhibitor sets a threshold for the onset of DNA replication. Nature *414*, 514–521.

Nasmyth, K. (1996). At the heart of the budding yeast cell cycle. Trends Genet. *12*, 405–412.

Neuert, G., Munsky, B., Tan, R.Z., Teytelman, L., Khammash, M., and van Oudenaarden, A. (2013). Systematic identification of signal-activated stochastic gene regulation. Science *339*, 584–587.

O Skinner, S., Xu, H., Nagarkar-Jaiswal, S., Freire, P.R., Zwaka, T.P., and Golding, I. (2016). Single-cell analysis of transcription kinetics across the cell cycle. Elife *5*, e12175.

Ogas, J., Andrews, B.J., and Herskowitz, I. (1991). Transcriptional activation of CLN1, CLN2, and a putative new G1 cyclin (HCS26) by SWI4, a positive regulator of G1-specific transcription. Cell *66*, 1015–1026.

Orlando, D. a, Lin, C.Y., Bernard, A., Wang, J.Y., Socolar, J.E.S., Iversen, E.S., Hartemink, A.J., and Haase, S.B. (2008). Global control of cell-cycle transcription by coupled CDK and network oscillators. Nature *453*, 944–947.

Ostapenko, D., and Solomon, M.J. (2011). Anaphase promoting complex-dependent degradation of transcriptional repressors Nrm1 and Yhp1 in Saccharomyces cerevisiae. Mol. Biol. Cell *22*, 2175–2184.

Palumbo, P., Mavelli, G., Farina, L., and Alberghina, L. (2010). Networks and circuits in cell regulation. Biochem. Biophys. Res. Commun. *396*, 881–886.

Paulsson, J. (2005). Models of stochastic gene expression. Phys. Life Rev. *2*, 157–175.

Peccoud, J., and Ycart, B. (1995). Markovian Modeling of Gene-Product Synthesis. Theor. Popul. Biol. *48*, 222–234.

Pelet, S., Rudolf, F., Nadal-Ribelles, M., de Nadal, E., Posas, F., Peter, M., and Nadal, E. De (2011). Transient activation of the HOG MAPK pathway regulates bimodal gene expression. Science *332*, 732–735.

Pereira, C., Coutinho, I., Soares, J., Bessa, C., Leão, M., and Saraiva, L. (2012). New insights into cancer-related proteins provided by the yeast model. FEBS J. *279*, 697–712.

Proft, M., Mas, G., de Nadal, E., Vendrell, A., Noriega, N., Struhl, K., and Posas, F. (2006). The stress-activated Hog1 kinase is a selective transcriptional elongation factor for genes responding to osmotic stress. Mol. Cell *23*, 241–250.

Querido, E., Gallardo, F., Beaudoin, M., Menard, C., and Chartrand, P. (2011). Stochastic and reversible aggregation of mRNA with expanded CUG-triplet repeats. J. Cell Sci. *124*, 1703–1714.

Raj, A., and van Oudenaarden, A. (2008). Nature, nurture, or chance: stochastic gene expression and its consequences. Cell *135*, 216–226.

Raj, A., and van Oudenaarden, A. (2009). Single-molecule approaches to stochastic gene expression. Annu. Rev. Biophys. *38*, 255–270.

Raj, A., Peskin, C.S., Tranchina, D., Vargas, D.Y., and Tyagi, S. (2006). Stochastic mRNA synthesis in mammalian cells. PLoS Biol. *4*, e309.

Raj, A., van den Bogaard, P., Rifkin, S.A., van Oudenaarden, A., and Tyagi, S. (2008). Imaging individual mRNA molecules using multiple singly labeled probes. Nat. Methods *5*, 877–879.

Raj, A., Rifkin, S.A., Andersen, E., and van Oudenaarden, A. (2010). Variability in gene expression underlies incomplete penetrance. Nature *463*, 913–918.

Rangamani, P., and Iyengar, R. (2008). Modelling cellular signalling systems. Essays Biochem. *45*, 83–94.

Reis, M., Kromer, J.A., and Klipp, E. (2018). General solution of the chemical master equation and modality of marginal distributions for hierarchic first-order reaction networks. J. Math. Biol. 1–43.

Reiser, V., D'Aquino, K.E., Ee, L.-S., and Amon, A. (2006). The stress-activated mitogen-activated protein kinase signaling cascade promotes exit from mitosis. Mol. Biol. Cell *17*, 3136–3146.

Reynaud, E.G., Krzic, U., Greger, K., and Stelzer, E.H.K. (2008). Light sheet-based fluorescence microscopy: more dimensions, more photons, and less photodamage. HFSP J. *2*, 266–275.

Richardson, H., Lew, D.J., Henze, M., Sugimoto, K., and Reed, S.I. (1992). Cyclin-B homologs in Saccharomyces cerevisiae function in S phase and in G2. Genes Dev. *6*, 2021–2034.

Rodriguez, A.J., Condeelis, J., Singer, R.H., and Dictenberg, J.B. (2007). Imaging mRNA movement from transcription sites to translation sites. Semin. Cell Dev. Biol. *18*, 202–208.

Romero-Santacreu, L., Moreno, J., Pérez-Ortín, J.E., and Alepuz, P. (2009). Specific and global regulation of mRNA stability during osmotic stress in Saccharomyces cerevisiae. RNA *15*, 1110–1120.

Rossi, R.L., Zinzalla, V., Mastriani, A., Vanoni, M., and Alberghina, L. (2005). Subcellular Localization of the Cyclin Dependent Kinase Inhibitor Sic1 is Modulated by the Carbon Source in Budding Yeast. Cell Cycle *4*, 1798–1807.

Saito, H., and Posas, F. (2012). Response to hyperosmotic stress. Genetics *192*, 289–318.

Saraiva, L., Fresco, P., Pinto, E., and Gonçalves, J. (2004). Characterization of phorbol esters activity on individual mammalian protein kinase C isoforms, using the yeast phenotypic assay. Eur. J. Pharmacol. *491*, 101–110.

Satyanarayana, A., and Kaldis, P. (2009). Mammalian cell-cycle regulation: several Cdks, numerous cyclins and diverse compensatory mechanisms. Oncogene *28*, 2925–2939.

Schmiedel, J.M., Klemm, S.L., Zheng, Y., Sahay, A., Blüthgen, N., Marks, D.S., and van Oudenaarden, A. (2015). Gene expression. MicroRNA control of protein expression noise. Science *348*, 128–132.

Schneiter, R. (2004). Genetics , Molecular and Cell Biology of Yeast.

Schreiber, G., Barberis, M., Scolari, S., Klaus, C., Herrmann, A., and Klipp, E. (2012). Unraveling interactions of cell cycle-regulating proteins Sic1 and B-type cyclins in living yeast cells: a FLIM-FRET approach. FASEB J. *26*, 546–554.

Schwob, E. (1994). The B-type cyclin kinase inhibitor p40SIC1 controls the G1 to S transition in S. cerevisiae. Cell *79*, 233–244.

Schwob, E., and Nasmyth, K. (1993). CLB5 and CLB6, a new pair of B cyclins involved in DNA replication in Saccharomyces cerevisiae. Genes Dev. *7*, 1160–1175.

Shahrezaei, V., and Marguerat, S. (2015). Connecting growth with gene expression: Of noise and numbers. Curr. Opin. Microbiol. *25*, 127–135.

Shahrezaei, V., and Swain, P.S. (2008). Analytical distributions for stochastic gene expression. Proc. Natl. Acad. Sci. U. S. A. *105*, 17256–17261.

Shepard, K. a, Gerber, a P., Jambhekar, A., Takizawa, P. a, Brown, P.O., Herschlag, D., DeRisi, J.L., and Vale, R.D. (2003). Widespread cytoplasmic mRNA transport in yeast: identification of 22 bud-localized transcripts using DNA microarray analysis. Proc. Natl. Acad. Sci. U. S. A. *100*, 11429–11434.

Shirayama, M., Tóth, A., Gálová, M., and Nasmyth, K. (1999). APC(Cdc20) promotes exit from mitosis by destroying the anaphase inhibitor Pds1 and cyclin Clb5. Nature *402*, 203–207.

Silverman, S.J., Petti, A.A., Slavov, N., Parsons, L., Briehof, R., Thiberge, S.Y., Zenklusen, D., Gandhi, S.J., Larson, D.R., Singer, R.H., et al. (2010). Metabolic cycling in single yeast cells from unsynchronized steady-state populations limited on glucose or phosphate. Proc. Natl. Acad. Sci. U. S. A. *107*, 6946–6951.

Simon, I., Barnett, J., Hannett, N., Harbison, C.T., Rinaldi, N.J., Volkert, T.L., Wyrick, J.J., Zeitlinger, J., Gifford, D.K., and Jaakkola, T.S. (2001). Serial Regulation of Transcriptional Regulators in the Yeast Cell Cycle. Cell *106*, 697–708.

Singer, R.H., and Ward, D.C. (1982). Actin gene expression visualized in chicken muscle tissue culture by using in situ hybridization with a biotinated nucleotide analog. Proc. Natl. Acad. Sci. U. S. A. *79*, 7331–7335.

Skotheim, J.M., Di Talia, S., Siggia, E.D., and Cross, F.R. (2008). Positive feedback of G1 cyclins ensures coherent cell cycle entry. Nature *454*, 291–296.

Slingerland, J., and Pagano, M. (2000). Regulation of the Cdk inhibitor p27 and its deregulation in cancer. J. Cell. Physiol. *183*, 10–17.

Spellman, P.T., Sherlock, G., Zhang, M.Q., Iyer, V.R., Anders, K., Eisen, M.B., Brown, P.O., Botstein, D., and Futcher, B. (1998). Comprehensive identification of cell cycle-regulated genes of the yeast Saccharomyces cerevisiae by microarray hybridization. Mol. Biol. Cell *9*, 3273–3297.

Spiesser, T., Kuehn, C., Krantz, M., and Klipp, E. (2016). The MYpop toolbox: Putting yeast stress responses in cellular context on single cell and population scales. Biotechnol. J. *11*, 1158–1168.

Spiesser, T.W., Kühn, C., Krantz, M., and Klipp, E. (2015). Bud-Localization of CLB2 mRNA Can Constitute a Growth Rate Dependent Daughter Sizer. PLoS Comput. Biol. *11*, e1004223.

Stehbens, S., Pemble, H., Murrow, L., and Wittmann, T. (2012). Imaging intracellular protein dynamics by spinning disk confocal microscopy. Methods Enzymol. *504*, 293–313.

Stewart-Ornstein, J., Weissman, J.S., and El-Samad, H. (2012). Cellular noise regulons underlie fluctuations in Saccharomyces cerevisiae. Mol. Cell *45*, 483–493.

Stuart, D., and Wittenberg, C. (1994). Cell cycle-dependent transcription of CLN2 is conferred by multiple distinct cis-acting regulatory elements. Mol. Cell. Biol. *14*, 4788–4801.

Di Talia, S., Skotheim, J.M., Bean, J.M., Siggia, E.D., and Cross, F.R. (2007). The effects of molecular noise and size control on variability in the budding yeast cell cycle. Nature *448*, 947–951.

Di Talia, S., Wang, H., Skotheim, J.M., Rosebrock, A.P., Futcher, B., and Cross, F.R. (2009). Daughter-specific transcription factors regulate cell size control in budding yeast. PLoS Biol. *7*, e1000221.

Taniguchi, Y., Choi, P.J., Li, G.W.G.-W., Chen, H., Babu, M., Hearn, J., Emili, A., Sunney Xie, X., and Xie, X.S. (2010). Quantifying E. coli Proteome and Transcriptome with Single-Molecule Sensitivity in Single Cells. Science (80-.). *329*, 533–538.

Thattai, M., and Van Oudenaarden, A. (2004). Stochastic gene expression in fluctuating environments. Genetics *167*, 523–530.

Thompson, M. a, Casolari, J.M., Badieirostami, M., Brown, P.O., and Moerner, W.E. (2010). Three-dimensional tracking of single mRNA particles in Saccharomyces cerevisiae using a double-helix point spread function. Proc. Natl. Acad. Sci. U. S. A. *107*, 17864–17871.

Thompson, R.E., Larson, D.R., and Webb, W.W. (2002). Precise nanometer localization analysis for individual fluorescent probes. Biophys. J. *82*, 2775–2783.

Tissier, F., Louvel, A., Grabar, S., Hagnéré, A.-M., Bertherat, J., Vacher-Lavenu, M.-C., Dousset, B., Chapuis, Y., Bertagna, X., and Gicquel, C. (2004). Cyclin E correlates with malignancy and adverse prognosis in adrenocortical tumors. Eur. J. Endocrinol. *150*, 809–817.

Toone, W.M., Johnson, A.L., Banks, G.R., Toyn, J.H., Stuart, D., Wittenberg, C., and Johnston, L.H. (1995). Rme1, a negative regulator of meiosis, is also a positive activator of G1 cyclin gene expression. EMBO J. *14*, 5824–5832.

Toyn, J.H., Johnson, A.L., Donovan, J.D., Toone, W.M., and Johnston, L.H. (1997). The Swi5 transcription factor of Saccharomyces cerevisiae has a role in exit from mitosis through induction of the cdk-inhibitor Sic1 in telophase. Genetics *145*, 85–96.

Trcek, T., Larson, D.R., Moldón, A., Query, C.C., and Singer, R.H. (2011). Single-molecule mRNA decay measurements reveal promoter- regulated mRNA stability in yeast. Cell *147*, 1484–1497.

Trcek, T., Chao, J.A., Larson, D.R., Park, H.Y., Zenklusen, D., Shenoy, S.M., and Singer, R.H. (2012). Single-mRNA counting using fluorescent in situ hybridization in budding yeast. Nat. Protoc. *7*, 408–419.

Tutucci, E., Vera, M., Biswas, J., Garcia, J., Parker, R., and Singer, R.H. (2018). An improved MS2 system for accurate reporting of the mRNA life cycle. Nat. Methods *15*, 81–89.

Uhlendorf, J., Miermont, A., Delaveau, T., Charvin, G., Fages, F., Bottani, S., Batt, G., and Hersen, P. (2012). Long-term model predictive control of gene expression at the population and single-cell levels. Proc. Natl. Acad. Sci. *109*, 14271–14276.

Vargas, D.Y., Shah, K., Batish, M., Levandoski, M., Sinha, S., Marras, S.A.E., Schedl, P., and Tyagi, S. (2011). Single-molecule imaging of transcriptionally coupled and uncoupled splicing. Cell *147*, 1054–1065.

Verma, R. (1997). Phosphorylation of Sic1p by G1 Cdk Required for Its Degradation and Entry into S Phase. Science (80-.). *278*, 455–460.

Voichek, Y., Bar-Ziv, R., and Barkai, N. (2016). Expression homeostasis during DNA replication. Science (80-.). *351*, 1087–1090.

Vos, T., Barber, R.M., Bell, B., Bertozzi-Villa, A., Biryukov, S., Bolliger, I., Charlson, F., Davis, A., Degenhardt, L., Dicker, D., et al. (2015). Global, regional, and national incidence, prevalence, and years lived with disability for 301 acute and chronic diseases and injuries in 188 countries, 1990–2013: a systematic analysis for the Global Burden of Disease Study 2013. Lancet *386*, 743–800.

Walker, J.M. (2011). Cell Cycle Synchronization (Totowa, NJ: Humana Press).

Wells, A.L., Condeelis, J.S., Singer, R.H., and Zenklusen, D. (2007). Imaging real-time gene expression in living systems with single-transcript resolution: image analysis of single mRNA transcripts. CSH Protoc. *2007*, pdb.prot4871.

Wilkinson, D.J. (2006). Stochastic Modelling for Systems Biology (Mathematical and Computational Biology Series) (Florida, Boca Raton: Chapman and Hall-CRC Press).

Wilkinson, D.J. (2009). Stochastic modelling for quantitative description of heterogeneous biological systems. Nat. Rev. Genet. *10*, 122–133.

Woldringh, C., Fluiter, K., and Huls, P. (1995). Production of senescent cells of Saccharomyces cerevisiae by centrifugal elutriation. Yeast *11*, 361–369.

Wu, B., Chao, J.A., and Singer, R.H. (2012). Fluorescence fluctuation spectroscopy enables quantitative imaging of single mRNAs in living cells. Biophys. J. *102*, 2936–2944.

Xiao, L., and Guo, J. (2015). Multiplexed single-cell in situ RNA analysis by reiterative hybridization. Anal. Methods *7*, 7290–7295.

Yaakov, G., Duch, A., García-Rubio, M., Clotet, J., Jimenez, J., Aguilera, A., and Posas, F. (2009). The stress-activated protein kinase Hog1 mediates S phase delay in response to osmostress. Mol. Biol. Cell *20*, 3572–3582.

Yang, F., Moss, L.G., and Phillips, G.N. (1996). The molecular structure of green fluorescent protein. Nat. Biotechnol. *14*, 1246–1251.

Yoshida, T., Sone, M., Ogawa, T., Nihei, H., Ozasa, H., Tsukada, K., and Horikawa, S. (1997). Molecular cloning of rat P38 mitogen-activated protein kinase and it's osmotic regulation in rat kidney. IUBMB Life *43*, 63–72.

Yunger, S., Rosenfeld, L., Garini, Y., and Shav-Tal, Y. (2010). Single-allele analysis of transcription kinetics in living mammalian cells. Nat. Methods *7*, 631–633.

Zapater, M., and Clotet, J. (2005). Control of Cell Cycle Progression by the Stress-Activated Hog1 MAPK. Cell Cycle *4*, 6–7.

Zenklusen, D., Larson, D.R., and Singer, R.H. (2008). Single-RNA counting reveals alternative modes of gene expression in yeast. Nat. Struct. Mol. Biol. *15*, 1263–1271.

Zhang, T., Schmierer, B., and Novák, B. (2011). Cell cycle commitment in budding yeast emerges from the cooperation of multiple bistable switches. Open Biol. *1*, 110009.

Zhivotovsky, B., and Orrenius, S. (2010). Cell cycle and cell death in disease: past, present and future. J. Intern. Med. *268*, 395–409.

Zipor, G., Haim-Vilmovsky, L., Gelin-Licht, R., Gadir, N., Brocard, C., and Gerst, J.E. (2009). Localization of mRNAs coding for peroxisomal proteins in the yeast, Saccharomyces cerevisiae. Proc. Natl. Acad. Sci. U. S. A. *106*, 19848–19853.

List of Figures

List of Tables

List of Supplementary Figures

List of Supplementary Tables